5-2014

A Method to Control Morphology of BHJ OPVs Using End-functionalized Poly(3-hexylthiophene)(P3HT) Grafted to SQDs

William Michael Kochemba
wkochemb@utk.edu

To the Graduate Council:

I am submitting herewith a dissertation written by William Michael Kochemba entitled "A Method to Control Morphology of BHJ OPVs Using End-functionalized Poly(3-hexylthiophene)(P3HT) Grafted to SQDs." I have examined the final electronic copy of this dissertation for form and content and recommend that it be accepted in partial fulfillment of the requirements for the degree of Doctor of Philosophy, with a major in Chemistry.

S. Michael Kilbey, II, Major Professor

We have read this dissertation and recommend its acceptance:

Jon P. Camden, Jimmy W. Mays, Gerd Duscher

Accepted for the Council:

Carolyn R. Hodges

Vice Provost and Dean of the Graduate School

(Original signatures are on file with official student records.)

A Method to Control Morphology of BHJ OPVs Using End-functionalized Poly(3-hexylthiophene)(P3HT) Grafted to SQDs

A Dissertation Presented for the
Doctor of Philosophy
Degree
The University of Tennessee, Knoxville

William Michael Kochemba

May 2014

Dedication

This dissertation is dedicated to my loving wife, Tara Kochemba, my children, Raya and Elijah Kochemba, and my beloved parents, Brenda and Chris Heck.

Acknowledgements

First of all, I would like to thank my advisor, Prof. S. Michael Kilbey II, for his patience and his everlasting enthusiasm for teaching. I am envious of his ability to communicate his thoughts and ideas in such a clear and concise manner. His professionalism is astounding and his kindness is infinite. Being a family man himself, he was companionate and understanding when I needed to spend time with my family. Not only am I honored to have him as a great mentor, but I am blessed to have him as friend.

I would also like to express my sincere gratitude to a number of family members, friends and colleagues who have helped me during my graduate studies at the University of Tennessee. First, I thank my wife, Tara, for keeping me in check and pushing me to excel in my research and my children, Raya and Elijah, who kept me motivated to be the best person and scientist that I can be. They have loved me unconditionally. I would also like to thank my parents, Brenda and Christopher Heck. I would not be where I am today without their guidance, advice and hospitality. My mother is an extremely strong woman who endured exceptionally difficult circumstances to keep my siblings and me protected and nurtured during our youth. My sister Jessica, her husband Bryan, and my niece and nephew, Lana and Luke, have provided me with encouraging conversations and motivation to push through challenging times. My brother Joseph participated in many long telephone conversions during my travels to Oak Ridge National Laboratory and taught me some basic computer programming skills along the way.

I acknowledge my colleagues at Oak Ridge National Laboratory who have always given me their sincere opinions and helpful advice. Those people include David Uhrig, Peter Bonneson, Brad Lokitz, Jamie Messman, Jose Alonzo, Bobby Sumpter, Rajeev Kumar, Suk-kyun Ahn,

Balaka Barkatay, Scott Hollenbeck and Joe Pickel. I am especially grateful for the support and guidance from Deanna Pickel, my research mentor at ORNL, whose friendship I will always treasure. She was an amazing teacher and an essential part of my graduate work- she helped me develop my laboratory skills and constantly encouraged me to think about problems from a unique perspective. Also, I thank Monojoy Goswami, a staff scientist in the theory group at the Center for Nanophase Materials Sciences, for his friendship, mentorship, and amazing Bengali Cuisine.

Finally, I would like to thank all of the members (past and present) of the Kilbey research group at the University of Tennessee for their support and friendship: Erick Soto-Cantu, Juan Pablo Hinestrosa, Chaitra Deodhar, Camille Kite, Jesse Davis, Kamlesh Bornani, Bethany Aden, Zach Siebers, and Xu Wang. Graduate school might have been unbearable without the immense amount of heart and soul that this group brought to work with them every single day.

Abstract

Improving the power conversion efficiency of organic photovoltaic devices based on polymer-nanoparticle bulk heterojunctions remains a significant challenge that limits the commercial production of these technologies. There are a number of factors that contribute to the efficiency of photovoltaic devices including absorption, charge generation and charge separation, which ultimately rely on the morphology of the bulk heterojunction active layer. My work aims to improve these processes by developing a method to prepare end-group functionalized π[pi]-conjugated polymers that will be used to decorate the surface of nanoparticles thereby tailoring the interface between the polymer and the nanoparticle. This work involves the preparation of a novel pyridine terminated poly (3-hexylthiophene) with the propensity to coordinate cadmium selenide semiconductor quantum dots. The polymers were synthesized by a modified Grignard metathesis polymerization in the presence of different additives and reactions conditions that improve the yield of monofunctional products.

The end-group composition of P3HTs prepared by *in situ* quenching of the GRIM polymerization method with tolyl-magnesium bromide was altered by adding reagents with an unsaturated double that coordinates with the active Ni^0[nickel zero] complex. The additives, 1-pentene and styrene, were shown to improve the monofunctional yield of tolyl-functionalized P3HTs, a model polymer, by interacting with the active Ni^0 species and preventing oxidation addition at the initiating chain end.

A method to tailor the donor/acceptor interface of bulk heterojunction organic photovoltaic devices by modifying the surface chemistry of semiconductor quantum dots (CdSe SQDs) will be presented. The ligands on CdSe SQD surfaces play an impactful role in their synthesis, solution

properties and nanophase organization in a polymer matrix. In this work, I report a method to stabilize cadmium selenide (CdSe) SQDs in a poly(3-hexylthiophene) (P3HT) matrix through a series of successive ligand exchanges that results in P3HT chains decorating the SQD surface.

Table of Contents

List of Tables

List of Figures

List of Schemes

Chapter 1: Introduction

1.1 Introduction to the synthesis of polythiophenes

The discovery of π-conjugated polymers in the late 1970s has led to both a Nobel Prize and a scurry to develop soft materials for organic optoelectronic applications. Driven in particular by a growing global demand for energy and environmental crises related to the use of fossil fuel, a large amount of research has been directed toward the use of π-conjugated polymers as active layer materials in organic photovoltaic (OPV) devices.[1-10] Organic photovoltaic devices have the potential to be lightweight, flexible and deployable over large surface areas with minimal cost associated with large scale manufacturing. However, the first π-conjugated polymers that were made and studied had the tendency to be insoluble in common organic solvents with relatively poor electronic properties.[11]

Over the past two decades, π-conjugated polymers have been rigorously studied to find ways to improve their physical and optoelectronic properties. For example, the preparation of π-conjugated polymers has converted from using harsh reaction conditions yielding poorly defined polymeric materials[12-13] to controlled chain-growth polymerization methods that yield well-defined polymers with relatively high hole mobilities.[14] Specifically, unsubstituted polythiophenes were first synthesized by electrochemical methods, yielding polymers with broad molecular weight distributions that were insoluble in most organic solvents.[12-13] Later, Elsenbaumer *et al.* prepared regiorandom alkyl-substituted polythiophenes, which improved the solubility of the polymers in organic solvents.[15] However, due to the lack of stereoselectivity of the polymerization mechanism, the resulting polymers had poor electronic properties due to the lack of planar stacking of the polymer chains. These problems of early preparations of P3HTs (as well as other pi-conjugated polymers) were recognized as a major barrier that would limit the

utility and adoption of pi-conjugated polymers in optoelectronic and photovoltaic devices. As a result, a driver of early research in the field revolved around better synthetic methods as well as monomer development.[11,16-18]

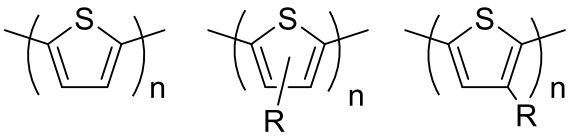

Figure 1-1. Chemical structures of unsubstituted 2,5-polythiophene (left), regiorandom, alkyl-substituted polythiophenes (middle), and regioregular poly(3-alkylthiophene), or P3AT (right).

A significant advance in the synthesis of π-conjugated polymers was made independently by McCullough and co-workers and by Rieke *et al*. in the early 1990's, who demonstrated that stereoregular monomers and metal-phosphine catalysts could be used to prepare regioregular poly(alkylthiophenes) coupled in a head-to-tail fashion (rrHT-P3AT).[16,19] For comparison, the chemical structures of the common types of polythiophenes are shown in Figure 1-1. As shown in the top of Scheme 1-2 below, the method developed by McCullough and coworkers to prepare rrHT-P3ATs begins with 2-bromo-3-alkylthiophene, which forms the regiospecific monomer by treatment with lithium diisopropylamide and successive addition of magnesium dibromide etherate at dry ice/acetone conditions. Then, a Ni^{II} catalyst is used to initiate a nickel-catalyzed cross coupling reaction. The Rieke method requires the use of a highly reactive zinc species, instead of magnesium, and a Pd^{0} catalyst to promote the cross coupling reaction.

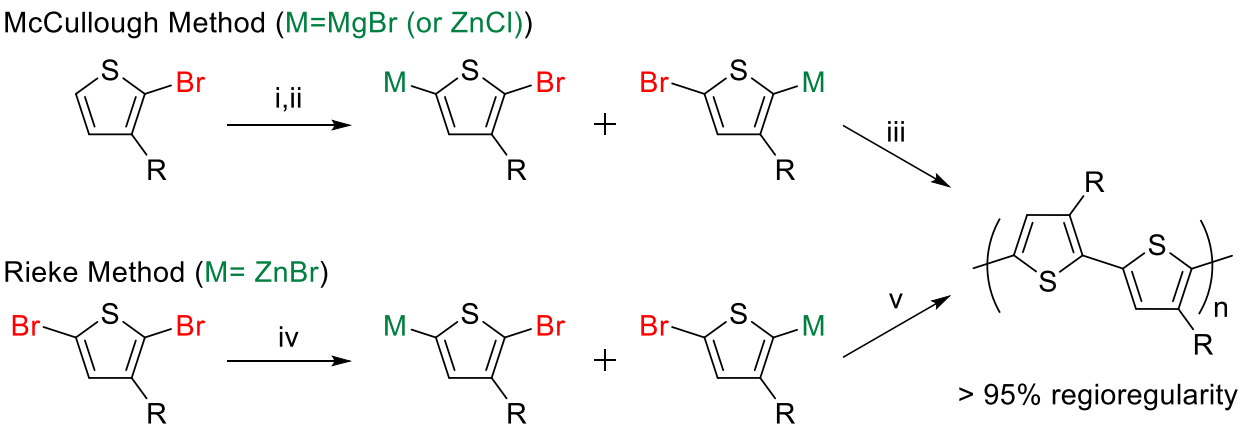

Scheme 1-1. Reaction schemes depicting the McCullough and Rieke methods for preparation of rrHT-P3ATs. i) lithium diisopropylamide (LDA)/THF, -40 °C, 40 min. ii) $MgBr_2$•OEt_2 ($ZnCl_2$), -60 to -40 °C, 40 min. iii) Ni(dppp)Cl_2, -5 to 25 °C, 18 h. iv) Zn*/THF, -78 °C, 4 h. v) Ni(dppe)Cl_2, 0 °C to rt, 24 h.

Both methods yield highly rrHT-P3HTs but necessitate long reaction times, cryogenic temperatures and high purity starting materials. Fortunately, the McCullough method was later modified into the Grignard metathesis (GRIM) method,[20] also known as the Kumada-catalyst transfer polycondensation (KCTP),[21] which makes use of less harsh reaction conditions and commercially available starting materials. Other methods to prepare rrHT-P3ATs are Suzuki[22] and Stille[23] cross-coupling reactions, which require palladium catalysts. Nevertheless, these methods are more cumbersome than the GRIM polymerization method because, like the original synthetic methods of McCullough and Rieke, cryogenic temperatures, strenuous monomer purification, and non-commercial starting materials are required.

A particular P3AT of great use is one having a hexyl side-chain [poly (3-hexylthiophene),

P3HT], because of P3HTs inherently good solubility and hole carrier mobility as compared to other P3ATs. The development of the GRIM polymerization method has made P3HT the benchmark material for many optoelectronic applications. The GRIM polymerization method provides the ability to prepare highly regioregular P3HT with control of molecular weight and narrow polydispersity. These three features lead to superior order and stacking of polymer chains, which leads to a relatively good hole carrier mobility. These traits, combined with the use of a 3-alkyl substitutent, such as a hexyl chain, make P3HT processible in organic solvents and, therefore, an efficient donor material for organic photovoltaics.

1.1.1 P3HT in active layers for OPVs

Because P3HT is an efficient donor material, the fabrication of any photovoltaic device also requires material that can transport electrons. Thus, it is necessary to mix P3HT with a good electron-carrying material (acceptor) in the active layer of a photovoltaic device to create a bulk heterojunction (BHJ) in order to transport electrons to the cathode. Examples of acceptor materials that are typically used in OPV devices include polymers, organic nanoparticles, and inorganic nanoparticles. Among these, the most commonly used material is the fullerene derivative, phenyl-C_{61}-butyric methyl ester (PCBM). The unique feature of PCBM is that it is miscible with amorphous P3HT and has a long-lived triplet state that provides excellent electron mobility. A detailed discussion of the different classes of OPV devices is given in Section 1-2.

Another type of nanoparticle, semiconductor quantum dots (SQDs), show much promise as acceptor-type materials for OPVs because their absorption band can be tuned by changing their size and shape. In spite of this desirable feature, SQDs are inorganic by nature, making them

immiscible in polymer matrices. Therefore, SQDs have a tendency to aggregate and form large domains of nanoparticles, hence diminishing electron transport in the active layer and leading to poor dispersion within a polymer matrix.

Because the mixing of inorganic nanoparticles and polymers is not thermodynamically favored, there is a need to develop a facile method to modify the surface of SQDs with P3HT chains and investigate how the nanoparticles organize in a polymer matrix. This necessarily involves preparation of P3HTs with specific end groups, and so in section 1-3, three methods to prepare end-functionalized P3HTs are discussed in detail. Also, an overview of recent progress in the synthesis and characterization of end-functionalized P3HTs is provided.

1.2 Motivation

The demand for energy is growing ever more rapidly with the development of new technologies and the increase in the world population. Currently, the United States relies on fossil fuels to meet at least half of its current energy demand.[24] A recent spike in shale gas extraction in the United States is expected to alleviate the stresses associated with being dependent on imported oil. However, natural gas is still a fossil fuel, and its combustion leads to the generation of the greenhouse gas, carbon dioxide, which is strongly implicated in global warming. Therefore, to secure and sustain energy independence, it is crucial that our country move toward renewable energy resources, such as wind, hydrogen, and solar.[9,25-27] Of the three energy sources, solar and hydrogen have been extensively studied due to the tremendous amount of solar energy that irradiates the surface of earth and the production of less harmful products when burned, respectively. Unfortunately, the hydrogen fuel technology is limited by inefficient production and

storage of hydrogen gas. Also, fossil fuels are the main source of energy for reaching high temperatures needed for steam methane reforming (SMR) for the production of hydrogen gas. On the other hand, an immense amount of solar energy contacts the surface of the earth each day, which makes solar energy conversion technologies promising for providing an affordable and sustainable energy future. Current solar conversion technologies utilize highly pure, crystalline silicon, which is costly to produce. This makes solar cells based on pi-conjugated polymers a promising alternative, particularly because of the variety of scalable methods that can be used to process polymer-based materials. Organic photovoltaic devices fabricated from conjugated polymers have the potential to be produced on a large-scale continuous manufacturing process at a relatively low cost.

There are several different types of organic photovoltaic technologies that are currently being developed, including dye-sensitized, polymer-polymer, and polymer-nanoparticle hybrid solar cells. The power conversion efficiency (PCE) of dye-sensitized solar cells (DSSC) have not improved greatly during the past two decades.[28] DSSC device performance is hindered by narrow absorption bands, unfavorable electrolyte-sensitizer interactions, and molecular aggregation of sensitizer moieties. Similarly, polymer-polymer OPVs are limited by poor electron carrier mobilities and narrow absorption ranges of the pi-conjugated polymers, which leads to low PCEs because of charge recombination and decreased exciton generation, respectively. Recent advances in band-gap engineered polymers is expected to improve the PCE of devices, however, because efforts to develop efficient low band gap polymer-based solar cells currently relies heavily on new monomer and new polymer synthesis, this topic will not be discussed here. Due in part to the barriers associated with DSSCs and polymer-polymer OPV systems, polymer-nanopartice (NP)

systems look particularly attractive due to high electron carrier mobility of the acceptor phase.

As stated previously, polymer-nanoparticle hybrid organic photovoltaics are promising if the dispersion of nanoparticles can be controlled so as to provide a pathway for electrons to be transported through the active layer. Recently, fill factors comparable to inorganic silicon solar cells (~80%) were observed from devices fabricated from blends of donor-acceptor type polymers and $PC_{71}BM$. The authors attribute the improvement in performance to organization of the active layer, with a highly ordered polymeric phase and good horizontal phase separation and vertical phase gradation.[29] One way to tailor the organization of nanoparticles in a polymer film is by grafting the nanoparticles with polymer chains and then blending the grafted nanoparticles with the corresponding homopolymer matrix.[30-31] The aforementioned examples that improve the arrangement of nanoparticles in polymer films lends promise to P3HT/semiconductor quantum dot OPVs because the quantum dots are donor-acceptor type nanoparticles that can be grafted with polymer chains to improve dispersion in a polymer matrix, while providing an additional source of exciton generation upon absorption of light.

Polymer-inorganic nanoparticle OPVs reported in the literature tend to have much lower PCEs than that of the polymer-fullerene solar cells. The lower efficiency of these devices is attributed mainly to the formation of large aggregates comprised of nanoparticles, which prevents transport of electrons through the active layer, leading to annihilation of the photogenerated charge carriers. The aggregation of the nanoparticles leads to phase segregation, creating large separated domains that are rich in polymer and nanoparticles. As suggested by the work of Akora *et al*.[31], a way to overcome unfavorable interactions between polymers and SQDs is by attaching polymer chains to the surface of the SQDs. Tethering polymer chains to the surface of nanoparticles requires an

anchoring group attached to the polymer chain at its end. Conceptually, this points to two related targets: A polymer group must be installed on the end group of the pi-conjugated polymer, and the chemical nature of the end group must be such that it interacts (preferably, strongly) with the inorganic semiconductor quantum dot. Because the solution based synthesis of CdSe SQDs requires the use of a long chain surfactant with phosphine oxide or carboxylate head groups to control growth and stabilize the nanoparticles in solution.[32] Therefore grafting the SQDs with polymer chains requires the use of a functional group that will coordinate the SQD and displace the native ligands. The ligands are displaced by ligand exchange either using a ligand that has a higher affinity to bind to CdSe or by bombarding the SQDs with an excess of the ligand.[33-34] Pyridine has also been used to modify the surface of CdSe SQDs both experimental and theoretically,[32,34-35] making them good candidates as end groups for P3HT that will promote grafting.

The most effective way to produce end-functional chains is to end-cap the growing chains at (or near) the end of the polymerization process. The GRIM polymerization method intrinsically provides a means to end-functionalize P3HT *in situ* by adding a monofunctional Grignard reagent once the monomer has been consumed, circumventing the need for performing post-polymerization modification reactions. Unfortunately, the accessibility of end groups is dependent on the tolerance of functional groups to Grignard conditions, which makes it challenging to prepare inherently functional end groups using this method. Also, the end-group composition depends on the Grignard reagent chosen to quench the polymerization. Because the mixing of polymers and nanoparticles is thermodynamically unfavorable and the performance of bulk heterojunction OPV devices hinges on having a morphology with optimal domain spacing, there is a need to prepare

an end-group functionalized P3HT having either a pyridine, carboxylate, or phosphine oxide end groups, or some other chemical group that will coordinate with the surface of SQDs.

1.3 Methods for preparing end-functional P3HTs

There are three major synthetic approaches that are used to prepare end-functionalized poly (3-hexylthiophene)s including post-polymerization modification, *ex situ* initiation, and *in situ* end-functionalization of the GRIM polymerization. In what follows, each of these methods will be described in general and noteworthy examples will be presented.

The post-polymerization functionalization method requires a premade polymer that is reacted under conditions that have been optimized for small molecules to promote coupling of the functional group with the chain end. With this route, the polymer can be thoroughly characterized before the end-functionalized step is performed and the functional group does not need to be tolerant to Grignard conditions typically used to synthesize P3HTs. Lee *et al*.[36] demonstrated the use two sequential post-polymerization reactions, a hydroboration reaction and an N,N'-dicyclohexylcarbodiimide (DCC) coupling reaction, to prepare fullerene-terminated P3HTs, and used these to compatibilize an organic photovoltaic device having an active layer comprised of a blend of P3HT and PCBM. The fullerene-terminated P3HT was found to stabilize the film morphology and prevent large-scale phase separation of P3HT and PCBM. Also, the power conversion efficiency (PCE) of the solar cell was stable over long thermal annealing times. In another example, a difunctional fullerene-terminated P3HT (C_{60}-P3HT-C_{60}) was prepared by Hillmyer and co-workers via a Vilsmeier Haack reaction.[37] The C_{60}-P3HT-C_{60} product exhibits lower melting temperatures than neat P3HT, but the percent crystallinity of the P3HT portion is

consistent with that of neat P3HT. Unfortunately, characterization by size exclusion chromatography (SEC) showed that the Vilsmeier Haack reaction led to the formation of a multimodal molecular weight distribution. Ultimately, post-polymerization functionalization methods are problematic and known to be low yielding due to the low concentration of end-groups and the reactions are generally limited to solvents that dissolve P3HT. Also, post-polymerization modifications require multiple reaction steps, additional purification time, and expensive coupling reagents. Therefore, alternative methods to prepare end-group functionalized P3HTs have been explored.

A second class of end-group functionalization methods, called *ex situ* initiation (a.k.a. external initiation), also has been used to prepare end-functional P3HTs.[38-42] The *ex situ* initiation method involves the use of an aryl halide initiating moiety that generates the active Ni^0 species prior to the polymerization. With this method, the preactivated Ar-Ni(L_2)X initiator and the active monomer are mixed to promote immediate transmetalation, leaving the Ar-group attached to the initiating chain end. This permits the use of a functional-group substituted Ar-Ni(L_2)X moiety, which provides the polymer with inherent end-group functionality, as shown in Scheme 1-2.

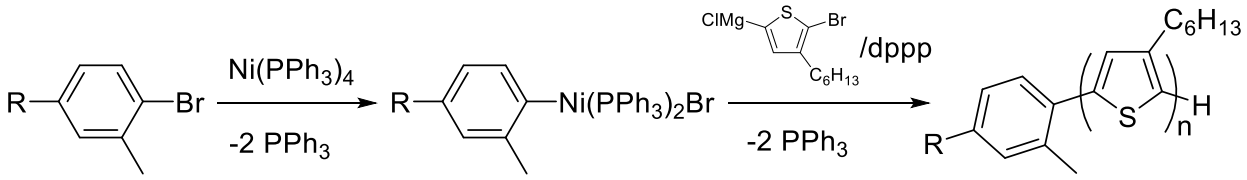

Scheme 1-2. External initiation of 2,5-dibomo-3-hexylthiophene to prepare monofunctional P3HT.

However, the functional groups must be tolerant to Grignard conditions used to polymerize the regiospecific monomer. Also, in order to access different types of end-groups, a new functional initiator must be prepared before every polymerization, which can be quite time consuming. In addition, the nickel catalyst has a tendency to diffuse, or "walk" through the solution during the polymerization. The loss of the catalyst from the growing chain end prevents complete chain-end functionalization because the catalyst begins polymerizing new polymer chains and the newly formed chains lack the initiating functional group. Kiriy *et* al.[40] developed a convenient method to prepare external initiators high initiation efficiency from sterically hindered Grignard reagents. Based on matrix assisted laser desorption ionization time-of-flight mass spectrometry (MALDI-TOF MS) analysis of the resulting P3HTs, the preparation of a tolyl-initiator from an *ortho*-tolyl-Grignard reagent produces greater than 95% o-tolyl-functionalized P3HT, which suggests high initiator efficiency. However, when the highly functional 4-(5-(9,9-dioctylfluorene)-4-hexyl-2-thienyl)-7-(5-bromo-4-hexyl-2-thienyl)-2,1,3-benzothiadiazole (F8TBT)-Ni(dppp)Cl initiator is used to polymerize the 2-bromo-5-chloromagnesium-3-hexylthiopene monomer, a variety of F8TBT end-group functionalized products are observed along with several unfunctionalized products.[40] Based on this it seems that the preparation of well-defined end-functionalized P3HTs by external initiation is limited not only to functional groups that are tolerant to the Grignard metathesis polymerization conditions, but to less exotic end groups. Therefore, in order to access end groups that are more useful (e.g. end-groups that can be used to couple P3HT chains to other polymers or that promote coordination or ligation) the use of post-polymerization modification reactions is often required following *ex situ* initiated polymerizations. To circumvent the limitations of post-polymerization modifications and *ex situ* initiation, it is necessary to develop a

method to prepared polymers with inherently useful end-groups using a more convenient and economical synthetic route.

Before discussing end-group functionalization approaches, it is insightful to first present and think about the GRIM polymerization mechanism, which proceeds via a chain growth mechanism that consists of three main catalytic steps: oxidative addition (OA), transmetalation (TM), and reductive elimination (RE), as shown in Scheme 1-3. Once all of the monomer has been consumed, the nickel catalyst remains associated with the chain end, providing a means directly end-functionalize P3HT by quenching with a monofunctional Grignard reagent, which is also depicted in Scheme 1-3.

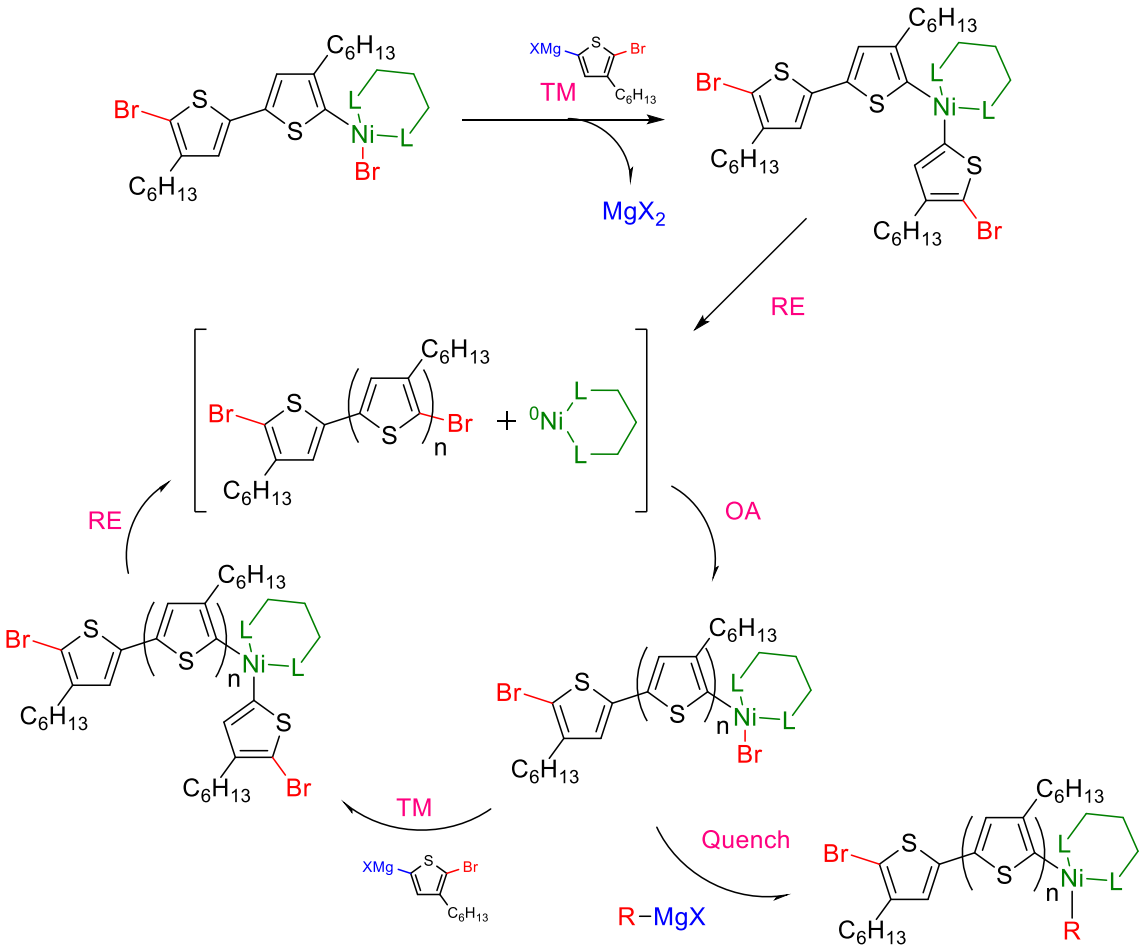

Scheme 1-3. Proposed mechanism for the GRIM polymerization and in situ quenching with a monofunctional Grignard reagent (R-MgX).

This method, which was developed by McCullough *et al.*, is referred to as *in situ* end functionalization of P3HT.[43-44] A variety of Grignard reagents have been used to end-functionalize P3HT, leading to vinyl-, allyl-, tolyl-, and phenyl-terminated P3HT, to name a few.[43-44] A more comprehensive list of Grignard reagents and the corresponding end groups that are installed on the chain ends of P3HT are shown in Figure 1-2.

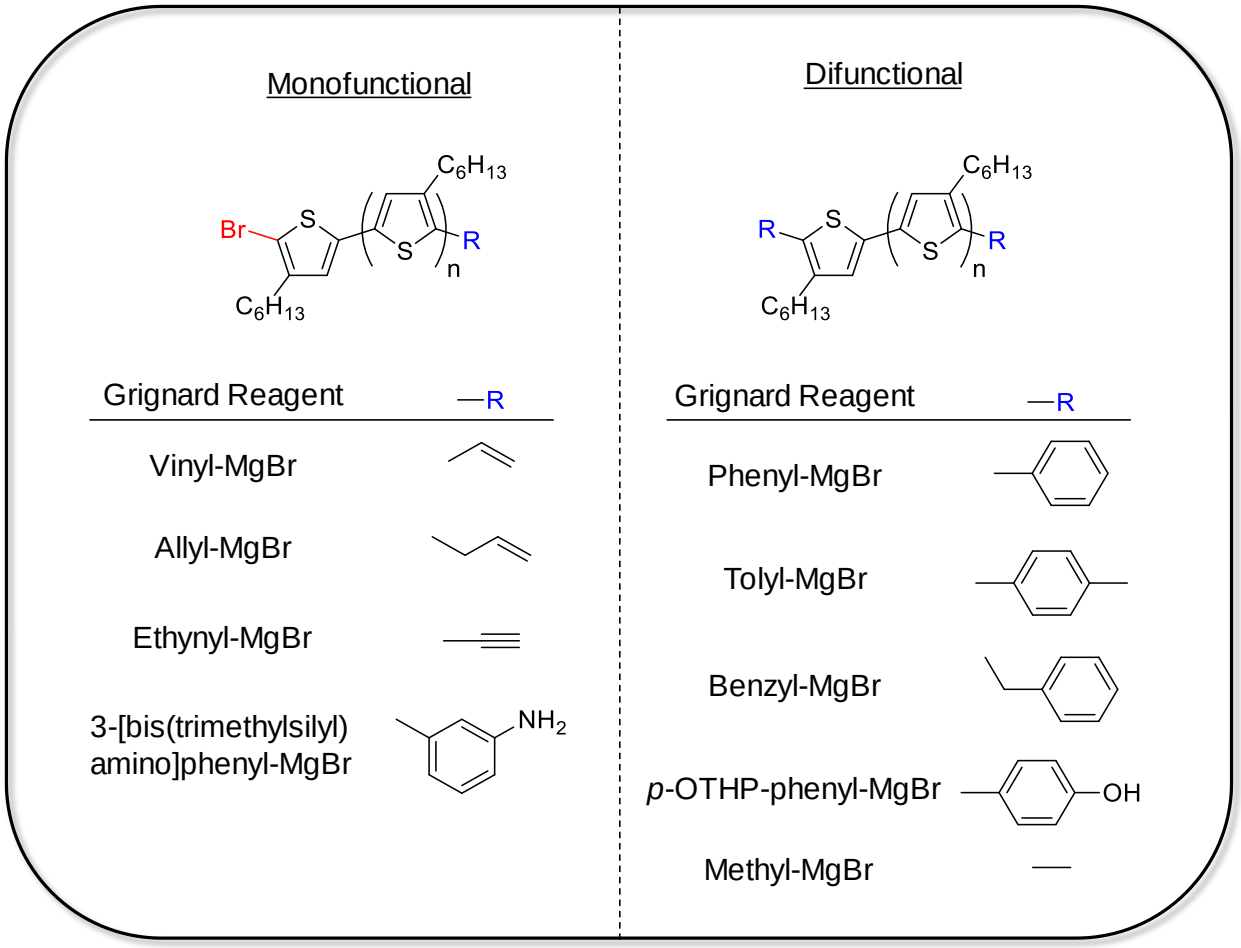

Figure 1-2. A comparison of monofunctional and difunctional products obtained from quenching the GRIM polymerization with the corresponding monofunctional Grignard reagent.

It is well known that quenching the GRIM polymerization with allyl and vinyl Grignard reagents leads to monofunctional P3HTs (~95% monofunctional) while quenching with aryl or alkyl Grignard reagents almost exclusively results in difunctional P3HT products. One exception to these generalities is the report by Takahashi and co-workers, who prepared monofunctional amine-terminated P3HT by quenching of the GRIM polymerization with a trimethylsilyl-protected

amine.[45] McCullough and co-workers attributed the near-exclusive formation of monofunctional vinyl and allyl P3HTs to coordination of the active Ni^0 species with the unsaturated groups of the Grignard, which prevents diffusion of the Ni^0 species and, therefore, prevents the Ni^0 species from oxidative addition at the other chain end where initiation took place.

Therefore, I hypothesized that an effective way to improve the diversity of end groups that can be installed using the in situ end-functionalization approach is to use an additive with a double bond (and that was tolerant to Grignard conditions) that would interact with the active Ni^0 catalyst species in solution and prevent oxidative addition at the initiating chain end. This strategy is discussed in more detail and experiments summarized in Chapters 2 and 3. It should be noted that of the Grignard reagents listed in Figure 1-2, none are inherently useful for coordination or ligation. For the purpose of grafting P3HT to the surface of SQDs, a pyridine Grignard reagent that can be used to end functionalize P3HT *in situ* while providing the opportunity to coordinate SQDs must be used.

1.4 Characterization of end-functional P3HTs

In order to classify materials as being well-defined and speculate about structure-property relationships of materials, it is important to have a good understanding of the chemical structure and properties of the individual starting materials. Therefore, an important part of my work includes rigorous characterization to provide a detailed understanding of the materials that were synthesized. First, the end-functional P3HTs are subject to molecular weight characterization and end-group analysis. There have been a number of methods developed to determine molecular weights and polydispersities of polymeric materials. Size exclusion chromatography (SEC) is one

of the most simple and versatile methods for determining the molar mass distribution, from which the number-average and weight-average molecular weights of a polymer sample and polydispersity can be obtained relative to a set of standards (usually polystyrene). For SEC analysis, a polymer sample is dissolved in a mobile phase (e.g., THF) and passed through a column that separates the polymer chains based on their hydrodynamic radius, which is directly proportional to molecular size. However, P3HT has been shown to adopt a rod-like conformation in solution leading to the overestimation of molecular weights obtained from SEC relative to polystyrene standards.[46-47] McCullough and coworkers found that SEC overestimates the molecular weight of P3ATs by a factor of 1.2-2.3 compared to measurements by MALDI-TOF MS.[46] Therefore, and certainly in the case of P3HT materials, a technique that measures the absolute molecular weight of a polymer sample should be used to compliment the SEC molecular weights.

MALDI-TOF MS is a soft ionization technique used in mass spectrometry to characterize macromolecules. (A soft ionization technique results in minimal or no fragmentation.) MALDI-TOF MS requires the use of a matrix that will absorb high energy radiation to indirectly ionize the analyte. Once ionized, the analytes travel down the time-of-flight tube and are separated based on their mass to charge ratio, *m*/z. MALDI-TOF MS provides good isotopic separation with high resolution, which is useful when performing end-group analysis. Obtaining a highly resolved mass spectrum is imperative when the molecular weights of two different products are very similar. This is exemplified in the Chapter 3, for example, when a 13-mer P3HT having one hydrogen and one bromine end group (2238.99 Da) are mixed with a 13-mer P3HT having one hydrogen and one pyridine end group (2238.10 Da). One limitation of MALDI-TOF MS is that it has the

tendency to underrepresent the higher molecular weight chains in a sample because of the mass-dependent desorption/ionization process.[46,48-49] Because SEC overestimates the molecular weight of P3HT and MALDI-TOF MS tends to bias lower molecular chains, especially in a the case of analyzing a polydisperse sample, low molecular weight P3HTs are used to study the end-functionalization of P3HT to facilitate high resolution in the MALDI-TOF MS.

Another technique that is frequently used to determine the absolute molecular weight and end-group composition of a polymer sample is nuclear magnetic resonance (NMR) spectroscopy. The molecular weight of an end-group functionalized polymer sample is found by integrating the signal attributed to the proton(s) on the end group against a proton on the repeating unit structure of the polymer chain. However, a challenge arises if the proton signals overlap or if the polymer is not ~100% functionalized. Because regioregular P3HT is composed of mainly head-to-tail coupled repeat units, the molecular weight may be estimated using ^{1}H-NMR by integrating the signals attributed to the methylene protons of the hexyl side chain that are nearest the thiophene ring as shown in Figure 1-3.

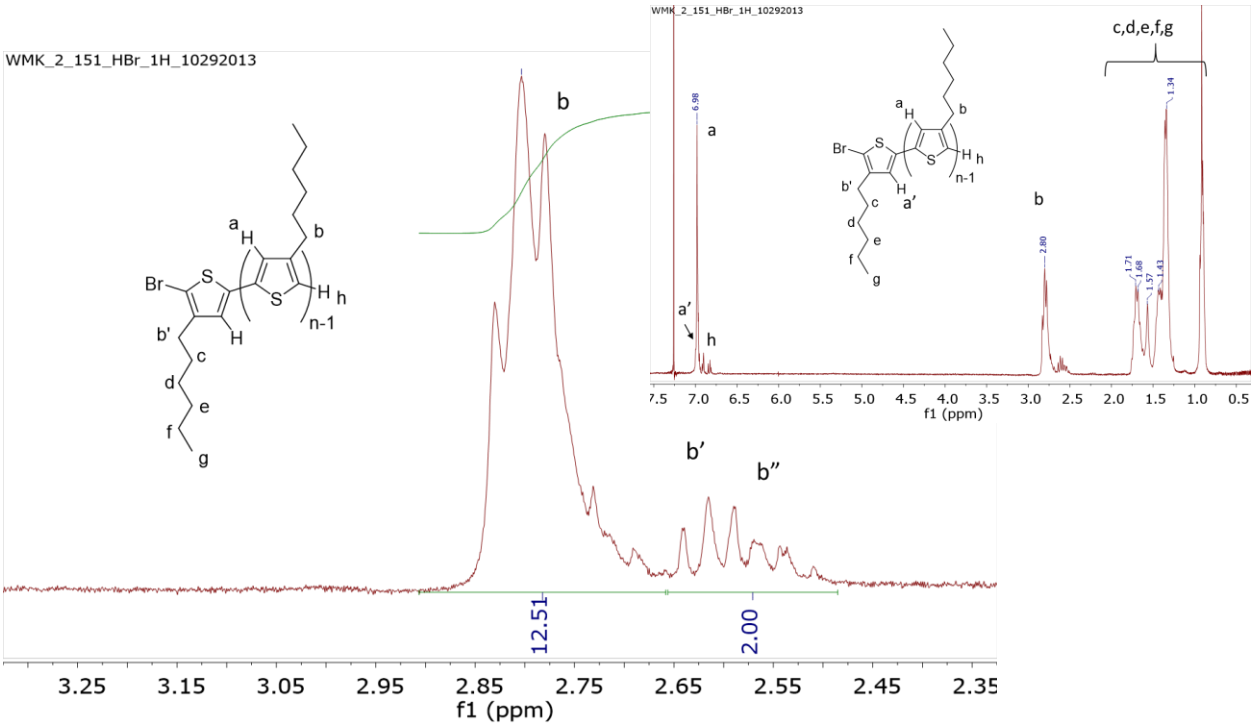

Figure 1-3. ^{1}H-NMR spectrum for a GRIM polymerization quenched with acid yielding hydrogen and bromine end-groups.

The methylene protons nearest the thienyl ring on a HT coupled repeating unit (labelled as b in Figure 1-3) appear at 2.80 ppm, whereas the methylene protons nearest the thienyl ring on the chain-ends are shifted upfield in the range of 2.5-2.68 ppm. This shift arises because the presence of end groups change the chemical environment at the chain end. For the example shown in Figure 1-3, protons labelled as b' and b" are assigned to the methylene protons nearest the thienyl ring bearing the end-groups. Integration of b' and b" against b gives a degree of polymerization (DP) of 15, which is consistent with the MALDI-TOF MS results and relates to a molecular weight of approximately 2,500 kDa. The molecular weight of this polymer sample by SEC gives an

estimated M_n=4,800 kDa. Unfortunately, integrating the signals from the aliphatic protons is not useful for definitive end-group analysis due to the similarity in chemical environments at each of the polymer chain ends and overlap of the proton signals. In addition, for higher molecular weight samples, molecular weight characterization and end-group analysis by NMR spectroscopy becomes less trivial because the concentration of end groups decreases with increasing molecular weight. Ultimately, NMR spectroscopy provides a good estimate of molecular weight for low molecular weight P3HT samples but only qualitative information about the end-group composition. Therefore, my work makes use of a "symbiotic" relationship between SEC, MALDI-TOF MS and ^{1}H-NMR characterization techniques to characterize the end-functionalized P3HTs that were synthesized.

1.5 Characterization: Organization of SQDs in P3HT thin films

The organization of nanoparticles in a polymer matrix can have a huge impact on the properties of their thin films. Therefore, it is necessary to investigate how nanoparticles arrange in a polymer matrix.[50-51] A technique that is most often used to study how nanoparticles organize in a polymer matrix is transmission electron microscopy (TEM). In TEM, the electrons that are transmitted through the sample are sensitive to changes in electron density of the sample: the electrons interact differently with heavier atoms in comparison to lighter atoms, which gives rise to contrast. For example, when a blend of inorganic nanoparticles and polymer are cast into a film and imaged using TEM, the inorganic nanoparticles have a much higher contrast than the polymer film, which provide a highly resolved image of how the nanoparticles organize [Figure 1-4 (left)].[52] On the other hand, when a P3HT/PCBM blend is cast into a thin film and imaged using TEM, only slight

contrast is observed due to the similarities in the organic chemical structures of the materials [Figure 1-4 (right)].[53]

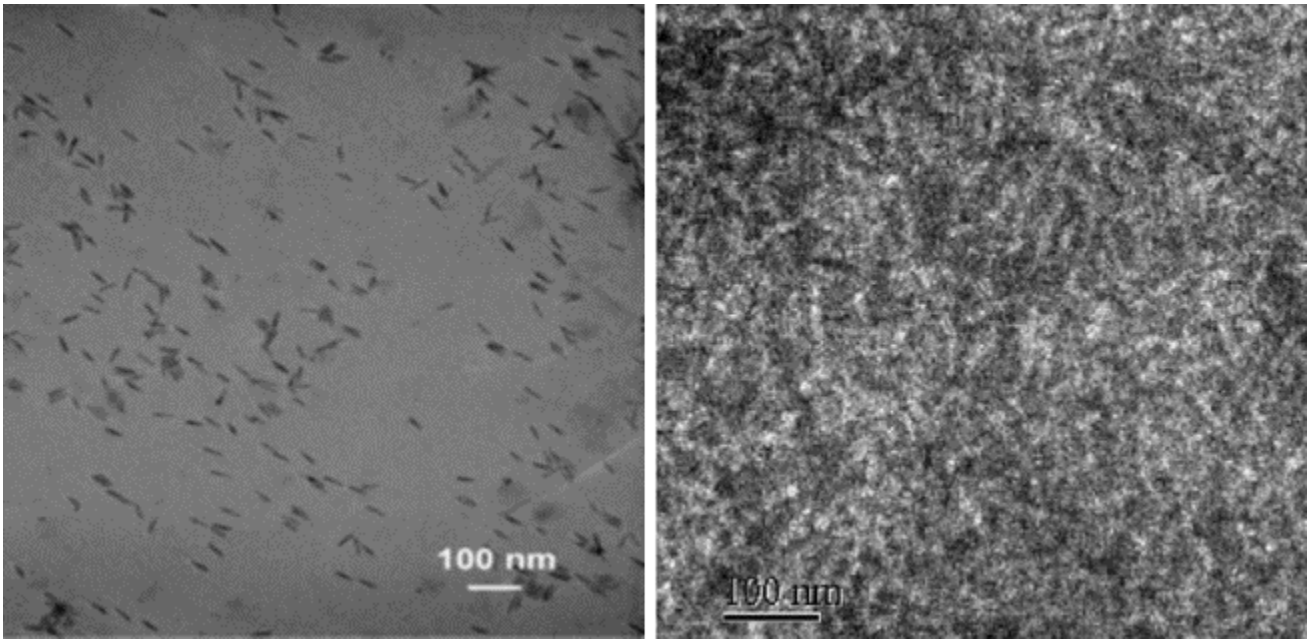

Figure 1-4. TEM images of P3HT/CdSe nanorod (left) and P3HT/PCBM (right) composite films. Taken from reference 52 and 53.

In addition to TEM, x-ray diffraction techniques can be used to investigate blends of polymers and inorganic nanoparticles. Because x-rays scatter from electrons, materials that have different atomic numbers show good contrast. X-ray diffraction can be used to examine how the nanoparticles organize within the P3HT matrix and how SQDs affect the ordering (crystallization) of the P3HT chains, too. X-ray diffraction (XRD) reveals information about how the polymer chains stack perpendicular to the substrate (e.g. silicon). In particular, for P3HT the first (100),

second (200) and third (300) order Bragg diffraction peaks from the edge-on stacking of P3HT chains can be observed. However, in order to probe longer length scales (i.e. lower q-range) a different technique is required. Therefore, small angle x-ray scattering (SAXS) techniques must be used to investigate long length scale features such as nanoparticle aggregates or domains with length scales on the range of 5-25 nm. In particular, grazing-incidence (GI) x-ray scattering techniques have gained much attention for probing the thin film morphology of bulk heterojunction OPV films because this type of geometry provides mesoscale structure information perpendicular to the substrate as well as lateral structure features in the film. For example, Chiu *et al*.[54] used a combination of grazing incidence small-angle (GISAXS) and wide-angle x-ray scattering (GIWAXS) techniques to study the morphology of P3HT/PCBM active layers for OPV devices. Scattering profiles from GIWAXS (edge-on P3HT stacking) and GISAXS (PCBM aggregation) were used to determine the size of P3HT crystallites and the radius of gyration of PCBM aggregates using Scherrer's relation and a Guinier approximation, respectively. The P3HT crystallite size and radius of gyration of PCBM were found to be 16 nm and 20 nm, respectively, for maximum device performance in this study. Also, Ruderer *et al*.[55] demonstrated the utility of GISAXS for probing the correlation length of the PCBM rich domains in bulk heterojunction films. The authors found that the PCBM domain sizes varied laterally in the sample depending on the casting solvent, but the device performance was relatively insensitive to these changes as long as the domains were within the excition diffusion length scale.

1.6 Research objectives

My thesis work addresses challenges associated with morphology development in P3HT/SQD BHJs by developing a novel method to control the morphology of polymer-nanoparticle systems through the use of end-functionalized P3HTs. This work was inspired in part by the work of Akcora *et al*.[31] who showed that it was possible to manipulate the organization of inorganic silica nanoparticles in a polymer (polystyrene) matrix by using surface-grafted chains. As mentioned in Section 1.1, the grafted PS chains not only prevent aggregation of the nanoparticles, but by tuning the number density of grafted chains and the relative difference between the grafted chain and matrix molecular weights, different morphologies could be accessed. Based on this work, my research objectives include:

i) Synthesize pyridine end-functionalized poly(3-hexylthiophene)s that can be used to ligate the P3HT chain with semi-conductor quantum dots (SQDs) through the pyridyl end group,

ii) Modify the surface of SQDs with P3HT ligands of different molecular weight using a series of ligand exchanges,

iii) Investigate how the molecular weight of the end-functionalized P3HT ligand and P3HT matrix affect the organization CdSe in a thin film of P3HT using transmission electron microscopy and x-ray scattering techniques.

The addition of functional end groups beyond those depicted in Figure 1-2 through a simple *in situ* quenching reaction represents both a major challenge in the chemistry of P3HTs that holds significant promise. In pursuit of this, Chapter 2 focuses on the use of additives and reaction

conditions to alter the end-group composition of tolyl-functionalized P3HTs prepared by *in situ* quenching of the GRIM polymerization. Tolyl-magnesium bromide was chosen as a model end-functionalization reagent due to its propensity to create mostly difunctional tolyl-functionalized P3HT. MALDI-TOF MS and NMR spectroscopy were used to estimate the molecular weight and end-group composition of the tolyl-functionalized P3HTs. When 1-pentene and styrene were used as additives, modest increases in the yield of monofunctional products was realized. Also, temperature and lithium chloride played impactful roles. The combination of these strategies (additives, LiCl, control of temperature) improved the yield of monofunctional tolyl-functionalized P3HTs, and as a result, this method was adapted to prepared monofunctional pyridyl end-functionalized P3HTs.

In Chapter 3, a facile one-pot method for preparing 2-pyridyl and 3-pyridyl P3HTs with high abundance of monofunctional products is described. The kinetics of the end-functionalization quenching reaction with lithium chloride complexes of 2- and 3-pyridyl Grignard reagents provided insight into the reaction mechanism of *in situ* quenching of the GRIM polymerization with pyridyl Grignard reagents. Density functional theory (DFT) calculations guided the selection of pyridine as a useful end group for P3HT to promote grafting of chains to the nanoparticle surface. The end-group composition was altered by the use of additives during *in situ* quenching of the GRIM polymerization, as determined by high resolution MALDI-TOF MS and NMR spectroscopy. TEM images of a blend of CdSe nanoparticles modified with P3HT ligands in a P3HT matrix revealed that the nanoparticles could be effectively dispersed in a matrix of P3HT chains, and that the dispersions are stable after 2 h of annealing at 150 °C.

In Chapter 4, a summary of the results from a morphology study using P3HT/CdSe blends

having P3HT ligands and P3HT matrices of varying molecular weights is given. The influence of P3HT ligand and P3HT matrix molecular weight on the dispersion of P3HT-decorated CdSe in a thin film was also investigated. A number of thermal, optical and thin film characterization techniques were used to study P3HT/CdSe composites. The P3HT-decorated CdSe SQDs were blended with the corresponding matrices to compare the organization of SQDs in composites having an ligand to matrix molecular weight ratios of 0.19, 0.56, 0.77, and 2.12. GISAXS was used to study the organization of CdSe SQDs in a P3HT film. It is noteworthy that even with high concentrations of CdSe SQDs (25 mass %) in a P3HT matrix, the P3HT-decorated CdSe SQDs remain dispersed in the thin films after thermal annealing for up to 24 h at 150 ^{o}C.

Finally, Chapter 5 summarizes the main results from my work and their impact. It also describes particular themes of future research that would be promising or logical extensions from my work.

Chapter 2: End-Group Composition of Poly(3-hexylthiophene)s Prepared by *in situ* Quenching of the GRIM Polymerization

This chapter describes work published in *J. Poly. Sci. Part A: Poly. Chem* **2012**, 50, 2762-2769. I synthesized and characterized all of the polymers described in this work and wrote the manuscript. Coauthors include Dr. Deanna L. Pickel, who provided guidance and helpful suggestions concerning synthesis and MALDI-TOF MS characterization, and Prof. S. Michael Kilbey II, who advised this work.

2.1 Abstract

The ability to prepare well-defined semiconducting polymers is essential for understanding the link between structure and function in organic photovoltaic devices. A general, one-pot method for altering the degree of functionality of end-functionalized poly(3-hexylthiophene)s (P3HTs) prepared by Grignard metathesis (GRIM) polymerization has been developed and is described in this chapter. In the absence of additives, the degree of functionality of end-functional P3HTs prepared by quenching of the GRIM polymerization with a Grignard reagent is dependent on the Grignard reagent utilized. In this chapter I describe how additives such as styrene and 1-pentene are able to alter the end-group composition of tolyl-functionalized P3HTs, which is determined by high resolution Matrix-assisted Laser Desorption Ionization Time-of-flight Mass Spectrometry (MALDI-TOF MS). In particular, when quenching the GRIM polymerization with tolyl-magnesium bromide, a modest decrease in the difunctional product is observed while the yield of the monofunctional product increases significantly. Temperature and lithium chloride (LiCl) addition also play impactful roles. Monofunctional P3HT is found to be the major product (72% abundance) when the functionalization is done in the presence of LiCl and styrene at 0 ^{o}C, whereas in the absence of additives the monofunctional product is present at only 11% abundance.

2.2 Introduction

Controlling end-group functionality of polymers provides vast opportunities to install sensing and recognition moieties,[56-57] promote supramolecular assembly,[58] enable chemical grafting to substrates[59] or extend chains with different types of monomers.[60] Because they are promising materials for applications such as biosensors, high performance organic voltaic devices and organic LEDs,[61-64] methods to prepare well-defined, end-functionalized semiconducting polymers are essential for fundamental studies that aim to link macromolecular design to structure and function. Poly(3-hexylthiophene) (P3HT) is one of the most extensively studied semiconducting polymers used in these applications due to ease of preparation and hole transport properties.[5,65-67] Well-defined, highly regioregular P3HTs with relatively low polydispersities can be prepared by the Grignard Metathesis (GRIM) polymerization method developed by McCullough *et al.*[68] and Yokozawa *et al*.[21] The GRIM polymerization method is advantageous because it utilizes commercially available starting materials and eliminates the need for cryogenic temperatures as compared to other methods.[8,21,68]

End-functional P3HTs can be prepared by quenching the GRIM polymerization with a Grignard reagent,[43-44] use of a functional initiator,[69-71] or by post-polymerization modification,[60,72] For example, post-polymerization modification reactions involving bromine coupling chemistry have been utilized to prepare dioctylphosphine oxide functionalized P3HT, and these were used to decorate CdSe nanocrystals for use in organic-inorganic nanocomposites.[72] The resulting P3HT-CdSe nanocomposites exhibited good dispersion of the CdSe in the P3HT matrix and enhanced the electronic interaction between these two components. Frechét and coworkers prepared primary amine-functionalized P3HTs via post-polymerization modification of GRIM prepared P3HT.[73]

Blends of the amine-terminated P3HTs and CdSe nanocrystals showed greater power conversion efficiencies as compared to the unfunctionalized P3HT. Unfortunately, post-polymerization end-functionalization techniques typically require multiple reactions steps, expensive coupling reagents, and result in low degrees of functionality.

To circumvent these problems, end-functional P3HTs can also be prepared by *in situ* end-functionalization (quenching) of the GRIM polymerization with a Grignard reagent, which was first reported by McCullough and coworkers.[43-44] Although this is a direct method to realize end-functional P3HTs, the end-group composition is dependent on the Grignard reagent used for quenching. For instance, when the GRIM polymerization is quenched with vinylmagnesium bromide or allylmagnesium bromide, >90% of the chains are monofunctional (i.e., one functional end-group per polymer chain) and the remaining chains are unfunctionalized. However, difunctional P3HTs predominate (60–90%) when the GRIM polymerization is quenched with alkyl or aryl Grignard reagents, such as phenylmagnesium bromide and tolylmagnesium bromide (tolyl-MgBr), with the remaining product being monofunctional (10–40%).[44] Yokozawa and coworkers[74] revisited this functionalization reaction utilizing 3,4-dimethylphenylmagnesium chloride as the quenching reagent and reported that only the difunctional product is observed. However, careful examination of their Matrix-assisted Laser Desorption Ionization Time-of-flight Mass Spectrometry (MALDI-TOF MS) spectra reveals that, in fact, multiple products are obtained, and the monofunctional product is obtained in approximately 10% abundance when compared to the difunctional product, which is consistent with broader sets of results.[43-44] Therefore, there are opportunities to improve the *in situ* end-functionalization to obtain either the monofunctional or difunctional products exclusively, and thus a more well-defined polymer.

More recently, externally initiated systems have been developed for the preparation of end-functionalized P3HTs.[69-70,75-76] Bronstein and Luscombe[69] reported the external initiation of P3HT with controlled molecular weights and narrow polydispersities by the use of *cis*-chloro(aryl)(dppp)nickel complex, and showed by MALDI-TOF MS that the main product was the end-functionalized P3HT. A small amount of unfunctionalized product was reported, but the amounts were not quantified. Kiriy[70] reported the formation of *in situ* initiators from the commercially available Ni(dppp)Cl_2 and Ni(dppe)Cl_2 species from sterically hindered Grignard reagents. By MALDI-TOF mass spectrometry the main distribution is attributed to the desired end-functionalized polymer, but a second distribution is observed and is not identified by the authors. When this method was used to prepare a functional P3HT bearing an electron-accepting group, nearly 20% of the product was unfunctionalized by MALDI. Koeckelberghs[71] also observed up to 20% unfunctionalized polymer when preparing P3HTs from externally initiated functional initiators. While these systems allow for better end group control in some cases, a new initiator must be prepared for each desired functionality, and issues remain with functional group tolerance.

Thus, a general method for the synthesis of monofunctional P3HTs by *in situ* quenching remains a significant challenge due to diffusion of the Ni^0 complex[44] and also because the functional groups accessible by end-quenching are limited to compounds that are tolerant to Grignard reagents. In addition, careful characterization of the resulting products is of the utmost importance and should include high resolution MALDI-TOF MS analysis for definitive end-group analysis of all of the products. This chapter focuses on a general, one-pot strategy for enhancing the control of end-group composition in P3HTs obtained by *in situ* end-functionalization via

Grignard quenching and their thorough characterization by MALDI-TOF MS. The ability to control the degree of functionality (i.e. mono- vs. di-functional) is important for understanding structure-property relationships in various systems. For example, grafting difunctional polymers to a nanoparticle substrate may result in loops (both chain ends binding to the same substrate) or bridging of nanoparticles, which can impact the behavior of the system.[64] Herein, I report the effect of chemical additives and temperature on the end-group composition of tolyl-functionalized P3HT prepared by GRIM polymerization and their full characterization by MALDI-TOF MS.

2.3 Results and Discussion

End-quenching of the GRIM polymerization of 3-hexylthiophene with a Grignard reagent yields the corresponding end-functionalized P3HT, where the degree of functionality is dependent on the choice of Grignard reagent. Aryl and alkyl Grignard reagents result in mostly difunctional P3HTs, while vinyl and allyl Grignard reagents yield monofunctional P3HTs.[43-44] Interestingly, quenching the GRIM polymerization with a dimethylsilyl-protected aniline group results in the monofunctional product exclusively.[77] McCullough and coworkers[43-44] attribute the high yield of difunctional products to the diffusion of the Ni^0 to the other chain end, where oxidative addition takes place, as shown in Scheme 2-1.

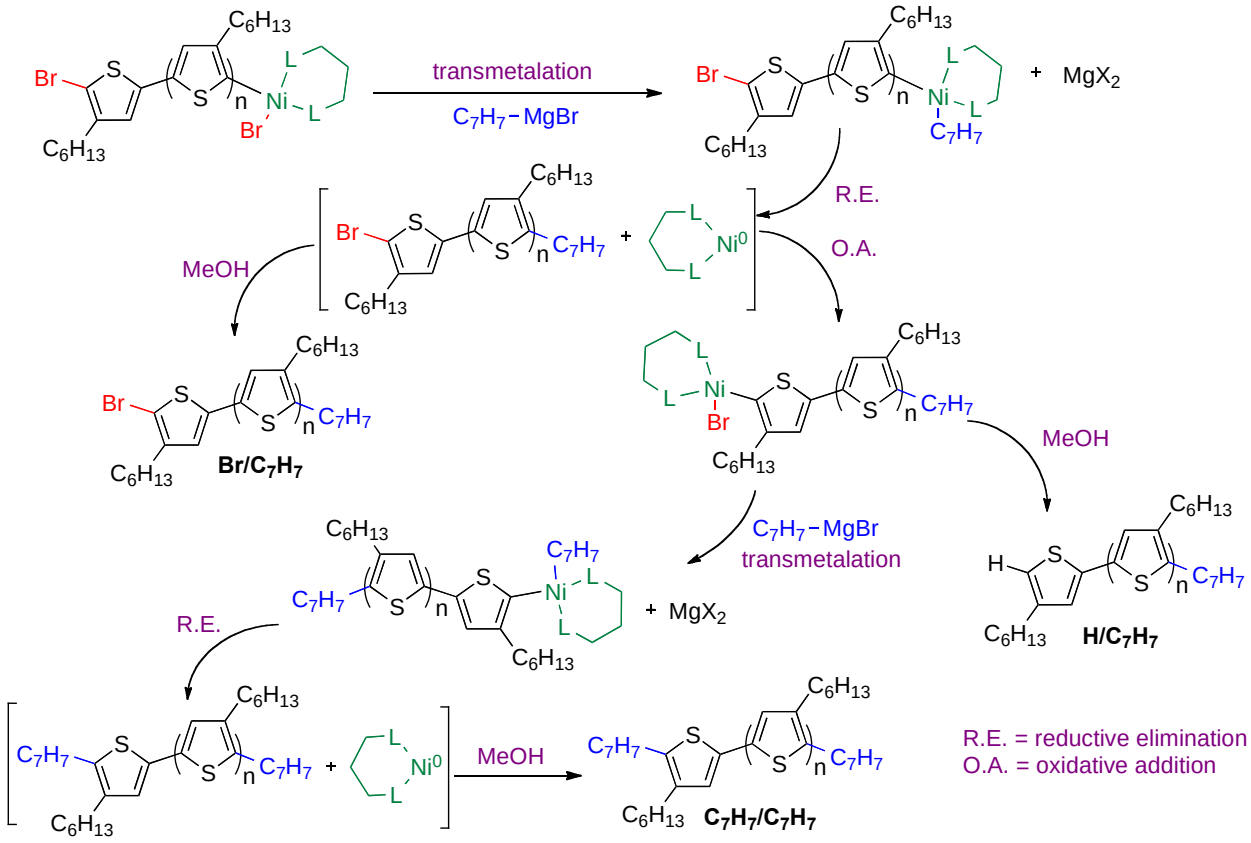

Scheme 2-1. Proposed mechanism showing the variety of products resulting from the *in situ* end-functionalization of GRIM prepared P3HT with tolyl-MgBr.

On the other hand, allyl, vinyl, or alkynyl groups of the Grignard interact with Ni^0, forming a stable π-complex that prevents oxidative addition at the other chain end as suggested by Scheme 2-2.[78-79] If this is the case, then the use of additives containing unsaturated groups may allow for the synthesis of monofunctional P3HTs with a wide variety of end group functionalities.

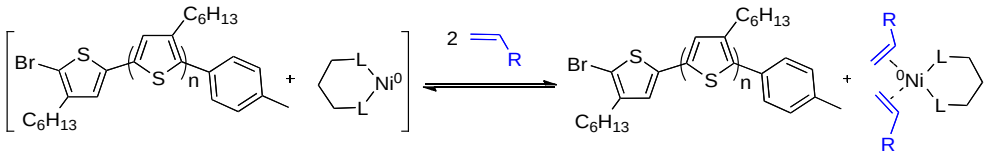

Scheme 2-2. Proposed interaction between Ni^0 and unsaturated group of additives to form the less active π-complex.

The end-functionalization of the GRIM polymerization with tolyl-MgBr was used as a model reaction in this study due to the propensity of this reaction to produce difunctional product in relatively high yield (>80%),[21,44] but the results can be extended to other Grignard reagents. Polymerizations were performed as previously described in the literature, and careful attention was paid to the monomer conversion as this can impact the composition of the final product.[24] The end-group composition of the P3HTs was determined by MALDI-TOF MS, and low molecular weight P3HTs were prepared (Mn < 3000 g/mol, see Appendix B for all molecular weight data) in order to obtain high resolution spectra for definitive end-group determination.[79] In all cases, spectra with isotopic resolution were obtained for definitive determination of the end-group composition. A typical MALDI spectrum of P3HT prepared by *in situ* end-functionalization using tolyl-MgBr (**P3HT1**) is shown in Figure 2-1. As expected, and in light of Scheme 2-1, several different products are observed. The major product is attributed to the 10-mer of the difunctional P3HT ($C_7H_7(C_{10}H_{14}S)_{10}C_7H_7$; Calc. monoisotopic mass 1842.93 Da, Obs. *m/z* 1842.88). In addition, several smaller distributions are observed, and these can be attributed to P3HTs with H/H, H/Br, Br/C_7H_7, and H/C_7H_7 end groups, as identified in Figure 2-1. McCullough did not observe the Br/C_7H_7 product, but this may be due to the lower sensitivity of MALDI when high

molecular weight materials are characterized.[43] In this study, all of the polymers are of relatively low molecular weight, allowing for spectra to be obtained with isotopic resolution and high sensitivity, whereas the spectra reported in previous work were not isotopically resolved.[43-44]

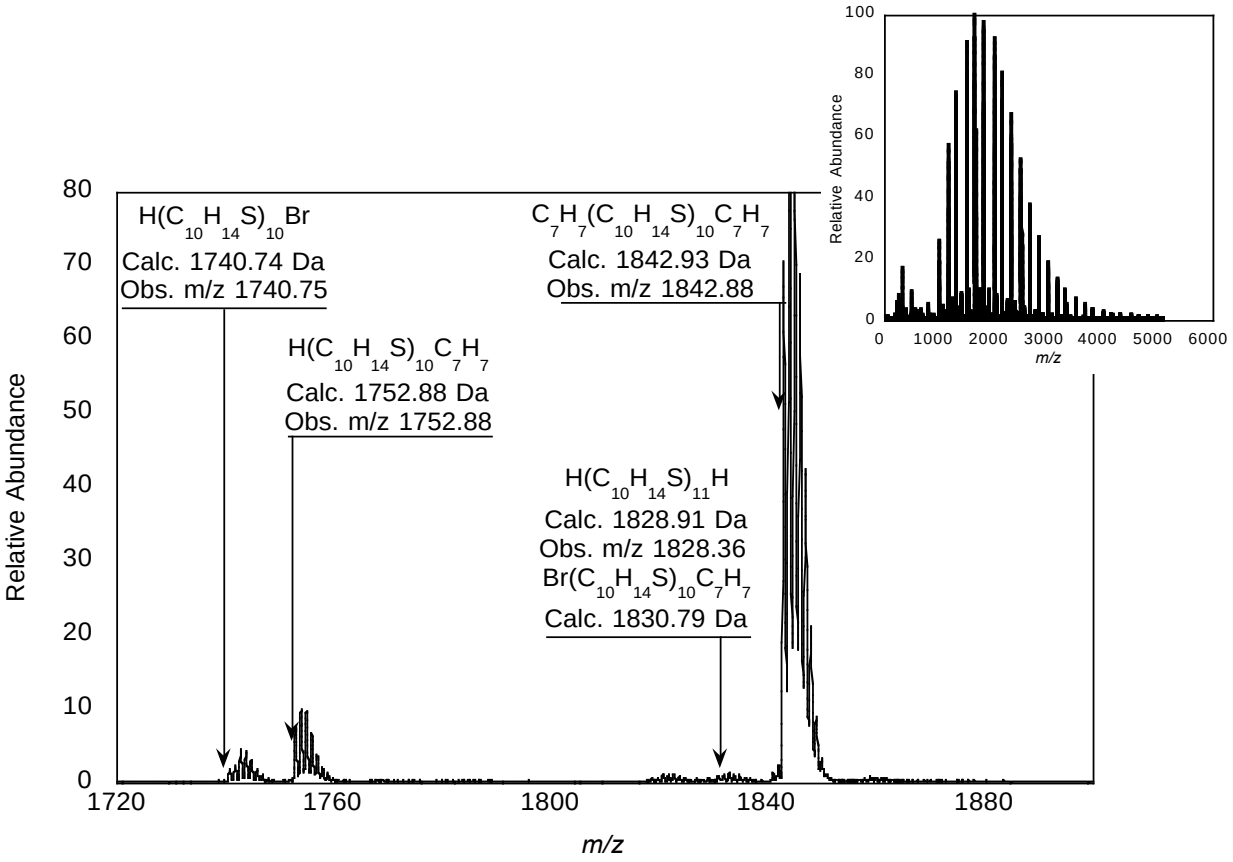

Figure 2-1. MALDI-TOF mass spectra of **P3HT1** obtained after quenching the polymerization with tolyl-MgBr (inset) and region of the 10-mer showing five products with end-groups: Br/H, H/H, Br/C_7H_7, H/C_7H_7, and C_7H_7/C_7H_7.

The origin of the observed products can be elucidated in view of the proposed mechanism of the GRIM polymerization. The GRIM polymerization proceeds by a transition-metal-catalyzed cross-coupling reaction involving three main catalytic steps: oxidative addition, transmetalation and reductive elimination.[8] Under "ideal" conditions when all of the monomer has been consumed, the nickel catalyst remains associated to one chain-end, and subsequent addition of tolyl-MgBr terminates the reaction to yield the ideal monofunctional product, Br/C_7H_7 (See Scheme 2-1). Because mostly difunctional product (e.g., C_7H_7/C_7H_7) is observed, it has been proposed that the Ni^0 oxidatively adds to the C-Br bond at the α-chain end via catalyst walking[80] or Ni^0 diffusion,[81] allowing for transmetalation with another tolyl-MgBr, followed by reductive elimination.[44] For the products where a proton is observed at the chain end, the Ni catalyst has been displaced by a quenching reagent, such as methanol, or termination has occurred prior to functionalization. The presence of H/Br end-groups suggests that tolyl-MgBr did not react with the active site of the Ni^{II} complex at the chain end prior to precipitation into methanol. Because of the complexity of these systems, one of the challenges is estimating the end-group composition. Traditional techniques such as ^1H NMR spectroscopy can provide some insight into the end-group composition but small amounts of side products are difficult to detect; however a fuller picture of the end group composition can be obtained with confidence by the use of high resolution MALDI-TOF MS.

The relative concentration of each product can be determined by MALDI-TOF MS from the monoisotopic peak height for each distribution. It is important to choose peaks in the same molecular weight region for each species, as MALDI-TOF MS is known to bias low molecular weight species due to their ease of ionization.[82] For this study, the 10-mer was chosen as the

molecular weight region for calculation of the composition. As shown in Figure 2-1, the distributions attributed to Br/H, C_7H_7/C_7H_7 and H/C_7H_7 in the MALDI spectrum are distinct from one another. Therefore, determining the concentration of these products is trivial. Calculation of the relative amounts of the chains with H/H [$H(C_{10}H_{14}S)_{11}H$; Calc. monoisotopic mass 1828.91 Da] and Br/C_7H_7 ($Br(C_{10}H_{14}S)_{10}C_7H_7$; Calc. monoisotopic mass 1830.79 Da) end-groups is more challenging because the two isotope distributions overlap (Figure 2-2). Using a program coded in MATLAB, a model distribution can be calculated to fit to the observed spectrum [Figure 2-2(c)] by adjusting the relative amounts of Br/C_7H_7 [Figure 2-2(a)] and H/H [Figure 2-2(b)] contributing to the distribution. The modeled and observed spectra for **P3HT12** are shown as an example in Figure 2-2. After determining the relative amounts of Br/C_7H_7 and H/H that contribute to the distribution, the monoisotopic peak heights can be calculated for each species, as described in Appendix B, to determine the overall end-group composition of the sample.

Using this methodology, **P3HT1** was found to contain 85% C_7H_7/C_7H_7, 9% H/C_7H_7, and 2% Br/C_7H_7. (See Appendix B for all of the fittings.) McCullough and coworkers reported 80% C_7H_7/C_7H_7 and 20% H/C_7H_7, but did not observe the Br/C_7H_7 product, which as noted previously is likely due to the lower sensitivity of MALDI-TOF MS at higher molecular weights, as McCullough prepared polymers in the 5000–7000 g/mol range.[43-44] This analysis demonstrates that high resolution MALDI-TOF MS is required for full end-group characterization of these materials, because if spectra are obtained without isotopic resolution, chains with H/H and Br/C_7H_7 end groups are not distinguishable. To my knowledge, this is the first comprehensive analysis of all of the products obtained by *in situ* quenching of the GRIM polymerization. In the past, little attention was paid to the side products that are present at low concentration.

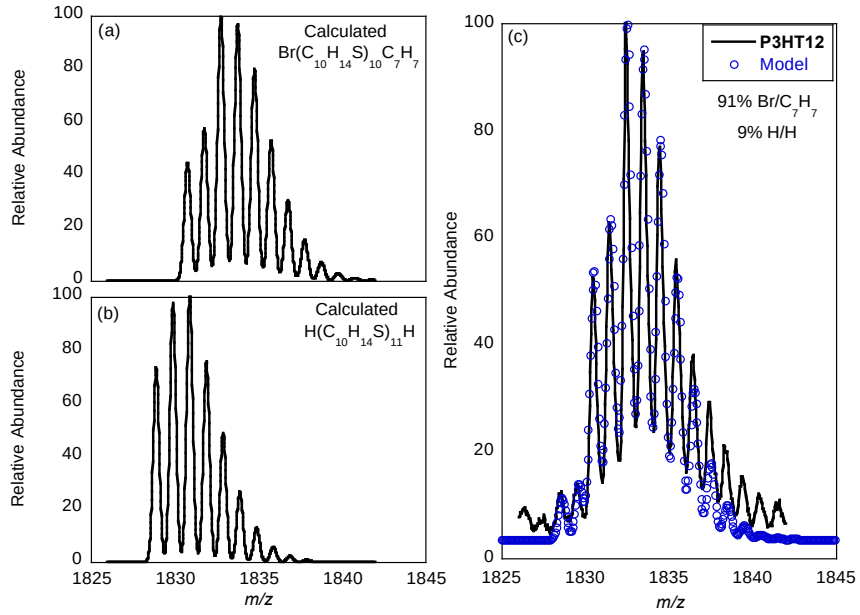

Figure 2-2. The calculated isotopic distributions for (a) $Br(C_{10}H_{14}S)_{10}C_7H_7$ and (b) $H(C_{10}H_{14}S)_{11}H$. The modeled spectrum of **P3HT12** (c) was obtained using the ratios of the two constituent spectra as a fitting parameter.

2.3.1 Effect of additives

McCullough *et al.* suggested that the formation of a π-complex between the Ni^0 species and unsaturated groups prevents the formation of difunctional products in cases where vinyl and allyl functionalized P3HTs are made by Grignard quenching.[43] Based on this, I postulated that additives containing unsaturation could prevent oxidative addition of Ni^0 to the α-chain end by complexing with the active Ni^0 complex, resulting in a higher yield of monofunctional product (see Scheme 2-2).[77-78]

To test this hypothesis, two different additives were utilized in this study, 1-pentene and styrene. 1-Pentene was added at various levels (20, 200, and 1000 times excess) relative to the

Ni(dppp)Cl_2 catalyst immediately before the addition of the tolyl-MgBr Grignard reagent used to quench the polymerizataion. Characterization of the resulting P3HTs by MALDI-TOF MS allows for the calculation of the end-group composition, and the results are shown in Table 2-1. As the ratio of 1-pentene to Ni^0 increases, the difunctional C_7H_7/C_7H_7 product decreases from 85% (**P3HT1**) to 60% (**P3HT4**), and the "ideal" monofunctional product, Br/C_7H_7, increases from 2% to 17%, which suggests that the additive suppresses oxidative addition at the α-chain end. Interestingly, the H/C_7H_7 product also increases from 9% to 14%, indicating that while the Ni^0 is still able to oxidatively add to the α-chain end, the presence of the 1-pentene interferes with the subsequent transmetalation step. Styrene was also investigated as an additive for the functionalization of P3HT with tolyl-MgBr. Styrene was chosen because it introduces extended conjugation that may enhance interaction with the active Ni^0 complex, and also because it is a bulkier ligand, which may sterically prevent oxidative addition and transmetalation. When styrene was present (**P3HT5**) the difunctional product decreased to 66% and the Br/C_7H_7 product increased to 23%, which is comparable to the results observed with 1-pentene. The amount of the H/C_7H_7 product did not change as compared to **P3HT1**, which suggests that styrene interacts more strongly with the Ni^0 complex. The change in end-group composition is confirmed by ^1H NMR spectroscopy by monitoring the aliphatic region attributed to the methylene carbon of the thiophene unit adjacent to the end-group. The ^1H NMR spectra region of interest for **P3HT1** and **P3HT5** are shown in Figure 2-3. The triplet at 2.65 ppm corresponds to the methylene protons of the thiophene unit adjacent to the tolyl functional group[43], and it dominates the spectrum of **P3HT1** (Figure 2-3a), which contains 85% difunctional product and 9% monofunctional product. In the **P3HT5** spectrum (Figure 2-3b), a triplet attributed to the methylene protons of the thiophene unit

adjacent to a Br end group appears at 2.57 ppm, which is consistent with the end-group composition attained by MALDI-TOF MS.[83] Peaks due to H-terminated polymer are also observed at 2.62 ppm in both spectra, but the signals are quite weak. ^{1}H NMR spectra of all of the P3HT polymers are included in Appendix B.

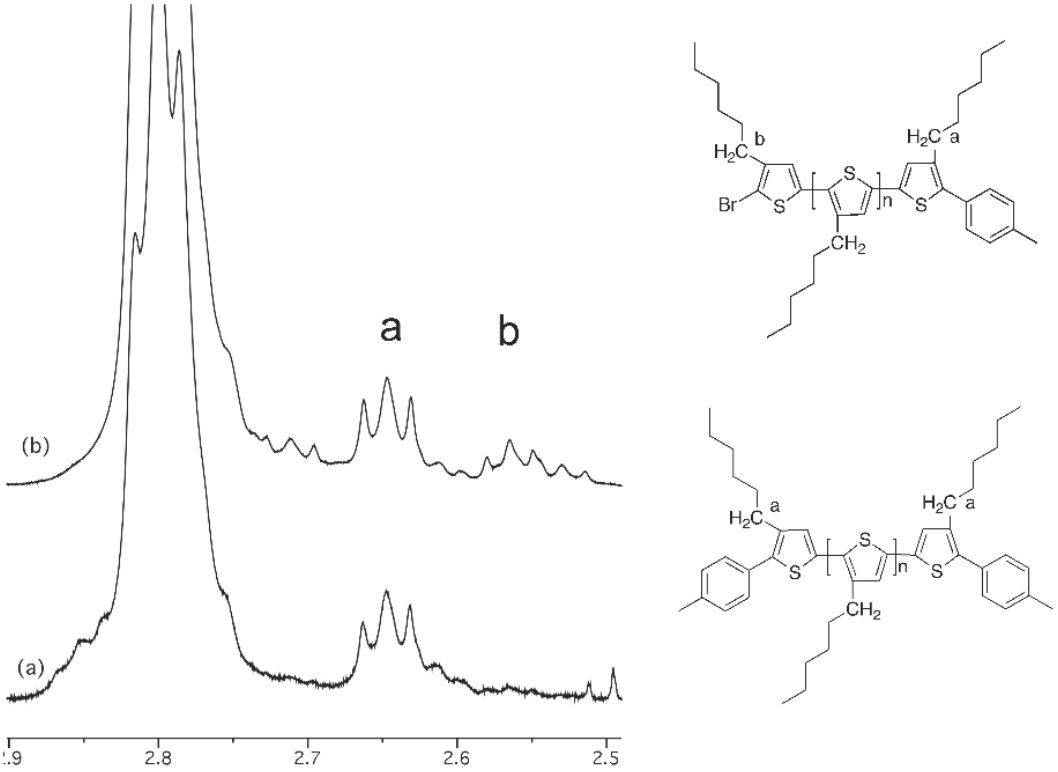

Figure 2-3. ^{1}H NMR spectra of tolyl-functionalized polymers (a) **P3HT1** and (b) **P3HT5**.

It should be noted that 1,3-dienes were also investigated as potential additives in the functionalization of P3HTs with tolyl-MgBr. Unfortunately, the 1,3-diene homopolymerized in the presence of the Ni catalyst[84] yielding a product with a multimodal GPC trace. While the

addition of styrene and 1-pentene as additives during the functionalization impacted the degree of functionality of the P3HT chains comprising the final product mixture, the difunctional species is still the major product observed. It should be noted that when a control experiment is performed wherein the GRIM polymerization is quenched with 5 M HCl (**P3HT0**) the only product observed is Br/H. This suggests that the polymerization proceeds by a chain growth mechanism in the absence of significant termination.

Table 2-1. Effect of 1-pentene and styrene on the end-group composition of tolyl-MgBr quenched P3HT at room temperature.

Sample	**Ni: additive**	**Additive**	**Br/C_7H_7**	**H/C_7H_7**	**C_7H_7/C_7H_7**	**Br/H**	**H/H**
P3HT0*	0	None	0	0	0	100	0
P3HT1	0	None	2	9	85	3	1
P3HT2	1:20	1-pentene	5	10	78	5	2
P3HT3	1:200	1-pentene	8	18	63	9	2
P3HT4	1:1000	1-pentene	17	14	60	7	2
P3HT5	1:1000	styrene	23	6	66	5	0

*__P3HT0__ was quenched with 5 N HCl as a control sample.

LiCl has been reported to significantly increase the rate of magnesium-halogen exchange for thiophenes and other aromatic compounds, as well as increase the yield of the metathesis polymerization.[45,85-86] The addition of LiCl to Grignard reagents decreases the degree of aggregation of the Grignard reagent, yielding a highly reactive Grignard-LiCl complex [$RMgCl_2^-Li^+$] and, in some cases, has been shown to increase the stability of aromatic Grignard reagents.[85,87]

In the GRIM polymerization of 2,5-dibromo-3-hexylthiophene, LiCl has been shown to increase the molecular weight and decrease the regioregularity of the resultant P3HTs.[86,88] Because of the ability of LiCl to alter the reactivity of Grignard reagents, its role in the *in situ* quenching of the GRIM polymerization is also investigated.

LiCl can be introduced into the polymerization during the metal-halogen exchange of 2,5-dibromo-3-hexylthiophene to yield the active Grignard·LiCl complex or a tolyl-MgBr·LiCl complex can be used as the functionalization reagent. In the first case, LiCl is present during the entire polymerization, while in the second case LiCl is only present during the functionalization step. The end-group compositions of samples prepared in the presence of LiCl are presented in Table 2-2. The addition of LiCl during the polymerization reduces the amount of difunctional P3HT formed (**P3HT6**) to a greater degree as compared to the case where it is only present during the functionalization (**P3HT8**). Addition of 1-pentene along with LiCl to the system further decreases the amount of difunctional P3HT (C_7H_7/C_7H_7) to 42% (**P3HT7**) and the amount of Br/C_7H_7 increases significantly to 28%. When LiCl is introduced as the tolyl-MgBr·LiCl complex, a modest decrease in the amount of difunctional product is observed (**P3HT8**), and in the presence of 1-pentene (**P3HT9**) or styrene (**P3HT10**) the difunctional product is found to account for 61% and 69% of the product, respectively. While the role of LiCl is not clear, it appears to suppress the formation of the difunctional product to some extent and enhance the effectiveness of 1-pentene as an additive.

Table 2-2. Effect of LiCl on the end-group composition of tolyl-MgBr quenched P3HT in the presence of 1-pentene and styrene at room temperature.

Sample	Ni: additive	Additive	LiCl[a]	Functionalization Reagent	Br/C_7H_7	H/C_7H_7	C_7H/C_7H_7	Br/H	H/H
P3HT6	0	None	Yes	tolyl-MgBr	3	19	71	4	3
P3HT7	1:1000	1-pentene	Yes	tolyl-MgBr	28	16	42	9	5
P3HT8	0	None	No	tolyl-MgBr·LiCl[b]	0	15	79	3	3
P3HT9	1:1000	1-pentene	No	tolyl-MgBr·LiCl[b]	12	16	61	8	3
P3HT10	1:1000	styrene	No	tolyl-MgBr·LiCl[b]	19	7	69	3	2

[a]LiCl was added during the preparation of the monomer. The ratio of 2,5-dibromo-3-hexylthiophene:LiCl was 1:0.95.

[b]LiCl was added during the preparation of the tolyl-MgBr reagent. The ratio of tolyl-MgBr:LiCl was 1:0.95.

2.3.2 Effect of Temperature

Because the oxidative addition of Ni^0 to the α-chain end needs to be suppressed to promote formation of the monofunctional P3HT products, a decrease in temperature should slow the rate of oxidative addition, as well as the diffusion of the Ni^0 catalyst. Functionalizations were performed at 0 ºC in the presence of 1-pentene or styrene and LiCl, and the results are presented in Table 2-3. When the GRIM polymerization is quenched with a tolyl-MgBr at 0ºC in the presence of LiCl (**P3HT11**), the difunctional product decreases to 61%. The addition of 1-pentene prior to the functionalization (**P3HT12**) decreases the difunctional product further to 27%, and the Br/C_7H_7 increases to 37%. When styrene is used as the additive, the difunctional product decreased to 20% and the "ideal" monofunctional P3HT, Br/C_7H_7, is present at 67% abundance. Taking into account the H/C_7H_7 monofunctional product, **P3HT13** contains 72% monofunctional species, which is a significant improvement when compared to **P3HT1**, where only 8% of the

product is monofunctional. The difunctional product is reduced from 85% in **P3HT1** to 20% in **P3HT13**. These results are comparable to those obtained with the external, functional initiators reported by Koeckelberghs, which results in 80-95% end-functionalized P3HT.[71]

Table 2-3. End-group composition of tolyl-MgBr quenched P3HT in the presence of LiCl and 1-pentene or styrene at 0°C.

Sample	Ni: additive	Additive	Br/C_7H_7	H/C_7H_7	C_7H_7/C_7H_7	Br/H	H/H
P3HT11	0	None	2	20	61	13	4
P3HT12	1:1000	1-pentene	36	15	28	17	4
P3HT13	1:1000	styrene	67	5	20	5	3

2.4 Conclusions

The work described in this chapter demonstrates a general, one-pot method for improved control of end-group composition of end-functionalized P3HTs prepared by GRIM polymerization followed by *in situ* quenching. Additives such as 1-pentene and styrene are shown to decrease the amount of difunctional P3HT, in some cases significantly, and increase the yield of the monofunctional P3HT. It is proposed that the additive interacts with the Ni^0 complex, preventing oxidative addition at the α-chain end and the formation of difunctional P3HT. Added LiCl present during the entire GRIM polymerization results in a greater decrease in difunctional P3HT as compared to cases where LiCl is present only during the functionalization. When the functionalization is done at 0°C in the presence of both LiCl and styrene, the monofunctional P3HT is observed in 72% yield, and the difunctional P3HT decreases to 20%. This strategy can be

extended to synthesize other well-defined end-functional P3HTs by changing the quenching reagent, providing the ability to prepare monofunctional materials for fundamental studies that link macromolecular design to structure and function in organic photovoltaic devices and organic LEDs. Additional optimization or exploration of other additives could potentially lead to complete deactivation of the Ni^0 complex after a single addition of a functional end-group to yield monofunctional P3HT exclusively.

2.5 Experimental

2.5.1 Characterization

Size exclusion chromatography (SEC) was performed using a Waters Alliance 2695 Separations Module equipped with three polymer Labs PLgel 5 μm mixed C columns (300 x 7.5 mm) in series in THF at 1.0 mL/min at 35 °C. The system is equipped with a Waters Model 2414 Refractive Index detector. Waters Empower™ 2 Software was used to generate a conventional calibration curve based on polystyrene standards.

Matrix Assisted Laser Desorption Ionization Time-of-Flight Mass Spectrometry (MALDI-TOF MS) was performed with a Bruker Daltonics Autoflex II mass spectrometer. The instrument is equipped with an N_2 laser (λ = 337 nm) with a frequency of 25 Hz and an accelerating voltage of 20 kV. *trans*-2-[3-(4-tert-Butylphenyl)-2-methyl-2-propenylidene]-malononitrile (DCTB, >99%, Fluka) was used as the matrix. Solutions of matrix (20 mg/mL) and analyte (10 mg/mL) were prepared in THF, and were mixed in a 5:1 ratio. Then, 1 μL was applied to the target and allowed to dry (Dried Droplet Method).[89] Mass spectra were collected in reflectron mode and the instrument was externally calibrated with polystyrene standards. Calculated isotope distributions

were obtained using iMass Version 1.1. A fitting program coded in MATLAB was used to obtain a modeled spectrum using the ratio of the two constituent spectra as a fitting parameter.

Gas chromatography coupled with mass spectrometry (GC-MS) was performed on an Agilent Technologies 7890A GC system with a 5975C inert XL EI/CI MSD mass spectrometer.

2.5.2 Preparation of p-tolylmagnesium bromide lithium chloride complex (tolyl-MgBr·LiCl)

The procedure used follows that of Knochel et al.[90] LiCl (0.919 g, 21.7 mmol) and magnesium turnings (0.554 g, 22.8 mmol) were added to a dry 100 mL 3-neck flask equipped with a 25 mL addition funnel, Teflon stopper, stir bar, and reflux condenser. Next, 20 mL of THF was transferred into the addition funnel *via* cannula. Sufficient THF (~5 mL) was added to the reaction vessel until the magnesium and LiCl were completely immersed. While stirring gently, the THF was gently heated under reflux and the solution of 4-bromotoluene (3.712 g, 21.7 mmol, 1.46 M in THF) was added dropwise. When the solution was vigorously refluxing, the heat was removed and the rate of addition of the 4-bromotoluene solution was adjusted to maintain a constant reflux. After complete addition of the 4-bromotoluene solution, the mixture was heated under reflux for an additional 3 h. The solution was transferred to glass vials via cannula and sealed with a Teflon coated septa. The concentration (1.6 M in THF) was determined by quenching an aliquot of the Grignard reagent with water followed by titration with a 1 M HCl solution. In instances where tolyl-MgBr is used as the functionalizing agent, lithium chloride was not added during the preparation.

2.5.3 Preparation of tolyl-functionalized P3HT via in situ end-functionalization

In a dry 500 mL 3-neck flask, 2,5-dibromo-3-hexylthiophene (1.08 g, 3.31 mmol) (and 0.95 eq. LiCl, if applicable) was dissolved in 40 mL of THF. The reaction vessel was equipped with a stir bar, condenser, and two Teflon stoppers. The solution was degassed with nitrogen for 30 min. *i*-PrMgCl (2.4 mL, 3.31 mmol) was transferred to the flask via syringe and the mixture was heated under reflux for 2 h. The reaction was monitored by GC-MS to ensure complete metal-halogen exchange. Once complete, the mixture was cooled to room temperature, Ni(dppp)Cl_2 (0.064 g, 0.118 mmol) was added, and the mixture was stirred for an additional 15 min. If an additive was to be used (i.e. styrene or 1-pentene, 20-1000 times excess compared to the nickel catalyst), it was transferred into the reaction vessel via syringe while stirring. Then 20 times molar excess of tolyl-MgBr or tolyl-MgBr·LiCl (2.36 mmol) compared to nickel catalyst was added to the mixture. To monitor the conversion of the end groups as a function of time, aliquots were taken, quenched in methanol, and analyzed. The final mixture was precipitated into methanol.

Chapter 3: *In situ* Formation of Pyridyl-Functionalized P3HTs via Quenching of the GRIM Polymerization

This chapter describes work published in *Chem. Mater.* **2012**, 24, 4459-4467. I synthesized and characterized all of the polymers described in this work and wrote the manuscript. Coauthors include Dr. Deanna L. Pickel, who provided guidance and helpful suggestions concerning synthesis and MALDI characterization, Dr. Bobby G. Sumpter performed the theoretical calculations, Dr. Jihua Chen provided the TEM results, Joseph D. Keene synthesized the semiconductor quantum dots, Prof. Sandra J. Rosenthal advised Joseph D. Keene, and Prof. S. Michael Kilbey II, who advised this work.

3.1 Abstract

The synthesis of well-defined, end-functional poly(3-hexylthiophene)s (P3HTs) by *in situ* quenching of the Grignard metathesis (GRIM) polymerization is complicated by the extreme tendency to favor difunctional products in all but a few cases. A facile one-pot method for preparing 2-pyridyl and 3-pyridyl P3HTs with high abundance of monofunctional products is established via an examination of the kinetics of the end-functionalization quenching reaction with lithium chloride complexes of 2- and 3-pyridyl Grignard reagents. Density functional theory calculations guide the selection of pyridine as a useful end group because it provides the capacity to ligate cadmium selenide (CdSe) nanocrystals and arrest aggregation upon thermal annealing when dispersed in a P3HT matrix. The relative abundances of various end-functional products, as ascertained by high resolution matrix assisted laser desorption ionization time-of-flight mass spectrometry, can be altered through the use of 1-pentene as an additive: GRIM polymerizations quenched with 3-pyridyl and 2-pyridyl Grignard reagents show 5% and 18% abundances of difunctional, pyridyl-capped P3HTs, respectively, when 1-pentene is present at 1000:1 relative to

the nickel catalyst. This represents a significant improvement compared to quenching with aryl Grignard reagents, where difunctional products predominate. The ability to manipulate end group compositions coupled with the propensity of pyridyl-functionalized P3HTs to ligate semiconductor quantum dots (SQD) opens new possibilities for tuning the morphology of conjugated polymer/SQD blends.

3.2 Introduction

End-functional π-conjugated polymers have attracted much attention as materials capable of improving the properties and performance of biosensors, organic field effect transistors, and organic photovoltaics because end-group functionality integrates the capacity for self-assembly and promotes interaction/reaction with other materials or surfaces.[3,7,10,37,52,64,91-98] Efforts in these areas often make use of poly(3-hexylthiophene) (P3HT) as a model polymer in part because the Grignard metathesis (GRIM) polymerization provides good control of molecular weight and results in relatively narrow polydispersity (PDI) while achieving high regioregularity through nearly exclusive head-to-tail couplings.[4,14,20-21,74,99-100] GRIM polymerization also provides a means to directly end-functionalize P3HT chains by quenching the polymerization with Grignard reagents.[44-45,101] The choice of the Grignard reagent has a strong impact on the relative proportion of monofunctional or difunctional products resulting from the end-functionalization: McCullough and coworkers[44,101] reported that *in situ* end functionalization using vinyl and allyl Grignard reagents leads almost exclusively to monofunctional products while aryl and alkyl Grignard reagents result in almost exclusive difunctional P3HT chains.

Control of end-group chemistry is conceptually important for controlling functionality that

hinges on association (i.e. recognition and/or binding) between the chains and other molecules or for enabling subsequent chemical modifications such as grafting to surfaces or chain extension. Tailoring end-group functionality has also been shown to be important for enhancing the efficiency of solar cell devices. For example, Krüger and coworkers prepared cyanoacrylic acid end-functionalized P3HTs for use as sensitizers in dye sensitized solar cells.[64] Difunctional cyanoacrylic acid end-functionalized P3HT sensitized the TiO_2 more efficiently, leading to a power conversion efficiency that was higher than if monofunctional or nonfunctional P3HTs were used.[64] Also, primary amine-terminated P3HTs prepared by Frechét *et al.* resulted in a significant increase in power conversion efficiency of hybrid organic photovoltaic devices made with cadmium selenide (CdSe) semiconductor quantum dots (SQDs). The increase in efficiency was attributed to coordination of the chain ends with the CdSe SQDs.[3]

Thus far, incorporation of end-groups on P3HT chains that function either as anchoring groups, chain extension moieties, or hydrogen bond donor/acceptors requires post-polymerization modification reactions that involve expensive reagents and multiple reaction steps that increase susceptibility to side reactions. For example, Hillmyer *et al.* prepared difunctional fullerene-terminated P3HTs via three successive post-polymerization reactions: a magnesium-halogen reaction, the Vilsmeier-Haack reaction, and a cycloaddition reaction.[37] However, the C_{60}-P3HT-C_{60} product also contained a product from chain coupling, which was observed by size exclusion chromatography (SEC). Lee and coworkers prepared monofunctional fullerene-terminated P3HTs with >90% functionality by Steglich esterification between a hydroxy-terminated P3HT and [6,6]-phenyl-C_{61}-butyric acid, which is a carboxylic acid derivative of [6,6]-phenyl-C_{61}-butyric acid methyl ester (PCBM).[102] These materials improve the stability of photovoltaic devices under

annealing conditions because the P3HT-C_{60} chains act as a compatibilizer. Lohwasser and coworkers[103] recently used post-polymerization methods to prepare dicarboxylate functionalized P3HT via a lithiation reaction. In the bulk, these difunctional P3HTs show a loss in crystallinity and a blue shift in the UV-vis spectrum, which is attributed to a loss of π-π stacking due to hydrogen bonding between the carboxylic acid end-groups of different P3HT chains.[103] Lohwasser *et al.* later reported the preparation of monocarboxylated P3HT by metal-halogen exchange of the bromine terminated P3HT followed by addition of gaseous CO_2.[86] DSC analysis showed that P3HT-COOH is less crystalline than its unfunctionalized counterpart; however, wide-angle X-ray scattering revealed that P3HT-COOH was highly ordered.[86] While multistep approaches are useful, simpler methods for creating well-defined end-functionalized polymers are preferred.

In this chapter, I report the synthesis of pyridyl-functionalized P3HT via quenching of the GRIM polymerization with 2- and 3-pyridyl Grignard reagents. This work capitalizes on my prior work, described in Chapter 2, where the end-group composition of tolyl-functionalized P3HT was controlled by the use of additives and reaction conditions.[104] Here I show that 1-pentene is effective as a complexing agent that prevents oxidative addition of Ni^0 at the α-chain end, promoting addition of pyridine at the growing chain end. The pyridyl-functionalized P3HTs are characterized using high resolution matrix assisted laser desorption ionization time-of-flight mass spectrometry (MALDI-TOF MS) to determine the relative abundance of end-groups. First principles calculations of heats of formation and electron density distributions were performed in order to rationalize the difference in reactivity of 2- and 3-pyridyl Grignard reagents with the propagating chain end. Binding strengths between different end groups and a CdSe surface were

also computed to assess which groups would present the best possible candidates for achieving appropriate ligand interactions. The impact of the CdSe surface ligands on the morphology of blends with P3HT were studied by TEM.

3.3 Results and Discussion

The GRIM polymerization (or Kumada Catalyst-Transfer Polycondensation, KCTP) has been rigorously studied and has proven to be a facile method for preparing well-defined, highly regioregular P3HTs for use in organic electronic applications.[3,14,4,20,44] Specifically, end-functional P3HTs are suitable candidates for tailoring morphology of donor-acceptor blends in these types of applications due to their potential to promote self-assembly. The degree of end-group functionality is sensitive to the reaction conditions employed during preparation of P3HT: reagent purity, monomer conversion, and catalyst choice collectively influence the outcome of the polymerization (i.e. end-group composition, molecular weight, and polydispersity index, PDI). Therefore, careful attention was given to the polymerization conditions in order to ensure that the end-groups observed were due to the end-functionalization step and not associated with side reactions during the polymerization. In particular, the polymers were prepared using clean, dry reagents and the Grignard exchange was strictly monitored to ensure a slight under conversion (<5%) of the 2,5-dibromo-3-hexylthiophene and complete consumption of i-PrMgCl during magnesium-halogen exchange. As a control, a polymerization quenched with 5 M HCl was characterized by MALDI-TOF MS and found to contain nearly 100% of chains having Br/H end-groups. (See Appendix C.) Also, molecular weight control for these polymerizations was observed while maintaining relatively low polydispersity, as evidenced by SEC, which indicates that the polymerization

proceeds by a chain growth mechanism with minimal termination. (See Appendix C.) These results are fully consistent with results from previous work of Yokozawa and Lohwasser.[4,86]

Based on the results of density functional theory (DFT) calculations described in section 3.4.2, pyridyl-functionalized P3HTs were chosen for synthetic development due to their favorable interaction with CdSe SQDs, which makes them good candidate materials for ligating CdSe SQDs. (See Appendix C.) Specifically, in order to have single point ligation, preparation of monofunctional, pyridyl-functionalized P3HTs was pursued by quenching the GRIM polymerization with the appropriate Grignard reagent. The proposed pathway to pyridyl-functionalized P3HT is shown in Scheme 3-1, illustrated with 2-pyridyl-MgCl·LiCl as the quenching reagent. Quenching with 3-pyridyl-MgCl·LiCl is not shown, but the pathway is assumed to be analogous. The accepted polymerization mechanism of the regiospecific monomer involves Ni-catalyzed cross-coupling with three steps: oxidative addition (OA), transmetallation (TM), and reductive elimination (RE).[105] It is known that quenching the GRIM polymerization with vinyl or allyl Grignard reagents yields mostly monofunctional P3HTs, while quenching with alkyl or aryl Grignard reagents produces difunctional P3HTs in high abundance (>80%).[44,101] Therefore, quenching with pyridyl Grignard reagents is expected to yield difunctional P3HT chains. For this reason Scheme 3-1 shows the various reaction pathways that give rise to products other than "ideal" monofunctional P3HTs that have a bromine at the α-end, due to the initial tail-to-tail dimer formed, and a pyridyl group at the ω-end that results from quenching the growing P3HT chain. I note that from here forward in this chapter, I refer to P3HT chains resulting from *in situ* quenching with pyridyl Grignard reagents by their end-groups only: for example, monofunctional pyridyl-capped P3HT with bromine at the α-end will be denoted as Br/C_5H_4N,

while unfunctionalized P3HT will be identified as Br/H.

The pyridyl-Grignard reagents were prepared by metal-halogen exchange of the corresponding bromopyridines with isopropyl magnesium chloride (i-PrMgCl) in the presence of lithium chloride (LiCl), according to a modified literature procedure.[106-112] Initial attempts to synthesize the pyridyl Grignard reagents without LiCl resulted in low yields for the 2-pyridyl Grignard or seemingly unsuccessful synthesis of the 3- and 4-pyridyl Grignard compounds. Interestingly, I observe that the 3-pyridyl Grignard reagent precipitates from solution if LiCl is not used during its preparation, yielding a highly reactive solid. In addition to this tendency to precipitate when forming the pyridyl Grignard reagents, I also observed that in the presence of LiCl, the metal-halogen exchange reaction reached completion more quickly for 3-bromopyridine (4 h at room temperature) than 2-bromopyridine (12 h at room temperature), which is in agreement with the work of Shi *et al.*[113]

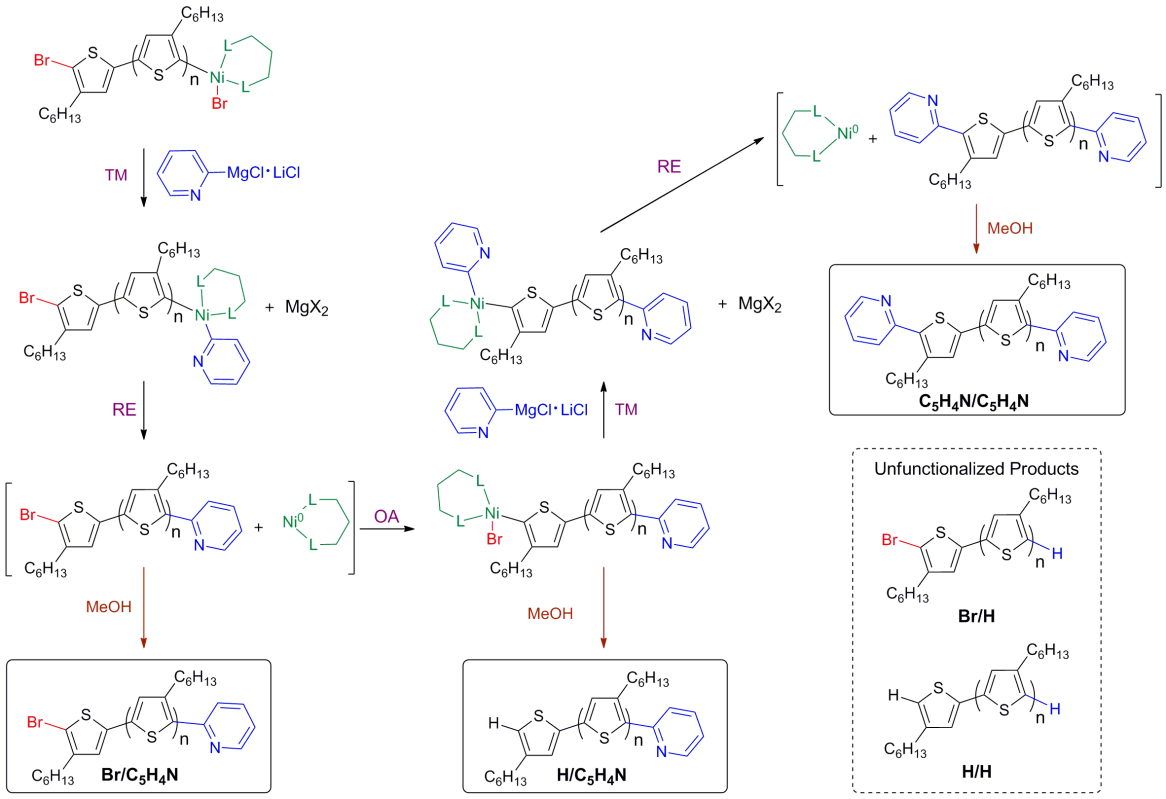

Scheme 3-1. Pyridyl-functionalized P3HT products (solid boxes) observed when transmetallation (TM), reductive elimination (RE), and oxidative addition (OA) steps occur after the GRIM polymerization is quenched with 2-pyridyl-MgCl·LiCl followed by precipitation into methanol. Unfunctionalized products (dashed box) resulting from incomplete conversion are also shown.

3.3.1 End-group analysis

Difunctional P3HTs are expected to be the major product when the GRIM polymerization is quenched with alkyl and aryl Grignard reagents, but quantitatively assessing the relative abundance of end-groups in a given sample is challenging. Only qualitative information about end-group composition can be obtained from 1H NMR spectroscopy due to overlapping chemical

shifts from protons having similar chemical environments. For example, ^{1}H NMR is not capable of distinguishing a pyridyl group at the α-chain end from one at the ω-chain end because the chemical environments are equivalent, resulting in similar chemical shifts. MALDI-TOF MS is an excellent analytical tool for definitive end-group analysis of functional polymers, an effort that is enhanced by the use of low molecular weight polymers (~2500 g/mol) for which spectra with isotopic resolution can be obtained.[79] A typical mass spectrum of P3HT quenched with 2-pyridyl-MgCl·LiCl (**P3HT1**) is shown in Figure 3-1. Just as difunctional P3HTs result from quenching with alkyl and aryl Grignard reagents, difunctional chains also are observed when heteroaryl Grignard reagents are used: The mass spectrum shows three distributions in the mass range associated with the 13-mer. Based on the observed *m/z* for the monoisotopic peaks and as identified in Figure 1, the distributions are nominally assigned as unfunctionalized P3HT [$H(C_{10}H_{14}S)_{13}H$, calc. monoisotopic 2161.08 Da, obs. *m/z* 2161.04], monofunctional P3HT [$H(C_{10}H_{14}S)_{13}C_5H_4N$, calc. monoisotopic 2238.10 Da, obs. *m/z* 2238.10] and difunctional P3HT [$C_5H_4N(C_{10}H_{14}S)_{13}C_5H_4N$, calc. monoisotopic 2315.13 Da, obs. *m/z* 2315.13]. Close examination reveals that the isotope distributions at *m/z* 2238.10 and 2315.13 have different patterns than the assigned calculated distributions. (See Appendix C.) This indicates that different products of similar mass overlap, resulting in an isotope pattern distinct from the two constituent species. In addition to confirming the presence of $H(C_{10}H_{14}S)_{13}C_5H_4N$ and $C_5H_4N(C_{10}H_{14}S)_{13}C_5H_4N$, the isotope distributions observed at *m/z* 2238.10 and 2315.13 also include contributions from $H(C_{10}H_{14}S)_{13}Br$ (calc. monoisotopic 2238.99 Da) and $Br(C_{10}H_{14}S)_{13}C_5H_4N$ (calc. monoisotopic 2316.01 Da), respectively. It is important to note that if the spectrum was obtained without isotopic resolution, those peaks would have been mistakenly attributed to a single product rather than

multiple products.

In order to determine the relative abundance of the different products, a MATLAB fitting program was used to calculate the composition of products that form the overlapping peaks based on the calculated isotope distributions of the proposed constituents. (See Appendix C.) This method was used in my previous work, described in Chapter 2, to quantify the end-group composition of tolyl-functionalized P3HTs.[104] Using this method, the end-group composition of **P3HT1** was found to be 51% C_5H_4N/C_5H_4N, 29% H/C_5H_4N, 13% H/H and 7% Br/H. This differs from results obtained when other aryl-Grignards (i.e. tolyl-MgBr) are used to quench the GRIM polymerization, where >85% of the product is reported to be difunctional.[44,101]

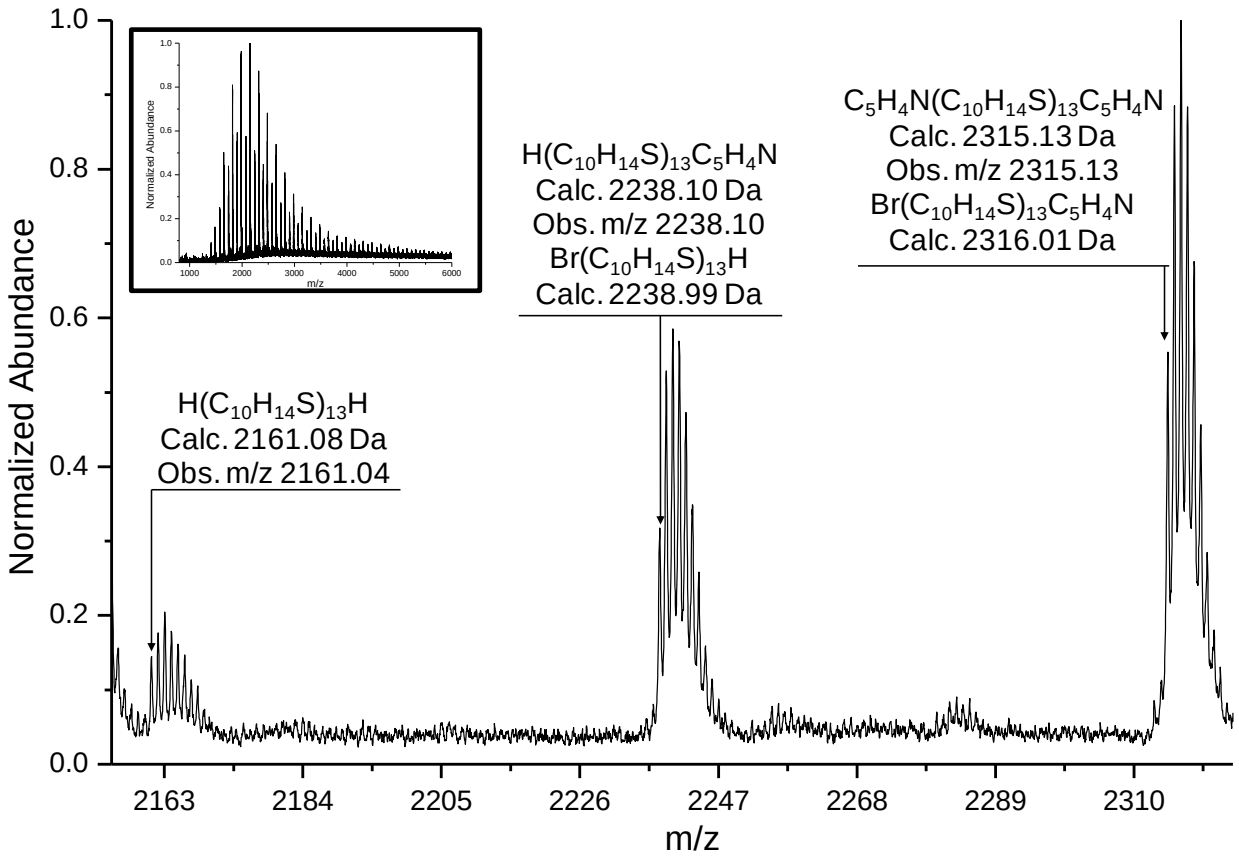

Figure 3-1. MALDI-TOF mass spectrum of **P3HT1** obtained after quenching the polymerization with 2-pyridyl-MgCl·LiCl (inset) and region of the 13-mer showing five products with Br/H, H/H, Br/C_5H_4N, H/C_5H_4N, and C_5H_4N/C_5H_4N end groups.

3.3.2 Investigation of the reactivity of 2- and 3-pyridyl-MgCl·LiCl with the propagating chain end

Initial quenching experiments revealed that the reactivity of 2- and 3-pyridyl-MgCl·LiCl complexes with the propagating chain end were dramatically different. Significantly longer reactions times were required for 3-pyridyl-MgCl·LiCl (90 minutes) to reach similar conversion

as compared to 2-pyridyl-MgCl·LiCl (40 minutes), whereas high conversion is achieved in less than 4 minutes when tolyl-MgBr was used to quench the GRIM polymerization.[44,101],[104] These differences in reactivity of the pyridyl-Grignard reagents with the propagating chain end as well as differences observed in their rate of formation motivated the kinetic studies presented in this chapter.

The kinetics of end-functionalization using 2- and 3-pyridyl-MgCl·LiCl as quenching reagents was investigated by monitoring, in an ex situ fashion, the evolution of the products as a function of time by MALDI-TOF MS. Table 3-1 shows the distribution of products that results from quenching the GRIM polymerization with 2-pyridyl-MgCl·LiCl. The desired monofunctional product, Br/C_5H_4N, is only found in 1% abundance after 40 minutes. The major product is C_5H_4N/C_5H_4N, which suggests that the Ni^0 complex diffuses or "walks" to the α-chain end, as previously reported,[80-81,114-115] where a second oxidative addition takes place, as shown in Scheme 3-1. It should be noted that the abundance of Br/C_5H_4N and H/C_5H_4N chains remains relatively constant throughout the reaction while the Br/H chains decrease and the C_5H_4N/C_5H_4N chains increase by similar amounts.

Table 3-1. End-group composition of P3HT quenched with 2-pyridyl-MgCl·LiCl as a function of time.

Time (min)	Br/C_5H_4N	H/C_5H_4N	C_5H_4N/C_5H_4N	Br/H	H/H	Br/Br
10	2	31	40	20	7	0
20	3	26	51	13	7	0
30	5	28	48	12	7	0
40	1	29	53	9	8	0

A similar study was done using 3-pyridyl-MgCl·LiCl as the quenching reagent, but longer reaction times were required to reach comparable conversion, as shown in Table 3-2. The abundance of chains having Br/C_5H_4N ends remains constant and relatively low (~7%) throughout the functionalization, similar to 2-pyridyl-MgCl·LiCl. However, when 3-pyridyl-MgCl·LiCl is used to quench the polymerization, the abundance of both H/C_5H_4N and C_5H_4N/C_5H_4N increases with time while the abundance of chains with Br/H end-groups decreases. It is also seen that the unfunctionalized product (Br/H), which is susceptible to oxidative addition, is still present in large amount (27%) even after 90 minutes. Comparison of the data in Tables 3-1 and 3-2 shows that reaction with the propagating chain end is faster for 2-pyridyl-MgCl·LiCl versus 3-pyridyl-MgCl·LiCl, as the total abundance of pyridyl-functionalized P3HT reaches 83% after approximately 40 minutes for 2-pyridyl-MgCl·LiCl, but only 65% after 90 minutes for 3-pyridyl-MgCl·LiCl. This exemplifies the lower reactivity of 3-pyridyl-MgCl·LiCl with the propagating chain end. The fact that in both cases, the decreases in the abundance of Br/H chains manifest as increases in H/C_5H_4N and/or C_5H_4N/C_5H_4N suggests that during quenching, the nickel catalyst remains active in the system, diffusing to and readily undergoing oxidative addition at the α-end

of P3HT chains. The fact that the formation of difunctional P3HT is suppressed for both 2- and 3-pyridyl Grignards as compared to the case of tolyl-MgBr suggests that the reactivity of the pyridyl-Grignards is significantly lower with the chain end (i.e. transmetallation is slower), despite the propensity for Ni^0 to oxidatively add to the α-chain end. This is also supported by the slow conversion of Br/H to pyridyl-functionalized products.

Table 3-2. End-group composition of P3HT quenched with 3-pyridyl-MgCl·LiCl as a function of time.

Time (min)	Br/C_5H_4N	H/C_5H_4N	C_5H_4N/C_5H_4N	Br/H	H/H	Br/Br
15	7	16	12	55	6	4
30	7	19	18	48	6	2
60	7	24	28	34	6	1
90	8	26	31	27	7	0

The observed differences in reactivity may be related to the stability of the Grignard reagents and the ability of the pyridine nitrogen to coordinate with the Ni^{II} at the chain end. The kinetics of magnesium-halogen exchange of bromopyridines with i-PrMgCl·LiCl has been studied by Shi et al.[113], and they report that 3- and 4-bromopyridines are considerably more reactive toward magnesium-halogen exchange than 2-bromopyridine, which they attribute to repulsion between the lone pairs when the anion is in the 2-position. A similar trend was reported for the regioselectivity of deprotonation of pyridine in the gas phase, where 70-80% of the 4-deprotonated pyridine and 20-30% of the 3-deprotonated pyridine were observed, which suggests that the

formation of the anion is thermodynamically more favorable in the 4- and 3-positions than the 2-position.[116] The relative acidities of the protons at various positions on the pyridine ring have also been reported, and based on the net charge densities at each position the relative stabilities of the anions is 4-pyridyl>3-pyridyl>>2-pyridyl.[117] These results are in agreement with my observation that the rate of magnesium-halogen exchange was faster for 3-bromopyridine versus 2-bromopyridine. (Here I note that due to stability issues with 4-bromopyridine, I did not include it in this study.[110]) The relative stabilities of the anions also provide some insight with regard to the different reactivity with the chain end. The 2-pyridyl-MgCl·LiCl, which forms the least stable anion, is more reactive with the active chain end than the 3-pyridyl-MgCl·LiCl, which explains why quenching with 2-pyridyl-MgCl-LiCl results in a high abundance of difunctional C_5H_4N/C_5H_4N product. A collaborator, Dr. Bobby Sumpter, calculated the heats of formation, ΔHf, and the electronic structures of the 2- and 3-pyridyl-MgCl·LiCl complexes in THF. His calculations indicate that Grignard formation at the 2- and 3- positions is equally favorable based on thermodynamics: ΔH_f = -110 kcal mol^{-1} for the 2-pyridyl-MgCl·LiCl and ΔH_f = -105 kcal mol^{-1} for the 3-pyridyl-MgCl·LiCl. (See Appendix C.) This suggests that the formation of the Grignard reagents is dominated by the deprotonation energies rather than by the heats of formation.

There are also several reports in the literature that pyridine can coordinate with Ni^{II} to form six-coordinate complexes.[118-121] Yokozawa and coworkers recently reported that coordination of pyridine with Ni^{II} at the propagating chain end during the synthesis of poly(3-(2-(2-(methoxyethoxy)propyl)pyridine) leads to disproportionation of growing polymer chains.[122] In my system, if pyridine interacts with Ni^{II} at the chain end when the Grignard is in the 2-position it may promote transmetallation due its closer proximity to the Ni active site as compared to when

the Grignard is in the 3-position. Both the stability of the Grignard and the ability of pyridine to coordinate to Ni^{II} may contribute to the higher pyridine functionality obtained with 2-pyridyl-MgCl·LiCl compared to 3-pyridyl-MgCl·LiCl.

3.3.3 Effect of 1-pentene on the functionalization

As evidenced by the mixture of products observed upon quenching the GRIM polymerization with pyridyl Grignards (see Tables 3-1 and 3-2) there is little control over end-group composition because, as pointed out earlier, the Ni^0 catalyst remains active during the quenching reaction. This tendency toward difunctional P3HT is consistent with previous work showing that difunctional P3HTs are obtained almost exclusively when aryl and alkyl Grignard reagents are used,[74,101] but stands in contrast with the observation of monofunctional P3HTs when vinyl and allyl Grignard reagents are used. I reported in Chapter 2 the use of 1-pentene and styrene to induce π-complexation of the alkene with the Ni^0 species, affecting an increase in the amount of monofunctional P3HT obtained from the in situ end-functionalization method when a tolyl Grignard reagent was used.[104] Based on those results, 1-pentene was used as an additive in an attempt to control the end-group composition of pyridyl-functionalized P3HT. Results obtained from the GRIM polymerization followed by quenching with 2-pyridyl-MgCl·LiCl in the presence of 1-pentene (40 min) are shown in Table 3-3. The yield of the monofunctional products (Br/C_5H_4N and H/C_5H_4N) increases from 29% to 48%, and the C_5H_4N/C_5H_4N product decreases substantially from 51% to 18% upon addition of 1000 equivalents of 1-pentene relative to Ni. There also is a slight increase in the amount of unfunctionalized P3HT (Br/H) formed with increasing 1-pentene. The increase in Br end-groups (from Br/C_5H_4N and Br/H) with increasing

1-pentene concentration was also confirmed by examining the aliphatic region of the ^{1}H-NMR spectra. The aliphatic region of the NMR spectra for P3HT1-P3HT4 is shown in Figure 3-2. For P3HT1, a triplet corresponding to the α-methylene protons adjacent to the pyridine ring dominates the spectrum at 2.90 ppm. In the P3HT4 spectrum, the triplet at 2.54 ppm corresponding to bromine adjacent to the α-methylene protons begins to dominate the spectrum, which is consistent with the trend observed from MALDI-TOF MS. It is worth noting that when nitrogen is in the 2-position on the ring the triplet is shifted downfield from the HT-HT diad (2.80 ppm)[17]; however, when the nitrogen is the 3-position of the ring, the triplet is shifted upfield to 2.65 ppm. (See Appendix C for the spectra showing the aliphatic region of P3HT5-P3HT8.)

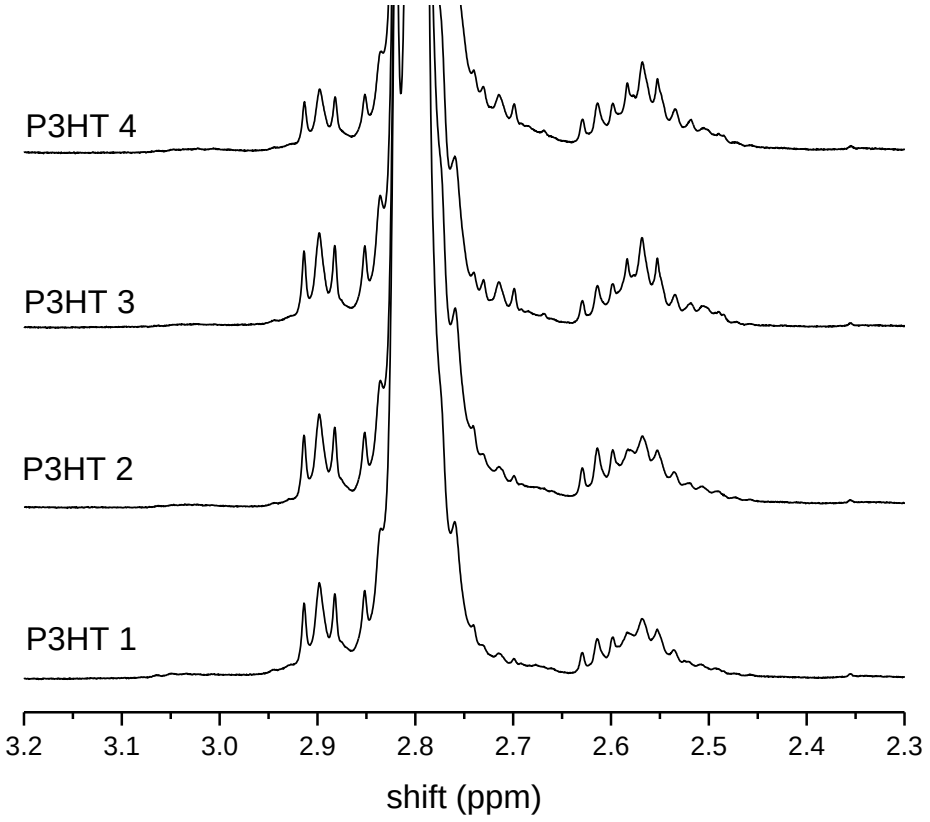

Figure 3-2. ^{1}H NMR spectra showing the aliphatic region that corresponds to the α-methylene protons adjacent to the chain ends for P3HT1-P3HT4.

Table 3-3. Effect of 1-pentene on the end-group composition of P3HTs quenched with 2-pyridyl-MgCl·LiCl.

Sample	**1-pentene:Ni**	**Br/C_5H_4N**	**H/C_5H_4N**	**C_5H_4N/C_5H_4N**	**Br/H**	**H/H**	**Br/Br**
P3HT1	0	0	29	51	7	13	0
P3HT2	20:1	3	39	34	5	19	0
P3HT3	200:1	18	27	34	8	9	4
P3HT4	1000:1	22	26	18	13	13	8

Similar results are observed when quenching with 3-pyridyl-MgCl·LiCl (60 min) in the presence of 1-pentene. As shown in Table 3-4, the abundance of the C_5H_4N/C_5H_4N product decreases significantly, from 41% to 5%, as the 1-pentene concentration is increased, and the amount of Br/C_5H_4N increases from 20% to 50%. The situation in which 1-pentene is added in a 20:1 ratio to Ni (P3HT6) is interesting as it seems to represent an optimization where the total abundance of monofunctional pyridyl-functionalized chains is highest at 60%, with two-thirds of that (40%) being the ideal product, Br/C_5H_4N, and the yield of unfunctionalized Br/H product is low (13%). At the highest 1-pentene to Ni ratio (1000:1), the unfunctionalized products account for 39% of the final end-group composition, and a decrease in total pyridine functionality is observed (61%). The results in Tables 3-3 and 3-4 suggest that Ni^0 interacts with the 1-pentene to form a π-complex, preventing oxidative addition at the α-chain end, leading to a lower abundance of the C_5H_4N/C_5H_4N product in both cases.

Table 3-4. Effect of 1-pentene on the end-group composition of P3HTs quenched with 3-pyridyl-MgCl·LiCl.

Sample	1-Pentene:Ni	Br/C_5H_4N	H/C_5H_4N	C_5H_4N/C_5H_4N	Br/H	H/H	Br/Br
P3HT5	0	20	16	39	16	9	0
P3HT6	20:1	40	19	23	13	5	0
P3HT7	200:1	34	9	7	32	5	13
P3HT8	1000:1	50	6	5	26	3	10

3.3.4 TEM imaging of surface modified CdSe/P3HT blends

Pyridyl-functionalized P3HTs were utilized as ligands for CdSe SQDs in order to investigate the influence of the CdSe ligand on the morphology of thin film blends of CdSe SQDs with P3HT. Preparation of the blends followed protocols established by Frechét et al.[3] To change the CdSe ligand, the native dodecylphosphonic acid (DPA) ligands were successively exchanged with pyridine and then with P3HT4. The resulting CdSe SQDs were blended with a high molecular weight P3HT (25 kg mol^{-1}) with Br/H end groups. TEM images of as cast and annealed films are shown in Figure 3-3. Additional TEM images with a 100 nm scale bar are displayed in Appendix C. Random dispersion of CdSe SQDs is observed in the as cast films, which are shown as the top row of images in Figure 3-3. After thermal annealing at 150ºC for 2 h, agglomerated clusters of CdSe SQDs are observed for blends where the CdSe ligands are the native DPA and pyridine. The DPA-CdSe agglomerated clusters range from 20-30 nm and pyridine-CdSe agglomerate in clusters of small size (10-20 nm). However, P3HT4-ligated CdSe nanocrystals remain dispersed and free of agglomeration even after thermal annealing at 150ºC for 2 h. The images suggest that by replacing the DPA and pyridine ligands with pyridyl-functionalized P3HT, the CdSe SQDs remain

dispersed in the P3HT matrix due to the favorable interactions between the P3HT ligands and the matrix P3HT. There are additional opportunities to use pyridyl-functionalized P3HTs in order to tune the morphology of thin films: as shown by Akcora and coworkers, who examined the morphology of blends of polystyrene-decorated silicon nanoparticles in polystyrene (PS) matrices, it is possible to access various morphologies by changing the molecular weight and tethering density of the PS chains ligating the nanoparticle or by changing the matrix molecular weight.[31] Further work in this area to understand the relationship between ligand molecular weight and blend morphology is discussed in Chapter 4.

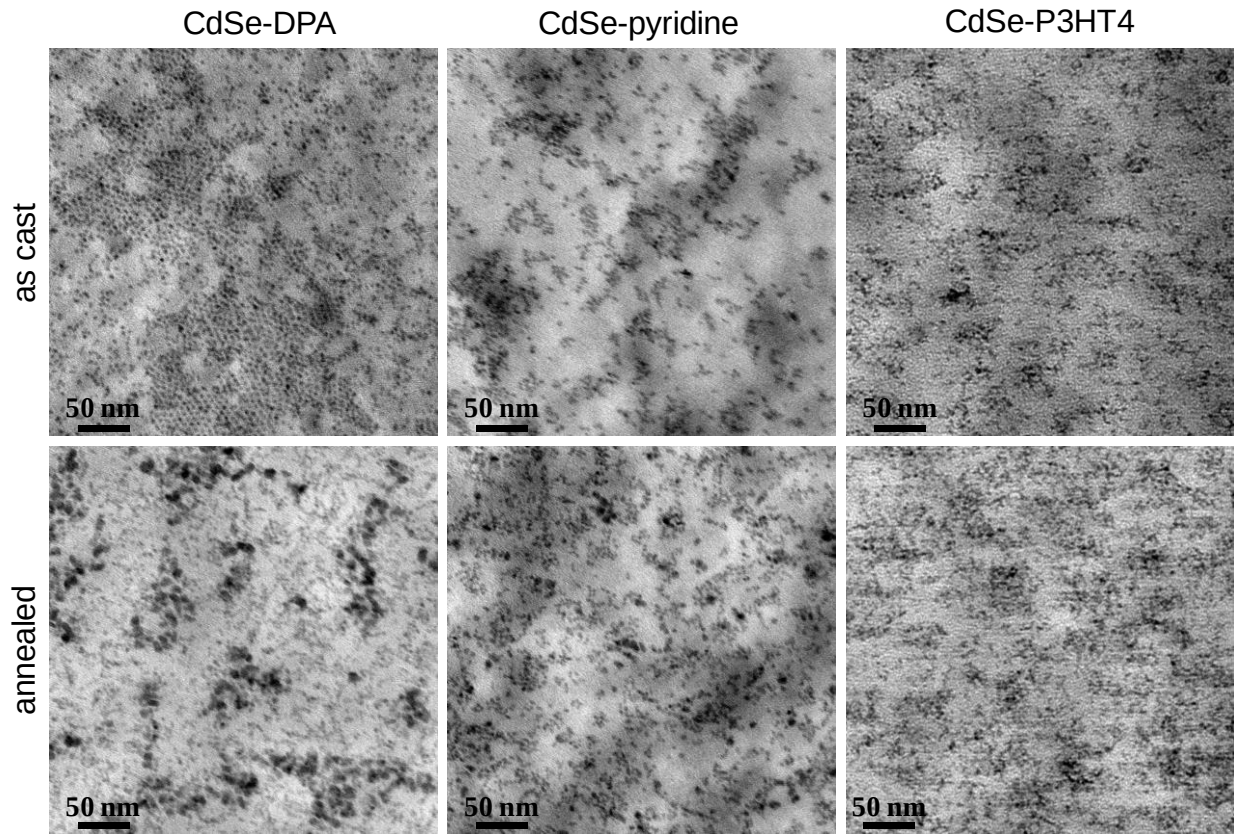

Figure 3-3. TEM micrographs of films consisting of 20 wt % surface-modified CdSe in a P3HT matrix (M_n = 25 kDa) made by drop casting from a 0.2 wt% solution in $CHCl_3$. The ligands decorating the CdSe surface are from left to right, DPA, pyridine and pyridyl-functionalized P3HT (P3HT4).

3.4 Conclusions

My work in this chapter demonstrates the utility of a "materials by design" approach, wherein theory, modeling, simulation, synthesis and characterization are used to rationally design materials for optoelectronic applications. This combination is brought to-bear to enhance end-group control in P3HTs prepared by the GRIM polymerization and allow heteroaromatic end-groups with useful functionality to be incorporated. Pyridyl-functionalized P3HT with a high degree of monofunctionality have been prepared by quenching the GRIM polymerization with 2- and 3-pyridyl Grignard reagents. As anticipated, diffusion of the Ni^0 complex and differences in the relative reactivities of the 2- and 3-pyridyl Grignard reagents leads to a mixture of products, including monofunctional, difunctional and unfunctionalized P3HT. The addition of 1-pentene, which interacts with Ni^0 and prevents oxidative addition at the α-chain end, increases the abundance of monofunctional products from 29% to 48% and from 36% to 56% when 2-pyridyl-MgCl·LiCl and 3-pyridyl-MgCl·LiCl are used as the quenching reagent, respectively.

Pyridyl-functionalized P3HTs were used as ligands to decorate CdSe SQDs and shown to stabilize the morphology of the CdSe/P3HT blends after thermal annealing at 150ºC for 2 h. This suggests that the pyridyl-functionalized P3HTs have the potential to improve hybrid organic photovoltaic devices by providing a way to manipulate blend morphology and by possibly creating intimate contact between the donor and acceptor phases in a bulk heterojunction.

3.5 Experimental

3.5.1 Materials

All reactions were performed under dry nitrogen in oven-dried glassware that was assembled while hot and cooled under nitrogen. [1,3-Bis(diphenylphosphino)propane] nickel (II) dichloride ($Ni(dppp)Cl_2$, 99%, Acros), 2,5-dibromo-3-hexylthiophene (Rieke Fine Chemicals), tetrahydrofuran (THF, Drisolv, EMD), 2-bromopyridine (99%, Aldrich), 3-bromopyridine (99%, Acros), methanol (>99.8%, Aldrich), 1-pentene (97%, Aesar), and 2-chloropropane (>99%, Acros) were used as received. Prior to their use, magnesium turnings (99.95%, Aldrich) were washed with 0.05 M HCl, water, and THF, and then vacuum dried. Isopropyl magnesium chloride (*i*-PrMgCl) was prepared by direct magnesium insertion into 2-chloropropane. The concentration of *i*-PrMgCl was determined by titration using a standard solution of HCl with phenolphthalein as the indicator. Lithium chloride (99%, EMD) was dried under vacuum at 100^{o}C, stored and weighed in a glovebox prior to use.

3.5.2 Simulations

To evaluate the relative binding strengths of candidate CdSe surface ligands, density functional theory (DFT) calculations were performed using the Vienna *ab initio* simulation package (VASP), version 4.6.6.[123-126] The Kohn-Sham equations were solved using the projector augmented wave (PAW) approach and a plane-wave basis with a 400 eV energy cutoff[127-128] using the spin polarized local density approximation (LDA).[129] Electronic convergence was defined as a consistency between successive cycles of less than 10-5 eV. A supercell consisting of 252 atoms with a vacuum layer of at least 10 Å over the surface when a candidate molecule was adsorbed was used to model

the CdSe. Binding energies of different molecular adsorbates, including pyridine (7.45 kcal mol^{-1}), phosphine oxide, (8.16 kcal mol^{-1}) and a carboxylic acid (4.93 kcal mol^{-1}) were computed. The respective binding energies for thiophene-functionalized analogues of these molecules revealed that pyridyl-functionalized thiophene had the largest binding energy (14.73 kcal mol^{-1}), indicating that a pyridyl-based ligand is a good candidate to pursue for synthetic development. As such, synthesis efforts were devoted along these lines.

The electronic structure and heats of formation of various pyridyl-MgCl·LiCl complexes were also determined using DFT calculations. These initial gas phase structures for 2- and 3-pyridyl Grignard/LiCl complexes were then placed in a simulation box with 80 THF molecules (explicit solvent) and the full system was optimized using the PM3 Hamiltonian.

3.5.3 Preparation of 2- and 3-pyridyl Grignard/LiCl complexes

LiCl (0.5002 g, 11.79 mmol), 3-bromopyridine (2.114 g, 13.35 mmol), and 10 mL of THF were added to a dry 100 mL 3-neck flask. The vessel was equipped with two Teflon stoppers, an addition funnel, and a stir bar. The solution was sparged with nitrogen for 30 min. i-PrMgCl in THF (13.4 mmol, 6.37 mL) was transferred to the addition funnel via syringe and diluted with 30 mL of THF, and then added dropwise to the reaction flask over a period of 10 min. In a matter of minutes the color of the reaction mixture changed from cloudy white to transparent maroon. The extent of reaction was monitored by GC-MS to ensure completion of metal-halogen exchange. The concentration of Grignard reagent was estimated based on the amounts of the reagents used and conversion measured by GC-MS from quenching a sample in water and extracting with hexanes. A similar procedure was used to synthesize 2-pyridylmagnesium chloride·LiCl.

3.5.4 Preparation of pyridyl-functionalized P3HT via in situ end-functionalization

In a dry 500 mL 3-neck flask, 2,5-dibromo-3-hexylthiophene (1.25 g, 3.83 mmol) was dissolved in 55 mL of THF. The reaction vessel was equipped with a stir bar, a condenser, and two Teflon stoppers. The solution was degassed with nitrogen for 30 min. i-PrMgCl (3.83 mmol, 7.8 mL) was transferred to the flask via syringe and the mixture was heated under reflux for 2 h. During this time the reaction was monitored by GC-MS to ensure complete metal-halogen exchange. Once complete, the mixture was cooled to room temperature, Ni(dppp)Cl_2 (62.9 mg, 0.116 mmol) was added, and the mixture was stirred for an additional 15 min. Then, the pyridyl Grignard (2.3 mmol) reagent was added to the mixture at 20 times molar excess relative to Ni. When monitoring the relative abundance of products having various end-groups as a function of reaction time, aliquots were periodically collected, quenched in methanol and analyzed. The final reaction mixture was precipitated into methanol. The recovered polymers were filtered into a Soxhlet thimble and washed with hot methanol and acetone then extracted with chloroform. When 1-pentene was used as an additive, it was added prior to introduction of the pyridyl Grignard reagent.

Chapter 4: Tailoring Nanoscale Organization of CdSe/poly (3-hexylthiophene) (P3HT) Blends by Ligand Modification

4.1 Abstract

A method to tailor the donor/acceptor interface of bulk heterojunction organic photovoltaic devices by modifying the surface chemistry of semiconductor quantum dots (CdSe SQDs) is described in this chapter. The ligands on CdSe SQD surfaces play an impactful role in their synthesis, solution properties and nanophase organization in a polymer matrix. In this work, I report a method to stabilize CdSe SQDs in a poly(3-hexylthiophene) (P3HT) matrix through a series of successive ligand exchanges that results in P3HT chains decorating the SQD surface. The surface ligands that were studied include dodecylphosphonic acid, pyridine, and pyridine end-functional P3HT. The pyridine end-group installed on P3HT chains has the propensity to coordinate to CdSe SQDs, thereby creating intimate contact between the donor and acceptor materials. Thin films of P3HT/CdSe blends were prepared under different annealing conditions and characterized using transmission electron microscopy and grazing incidence x-ray scattering techniques.

4.2 Introduction

The addition of nanoparticles to polymer matrices is an attractive route for creating composite materials that offer improved mechanical, optoelectronic or biomedical properties, or provide new functionality, such as the ability to self-heal. In each of these applications, the performance of the nanocomposite is dictated by the arrangement of nanoparticles in the organic polymer phase. Moreover, the choice of nanoparticle (organic versus inorganic) will have a dramatic impact on their arrangement because inorganic nanoparticles are typically immiscible with polymers.[130-131] The incompatibility of inorganic nanoparticles with polymers tends to result in segregation and

agglomeration of nanoparticles due to their van der Waals interactions. Therefore, to overcome this behavior, it is important to understand how to tailor the interactions between nanoparticles and polymers in order to develop a method that allows the nanoscale organization of the system to be controlled.

There are numerous reports in the literature that focus on developing methods to control the arrangement and distribution of inorganic nanoparticles in a polymer matrix to achieve an improvement in the corresponding nanocomposite.[3,7,9-10,35,39,50,98,107,130,132-139] For example, Hartmann and coworkers[140] mechanically rubbed poly (3-hexylthiophene)(P3HT)/CdSe nanorod (NR) thin films and found that the CdSe NRs and P3HT chains align parallel and in-plane to the rubbing direction, as evidenced by transmission electron miscroscopy (TEM) and grazing incident x-ray diffraction (GIXD). The authors suggest that the application of a mechanical force (rubbing) to manipulate arrangement can be extended to other hybrid polymer nanocomposites, perhaps leading to improved properties. In addition to mechanic rubbing, block copolymers have been shown to produce interesting arrangements of nanoparticles due to their tendency to microphase segregate.[139,141-147] Noro and coworkers[142] prepared polymer nanocomposites via hydrogen bonding of polystyrene-block-poly(4-vinylpyridine) (PS-P4VP) and hydroxyl-functionalized cadmium selenide (CdSe-OH) semiconductor quantum dots (SQDs). They demonstrated that the volume fraction of the P4VP block influences the morphology of the nanoparticles: a low volume fraction P4VP produces well-dispersed spheres while a symmetric copolymer having equal volume fractions of PS and P4VP yield a lamellae structure with the CdSe-OH nanoparticles residing in the P4VP phase. Similarly, Kramer and coworkers[139] demonstrated precise control of gold nanoparticle location in a symmetric PS-PVP block copolymer matrix by modifying the surface of

gold with the corresponding thiol-terminated homopolymers. The nanoparticles can be driven to segregate into either block domain depending on the compatibility of the surface ligands and they can also be organized at the interface between the domains if a mixture of homopolymers are used to coat the nanoparticle surfaces. Nanophase segregation of block copolymers provides heterogeneity in the form of distinct phases for templating the organization of nanoparticles, however, organizing nanoparticles in a homopolymer matrix is challenging due to the lack of compositionally distinct phases to direct self-assembly.

Grafting polymer chains to the surface of nanoparticles has been shown to improve the compatibility of inorganic nanoparticles in a nanocomposite. Emrick and coworkers demonstrated a "grafting-from" approach to prepare poly (*p*-phenylene vinylene) grafted spherical CdSe SQDs.[148] The PPV-decorated CdSe SQDs remained dispersed in the as cast film, as evidence by TEM images. However, with a grafting-from approach, the polymer chains that are bound to a surface are not well characterized, which leads to ambiguity in terms of correlating nanocomposite structures with chain properties and chain grafting density. To address this gap, end-functionalized polymers that can tether to the surface of nanoparticles can be prepared and characterized, followed by attachment of those chains via a grafting-to approach.

Modifying the interface between π-conjugated polymers and SQDs offers promise for tuning the nanoscale organization of the quantum dots in a polymer matrix for improving power conversion efficiency in hybrid organic photovoltaic devices. In particular, grafting π-conjugated polymers to the surface of inorganic nanoparticles has been extensively studied, however, the current methods have been limited by the lack of handles that can be tuned to exhibit different structures. For example, Skaff *et al.*[148] grafted PPV chains to the surface of CdSe SQDs and

studied the composite material as a binary system. With this method, the concentration of SQDs in polymer matrix was dictated by the amount of polymer that polymerized on the surface. In addition, Zhang and coworkers[7] reported the dispersion of P3HT-grated nanorods blended in a P3HT homopolymer matrix, without studying the effect of grafted chain and matrix molecular weight on the organization of nanoparticles in the polymer film. On the other hand, Akcora and coworkers[31] reported an exemplary method that demonstrated the self-assembly of spherical polymer-grafted-nanoparticles into a variety of anisotropic structures when blended with the corresponding homopolymer matrix. The authors varied the grafted chain molecular weight, grafting densities and matrix molecular weight and observed a range of exotic structures from full dispersion of the nanoparticles to arrangements that were termed "sheets" and "strings".[31] Most recently, the assembly of polymer-grafted magnetic nanoparticles in a polymer melt was investigated by Akcora and Jiao.[30] The authors found that brush-brush entanglements play a impacful role at low grafting densities, resulting in long strings of particles. For high grafting densities, the nanoparticles remained mostly dispersed with low correlation between particles. These contributions are inspiring because they demonstrate a new method for tuning the morphology of nanoparticles in a polymer matrix; however, the investigations are limited to flexible polymers (e.g. polystyrene). Although systematic studies of the role of nanoparticle size are yet to emerge, and high loadings have not been investigated, in some instances, such as hybrid photovoltaics based on SQDs,[7,10,73,148] ZnO nanoparticles,[149] and TiO_2[133] nanoparticles, nanoparticle loading ranging from 20-60 wt% is needed in order to access useful properties of polymer nanoparticle blends. Nevertheless, the work of Akcora and coworkers holds promise because it shows that the polymer-nanoparticle interactions can be tailored, which should facilitate

the use of higher nanoparticle loadings without nanoparticle aggregation dominating the morphology.

Here I adapt the concepts developed by Akcora and coworkers on polystyrene/silica nanocomposites to a system consisting of P3HT, a semiflexible conjugated polymer, and CdSe nanoparticles. Specifically, the CdSe SQDs are modified by tethered P3HT ligands and then blended in a P3HT matrix leading to stable dispersions of nanoparticles. To accomplish thisCdSe SQDs were grafted with pyridine-functionalized P3HTs (pyr-P3HTs) and then dispersed in a P3HT matrix. The concentration of SQDs remained constant at 25 mass % and the molecular weight of the pyr-P3HT ligand and the P3HT matrix was varied from 5-14 kDa and 6.5-14 kDa, respectively. Thermal gravimetric analysis and UV-vis spectroscopy were used to investigate the P3HT-decorated CdSe SQDs before dispersing them into the matrix P3HT. The morphology of ternary blends of P3HT-decorated CdSe-SQDs in P3HT was investigated using small angle x-ray scattering and transmission electron microscopy techniques. Pyridine-decorated CdSe SQDs were also blended with both P3HT matrix polymers as controls. The P3HT-decorated CdSe SQDs in a P3HT matrix were well-dispersed upon casting and remained well-dispersed even after 24 h of annealing at 150 ^{o}C.

4.3 Results and Discussion

As discussed in Chapter 3, transmission electron microscopy was used to investigate how dodecyl phoshponic acid (DPA), pyridine, and pyridine-functionalized P3HT-decorated CdSe SQDs organize in a 25 kDa matrix of P3HT. (I will refer to the pyridine-functionalized P3HT as pyrP3HT.) I found that the pyrP3HT-decorated SQDs were well-dispersed in the matrix when

drop cast in a thin film. It was also found that the dispersion of the pyr-P3HT-decorated CdSe SQDs was stabile after 2 h of thermal annealing at 150 ^{o}C. Therefore, grazing incidence wide-angle x-ray scattering (GI-WAXS) techniques were used to examine the morphology of the thin films containing surface-modified CdSe SQDs blended with a P3HT matrix. Figure 4-1 shows GI-WASXS patterns that were acquired for thin films of DPA-CdSe, pyridine-CdSe, and pyrP3HT-decorated CdSe SQDs that were each blended with a 25 kDa P3HT matrix and thermal annealed at 150 ^{o}C for 2 h. The GI-WAXS patterns for a thin film of DPA-decorate CdSe SQDs (Figure 4-1a) and the P3HT matrix polymer (Figure 4-1b) used for these studies are also shown. It is noted that the grazing incidence diffraction pattern shown in Figure 4-1a indicates that the CdSe SQDs are organizing in a hexagonal close packed structure. The scattering patterns observed for the samples that contain a P3HT matrix polymer look very similar to one another, however, in the low q region (surrounding the main beam), vast difference are observed. For example, the P3HT matrix pattern (Figure 4-1b) does not have much scattering in the low q region, whereas intense scattering is observed in the low q regime in Figures 4-1c-e. The scattering intensity in the low q regime is due to presence of CdSe SQDs and how they organize in the P3HT matrix. Interestingly, the angular intensity of the Bragg diffraction peaks from the edge-on stacking of P3HT chains changes between samples. This suggests that the surface modified CdSe SQDs affect the orientation the P3HT crystallites that are forming in the film. The x-ray scattering experiments shown here constitute a set of preliminary results that motivated the remainder of the experiments described in this chapter. Specifically and as described in this chapter, I investigate how changing the P3HT ligand and matrix molecular weight affect the organization of nanoparticles in thin films using TEM and GI small-angle x-ray scattering. The GI-SAXS technique provides better

resolution of the low q regime, which gives information about the organization of the CdSe SQDs.

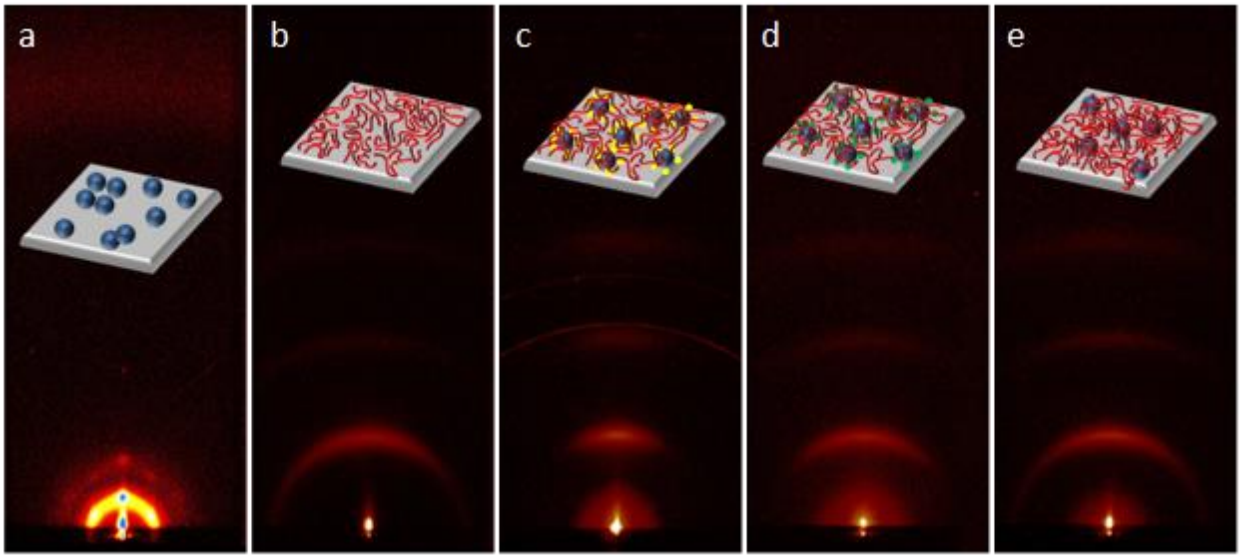

Figure 4-1. The GI-WAXS patterns for films of a) CdSe-DPA, b) P3HT matrix, c) CdSe-OA blended with P3HT matrix, d) CdSe-Pyr blended with P3HT matrix and 3) CdSe-P3HT blended with the P3HT matrix. The low angle scattering is due to the CdSe in the P3HT film, while the halos at higher angle are from Bragg diffraction of the P3HT crystals that form in the thin film.

4.3.1 Decorating SQDs with pyridine-functionalized P3HT

The ability to prepare monodisperse, crystalline CdSe SQDs with good control over their size and shape relies on the use of coordinating solvents.[32] The role of the coordinating solvent is to passivate the surface of the CdSe SQDs and prevent agglomeration.[32] Initially, trioctylphosphine oxide (TOPO) combined with other aliphatic surfactant co-solvents were used because the high boiling points facilitate the high-temperature synthesis of the CdSe nanocrystals.[32] New synthetic

methodologies were later pursued, which led to the use of oleic acid (vegetable oil) as a solvent to prepare CdSe SQDs in a more "green" fashion.[150] Because the coordinating solvent used to prepare CdSe SQDs must be able to withstand high temperatures and must have a high affinity to bind the newly formed SQDs, the solvothermal preparation technique is limited to the coordinating solvents that were previously mentioned. Therefore, in order to create SQDs modified with polymeric ligands, a ligand exchange process to displace the coordinating solvent molecules on pre-synthesized SQDs is needed.

CdSe SQDs were decorated with pyridine-functionalized P3HT ligands having molecular weights of 5 and 14 kDa as determined by SEC relative to polystyrene standards. The P3HT-decorated CdSe SQDs were prepared by a grafting-to approach involving two consecutive ligand exchange steps, which are depicted in Scheme 4-1. Because pyridine has a lower binding affinity for CdSe than OA, the OA ligands must be removed by bombarding the SQDs with neat pyridine. First, the native OA-coated CdSe SQDs were precipitated from a toluene solution using ethanol, followed by centrifugation and decanting to remove the supernatant. Then, anhydrous pyridine was added to reconstitute the OA-CdSe SQDs. The OA ligands were displaced with pyridine, forming the pyridine-decorated CdSe intermediate after 24 h of heating at 60 ^{o}C as evidence by quenching of their photoluminescence that was visually observed by viewing the SQDs under a 365 nm UV light. (See Appendix D.) In a second ligand exchange step, the small molecule pyridine ligands are replaced with macromolecular pyridine-functionalized P3HT ligands, which was demonstrated in our previous work.[35] For this step, pyridine-decorated CdSe SQDs in pyridine were added to a solution of pyridine-functionalized P3HT in $CHCl_3$ and the mixture was heated to 60 ^{o}C to facilitate the exchange. After allowing 1 week for the exchange to take place,

the mixtures were dried under with N_2 to remove $CHCl_3$ and any remaining pyridine and then reconstituted in $CHCl_3$, yielding a solution of P3HT-decorated CdSe SQDs.

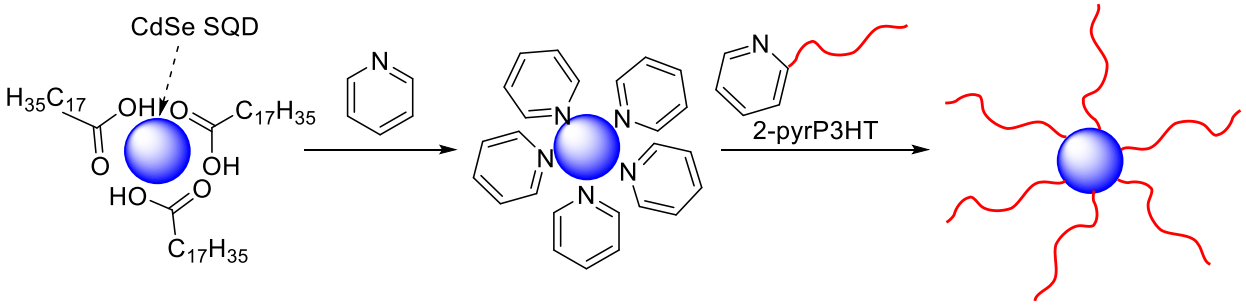

Scheme 4-1. Ligand exchange process used to prepare P3HT-decorated CdSe SQDs.

4.3.2 UV-Vis spectroscopy of surface-modified CdSe SQDs

The optical absorbance spectra for the P3HT-decorated CdSe SQDs and the individual components are shown in Figure 4-2. The absorption maximum at the band edge for pyridine-decorated CdSe SQDs, which indicates the size of the SQDs, appears at 590 nm, and corresponds to an average SQD diameter of 4.2 nm.[32] The absorption maximum of the 5kDa pyrP3HT in chloroform (designated in the text as $P3HT_5$) is at 444 nm whereas the absorption maximum of $P3HT_{14}$ in chloroform is slightly red shifted to 453 nm. This suggests that the conjugation length of the pristine pyridine-functionalized P3HT increases with P3HT molecular weight. After coordinating to SQDs, the absorption maxima for $P3HT_5$- and $P3HT_{14}$-decorated CdSe SQDs blue shift from 444 to 425 nm and from 453 to 446 nm, respectively. I believe that the blue shift can be explained by the interactions and packing of the P3HT chains: In both cases, the P3HT chains

go from a somewhat aggregated state in solution to a surface constrained state when grafted to the SQDs. This confinement effect makes it difficult for the P3HT chains to pack due to intermolecular interactions, which results in the blue shift observed in the absorbance spectra. The blue shift is more pronounced for SQDs decorated with the low molecular weight P3HT chains ($P3HT_5$) because the shorter chain length restricts motion when confined to the surface due to the semiflexible chain having fewer Kuhn steps. However, the higher degree of polymerization of $P3HT_{14}$ provides additional conformational freedom that enable π-π intermolecular interactions to drive aggregation of the chains even when one end is tethered to the SQD surface. In addition to the blue shifts, it is apparent that the absorbance spectrum of the P3HT-decorated SQDs is the sum of the absorption spectra of their constituent materials.

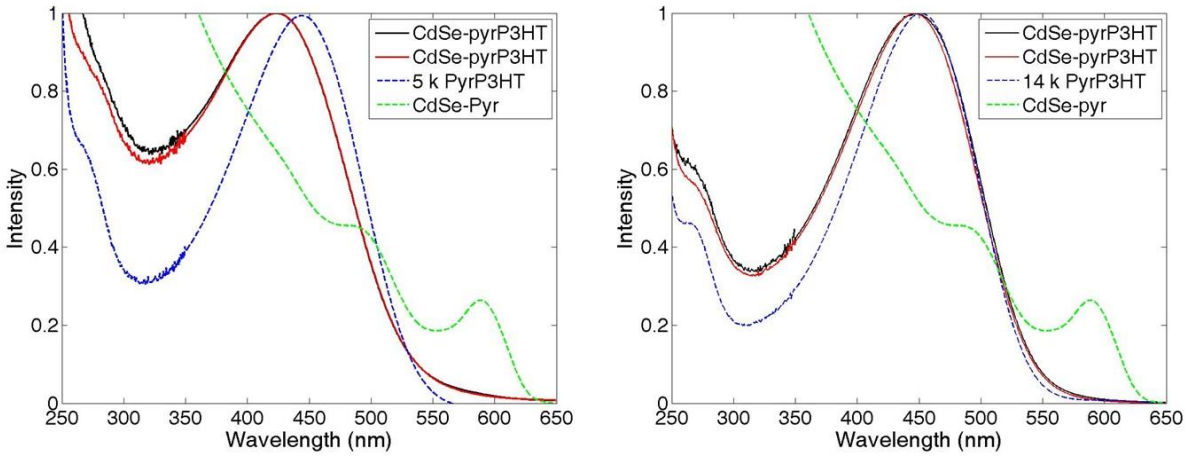

Figure 4-2. Optical absorbance spectra for CdSe-pyr intermediate (green dashed line), pyridine-functionalized P3HTs (dashed blue line), and P3HT-decorated CdSe (solid lines).

4.3.3 Thermal gravimetric analysis of surface-modified CdSe SQDs

Thermal gravimetric analysis was used to evaluate the P3HT-decorated CdSe SQDs. The thermal gravimetric profiles of $P3HT_5$ and $P3HT_{14}$ homopolymers indicate an onset of degradation between 380-440 ^oC, and char yields of 23 and 28% respectively, as shown in Figure 4-2. These char yields are comparable to values reported by Emrick and coworkers.[7] As expected, the P3HT-decorated CdSe SQDs exhibited a significant mass loss from 350-500 ^oC, due to degradation of the P3HT chains covering the CdSe SQDs. Interestingly, the degradation of the CdSe nanocrystals depends on the type of ligand modifying the surface. The onset of degradation of CdSe occurs around 650-700 ^oC when the surfaces are grafted with P3HT chains, but the onset of degradation of CdSe occurs around 900-950 ^oC when the SQDs are ligated with pyridine. Also, the rate of CdSe degradation is much slower for the SQDs decorated with higher molecular weight P3HT chains. The results obtained from UV-vis and TGA suggest that the CdSe SQDs are modified by the pryP3HT ligands; however, blending the P3HT-decorated CdSe SQDs with a P3HT matrix should provide more insight on the interaction between the CdSe SQDs and P3HT.

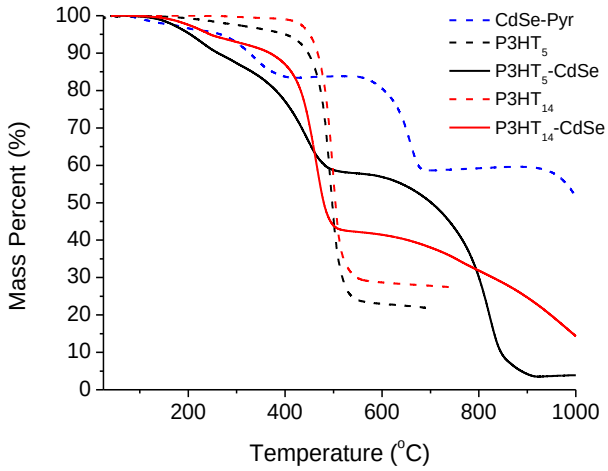

Figure 4-3. Mass loss obtained by thermal gravimetry of Pyr-CdSe, $P3HT_5$, $P3HT_5$-CdSe, $P3HT_{14}$, and $P3HT_{14}$-CdSe. All of these experiments were performed under an N_2 atmosphere.

4.3.4 Transmission Electron Microscopy

To investigate how the molecular weights of the P3HT ligands and P3HT matrix affect the dispersion of CdSe nanoparticles in a thin film, the P3HT-decorated CdSe SQDs were blended with two different molecular weight P3HT matrix polymers. The P3HT ligand, P3HT matrix, and ligand to matrix ratio (L/M) for the various composites made here are recorded in Table 4-1.

Table 4-1. Molecular characteristics and L/M for the various composites.

Composite	Ligand (M_n RI-SEC)	Matrix (M_n RI-SEC)	L/M
5L-6.5M	5 000	6 500	0.77
5L-26.2M	5 000	26 200	0.19
14L-6.5M	13 800	6 500	2.12
14L-26.2M	13 800	26 200	0.52
pyrL-6.5M*	-	6 500	-
pyrL-26.2M*	-	26 200	-

*Pyridine-decorated CdSe SQDs (pyrL) were blended with each P3HT matrix as a control sample.

Based on the work of Akcora and coworkers,[30-31] blending PS-grafted spherical nanoparticles in a polystyrene matrix leads to the formation of a variety of anisotropic structures. They reported that when the ligand to matrix molecular weight ratio (L/M) is large (3-4) at high grafting densities (0.1 chains/nm^2), the PS-grafted nanoparticles are dispersed in the polymer matrix. On the other hand, when the L/M ratio is small (< 1) and the grafting density is low (0.01 chains/nm^2), the polymer-grafted nanoparticles agglomerate into large spherical aggregates. However, PS is a flexible polymer whereas P3HT is described as being much more rigid due to the intermolecular interactions and rigid thiophene ring structure of the backbone. Therefore, studying the arrangement of P3HT grafted CdSe SQDs in a P3HT matrix will provide fundamental insight into the structure-property relationships that exists when semi-flexible polymer-grafted nanoparticles are dispersed in a matrix comprised of semi-flexible polymers. For this study and as reflected in Table 4-1 the P3HT-decorated CdSe SQds blended in P3HT matrix polymers have L/M values of 0.19 0.52, 0.77, and 2.12.

The arrangement of CdSe nanoparticles in the P3HT matrix was imaged using TEM. The films, made by drop casting 0.2 wt % solutions from $CHCl_3$, are on carbon-coated copper grids. Figure 4-4 displays in two vertical columns TEM images of the nanocomposite blends and particle distribution analyses that were acquired from each of the P3HT-grafted nanocomposites as cast (Figure 4-4, left column) and after 24 h of thermal annealing at 150 ^oC (Figure 4-4 ,right column). The nanocomposites were also imaged after 8 and 16 h of thermal annealing at 150 ^oC and those images are given in the Appendix D. It should be noted that the high electron density of the CdSe SQDs provides excellent contrast when imaging P3HT/CdSe films by TEM. The images and particle size analyses show that the P3HT-decorated CdSe SQDs remain dispersed for all L/M values, even after 24 h of thermal annealing at 150 ^oC. The histograms in Figure 4-4, which are frequency distributions of the number of particles per aggregate, show that the number of particles per aggregate does not change significantly as matrix and graft molecular weights are changed and as the samples are subjected to thermal annealing. It is worth noting that replicate TEM samples were not made for this study. In fact, the same TEM grids were imaged and thermally annealed successively over the range of annealing times, which demonstrates the stability of the films. This provides the ability to obtain sets of images that reflect how the morphology evolves during the thermal annealing process, and those figures (see Appendix D) demonstrate the stability of the nanoparticle dispersions. Although TEM allows the dispersion of P3HT-grafted CdSe in P3HT matrices to be imaged directly, grazing incidence small angle x-ray scattering (GI-SAXS) was also used to investigate the organization of nanoparticles in the thin films.

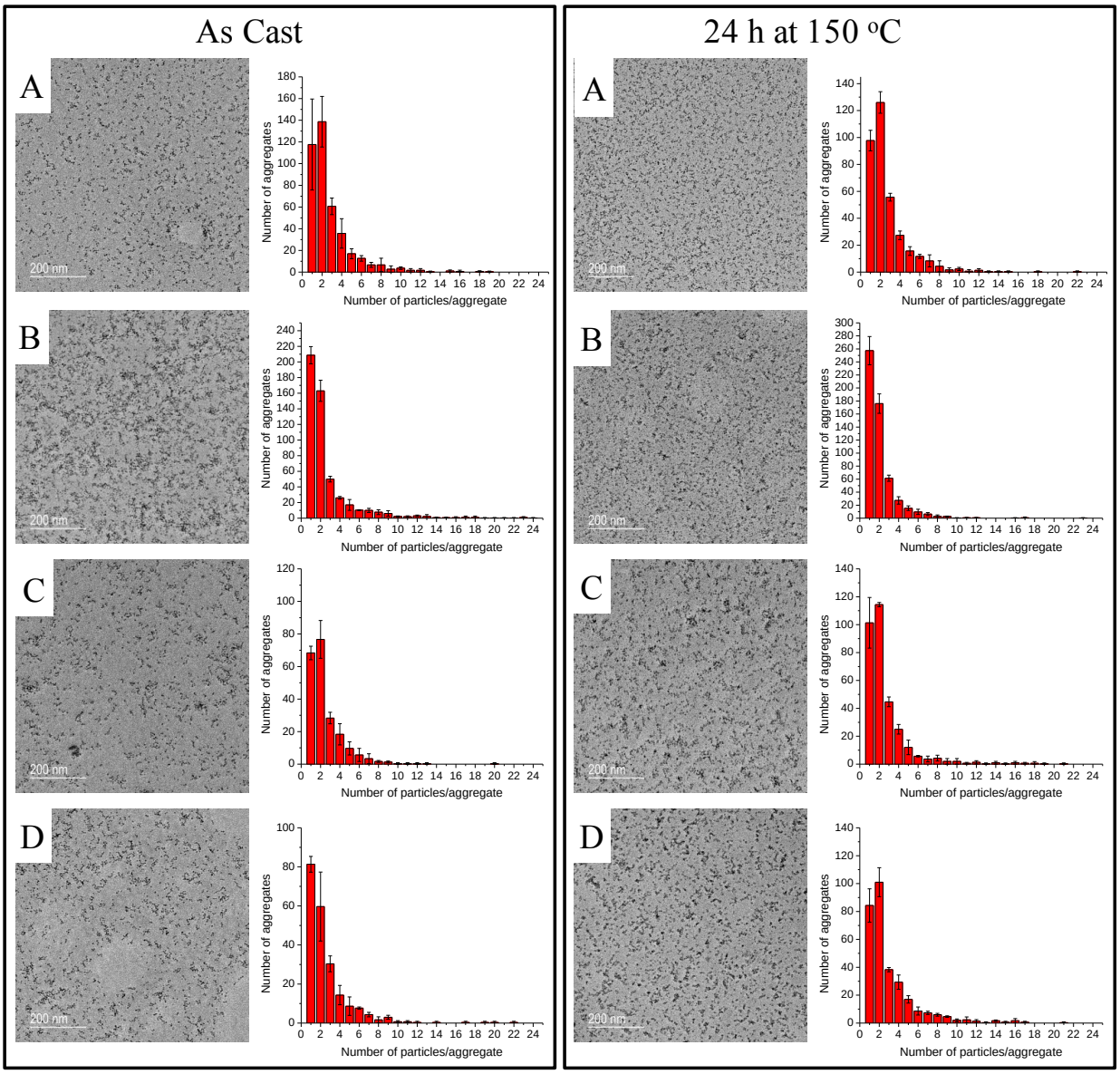

Figure 4-4. TEM images and the resulting particle distribution analysis showing that the number of particles/aggregate as a function of the number of aggregates remains constant even after 24 h of thermal anealing.

4.3.5 Grazing-incidence small-angle x-ray scattering of nanocomposites

The in-plane GISAXS curves for the as-cast and annealed films of surface-modified CdSe SQD mixtures were fit using a combined model of Schulz sphere[151] and power-law model as exemplified in Figure 4-5. In this combined model, the Schulz sphere model represents the scattering due to the spherical CdSe quantum dots that are dispersed in the P3HT matrix and the power-law model accounts for the scattering of crystalline P3HT domains surrounded by amorphous P3HT chains. The combined model is expressed as

$$I(Q_{xy}) = f_{s1}\int_0^\infty f(R)R^6F^2(Q_{xy}R)dR + f_{s1}Q_{xy}^{-n} + B \quad (1)$$

where f_{s1} and f_{s2} are the scale factors, n is the power-law exponent and B is the incoherent scattering background. R is the average radius of the sphere (quantum dots) and Q_{xy} is the in-plane momentum transfer of the scattered X-ray beam, which is given by $Q_{xy}=(4\pi/\lambda)\sin\theta_{xy}$ with θ_{xy} being one-half of the in-plane scattering angle. $f(R)$ is the normalized Schulz distribution of R and $F(Q_{xy}R)$ is the scattering amplitude of spheres having radius R. $F(Q_{xy}R)$ is given by,[152]

$$F(Q_{xy}R) = \frac{3[\sin(Q_{xy}R) - Q_{xy}R\cos(Q_{xy}R)]}{(Q_{xy}R)^3} \quad (2)$$

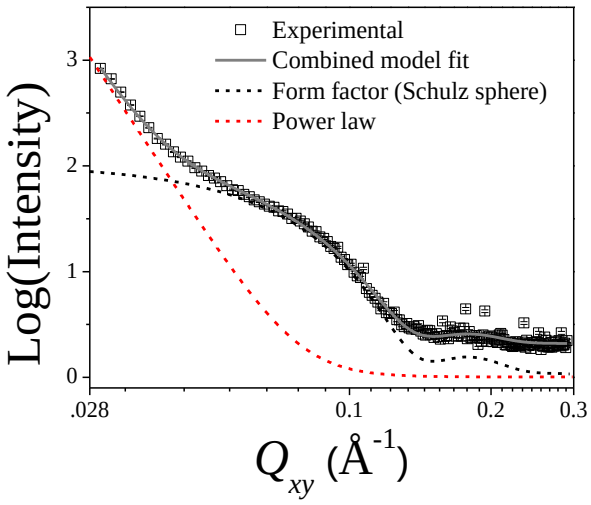

Figure 4-5. Example showing the models used (individual and combined) to fit the in-plane GI-SAXS measured for composites containing 25 wt % CdSe in P3HT. Here, the circularly averaged in-plane scattering was extracted from the 2D GISAXS pattern for the as-cast film of 5L-6.5M and fit using the combined model shown in Equation (1).

Figure 4-6a and 4-6b show the experimental in-plane GISAXS curves for as-cast and annealed P3HT and 5L-6.5M films. The GISAXS curves for the as-cast and annealed 5L-6.5M films were fit using Equation (1) and the results are shown in Figure 4-6. Also, the out-of-plane GIWAXS patterns for the as cast and annealed films, which show the (100) reflection due to crystallization of P3HT chains, are depicted in the insets of Figure 4-6a and 4-6b. As seen in Figure 4-6a, the scattering curves acquired for the as-cast and annealed P3HT films merely exhibit monotonic decays without Guinier regime scattering (leveling-off in slope in the low-Q_{xy} region). The absence of Guinier scattering regime implies that the P3HT crystals are large beyond the detection limit of the GISAXS set-up used. (The Guinier regime is $Q_{xy}R << 1$.) Although the size of the

P3HT crystals could not be determined due to instrumental limitation, the scattering curve of the annealed P3HT film is shifted toward the lower-Q_{xy} region in comparison to that of as-cast P3HT film. This behavior might indicate that thermal annealing induced the growth of P3HT crystals. Clearly, the increased crystallinity as a result of growth of P3HT crystals manifests in the inset GIWAXS patterns, where the (100) reflection intensifies as a result of the thermal annealing. One of the notable scattering features that can be seen by comparing 5L-6.5M and as-cast P3HT films is the bulged scattering shoulder observed at approximately Q_{xy}=0.095 $Å^{-1}$. The scattering shoulders were due to the form factor of isolated CdSe spheres, which is gives an R = 29.9 Å and polydispersity, p_R= 0.12. The CdSe R obtained from the model fits remains unchanged by thermal annealing (over 24 h of thermal annealing) and the size resulting from the fit are consistent with the radii obtained by TEM imaging and UV-vis data. The ability of the scattering to be described by a form factor of single CdSe SQDs and the absence of any noticeable correlation peak or need for adding another form factor associated with CdSe SQD clusters implies that CdSe SQDs are well dispersed in the P3HT matrix without correlation (interaction between quantum dots). Films of 5L-26.2M, 14L-6.5M and 14L-26.2M exhibit, more or less, the same characteristics in their GISAXS patterns leading to similar fitting results as films of 5L-6.5M. (See Appendix D.) Those similarities imply that the P3HT-grafted CdSe SQDs are well-dispersed (isolated and uncorrelated) in the CdSe SQDs at all of the L/M and graft and matrix molecular weights examined.

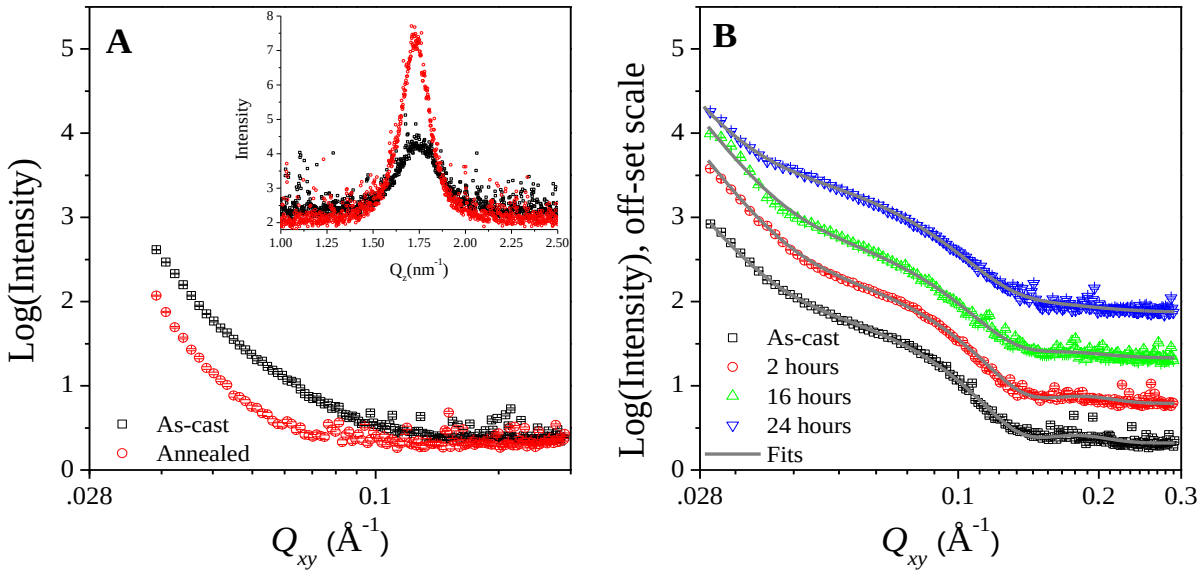

Figure 4-6. In-plane GISAXS curves and model fits for films of 26.2M (left) and 5L-6.5M (right). Each of the scattering curves result from the circularly averaged in-plane scattering for each film, which are extracted from the corresponding 2D GI-SAXS patterns.

In the case of pyrL-6.5M and pyrL-26.2M films, however, the change in the in-plane GISAXS patterns are somewhat different from those obtained for 5L-6.5M, 5L-26.2M, 14L-6.5M and 14L-26.2M as shown in Figure 4-7. In Figure 4-7, it is noted that the scattering becomes more intense at q~0.1 A^{-1} for the as-cast films of pyrL-6.5M and pyrL-6.3M, but only power law scattering is noticeable in the GISAXS curve for the annealed films. These results suggest that the CdSe SQDs are well-dispersed in the as-cast pyrL-6.5M and pyrL-26.2M films, but aggregate after thermal annealing at 150 ^{o}C for 2 h. It can be implied that the form factor of CdSe SQDs overlaps with the form factor of CdSe SQD clusters, which are larger in size and hence more intense in scattering.

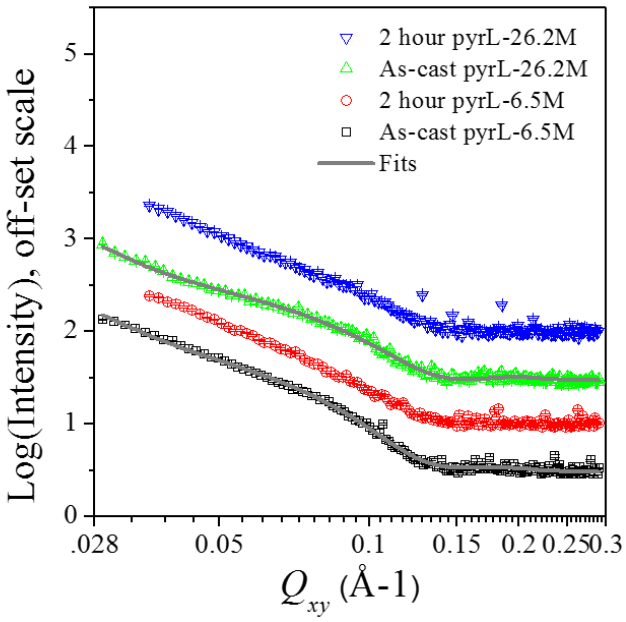

Figure 4-7. In-plane GISAXS curves and model fits for films of pyrL-6.5M and pyrL-26.2M.

4.4 Conclusions

The work described in this chapter demonstrates the utility of grafting P3HT chains to CdSe SQDs as a method to improve their dispersion in P3HT matrices. Grafting P3HT chains to the surface of CdSe SQDs changes the optoelectronic and degradation behaviors of the corresponding composites. UV-vis spectroscopy measurements show a blue shift in the absorption maxima of P3HT when grafted to CdSe SQDs due to a decrease in intermolecular interactions resulting from tethering (constraining) the P3HT chains. This blue shift is more pronounce for the lower molecular weight P3HT grafts. In addition, the CdSe SQDs degrade at a much lower temperature (650 ^{o}C) when grafted with P3HT as compared to pyr-decorated CdSe SQDs (900 ^{o}C). Also, CdSe SQDs grafted with high molecular weight P3HT chains tend to degrade at a much slower rate. It

is noteworthy that even with high concentrations of CdSe SQDs (25 mass %) in a P3HT matrix, the P3HT-decorated CdSe SQDs remain dispersed in the thin films, even after thermal annealing for up to 24 h at 150 ºC, independent of ligand and matrix molecular weight. This work is promising because it shows that large-scale aggregation of CdSe SQDs in P3HT can be eliminated. This should translate to an improvement in charge separation of hybrid organic photovoltaic devices, a hypothesis that can be examined by making devices and testing their performance.

4.5 Experimental

4.5.1 Materials

Pyridine functionalized P3HTs were prepared according to methods described in Chapter 3. The molecular characteristics of the pyrP3HTs as well as "plain" P3HTs with H/Br end groups are reported in Table 4-2.[35] Chloroform (Drisolv, EMD), pyridine (Drisolv, EMD), benzene (Drisolv, EMD), hexanes (>99.8%, Aldrich) and ethanol (>99.8%, Aldrich) were used as received. Oleic acid-covered cadmium selenide nanoparticles (~5 nm) were prepared by the Rosenthal research group at Vanderbilt University. Silicon wafers of size 1 × 1.2 cm (Silicon Quest) were cleaned with piranha acid, rinsed with nanopure deionized water and dried thoroughly with N_2 prior to use.

Table 4-2. Molecular weight and polydispersity, obtained by RI-SEC of P3HTs used.

Sample	M_n	M_w	PDI
6.5 k P3HT	6 500	8 600	1.31
25 k P3HT	26 200	31 600	1.20
5 k Pyr-P3HT	5 000	6 300	1.23
14 k Pyr-P3HT	13 800	15 000	1.09

4.5.2 Characterizations

Size exclusion chromatography (SEC) was performed using a Waters Alliance 2695 Separations Module equipped with three Polymer Laboratories PLgel 5 μm mixed C columns (300 × 7.5 mm) in series in THF at 1.0 mL/min and 35 °C. The RI detector (Waters model 2414) was used to determine molecular weight relative to polystyrene standards. MALDI-TOF MS spectra were collected using a Bruker Daltonics Autoflex II mass spectrometer, which is equipped with a N2 laser, (λ = 337 nm) operating at a frequency of 25 Hz and an accelerating voltage of 20 kV. trans-2-[3-(4-tert- Butylphenyl)-2-methyl-2-propenylidene]malononitrile (DCTB) (>99%, Fluka) was used as the matrix. Solutions of DCTB (20 mg/mL) and the analyte (10 mg/mL) were prepared in THF and then mixed in a 10:2 ratio. A volume of 1 μL was applied to the target via the dried droplet method.36 Mass spectra were collected in reflectron mode, and the instrument was externally calibrated with polystyrene standards. UV-Vis absorption spectra were recorded using a Cary 5000 spectrometer.

Grazing incidence x-ray scattering measurements were performed on an Anton Paar SAXSess mc^2 instrument equipped with a multipurpose VarioStage. The diffracted beam was recorded on either an imaging plate (Multisensitive Storage Phosphor) that was read using a Perkin Elmer

Cyclon® 2D imaging plate reader for WAXD, or a CCD detector (Princeton Instruments, 2084 x 2084 pixels array with 24 x 24 μm² pixel size) for SAXS data. The x-ray diffraction (XRD) measurements were performed on a PANalytical X'Pert Pro MPD equipped with an X'Celerator solid-state detector. For the GIWAXS and XRD measurements, X-rays were generated at 45 kV/40 mA and 40 kV/50 mA, respectively, and X-ray beam wavelength was 1.541 Å (Cu Kα radiation). Polymer thin films were prepared by drop casting solutions of ligated CdSe nanocrystals blended with a P3HT matrix onto silicon substrates. The prepared polymer films were analyzed using a 2θ scan from 3º-25º with an omega offset of 1.5º.

Images of P3HT/CdSe blends were acquired using a Zeiss Libra 120 TEM at 120 kV. The samples for TEM were prepared by dropcasting a 0.2 wt % solution of surface-modified CdSe SQDs blended with a P3HT matrix from $CHCl_3$ onto amorphous carbon-coated copper grids (400 mesh, Ted Pella).

4.5.3 Ligand exchange protocol used to prepare P3HT-decorated CdSe

A typical ligand exchange began when OA-CdSe (10 ml, 2.52×10^{-6} mol) in toluene was precipitated using a minimal amount of ethanol (~15 mL) and then centrifuged. The supernatant was decanted off and then anhydrous pyridine (~10 mL) was added. The mixture was heated to 60 ºC for 24 h to yield the pyridine-CdSe. Next, the suspension of pyr-CdSe (500 μL, 7.3×10^{-8} mol) in pyridine was added to a 20 mL scintillation vial and dissolved in 5 mL of $CHCl_3$. The pyridine-functionalized P3HT (0.01825 g, 7.3×10^{-6} mol) was added to the pyr-CdSe solution and heated to 40 ºC to fully dissolve the polymer. Then, the mixture was dried with N_2 and then reconstituted in 5 mL of $CHCl_3$. The solution was heated to 60 ºC for 1 week, after which the

solvent was removed by evaporation with N_2 until the material was dry.

4.5.4 Solution and film preparation

The P3HT-decorated CdSe SQDs were re-dissolved in $CHCl_3$ to make a solution that was 0.2 wt % total solid concentration. Before adding the matrix P3HT, a 0.5 mL aliquot of each solution was reserved for UV-vis and TGA experiments. Next, the matrix P3HT (predissolved in $CHCl_3$) was added to the P3HT-decorated CdSe SQDs and mixed thoroughly. Once more, the $CHCl_3$ solvent was removed and films were dried. Finally, the mixtures were re-dissolved in $CHCl_3$ to make solutions that were 0.2 wt % total solids for drop casting.

Thin films of surface-modified CdSe SQDs blended with a P3HT matrix for x-ray scattering measurements were prepared by drop casting from 0.2 wt % $CHCl_3$ solutions onto silicon wafers that had been freshly cleaned using piranha acid. Using AFM imaging and the scratch test method, films thicknesses were measured to be approximately 300-400 nm. The P3HT thin films on silicon wafers were stored in a vacuum oven, wrapped in aluminum foil, to preserve the samples (minimize light exposure, oxygen, and water vapor).

Chapter 5: Summary, Conclusions and Future Work

The ability to formulate structure-property relationships that describe the behaviour of polymeric systems hinges on the preparation of well-defined materials, and oftentimes this demands creative routes to overcome synthetic challenges. The work described in this dissertation exemplifies this notion. My work demonstrates a general, one-pot method that enables improved control of end-group functionality and composition in P3HTs prepared by GRIM polymerization followed by *in situ* quenching. Additives such as 1-pentene and styrene are shown to decrease the amount of difunctional P3HT produced, and in some cases there are significant decreases in the amount of difunctional products and an increase in the yield of the monofunctional P3HT product. My studies point to the idea that the additive interacts with the Ni^0 complex, preventing oxidative addition at the α-chain end, which suppresses formation of difunctional P3HTs. The addition of LiCl during the entire GRIM polymerization results in a greater decrease in difunctional P3HT as compared to cases where LiCl is present only during the functionalization by in situ quenching with a Grignard reagent. When functionalization (quenching) with tolyl-magnesium-bromide is done at 0°C in the presence of both LiCl and styrene, the monofunctional, tolyl-terminated P3HT is observed in 72% yield and the difunctional P3HT (tolyl groups at both chain ends) decreases to 20%. This represents a significant improvement because quenching with tolyl-magnesium bromide alone results exclusively in difunctional product.

Perhaps more importantly, my work shows that this use of additives is a general strategy that can be extended to synthesize other well-defined, end-functional P3HTs by changing the quenching reagent. This advance provides the ability to prepare (nearly-)monofunctional materials for fundamental studies that link macromolecular design of the conjugated polymer to structure and function in organic photovoltaic devices and organic LEDs. Additional optimization or

exploration of other additives offers the potential to completely deactivate the Ni^0 complex after a single addition of a functional end-group, which would result in the exclusive synthesis of monofunctional P3HTs.

My thesis work also makes use of and demonstrates the utility of a "materials by design" approach, wherein theory, modeling, simulation is used to guide the selection of the synthetic target molecules. Here theory, modelling and simulation pointed to pyridine end groups as useful for ligating CdSe semiconductor quantum dots, which can be used to rationally design materials for optoelectronic applications. This combination of synthetic capability and calculation-guided identification of a synthetic target is brought to-bear to enhance end-group control in P3HTs prepared by the GRIM polymerization and allow heteroaromatic end-groups with useful functionality to be incorporated. Specifically, pyridyl-functionalized P3HTs with a high degree of monofunctionality have been prepared by quenching the GRIM polymerization with 2- and 3-pyridyl Grignard reagents. As anticipated, diffusion of the Ni^0 complex and differences in the relative reactivity of the 2- and 3-pyridyl Grignard reagents leads to a mixture of products, including monofunctional, difunctional and unfunctionalized P3HT. The addition of 1-pentene, which interacts with Ni^0 and prevents oxidative addition at the α-chain end, increases the abundance of monofunctional products from 29% to 48% and from 36% to 56% when 2-pyridyl-MgCl·LiCl and 3-pyridyl-MgCl·LiCl are used as the quenching reagent, respectively. Pyridyl-functionalized P3HTs were used as ligands to decorate CdSe SQDs and shown to stabilize the morphology of the CdSe/P3HT blends after thermal annealing at 150 °C for 2 h. This suggests that the pyridyl-functionalized P3HTs have the potential to improve hybrid organic photovoltaic devices by providing a way to manipulate blend morphology and by possibly creating intimate

contact between the donor and acceptor phases in a bulk heterojunction thin film.

The influence of P3HT ligand and P3HT matrix molecular weights on the dispersion of P3HT-decorated CdSe in a thin film was also investigated. Thermal gravimetric analysis and UV-vis spectroscopy were used to investigate the P3HT-decorated CdSe SQDs before dispersing them into a matrix. The absorption maxima of P3HT exhibited a blue shift when P3HT chains were grafted to CdSe SQDs, and the shift was more pronounced when the lower molecular weight P3HTs were tethered due to fewer Kuhn steps for lower molecular weight P3HTs resulting in lower flexibility, which decreases conformation freedom of P3HT chains leading to a decrease in chain ordering when in a surface constrained state. In addition, the CdSe SQDs degrade at a much lower temperature (650 °C) when grafted with P3HT as compared to pyridine-decorated CdSe SQDs (900 °C). Also, CdSe-SQDs grafted with high molecular weight P3HT chains tend to degrade at a much slower rate. The P3HT-decorated CdSe SQDs were blended with the different P3HT matrices to examine the organization of the P3HT-decorated SQDs at various ligand-to-matrix molecular weight ratios (L/M), including L/M values of 0.19, 0.56, 0.77, and 2.12. Preliminary GIWAXS studies suggest that the P3HT CdSe SQDs are not well order in the polymer film, however, an intense halo is observed in the low q regime. To provide better resolution and access to the low q regime, GISAXS was used to study the organization of CdSe SQDs in a P3HT film. The GISAXS data suggest that the scattering in the low q-regime is due to the form factor of the CdSe SQDs. For all L/M ratios examined, the GISAXS data acquired for nanocomposites containing P3HT-decorated CdSe SQDs and P3HT chains could be modelled using a Schulz sphere plus a power law function. This modelling yielded a length scale of 2.9 nm corresponding to the radius of the CdSe SQDs. The fact that the scattering is dominated by single spheres plus

scattering due to the chains suggests that the nanoparticles are mostly isolated (dispersed) in the thin film. However, when pyridine-decorated CdSe SQDs are blended in the same P3HT matrix polymers and cast into thin films, the nanoparticles are dispersed initially but become aggregated upon thermal treatment at 150 °C for 2h, which is evidenced by the disappearance of a bulge in the scattering around q = 0.1. It is noteworthy that even with high concentrations of CdSe SQDs (25 mass %) in a P3HT matrix, the P3HT-decorated CdSe SQDs remain dispersed in the thin films after thermal annealing for up to 24 h at 150 °C. The P3HT-decorated CdSe SQDs are well dispersed in the 6.5 kDa and 26.2 kDa P3HT matrices, and they remained dispersed even when annealed for 24 h at 150 °C. A series of GIWAXS experiments should be performed in order to compare the changes in P3HT crystallinity upon thermal treatment of these films. Another way to advance this work would be to include studies that characterize electronic properties of these thin films. Studies that specifically examine device performance as a function of L/M and particle loading levels may be insightful.

Due to the modularity of the approach, it would be interesting to prepare different types of end-functional P3HTs that coordinate CdSe SQDs and study the morphology of the corresponding films. Understanding trade-offs between the ligation strength and the surface density of grafted chains may provide insight that helps guide the design of polymer-decorated nanoparticle systems. Also, studying a broader range of ligand and matrix molecular weights may prove to be insightful because based on the work of Akcora and coworkers, interesting morphologies resulting from the trade-offs between the ability of the grafted chains to stabilize the SQD surface and the ability of the matrix chains to wet the tethered chains may prove to be a useful way to manipulate morphology. However, it may prove to be challenging to prepare well-defined (nearly-)

monofunctional P3HTs of high molecular weight due to the limited solubility of P3HT and the increased difficulty of thorough characterization of high molecular weight samples. Finally, while we targeted the synthesis of monofunctional P3HTs so that each chain would have single-point attachment to the SQD surface, it might be interesting to explore difunctional chains to see if "bridging" would, in fact, be problematic to efforts to manipulate the morphology by changing graft chain molecular weight, tethering density and matrix chain molecular weight.

List of References

1. Andersson, M. R.; Thomas, O.; Mammo, W.; Svensson, M.; Theander, M.; Inganas, O., Substituted Polythiophenes Designed for Optoelectronic Devices and Conductors. *J. Mater. Chem.* **1999**, *9*, 1933-1940.
2. Huynh, W. U.; Dittmer, J. J.; Libby, W. C.; Whiting, G. L.; Alivisatos, A. P., Controlling the Morphology of Nanocrystal-polymer Composites for Solar Cells. *Adv. Funct. Mater.* **2003**, *13*, 73-79.
3. Liu, J. S.; Tanaka, T.; Sivula, K.; Alivisatos, A. P.; Frechet, J. M. J., Employing End-functional Polythiophene to Control the Morphology of Nanocrystal-polymer Composites in Hybrid Solar Cells. *J. Am. Chem. Soc.* **2004**, *126*, 6550-6551.
4. Miyakoshi, R.; Yokoyama, A.; Yokozawa, T., Synthesis of Poly(3-hexylthiophene) with a Narrower Polydispersity. *Macromol. Rapid Commun.* **2004**, *25*, 1663-1666.
5. Zhokhavets, U.; Erb, T.; Hoppe, H.; Gobsch, G.; Sariciftci, N. S., Effect of Annealing of Poly(3-hexylthiophene)/Fullerene Bulk Heterojunction Composites on Structural and Optical Properties. *Thin Solid Films* **2006**, *496*, 679-682.
6. Wang, L.; Liu, Y. S.; Jiang, X.; Qin, D. H.; Cao, Y., Enhancement of Photovoltaic Characteristics Using a Suitable Solvent in Hybrid Polymer/multiarmed CdS Nanorods Solar Cells. *Phys. Chem C* **2007**, *111*, 9538-9542.
7. Zhang, Q. L.; Russell, T. P.; Emrick, T., Synthesis and Characterization of CdSe Nanorods Functionalized with Regioregular Poly(3-hexylthiophene)". *Chem. Mat.* **2007**, *19*, 3712-3716.
8. Osaka, I.; McCullough, R. D., Advances in Molecular Design and Synthesis of Regioregular Polythiophenes. *Acc. Chem. Res.* **2008**, *41*, 1202-1214.

9. Saunders, B. R.; Turner, M. L., Nanoparticle-polymer Photovoltaic Cells. *Adv. Colloid Interface Sci.* **2008**, *138*, 1-23.

10. Palaniappan, K.; Murphy, J. W.; Khanam, N.; Horvath, J.; Alshareef, H.; Quevedo-Lopez, M.; Biewer, M. C.; Park, S. Y.; Kim, M. J.; Gnade, B. E.; Stefan, M. C., Poly(3-hexylthiophene)-CdSe Quantum Dot Bulk Heterojunction Solar Cells: Influence of the Functional End-Group of the Polymer. *Macromolecules* **2009**, *42*, 3845-3848.

11. Roncali, J., Conjugated Poly(thiophenes): Synthesis, Functionalization, and Applications. *Chem. Rev.* **1992**, *92*, 711-738.

12. Lin, J. W. P.; Dudek, L. P., Sythesis and Properties of Poly(2,5-thienylene). *J. Polym. Sci. Pol. Chem.* **1980**, *18*, 2869-2873.

13. Yamamoto, T.; Sanechika, K.; Yamamoto, A., Preparation of Thermostable and Electric-conducting Poly(2,5-thienylene). *J. Polym. Sci. Part C-Polym. Lett.* **1980**, *18*, 9-12.

14. Loewe, R. S.; Khersonsky, S. M.; McCullough, R. D., A Simple Method to Prepare Head-to-Tail Coupled, Regioregular Poly(3-alkylthiophenes) Using Grignard Metathesis. *Advanced Materials* **1999**, *11*, 250-253.

15. Elsenbaumer, R. L.; Jen, K. Y.; Oboodi, R., Processible and Environmentally Stable Conducting Polymers. *Synth. Met.* **1986**, *15*, 169-174.

16. Chen, T. A.; Rieke, R. D., The 1st Regioregular Head-to-Tail Poly(3-hexylthiophene-2,5-diyl) and a Regiorandom Isopolymer- Ni vs Pd Catalysis of 2(5)-bromo-5(2)-bromozincio)-3-hexylthiophene Polymerization. *J. Am. Chem. Soc.* **1992**, *114*, 10087-10088.

17. Chen, T. A.; Wu, X. M.; Rieke, R. D., Regiocontrolled Synthesis of Poly(3-alkylthiophenes) Mediated by Rieke Zinc- Their Characterization and Solid-State Properties. *J. Am. Chem.*

Soc. **1995**, *117*, 233-244.

18. McCullough, R. D.; Tristramnagle, S.; Williams, S. P.; Lowe, R. D.; Jayaraman, M., Self-orienting Heat-to-Tail Poly(alkylthiophenes)- New Insights on Structure-Property Relationships in Conducting Polymers. *J. Am. Chem. Soc.* **1993**, *115*, 4910-4911.
19. McCullough, R. D.; Lowe, R. D., Enhanced Electrical Conductivity in Regioselectively Synthesized Poly(3-alkylthiophenes). *J. Chem. Soc.-Chem. Commun.* **1992**, 70-72.
20. Loewe, R. S.; Ewbank, P. C.; Liu, J.; Zhai, L.; McCullough, R. D., Regioregular, Head-to-Tail Coupled Poly(3-alkylthiophenes) Made Easy by the GRIM Method: Investigation of the Reaction and the Origin of Regioselectivity. *Macromolecules* **2001**, *34*, 4324-4333.
21. Yokoyama, A.; Miyakoshi, R.; Yokozawa, T., Chain-Growth Polymerization for Poly(3-hexylthiophene) with a Defined Molecular Weight and a Low Polydispersity. *Macromolecules* **2004**, *37*, 1169-1171.
22. Suzuki, A., Recent Advances in the Cross-coupling Reactions of Organoboron Derivatives with Organic Electrophiles. *J. Organomet. Chem.* **1999**, *576*, 147-168.
23. Stille, J. K., The Palladium-catalyzed Cross-Coupling Reactions of Organothin Reagents with Organic Electrophiles. *Angew. Chem.-Int. Ed.* **1986**, *25*, 508-523.
24. Administration, U. S. E. I., The Annual Energy Outlook 2013 (AEO2013). **2013**.
25. Hoppe, H.; Sariciftci, N. S., Polymer Solar Cells. In *Photoresponsive Polymers Ii*, Springer-Verlag Berlin: Berlin, 2008; Vol. 214, pp 1-86.
26. Lattin, W. C.; Utgikar, V. P., Transition to Hydrogen Economy in the United States: A 2006 Status Report. *Int. J. Hydrog. Energy* **2007**, *32*, 3230-3237.
27. Wei, D., Dye Sensitized Solar Cells. *Int. J. Mol. Sci.* **2010**, *11*, 1103-1113.

28. Ning, Z.; Fu, Y.; Tian, H., Improvement of Dye-sensitized Solar Cells: What We Know and What We Need to Know. *Energy Environ. Sci.* **2010**, *3*, 1170-1181.

29. Guo, X.; Zhou, N.; Lou, S. J.; Smith, J.; Tice, D. B.; Hennek, J. W.; Ortiz, R. P.; Navarrete, J. T. L.; Li, S.; Strzalka, J.; Chen, L. X.; Chang, R. P. H.; Facchetti, A.; Marks, T. J., Polymer Solar Cells with Enhanced Fill Factors. *Nature Photonics* **2013**, *7*, 825-833.

30. Jiao, Y.; Akcora, P., Assembly of Polymer-Grafted Magnetic Nanoparticles in Polymer Melts. *Macromolecules* **2012**, *45*, 3463-3470.

31. Akcora, P.; Liu, H.; Kumar, S. K.; Moll, J.; Li, Y.; Benicewicz, B. C.; Schadler, L. S.; Acehan, D.; Panagiotopoulos, A. Z.; Pryamitsyn, V.; Ganesan, V.; Ilavsky, J.; Thiyagarajan, P.; Colby, R. H.; Douglas, J. F., Anisotropic Self-assembly of Spherical Polymer-grafted Nanoparticles. *Nat. Mater.* **2009**, *8*, 354-U121.

32. Rosenthal, S. J.; McBride, J.; Pennycook, S. J.; Feldman, L. C., Synthesis, Surface Studies, Composition and Structural Characterization of CdSe, Core/shell and Biologically Active Nanocrystals. *Surf. Sci. Rep.* **2007**, *62*, 111-157.

33. Owen, J. S.; Park, J.; Trudeau, P. E.; Alivisatos, A. P., Reaction Chemistry and Ligand Exchange at Cadmium-selenide Nanocrystal Surfaces. *J. Am. Chem. Soc.* **2008**, *130*, 12279-12281.

34. Martinez-Ferrero, E.; Albero, J.; Palomares, E., Materials, Nanomorphology, and Interfacial Charge Transfer Reactions in Quantum Dot/Polymer Solar Cell Devices. *J. Phys. Chem. Lett.* **2010**, *1*, 3039-3045.

35. Kochemba, W. M.; Pickel, D. L.; Sumpter, B. G.; Chen, J.; Kilbey II, S. M., In Situ Formation of Pyridyl-Functionalized Poly(3-hexylthiophene)s via Quenching of the Grignard

Metathesis Polymerization: Toward Ligands for Semiconductor Quantum Dots. *Chem. Mat.* **2012**, *24*, 4459-4467.

36. Lee, J. U.; Jung, J. W.; Emrick, T.; Russell, T. P.; Jo, W. H., Synthesis of C60-end Capped P3HT and its Application for High Performance of P3HT/PCBM Bulk Heterojunction Solar Cells. *J. Mater. Chem.* **2010**, *20*, 3287-3294.
37. Boudouris, B. W.; Molins, F.; Blank, D. A.; Frisbie, C. D.; Hillmyer, M. A., Synthesis, Optical Properties, and Microstructure of a Fullerene-Terminated Poly(3-hexylthiophene). *Macromolecules* **2009**, *42*, 4118-4126.
38. Kiriy, A.; Senkovskyy, V.; Sommer, M., Kumada Catalyst-Transfer Polycondensation: Mechanism, Opportunities, and Challenges. *Macromol. Rapid Commun.* **2011**, *32*, 1503-1517.
39. Senkovskyy, V.; Tkachov, R.; Beryozkina, T.; Komber, H.; Oertel, U.; Horecha, M.; Bocharova, V.; Stamm, M.; Gevorgyan, S. A.; Krebs, F. C.; Kiriy, A., "Hairy" Poly(3-hexylthiophene) Particles Prepared via Surface-Initiated Kumada Catalyst-Transfer Polycondensation. *J. Am. Chem. Soc.* **2009**, *131*, 16445-16453.
40. Senkovskyy, V.; Sommer, M.; Tkachov, R.; Komber, H.; Huck, W. T. S.; Kiriy, A., Convenient Route To Initiate Kumada Catalyst-Transfer Polycondensation Using Ni(dppe)Cl_2 or Ni(dppp)Cl_2 and Sterically Hindered Grignard Compounds. *Macromolecules* **2010**, 10157-10161.
41. Bronstein, H. A.; Luscombe, C. K., Externally Initiated Regioregular P3HT with Controlled Molecular Weight and Narrow Polydispersity. *J. Am. Chem. Soc.* **2009**, *131*, 12894-12895.
42. Doubina, N.; Paniagua, S. A.; Soldatova, A. V.; Jen, A. K. Y.; Marder, S. R.; Luscombe, C.

K., Steric Effects of the Initiator Substituent Position on the Externally Initiated Polymerization of 2-Bromo-5-iodo-3-hexylthiophene. *Macromolecules* **2011**, *44*, 512-520.

43. Jeffries-El, M.; Sauve, G.; McCullough, R. D., Facile Synthesis of End-functionalized Regioregular Poly(3-alkylthiophene)s via Modified Grignard Mmetathesis Reaction. *Macromolecules* **2005**, *38*, 10346-10352.
44. Jeffries-El, M.; Sauve, G.; McCullough, R. D., In-situ End-group Functionalization of Regioregular Poly(3-alkylthiophene) Using the Grignard Metathesis Polymerization Method. *Adv. Mater.* **2004**, *16*, 1017-1019.
45. Takahashi, A.; Rho, Y.; Higashihara, T.; Ahn, B.; Ree, M.; Ueda, M., Preparation of Nanoporous Poly(3-hexylthiophene) Films Based on a Template System of Block Copolymers via Ionic Interaction. *Macromolecules* **2010**, *43*, 4843-4852.
46. Liu, J. S.; Loewe, R. S.; McCullough, R. D., Employing MALDI-MS on Poly(alkylthiophenes): Analysis of Molecular weights, Molecular Weight Distributions, End-group Structures, and End-group Modifications. *Macromolecules* **1999**, *32*, 5777-5785.
47. Holdcroft, S., Determination of Molecular Weights and Mark-Houwink Constants for Soluble Electrically Conducting Polymers. J. Polym. Sci. *Part B-Polym. Phys.* **1991**, *29*, 1585-1588.
48. Montaudo, G.; Montaudo, M. S.; Puglisi, C.; Samperi, F., Characterization of Polymers by Matrix-assisted Laser Desorption/ionization Time-of-flight Mass Spectrometry: Molecular Weight Estimates in Samples of Varying Polydispersity. *Rapid Commun. Mass Spectrom.* **1995**, *9*, 453-460.
49. Montaudo, G.; Garozzo, D.; Montaudo, M. S.; Puglisi, C.; Samperi, F., Molecular and Structural Characterization of Polydisperse Polymers and Copolymers by Combining

MALDI-TOF Mass Spectrometry with GPC Fractionation. *Macromolecules* **1995**, *28*, 7983-7989.

50. Vaia, R. A.; Maguire, J. F., Polymer Nanocomposites With Prescribed Morphology: Going Beyond Nanoparticle-filled Polymers. *Chem. Mat.* **2007**, *19*, 2736-2751.
51. Koerner, H.; Drummy, L. F.; Benicewicz, B.; Li, Y.; Vaia, R. A., Nonisotropic Self-Organization of Single-Component Hairy Nanoparticle Assemblies. *ACS Macro Lett.* **2013**, *2*, 670-676.
52. Lin, Z., Organic–Inorganic Nanohybrids through the Direct Tailoring of Semiconductor Nanocrystals with Conjugated Polymers. *Chem. Eur. J.* **2008**, *14*, 6294-6301.
53. Vanlaeke, P.; Swinnen, A.; Haeldermans, I.; Vanhoyland, G.; Aernouts, T.; Cheyns, D.; Deibel, C.; D'Haen, J.; Heremans, P.; Poortmans, J.; Manca, J. V., P3HT/PCBM bulk Heterojunction Solar Cells: Relation Between Morphology and Electro-optical Characteristics. *Sol. Energy Mater. Sol. Cells* **2006**, *90*, 2150-2158.
54. Chiu, M.-Y.; Jeng, U. S.; Su, C.-H.; Liang, K. S.; Wei, K.-H., Simultaneous Use of Small- and Wide-Angle X-ray Techniques to Analyze Nanometerscale Phase Separation in Polymer Heterojunction Solar Cells. *Adv. Mater.* **2008**, *20*, 2573-2578.
55. Ruderer, M. A.; Guo, S.; Meier, R.; Chiang, H.-Y.; Körstgens, V.; Wiedersich, J.; Perlich, J.; Roth, S. V.; Müller-Buschbaum, P., Solvent-Induced Morphology in Polymer-Based Systems for Organic Photovoltaics. *Adv. Funct. Mater.* **2011**, *21*, 3382-3391.
56. Mather, B. D.; Lizotte, J. R.; Long, T. E., Synthesis of Chain End Functionalized Multiple Hydrogen Bonded Polystyrenes and Poly(alkyl acrylates) Using Controlled Radical Polymerization. *Macromolecules* **2004**, *37*, 9331-9337.

57. Nicolas, J.; Mantovani, G.; Haddleton, D. M., Living Radical Polymerization as a Tool for the Synthesis of Polymer-Protein/Peptide Bioconjugates. *Macromol. Rapid Commun.* **2007**, *28*, 1083-1111.

58. Huh, J.; Jung, J. Y.; Lee, J. U.; Cho, H.; Park, S.; Park, C.; Jo, W. H., Supramolecular Assembly of End-Functionalized Polymer Mixtures Confined in Nanospheres. *ACS Nano* **2010**, *5*, 115-122.

59. Zdyrko, B.; Luzinov, I., Polymer Brushes by the "Grafting to" Method. *Macromol. Rapid Commun.* **2011**, *32*, 859-869.

60. Iovu, M. C.; Jeffries-El, M.; Sheina, E. E.; Cooper, J. R.; McCullough, R. D., Regioregular Poly(3-alkylthiophene) Conducting Block Copolymers. *Polymer* **2005**, *46*, 8582-8586.

61. Bangar, M. A.; Chen, W.; Myung, N. V.; Mulchandani, A., Conducting Ppolymer 1-dimensional Nanostructures for FET Sensors. *Thin Solid Films* **2010**, *519*, 964-973.

62. Coropceanu, V.; Cornil, J.; da Silva, D. A.; Olivier, Y.; Silbey, R.; Bredas, J. L., Charge Transport In Organic Semiconductors. *Chem. Rev.* **2007**, *107*, 926-952.

63. Jiu, T. G.; Reiss, P.; Guillerez, S.; de Bettignies, R.; Bailly, S.; Chandezon, F., Hybrid Solar Cells Based on Blends of CdSe Nanorods and Poly(3-alkylthiophene) Nanofibers. *IEEE J. Sel. Top. Quantum Electron.* **2010**, *16*, 1619-1626.

64. Krueger, R. A.; Gordon, T. J.; Baumgartner, T.; Sutherland, T. C., End-Group Functionalization of Poly(3-hexylthiophene) as an Efficient Route to Photosensitize Nanocrystalline TiO2 Films for Photovoltaic Applications. *ACS Appl. Mater. Interfaces* **2011**, *3*, 2031-2041.

65. Dayal, S.; Reese, M. O.; Ferguson, A. J.; Ginley, D. S.; Rumbles, G.; Kopidakis, N., The Effect

of Nanoparticle Shape on the Photocarrier Dynamics and Photovoltaic Device Performance of Poly(3-hexylthiophene):CdSe Nanoparticle Bulk Heterojunction Solar Cells. *Adv. Funct. Mater.* **2010**, *20*, 2629-2635.

66. Kim, J. S.; Lee, Y.; Lee, J. H.; Park, J. H.; Kim, J. K.; Cho, K., High-Efficiency Organic Solar Cells Based on End-Functional-Group-Modified Poly(3-hexylthiophene). *Adv. Mater.* **2010**, *22*, 1355-1360.
67. Truong, N. T. N.; Kim, W. K.; Park, C., Effect of CdSe/P3HT Composition on Electrical and Structural Properties of Bulk Hetero-junction Solar Cell Active Layer. *Sol. Energy Mater. Sol. Cells* **2011**, *95*, 167-170.
68. Loewe, R. S.; Khersonsky, S. M.; McCullough, R. D., A Simple Method to Prepare Head-to-Tail Coupled, Regioregular Poly(3-alkylthiophenes) Using Grignard Metathesis. *Adv. Mater.* **1999**, *11*, 250-253.
69. Bronstein, H. A.; Luscombe, C. K., Externally Initiated Regioregular P3HT with Controlled Molecular Weight and Narrow Polydispersity. *J. Am. Chem. Soc.* **2009**, *131*, 12894-12895.
70. Senkovskyy, V.; Sommer, M.; Tkachov, R.; Komber, H.; Huck, W. T. S.; Kiriy, A., Convenient Route To Initiate Kumada Catalyst-Transfer Polycondensation Using Ni(dppe)Cl_2 or Ni(dppp)Cl_2 and Sterically Hindered Grignard Compounds. *Macromolecules* **2010**, *43*, 10157-10161.
71. Smeets, A.; Van Den Bergh, K.; De Winter, J.; Gerbaux, P.; Verbiest, T.; Koeckelberghs, G., Incorporation of Different End Groups in Conjugated Polymers Using Functional Nickel Initiators. *Macromolecules* **2009**, *42*, 7638-7641.
72. Xu, J.; Wang, J.; Mitchell, M.; Mukherjee, P.; Jeffries-El, M.; Petrich, J. W.; Lin, Z.,

Organic−Inorganic Nanocomposites via Directly Grafting Conjugated Polymers onto Quantum Dots. *J. Am. Chem. Soc.* **2007**, *129*, 12828-12833.

73. Liu, J.; Tanaka, T.; Sivula, K.; Alivisatos, A.; Frechet, J., Employing End-functional Polythiophene to Control the Morphology of Nanocrystal-polymer Composites in Hybrid Solar Cells. *J. Am. Chem. Soc.* **2004**, *126*, 6550-6551.
74. Miyakoshi, R.; Yokoyama, A.; Yokozawa, T., Catalyst-transfer Polycondensation. Mechanism of Ni-catalyzed Chain-growth Polymerization Leading to Well-defined Poly(3-hexylthiophene). *J. Am. Chem. Soc.* **2005**, *127*, 17542-17547.
75. Senkovskyy, V.; Khanduyeva, N.; Komber, H.; Oertel, U.; Stamm, M.; Kuckling, D.; Kiriy, A., Conductive Polymer Brushes of Regioregular Head-to-Tail Poly(3-alkylthiophenes) via Catalyst-Transfer Surface-Initiated Polycondensation. *J. Am. Chem. Soc.* **2007**, *129*, 6626-6632.
76. Sontag, S. K.; Marshall, N.; Locklin, J., Formation of Conjugated Polymer Brushes by Surface-initiated Catalyst-transfer Polycondensation. *Chem. Commun.* **2009**, 3354-3356.
77. Tolman, C. A.; Seidel, W. C.; Gosser, L. W., Formation of Olefin Complexes of Nickel(0). Steric and Electronic Effects of Phosphorus Ligands. *Organometallics* **1983**, *2*, 1391-1396.
78. Crabtree, R. H., In *The Organometallic Chemistry of the Transition Metals*, 3rd ed.; John Wiley & Sons: New York, 2001; p 534.
79. Arnould, M. A.; Polce, M. J.; Quirk, R. P.; Wesdemiotis, C., Probing Chain-end Functionalization Reactions in Living Anionic Polymerization via Matrix-assisted Laser Desorption Ionization Time-of-flight Mass Spectrometry. *Int. J. Mass Spectrom.* **2004**, *238*, 245-255.

80. Tkachov, R.; Senkovskyy, V.; Komber, H.; Sommer, J.-U.; Kiriy, A., Random Catalyst Walking along Polymerized Poly(3-hexylthiophene) Chains in Kumada Catalyst-Transfer Polycondensation. *J. Am. Chem. Soc.* **2010**, *132*, 7803-7810.

81. Achord, B. C.; Rawlins, J. W., Evidence of Ni(0) Complex Diffusion during Grignard Metathesis Polymerization of 2,5-Dibromo-3-hexylthiophene. *Macromolecules* **2009**, *42*, 8634-8639.

82. Montaudo, G.; Montaudo, M. S.; Puglisi, C.; Samperi, F., Characterization of Polymers by Matrix-assisted Laser Desorption/ionization Time-of-flight Mass Spectrometry: Molecular Weight Estimates in Samples of Varying Polydispersity. *Rapid Commun. Mass Spectrom.* **1995**, *9*, 453-460.

83. Iovu, M. C.; Sheina, E. E.; Gil, R. R.; McCullough, R. D., Experimental Evidence for the Quasi-"Living" Nature of the Grignard Metathesis Method for the Synthesis of Regioregular Poly(3-alkylthiophenes). *Macromolecules* **2005**, *38*, 8649-8656.

84. Osakada, K.; Takeuchi, D., Coordination Polymerization of Dienes, Allenes, and Methylenecycloalkanes. *Adv. Polym. Sci.* **2004**, *171*, 137-194.

85. Krasovskiy, A.; Knochel, P., A LiCl-mediated Br/Mg Exchange Reaction for the Preparation of Functionalized Aryl- and Heteroarylmagnesium Compounds from Organic Bromides. *Angew. Chem., Int. Ed. Eng.* **2004**, *43*, 3333-3336.

86. Lohwasser, R. H.; Thelakkat, M., Toward Perfect Control of End Groups and Polydispersity in Poly(3-hexylthiophene) via Catalyst Transfer Polymerization. *Macromolecules* **2011**, *44*, 3388-3397.

87. Piller, F. M.; Appukkuttan, P.; Gavryushin, A.; Helm, M.; Knochel, P., Convenient Preparation

of Polyfunctional Aryl Magnesium Reagents by a Direct Magnesium Insertion in the Presence of LiCl. *Angew. Chem., Int. Ed. Eng.* **2008**, *47*, 6802-6806.

88. Lanni, E. L.; McNeil, A. J., Mechanistic Studies on Ni(dppe)Cl-2-Catalyzed Chain-Growth Polymerizations: Evidence for Rate-Determining Reductive Elimination. *J. Am. Chem. Soc.* **2009**, *131*, 16573-16579.
89. Pasch, H.; W.Schrepp, *MALDI-TOF Mass Spectrometry of Synthetic Polymers*. Springer: Berlin, 2003.
90. Knochel, P.; Dohle, W.; Gommermann, N.; Kneisel, F. F.; Kopp, F.; Korn, T.; Sapountzis, I.; Vu, V. A., Highly Functionalized Organomagnesium Reagents Prepared Through Halogen-metal Exchange. *Angew. Chem., Int. Ed. Engl.* **2003**, *42*, 4302-4320.
91. Lohwasser, R. H.; Bandara, J.; Thelakkat, M., Tailor-made Synthesis of Poly(3-hexylthiophene) with Carboxylic End Groups and its Application as a Polymer Sensitizer in Solid-state Dye-sensitized Solar Cells. *J. Mater. Chem.* **2009**, *19*, 4126-4130.
92. Boon, F.; Desbief, S.; Cutaia, L.; Douheret, O.; Minoia, A.; Ruelle, B.; Clement, S.; Coulembier, O.; Cornil, J.; Dubois, P.; Lazzaroni, R., Synthesis and Characterization of Nanocomposites Based on Functional Regioregular Poly(3-hexylthiophene) and Multiwall Carbon Nanotubes. *Macromol. Rapid Commun.* **2010**, *31*, 1427-1434.
93. Zhao, L.; Lin, Z., Crafting Semiconductor Organic−Inorganic Nanocomposites via Placing Conjugated Polymers in Intimate Contact with Nanocrystals for Hybrid Solar Cells. *Adv. Mater.* **2012**, *24*, 4353-4368.
94. Zhao, L.; Pang, X.; Adhikary, R.; Petrich, J. W.; Lin, Z., Semiconductor Anisotropic Nanocomposites Obtained by Directly Coupling Conjugated Polymers with Quantum Rods.

Angew. Chem., Int. Ed. Eng. **2011**, *50*, 3958-3962.

95. Zhao, L.; Pang, X.; Adhikary, R.; Petrich, J. W.; Jeffries-El, M.; Lin, Z., Organic−Inorganic Nanocomposites by Placing Conjugated Polymers in Intimate Contact with Quantum Rods. *Adv. Mater.* **2011**, *23*, 2844-2849.
96. Pang, X.; Zhao, L.; Feng, C.; Lin, Z., Novel Amphiphilic Multiarm, Starlike Coil–Rod Diblock Copolymers via a Combination of Click Chemistry with Living Polymerization. *Macromolecules* **2011**, *44*, 7176-7183.
97. Goodman, M. D.; Xu, J.; Wang, J.; Lin, Z., Semiconductor Conjugated Polymer−Quantum Dot Nanocomposites at the Air/Water Interface and Their Photovoltaic Performance. *Chem. Mat.* **2009**, *21*, 934-938.
98. Xu, J.; Wang, J.; Mitchell, M.; Mukherjee, P.; Jeffries-El, M.; Petrich, J. W.; Lin, Z., Organic−Inorganic Nanocomposites via Directly Grafting Conjugated Polymers onto Quantum Dots. *J. Am. Chem. Soc.* **2007**, *129*, 12828-12833.
99. Sheina, E. E.; Liu, J. S.; Iovu, M. C.; Laird, D. W.; McCullough, R. D., Chain growth mechanism for regioregular nickel-initiated cross-coupling polymerizations. *Macromolecules* **2004**, *37*, 3526-3528.
100. Iovu, M. C.; Sheina, E. E.; Gil, R. R.; McCullough, R. D., Experimental Evidence for the Quasi-"living" Nature of the Grignard Metathesis Method for the Synthesis of Regioregular Poly(3-alkylthiophenes). *Macromolecules* **2005**, *38*, 8649-8656.
101. Jeffries-El, M.; Sauve, G.; McCullough, R., Facile Synthesis of End-functionalized Regioregular Poly(3-alkylthiophene)s via Modified Grignard Metathesis Reaction. *Macromolecules* **2005**, *38*, 10346-10352.

102. Lee, J. U.; Jung, J. W.; Emrick, T.; Russell, T. P.; Jo, W. H., Synthesis of C(60)-end Capped P3HT and its Application for High Performance of P3HT/PCBM Bulk Heterojunction Solar Cells. *J. Mater. Chem.* **2010**, *20*, 3287-3294.

103. Lohwasser, R. H.; Thelakkat, M., Synthesis and Characterization of Monocarboxylated Poly(3-hexylthiophene)s via Quantitative End-Group Functionalization. *Macromolecules* **2010**, *43*, 7611-7616.

104. Kochemba, W. M.; Kilbey II, S. M.; Pickel, D. L., End-group Composition of Poly(3-hexylthiophene)s Prepared by In Situ Quenching of the Grignard Metathesis Polymerization: Influence of Additives and Reaction Conditions. *J. Polym. Sci. Part A: Polymer Chemistry* **2012**, *50*, 2762–2769.

105. Osaka, I.; McCullough, R. D., Advances in Molecular Design and Synthesis of Regioregular Polythiophenes. *Accounts Chem. Res.* **2008**, *41*, 1202-1214.

106. Cai, W. L.; Ripin, D. H. B., A Practical Synthesis of Pyridylboranes via Magnesium-halogen Exchange. *Syn. Lett.* **2002**, 273-274.

107. Antoun, T.; Brayner, R.; Al terary, S.; Fievet, F.; Chehimi, M.; Yassar, A., Facile Synthesis of Oligothiophene-capped CdS Nanoparticles. *Eur. J. Inorg. Chem.* **2007**, 1275-1284.

108. Bhasin, K. K.; Arora, V.; Sharma, S. K.; Venugopalan, P., A Novel and Facile One-pot Synthesis of Pyridylselenium Compounds through Selective Bromine-magnesium Exchange with Isopropylmagnesium Halide. *Appl. Organomet. Chem.* **2005**, *19*, 161-166.

109. Trecourt, F.; Breton, G.; Bonnet, V.; Mongin, F.; Marsais, F.; Queguiner, G., Pyridylmagnesium Chlorides from Bromo and Dibromopyridines by Bromine-magnesium Exchange: A Convenient Access to Functionalized Pyridines. *Tetrahedron Lett.* **1999**, *40*,

4339-4342.

110. Trecourt, F.; Breton, G.; Bonnet, V.; Mongin, F.; Marsais, F.; Queguiner, G., New Syntheses of Substituted Pyridines via Bromine-magnesium Exchange. *Tetrahedron* **2000**, *56*, 1349-1360.

111. Piller, F. M.; Metzger, A.; Schade, M. A.; Haag, B. A.; Gavryushin, A.; Knochel, P., Preparation of Polyfunctional Arylmagnesium, Arylzinc, and Benzylic Zinc Reagents by Using Magnesium in the Presence of LiCl. *Chemistry- A European Journal* **2009**, *15*, 7192-7202.

112. Krasovskiy, A.; Knochel, P., A LiCl-mediated Br/Mg Exchange eaction for the Preparation of Functionalized Aryl- and Heteroarylmagnesium Compounds from Organic Bromides. *Angew. Chem. Int. Ed.* **2004**, *43*, 3333-3336.

113. Shi, L.; Chu, Y. Y.; Knochel, P.; Mayr, H., Kinetics of Bromine-Magnesium Exchange Reactions in Heteroaryl Bromides. *Org. Lett.* **2009**, *11*, 3502-3505.

114. Komber, H.; Senkovskyy, V.; Tkachov, R.; Johnson, K.; Kiriy, A.; Huck, W. T. S.; Sommer, M., Ring Walking versus Trapping of Nickel(0) during Kumada Catalyst Transfer Polycondensation Using Externally Initiated Electron-Accepting Thiophene-Benzothiadiazole-Thiophene Precursors. *Macromolecules* **2011**, *44*, 9164-9172.

115. Verswyvel, M.; Monnaie, F.; Koeckelberghs, G., AB Block Copoly(3-alkylthiophenes): Synthesis and Chiroptical Behavior. *Macromolecules* **2011**, *44*, 9489-9498.

116. Schafman, B. S.; Wenthold, P. G., Regioselectivity of Pyridine Deprotonation in the Gas Phase". *J. Org. Chem.* **2007**, *72*, 1645-1651.

117. Meotner, M.; Kafafi, S. A., Carbon Acidities of Aromatic-Compounds. *J. Am. Chem. Soc.*

1988, *110*, 6297-6303.

118. Antonov, A. A.; Semikolenova, N. V.; Zakharov, V. A.; Zhang, W.; Wang, Y.; Sun, W.-H.; Talsi, E. P.; Bryliakov, K. P., Vinyl Polymerization of Norbornene on Nickel Complexes with Bis(imino)pyridine Ligands Containing Electron-Withdrawing Groups. *Organometallics* **2012**, *31*, 1143-1149.
119. Handa, M.; Farida, A.; Thompson, L. K.; Hayashibara, C.; Sugimori, T.; Hiromitsu, I.; Kasuga, K., Dinuclear Phenoxo-Bridged Nickel(II) Complexes of Macrocyclic Ligands with Cyano Groups Laterally Introduced on a Conjugated System within the Ligands. *Molecular Crystals and Liquid Crystals Science and Technology. Section A. Molecular Crystals and Liquid Crystals* **2000**, *342*, 75-80.
120. Thoi, V. S.; Chang, C. J., Nickel N-heterocyclic Carbene-pyridine Complexes that Exhibit Selectivity for Electrocatalytic Reduction of Carbon Dioxide over Water. *Chem. Commun.* **2011**, *47*, 6578-6580.
121. Duval, H.; Bulach, V.; Fischer, J.; Weiss, R., Four-Coordinate, Low-Spin (S = 0) and Six-Coordinate, High-Spin (S = 1) Nickel(II) Complexes of Tetraphenylporphyrins with β-Pyrrole Electron-Withdrawing Substituents: Porphyrin-Core Expansion and Conformation. *Inorg. Chem.* **1999**, *38*, 5495-5501.
122. Nanashima, Y.; Yokoyama, A.; Yokozawa, T., Synthesis of Novel Blue-light-emitting Polypyridine. *J. Polym. Sci. Pol. Chem.* **2012**, *50*, 1054-1061.
123. Kresse, G.; Furthmuller, J., Efficiency of Ab-Initio Total Energy Calculations for Metals and Semiconductors Using a Plane-Wave Basis Set. *Comput. Mat. Sci.* **1996**, *6*, 15-50.
124. Kresse, G.; Furthmuller, J., Efficient Iterative Schemes for Ab Initio Total-Energy

Calculations Using a Plane-Wave Basis Set. *Phys. Rev. B.* **1996**, *54*, 11169-11186.

125. Kresse, G.; Hafner, J., Ab Initio Molecular-Dynamics Simulation of the Liquid-Metal-Amorphous-Semiconductor Transition in Germanium. *Phys. Rev. B.* **1994**, *49*, 14251-14269.
126. Kresse, G.; Hafner, G., Ab Initio Molecular Dynamics for Liquid Metals. *Phys. Rev. B.* **1993**, *47*, 558-561.
127. Kresse, G.; Joubert, D., From Ultrasoft Pseudopotentials to the Projector Augmented-Wave. *Phys. Rev. B.* **1999**, *59*, 1758-1775.
128. Blochl, P. E., Projector Augmented-Wave Method. *Phys. Rev. B.* **1994**, *50*, 17953-17979.
129. Ceperley, D. M.; Alder, B. J., Ground State of the Electron Gas by aw Stochastic Method. *Phys. Rev. Lett.* **1980**, *45*, 566-569.
130. Frischknecht, A. L.; Padmanabhan, V.; Mackay, M. E., Surface-induced Phase Behavior of Polymer/nanoparticle Blends with Attractions. *J. Chem. Phys.* **2012**, *136*, 164904-164913.
131. Amitabh, B.; Hoichang, Y.; Chunzhao, L.; Kilwon, C.; Brian, C. B.; Sanat, K. K.; Linda, S. S., Quantitative Equivalence Between Polymer Nanocomposites and Thin Polymer Films. *Nat. Mater.* **2005**, *4*, 693-698.
132. Kumar, U.; Kumari, K.; Sharma, S. N.; Kumar, M.; Vankar, V. D.; Kakkar, R.; Kumar, V., Role of Surface Modification of Colloidal CdSe Quantum Dots on the Properties of Hybrid Organic-inorganic Nanocomposites. *Colloid Polym. Sci.* **2010**, *288*, 841-849.
133. Boon, F.; Thomas, A.; Clavel, G.; Moerman, D.; De Winter, J.; Laurencin, D.; Coulembier, O.; Dubois, P.; Gerbaux, P.; Lazzaroni, R.; Richeter, S.; Mehdi, A.; Clément, S., Synthesis and Characterization of Carboxystyryl End-functionalized Poly(3-hexylthiophene)/TiO_2 Hybrids in View of Photovoltaic Applications. *Synth. Met.* **2012**, *162*, 1615-1622.

134. Li, Q. W.; Sun, B. Q.; Kinloch, I. A.; Zhi, D.; Sirringhaus, H.; Windle, A. H., Enhanced Self-assembly of Pyridine-capped CdSe Nanocrystals on Individual Single-walled Carbon Nanotubes. *Chem. Mat.* **2006**, *18*, 164-168.

135. Shallcross, R. C.; D'Ambruoso, G. D.; Korth, B. D.; Hall, H. K.; Zheng, Z.; Pyun, J.; Armstrong, N. R., Poly(3,4-ethylenedioxythiophene)−Semiconductor Nanoparticle Composite Thin Films Tethered to Indium Tin Oxide Substrates via Electropolymerization. *J. Am. Chem. Soc.* **2007**, *129*, 11310-11311.

136. Lee, J.; Kim, J.; Yang, C., Organic–Inorganic Nanostructure Architecture via Directly Capping Fullerenes onto Quantum Dots. *Nanoscale Res. Lett.* **2010**, *6*, 1-4.

137. Lokteva, I.; Radychev, N.; Witt, F.; Borchert, H.; Parisi, J. r.; Kolny-Olesiak, J., Surface Treatment of CdSe Nanoparticles for Application in Hybrid Solar Cells: The Effect of Multiple Ligand Exchange with Pyridine. *J. Phys. Chem. C.* **2010**, *114*, 12784-12791.

138. Chen, H.; Chen, J.; Yin, W.; Yu, X.; Shao, M.; Xiao, K.; Hong, K.; Pickel, D. L.; Kochemba, W. M.; Kilbey II, S. M.; Dadmun, M., Correlation of Polymeric Compatibilizer Structure to its Impact on the Morphology and Function of P3HT:PCBM Bulk Heterojunctions. *J. Mater. Chem. A* **2013**, *1*, 5309-5319.

139. Chiu, J. J.; Kim, B. J.; Kramer, E. J.; Pine, D. J., Control of Nanoparticle Location in Block Copolymers. *J. Am. Chem. Soc.* **2005**, *127*, 5036-5037.

140. Hartmann, L.; Djurado, D.; Florea, I.; Legrand, J.-F.; Fiore, A.; Reiss, P.; Doyle, S.; Vorobiev, A.; Pouget, S.; Chandezon, F.; Ersen, O.; Brinkmann, M., Large-scale Simultaneous Orientation of CdSe Nanorods and Regioregular Poly(3-hexylthiophene) By Mechanical Rubbing. *Macromolecules* **2013**, *46*, 6177-6186.

141. Balazs, A. C.; Emrick, T.; Russell, T. P., Nanoparticle Polymer Composites: Where Two Small Worlds Meet. *Science* **2006**, *314*, 1107-1110.

142. Noro, A.; Higuchi, K.; Sageshima, Y.; Matsushita, Y., Preparation and Morphology of Hybrids Composed of a Block Copolymer and Semiconductor Nanoparticles via Hydrogen Bonding. *Macromolecules* **2012**, *45*, 8013-8020.

143. Arora, H.; Li, Z.; Sai, H.; Kamperman, M.; Warren, S. C.; Wiesner, U., Block Copolymer Directed Nnanoporous Metal Thin Films. *Macromol. Rapid Commun.* **2010**, *31*, 1960-1964.

144. Chiu, J. J.; Kim, B. J.; Yi, G.-R.; Bang, J.; Kramer, E. J.; Pine, D. J., Distribution of Nanoparticles in Lamellar Domains of Block Copolymers. *Macromolecules* **2007**, *40*, 3361-3365.

145. Bockstaller, M. R.; Mickiewicz, R. A.; Thomas, E. L., Block Copolymer Nanocomposites: Perspectives for Tailored Functional Materials. *Adv.Mater.* **2005**, *17*, 1331-1349.

146. Bockstaller, M. R.; Lapetnikov, Y.; Margel, S.; Thomas, E. L., Size-selective Organization of Enthalpic Compatibilized Nanocrystals in Ternary Block Copolymer/particle Mixtures. *J. Am. Chem. Soc.* **2003**, *125*, 5276-5277.

147. Cheng, J. Y.; Ross, C. A.; Chan, V. Z. H.; Thomas, E. L.; Lammertink, R. G. H.; Vancso, G. J., Formation of a Cobalt Magnetic Dot Array via Block Copolymer Lithography. *Adv. Mater.* **2001**, *13*, 1174-1178.

148. Skaff, H.; Sill, K.; Emrick, T., Quantum Dots Tailored with Poly(para-phenylene vinylene). *J. Am. Chem. Soc.* **2004**, *126*, 11322-11325.

149. Das, N. C.; Sokol, P. E., Hybrid Photovoltaic Devices from Regioregular Polythiophene and ZnO Nanoparticles Composites. *Renew. Energy* **2010**, *35*, 2683-2688.

150. Yu, W. W.; Peng, X. G., Formation of High-quality CdS and other II-VI Semiconductor Nanocrystals in Noncoordinating Solvents: Tunable Reactivity of Monomers. *Angew. Chem. Int. Edit.* **2002**, *41*, 2368-2371.

151. Schulz, G. V., The Kinetics of Chain Polymerization. The Effect of Various Reaction Species on the Multimolecularity. *Z. Physik. Chem.* **1939**, *B43*, 25-46.

152. Guinier, A. F. G., *Small-angle scattering of X-rays*. Wiley: New York, 1955.

153. Wu, S.; Huang, L.; Tian, H.; Geng, Y.; Wang, F., LiCl-Promoted Chain Growth Kumada Catalyst-Transfer Polycondensation of the "Reversed" Thiophene Monomer. *Macromolecules* **2011**, *44*, 7558-7567.

154. Sullivan, J. T.; Harrison, K. E.; Mizzell, J. P.; Kilbey, S. M., Contact Angle and Electrochemical Characterization of Multicomponent Thiophene-Capped Monolayers. *Langmuir* **2000**, *16*, 9797-9803.

Appendices

Appendix A- Precision synthesis of end-functionalized poly(3-hexylthiophene)s

Detailed synthetic protocols

The successful preparation of well-defined end-functionalized poly (3-hexylthiophenes) will be described in this appendix. There are several steps in the synthetic protocol that are crucial for obtaining P3HTs with good control over molecular weight, polydispersity, and end-group functionality, which will be discussed throughout this appendix. As discussed in Chapter 1, the most common method to prepare P3HT is by the Grignard Metathesis (GRIM) polymerization method (a.k.a. Kumada Catalyst-transfer polycondenstation, KCTP). As described by the name, the GRIM polymerization utilizes the highly reactive alkyl halomagnesio (MgX) reagent, which is extremely moisture sensitive, in a metathesis reaction with 2,5-dibromo-3-hexylthiophene yielding a regiospecific monomer that will readily undergo nickel-catalyzed cross coupling at room temperature. **Note: Grignard reagents react violently in the presence of moisture. Proper PPE should be worn at all times while working with Grignard reagents.** Therefore, the remainder of this appendix will discuss in detail the materials that are required to prepare well-defined end-functional P3HT using the GRIM polymerization method.

The laboratory-scale preparation of P3HT requires several materials that should be prepared/purchased prior to beginning the experiment, including 2,5-dibromo-3-hexylthiophene, isopropyl magnesium chloride (*i*-PrMgCl), anhydrous tetrahydrofuran, 1,3-bis(diphenylphosphino)propane nickel (II) dichloride, and either methanol or 5M HCl. I have found it beneficial to prepare isopropyl magnesium chloride by direct insertion of magnesium into

the C-Cl bond of 2-chlorpropane in THF. This eliminates batch-to-batch variation in purity and concentration typically observed for commercial Grignard reagents. The procedure to synthesize isopropyl magnesium chloride is detailed below.

Synthesis of isopropyl magnesium chloride

Magnesium shavings (11.396g, 0.469mol) were added to a dry 500 mL 3-neck flask equipped with a 250 mL addition funnel, Teflon stopper, stir bar, and reflux condenser. Next, 165 mL of THF were transferred into the addition funnel via canula (two ended needle). THF (~30 mL) was allowed to pass through the stopcock until the magnesium was completely immersed. The 2-chloropropane (36.096g, 0.459mol) was added to the addition funnel via syringe. Stirring gently, the THF was brought to a gentle reflux and the solution of 2-chloropropane was added dropwise until the reflux grew slightly more vigorous. Then the heat was removed and the rate of addition was adjusted to keep the reaction mixture at a constant controlled reflux. After complete addition of 2-chloropropane, the heat was re-applied to allow an additional 2 h of refluxing. The solution was removed from the heat and allowed to cool without stirring, which allows the unreacted magnesium to settle to the bottom of the flask. (Be sure not to transfer solids when collecting the solution) The solution was collected in glass vials and sealed with a Teflon-coated septa for storage. The solution was titrated to determine the Grignard concentration, as discussed below.

To estimate the concentration of *i*-PrMgCl, ~1-2 mL (record accurate volume for back calculation) of the Grignard reagent is accurately drawn into a 2 mL disposable syringe and quenched by dropwise addition into ~40 mL 3:1 THF/H_2O mixture in a 250 mL Erlenmeyer flask. Next, a stir bar and 2-3 drops phenolthalein indicator are added to the flask. While stirring, a

standard solution of 0.1M HCl (or similar concentration) is added dropwise to titrate the solution until the endpoint is reached. From the volume of HCl added, the number of moles of HCl required to reach the endpoint is calculated. By equivalence, this equals the number of moles of *i*-PrMgCl, so from the volume that was initially added, the concentration of *i*-PrMgCl can be calculated. In my experience, this titration method will generally overestimate the concentration of the Grignard reagent by about 20-30%. Therefore, a test reaction will need to be performed to recalculate the concentration of *i*-PrMgCl, which is detailed in the next section.

Preparation of the active monomer: the test reaction and monomer conversion

In addition to needing an inert and moisture free environment for the successful synthesis of P3HT, the conversion of 2,5-dibromo-3-hexylthiophene (DB3HT) to the active monomer form is extremely important. The active monomer is the isomer that is produce when the Grignard metathesis occurs at the 5-position, yielding 2-bromo-5-chlormagnesio-3-hexylthiophene as shown in Scheme A-1. This isomer has been called "active" because this isomer is incorporated into the polymer chain exclusively when a nickel catalyst with a bulky phosphine ligand (diphenylphosphinopropane or diphenylphosphinoethane) is used during the polymerization, leading to a majority of head-to-tail couplings. However, it has been reported that the use of LiCl leads to a decrease in the regioregularity due to the incorporation of the reverse monomer in the polymer chain.[153] This needs to be considered when using LiCl to prepare the active monomer or when LiCl is used during an end-functionalization step. It is also important to note that the abundance of each isomer depends on the Grignard reagent chosen for the exchange. *i*-PrMgCl is used most often because it remains active after long periods of storage and when used in the

Grignard metathesis reaction a high abundance of the active monomer is produced.

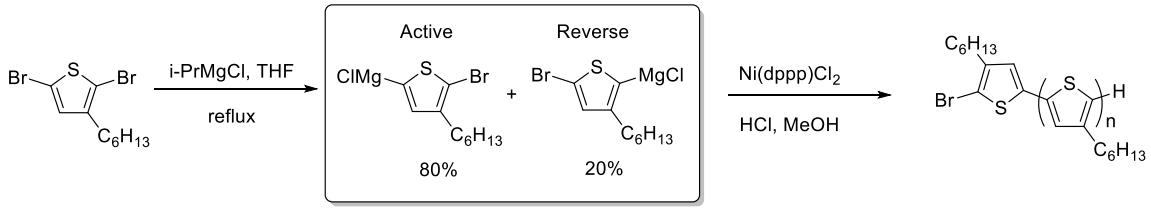

Scheme A-1. Reaction scheme for the synthesis of P3HT highlighting the formation of two isomers produced by the Grignard metathesis reaction of 2,5-dibromo-3-hexylthiophene with *i*-PrMgCl.

Gas chromatography-mass spectrometry (GC-MS) is a powerful tool for measuring the relative abundance of each monomer adduct, which gives insight into products that are obtained after the polymerization.

The stoichiometry of the GRIM reaction is also key to obtaining well-defined P3HT. Therefore, I consider the scenarios where the monomer can be "overconverted" or "underconverted". The overconverted scenario occurs when more than one equivalent of *i*-PrMgCl is used compared to the DB3HT starting material, which yields the 2,5-chloromagnesio-3-hexylthiophene product. This product is unfavourable because it terminates the polymer chain, preventing the nickel catalyst from reinserting and propagating. Also, if this overconverted monomer is added to the polymer chain, the polymer chain becomes a macromonomer and the polymerization mechanism may become more of a step growth mechanism rather than a chain growth mechanism. On the other hand, the underconverted scenario occurs when less than one

equivalent of *i*-PrMgCl is used compared to DB3HT. Once the *i*-PrMgCl is consumer, DB3HT is left over in the reaction pot, creating more sites from chain initiation. Therefore, I have found that the optimal ratio of DB3HT to *i*-PrMgCl is 1:0.95, which makes it crucial to know the exact concentration of the *i*-PrMgCl reagent.

Previously, I discussed how the titration of *i*-PrMgCl, either prepared in-house or purchased from a commercial source, usually provides an over-estimate of the concentration. Thus, a "test" reaction is needed to more accurately define the concentration. The test reaction is done on a small scale, typically 0.5 g to 1.0 g of DB3HT, in case the monomer conversion is not satisfactory (which is usually the cases and why I do a test reaction). The test reaction is performed exactly like a standard GRIM polymerization, except when an aliquot is taken and analysed by GC-MS, the new concentration of *i*-PrMgCl can be calculated from the abundance of each product observed in the chromatogram. This will be discussed in detail in the next section. The aliquot for GC-MS is obtained by carefully taking several tenths-of-a-milliliter of solution from the reaction vessel into a dry syringe that is equipped with an eight inch stainless steel needle (clean) and quenching this aliquot in the aqueous portion (bottom) a biphasic solution of 1:1 hexanes to 5 M HCl (~ 3-4 mL total in a scintillation vial). Then, the hexanes fraction is removed from the top via pipette and transferred into a vial compatible with the GC-MS instrument. The method on the GC-MS may need to be tuned to provide good resolution, depending on the instrument. Example GC chromatograms from each conversion scenario are shown in Figure A-1.

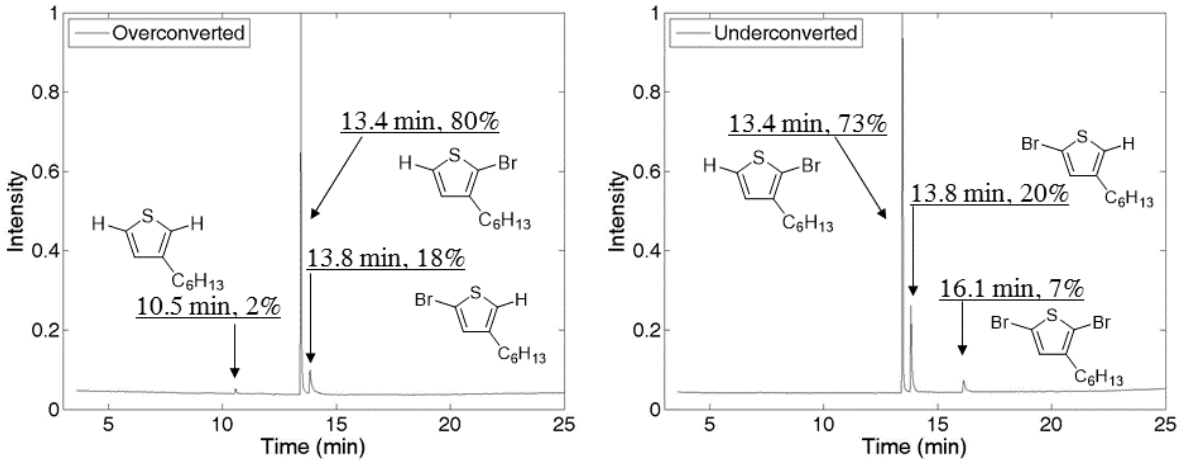

Figure A-1. Gas chromatograms from an overconverted (left) and an underconverted (right) batch of monomer.

The peaks at 13.4 min and 13.8 min correspond to the 2-bromo-3-hexylthiophene (active monomer) product and the 5-bromo-3-hexylthiophene (reverse monomer) product, respectively. It is important to note that when the isomers are quenched in the acid portion of the biphasic extraction solution, the -MgX functional group is replaced by a proton. The ratio of the peaks for each chromatogram is between 80:20 and 75:25, active monomer to reverse monomer. In Figure A-1 (left), the peak observed at 10.5 min corresponds to 3-hexylthiophene, which is indicative of an overconverted monomer scenario. On the other hand, in Figure A-1 (right) the peak at 16.1 min corresponds to unreacted 2,5-dibromo-3-hexylthiophene, indicating an underconverted monomer scenario. As stated before, overconverison is undesirable.

Once the test reaction is completed and the GC chromatogram is acquired, the GC chromatogram can be anaylzed in order to calculate the concentration of the *i*-PrMgCl that was used. This is done be simply multiplying the original number of moles of DB3HT that were used

in the reaction by the percentage of DB3HT that reacted with *i*-PrMgCl and then dividing this result by the volume of *i*-PrMgCl that was initially transferred to the reaction vessel via syringe. This is represented by Equation A-1, where $C_{i\text{-PrMgCl}}$, n_{DB3HT}, $\%_{DB3HT}$, and $V_{i\text{-PrMgCl}}$ are the corrected concentration of *i*-PrMgCl, the number of moles of DB3HT used in the test reaction, the percent abundance of unreacted DB3HT found from the GC chromatogram, and the volume of *i*-PrMgCl used in the test reaction, respectively.

$$C_{i-\mathrm{Pr}MgCl} = \frac{n_{DB3HT} * (100\% - \%_{DB3HT})}{V_{i-\mathrm{Pr}MgCl}} \quad \text{(A-1)}$$

The contents of the test reaction may be polymerized or properly disposed of in the appropriate waste container. The yield of the corresponding polymer is typically low (large abundance of unreacted DB3HT) and not well defined, but the polymer will be comparable to commercially prepared materials.

Preparation of P3HT using the standard GRIM polymerization method

In a dry 500 mL 3-neck flask, 2,5-dibromo-3-hexylthiophene (1.08 g, 3.31 mmol) (and 0.95 eq. LiCl, if applicable) was dissolved in 40 mL of THF. The reaction vessel was equipped with a stir bar, condenser, and two Teflon stoppers. The solution was sparged with nitrogen for 30 min. *i*-PrMgCl (2.3 mL, 3.14 mmol) was transferred to the flask via syringe and the mixture was heated under reflux for 2 h. The reaction was monitored by GC-MS to ensure complete metal-halogen exchange (target 95% conversion), and the absence of overconversion of the monomer. Once complete, the mixture was cooled to room temperature, $Ni(dppp)Cl_2$ (0.064 g, 0.118 mmol) was added, and the mixture was stirred for an additional 15 min. Then, 20 times molar excess of

monofunctional Grignard reagent compared to nickel catalyst can be added to end-functionalize the polymer. Otherwise, the reaction should be quenched with 5M HCl and allowed to stir for several minutes. The final mixture was precipitated into methanol.

As previously stated, the monomer conversion is very important for preparing well-defined P3HT. In addition, the reaction mixture should be at room temperature before addition of the nickel catalyst. A water bath can be placed under the reaction vessel to expedite the process and minimize temperature fluctuations. It should be noted that the color of the reaction solution will become a vibrant reddish color several minutes after addition of the nickel catalyst. Also, a distinct yellow film will be observed on the glass walls of the reaction vessel if lightly swirled, which can be used as another indication that poly(3-hexylthiophene) is forming. The most obvious indication of a successful polymerization occurs when the polymer is precipitated into methanol. A light red to dark purple precipitate forms immediately when the reaction mixture is slowly added to methanol.

As far as quenching reagents are concerned, HCl is the most useful but cannot be used with end-groups that are sensitive to strong acids. In that case, methanol is the second best choice. Do not use water to precipitate the polymer solution! A multimodal distribution typically forms and this has been well documented.[4]

Preparation of P3HT-$SiCl_3$: Polymer brushes for anode buffer layers

Trichlorosilane terminated P3HT was prepared according to a modified literature procedure.[154] In a new dry 20 mL scintillation vial, allyl (or vinyl) terminated P3HT (0.100g, M_n=2.5 kDa by MALDI-TOF MS) was dissolved in ~15 mL of dry benzene (may need to heat to ~50 ^oC for full

dissolution). Then, the solution of allyl-P3HT in benzene was transferred to a clean, dry 100 mL custom-made glass reaction vessel (example displayed in Figure A-2) via canula. **NOTE: Silanizing the glassware may make the glassware easier to clean.** The custom reaction vessel is equipped with a clean stir bar, diluted with 20 mL of dry benzene and then placed on the Schlenk line. The reaction mixture was degassed. Then, the vessel was refilled with N_2 and allowed to purge with N_2 for several minutes before continuing. All future additions and extractions of material were performed with a positive flow of N_2 to prevent contamination by ambient air. Next, an excess of $HSiCl_3$ (0.5 mL) was added to the reaction vessel via syringe. Finally, Karstedt's catalyst (0.2 mL, 1 wt % in xylene) was added to the reaction mixture and the reaction was sealed off and heated to 90 ^oC with stirring for ~18 h. Please note that Speier's catalyst was used initially, but the Karstedt's catalyst was later used due to its improved solubility in benzene. Once the reaction is complete, the excess $HSiCl_3$ was removed by repeated vacuum transfers of clean benzene into and out of the reaction vessel. (When benzene is removed by applying vacuum, a vacuum trap cooled by liquid nitrogen must be used to prevent pump damage. A clean trap should be used with each cycle.) Then, the vessel was dried under vacuum for 18 h. The product was reconstituted by adding dry chloroform via syringe. It should be noted that other solvents may be used to reconstitute the P3HT-$SiCl_3$ such as dichlorobenzene, which may improve the formation of films when spin casting.

Figure A-2. A custom-made glass reaction vessel used to prepare and store P3HT-$SiCl_3$.

Appendix B- Chapter 2: End-Group Composition of Poly(3-hexylthiophene)s Prepared by in situ Quenching of the GRIM Polymerization

Molecular weight data for tolyl-functionalized P3HTs

The molecular weight of each P3HT sample described in Chapter 2 was determined by both SEC (relative to polystyrene standards) and MALDI-TOF MS, and the results are shown in Table B-1.

Table B-1. SEC and MALDI-TOF MS molecular weight data for tolyl-functionalized P3HTs.

	SEC-RI			MALDI-TOF MS		
	M_n	M_w	PDI	M_n	M_w	PDI
P3HT0	-	-	-	-	-	-
P3HT1	3200	4200	1.30	1850	2040	1.13
P3HT2	2700	3600	1.34	1720	1880	1.09
P3HT3	3400	4500	1.33	1650	1820	1.10
P3HT4	3200	4300	1.35	1660	1840	1.11
P3HT5	3200	4000	1.27	1800	2030	1.12
P3HT6	3300	5000	1.51	1350	1520	1.12
P3HT7	3400	5400	1.56	1480	1570	1.07
P3HT8	4400	5600	1.27	1870	2090	1.12
P3HT9	4700	6000	1.28	1810	1960	1.12
P3HT10	4000	5300	1.30	1720	1840	1.09
P3HT11	4700	7500	1.59	1680	1800	1.07
P3HT12	3700	5800	1.54	1700	2000	1.18
P3HT13	4500	6100	1.37	1710	1880	1.10

Calculation of end-group composition based on modeled spectra

In general, the relative amounts of different species observed by MALDI-TOF MS can be calculated from the monoisotopic peak heights within a given mass range. When the distributions are distinguishable from each other, determining the end-group composition is trivial, but as discussed in Chapter 2 when two distributions overlap (i.e. Br/C_7H_7 and H/H) the composition of the peak must first be determined using the MATLAB fitting program in order to calculate the end-group composition. As shown in Figure 2-2 of Chapter 2 for **P3HT12**, the distributions for $Br(C_{10}H_{14}S)_{10}C_7H_7$ and $H(C_{10}H_{14}S)_{11}H$ differ in mass by 2 amu and thus overlap. Using the MATLAB program it was determined that the observed distribution was composed of 91% $Br(C_{10}H_{14}S)_{10}C_7H_7$ and 9% $H(C_{10}H_{14}S)_{11}H$. The monoisotopic peak intensity for the $H(C_{10}H_{14}S)_{11}H$ species at *m/z* 1828.59 is found to be 727 using the Bruker FlexAnalysis software. The monoisotopic peak height for the $Br(C_{10}H_{14}S)_{10}C_7H_7$ species can then be calculated using Equation B-1 where $\%H(Th)_nH$ is the percent of the n-mer with H/H end-groups

$$\%H(Th)_nH = \frac{I_{H(Th)_nH}}{I_{H(Th)_nH} + I_{Br(Th)_{n-1}C_7H_7}} \quad \text{(B-1)}$$

in the distribution as determined using the MATLAB program, $I_{H(Th)_nH}$ is the monoisotopic peak intensity of the n-mer with H/H end groups and $I_{Br(Th)_{n-1}C_7H_7}$ is the monoisotopic peak intensity of the n-1 mer with Br/C_7H_7 end groups. For clarity purposes, the abbreviation Th was used to represent $C_{10}H_{14}S$. For **P3HT12**,

$$9\% = \frac{727}{727 + I_{Br(Th)_{10}C_7H_7}} \times 100$$

$$I_{Br(Th)_{10}C_7H_7} = 7351$$

It is important to note that because the 10-mer $Br(C_{10}H_{14}S)_{10}C_7H_7$ overlaps with the 11-mer $H(C_{10}H_{14}S)_{11}H$ distribution in the mass spectrum, it is appropriate to use the intensity of the monoisotopic peak for the 10-mer $H(C_{10}H_{14}S)_{10}H$ in the calculation of the end-group composition. This ensures that the end-group composition is calculated using the intensities of species with the same number of repeat units. Table B-2 shows the monoisotopic peak heights for each species observed by MALDI-TOF MS, and the relative abundance of each calculated from the monoisotopic peak height. Using this methodology, **P3HT12** was found to contain 27% C_7H_7/C_7H_7, 15% H/C_7H_7, 37% Br/C_7H_7, 17% Br/H and 4% H/H. The remainder of the end-group compositions are provided in Tables 2-1, 2-2 and 2-3 in Chapter 2.

Table B-2. Monoisotopic peak heights used in the calculation of the end-group composition for the 10-mer of P3HT12.

Species	Obs. *m/z*	Monoisotopic Peak Height	Relative Abundance (%)
$Br(C_{10}H_{14}S)_{10}C_7H_7$	--	7351	37
$H(C_{10}H_{14}S)_{10}C_7H_7$	1752.55	2937	15
$C_7H_7(C_{10}H_{14}S)_{10}C_7H_7$	1842.60	5329	27
$Br(C_{10}H_{14}S)_{10}H$	1740.39	3380	17
$H(C_{10}H_{14}S)_{10}H$	1662.43	695	4
$H(C_{10}H_{14}S)_{11}H$	1828.59	727	--

MALDI-TOF MS spectra, modeled spectra, and SEC chromatograms for tolyl-functionalized P3HTs

P3HT1: The MALDI-TOF mass spectra of **P3HT1** is given in Figure 2-1 in Chapter 2.

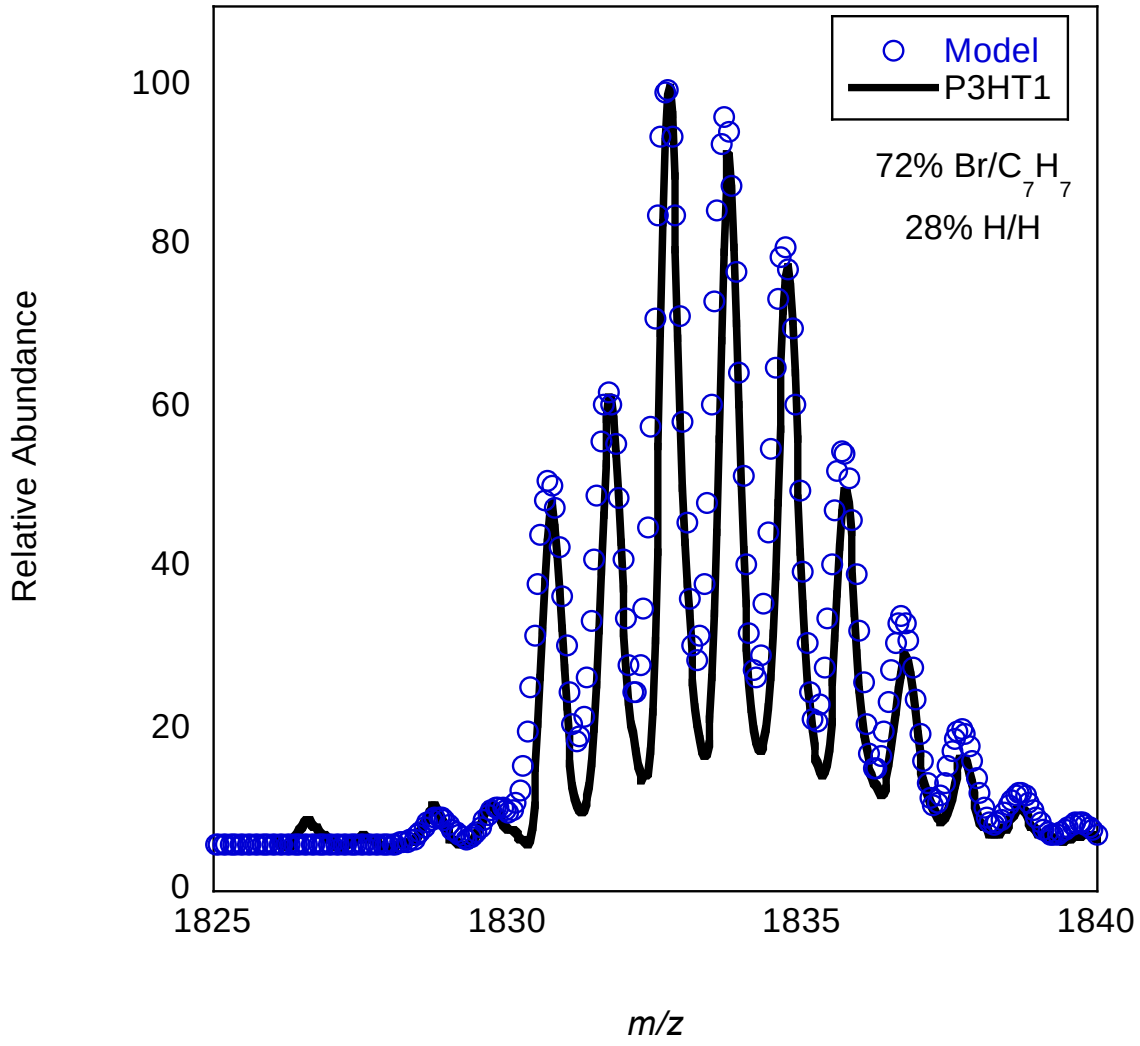

Figure B-1. Modeled spectrum for **P3HT1** showing the estimated abundance of Br/C_7H_7 and H/H terminated chains in the overlapping distribution.

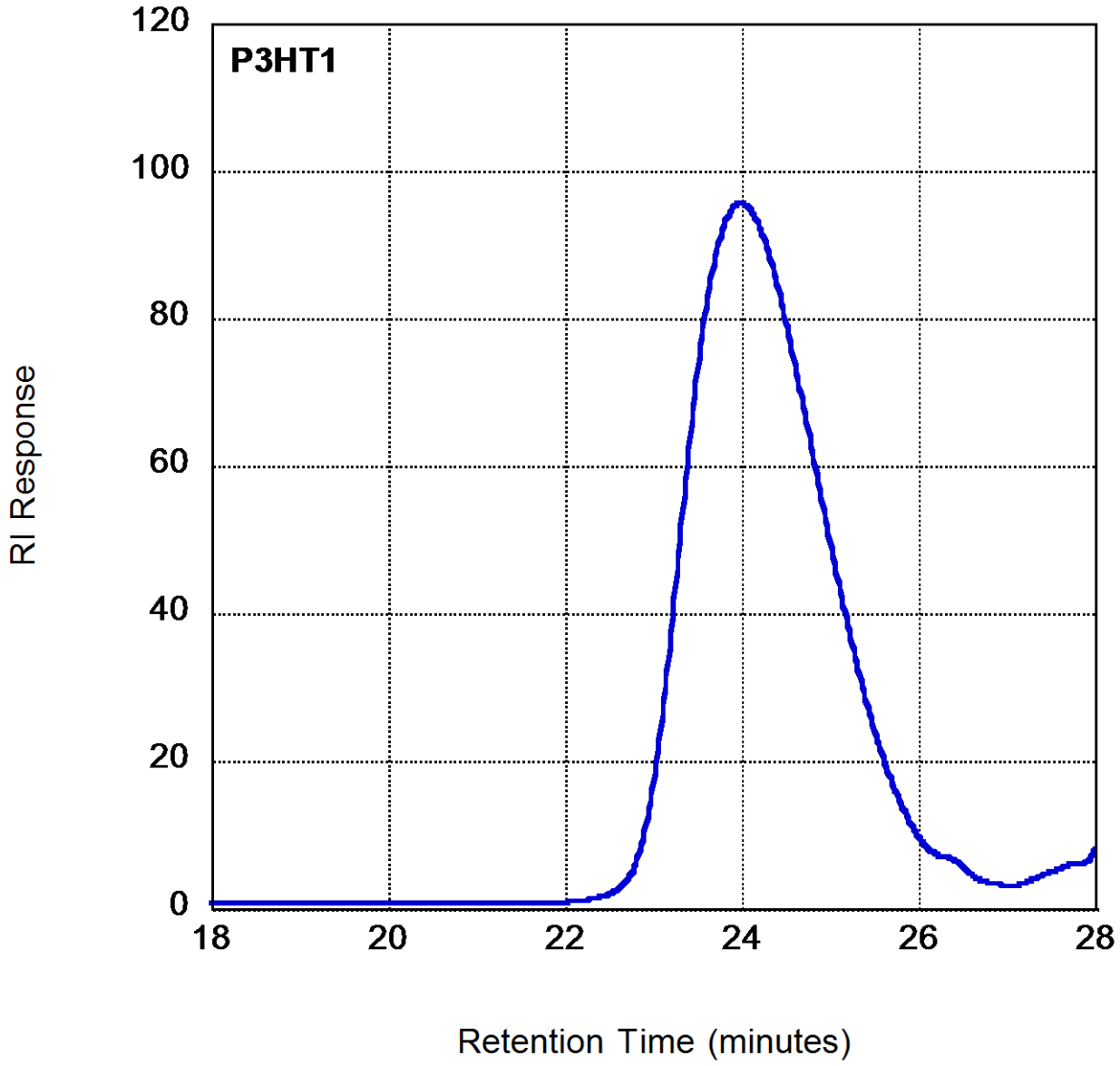

Figure B-2. SEC chromatogram for **P3HT1**.

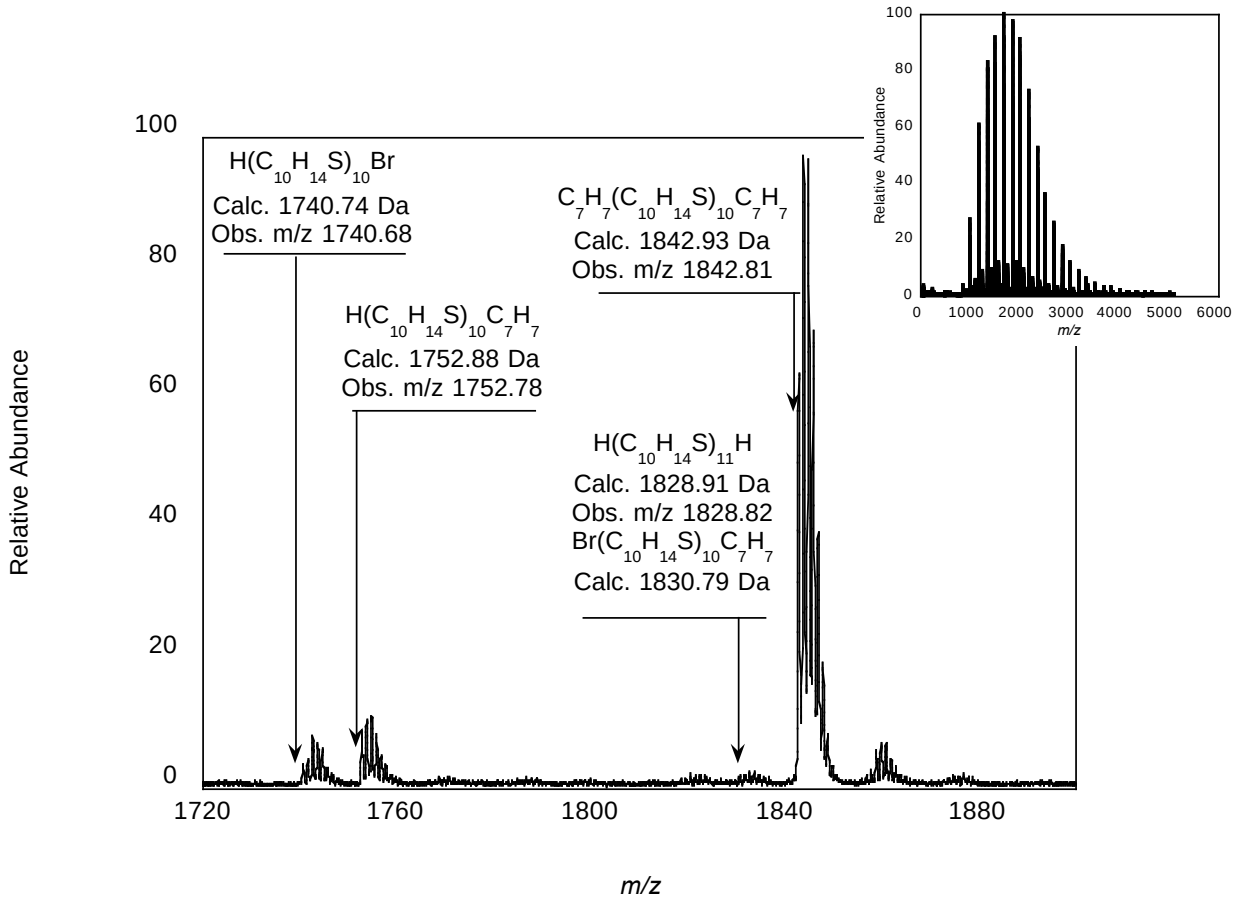

Figure B-3. Magnification of the 10-mer region of **P3HT2** with the full mass spectrum shown as an inset.

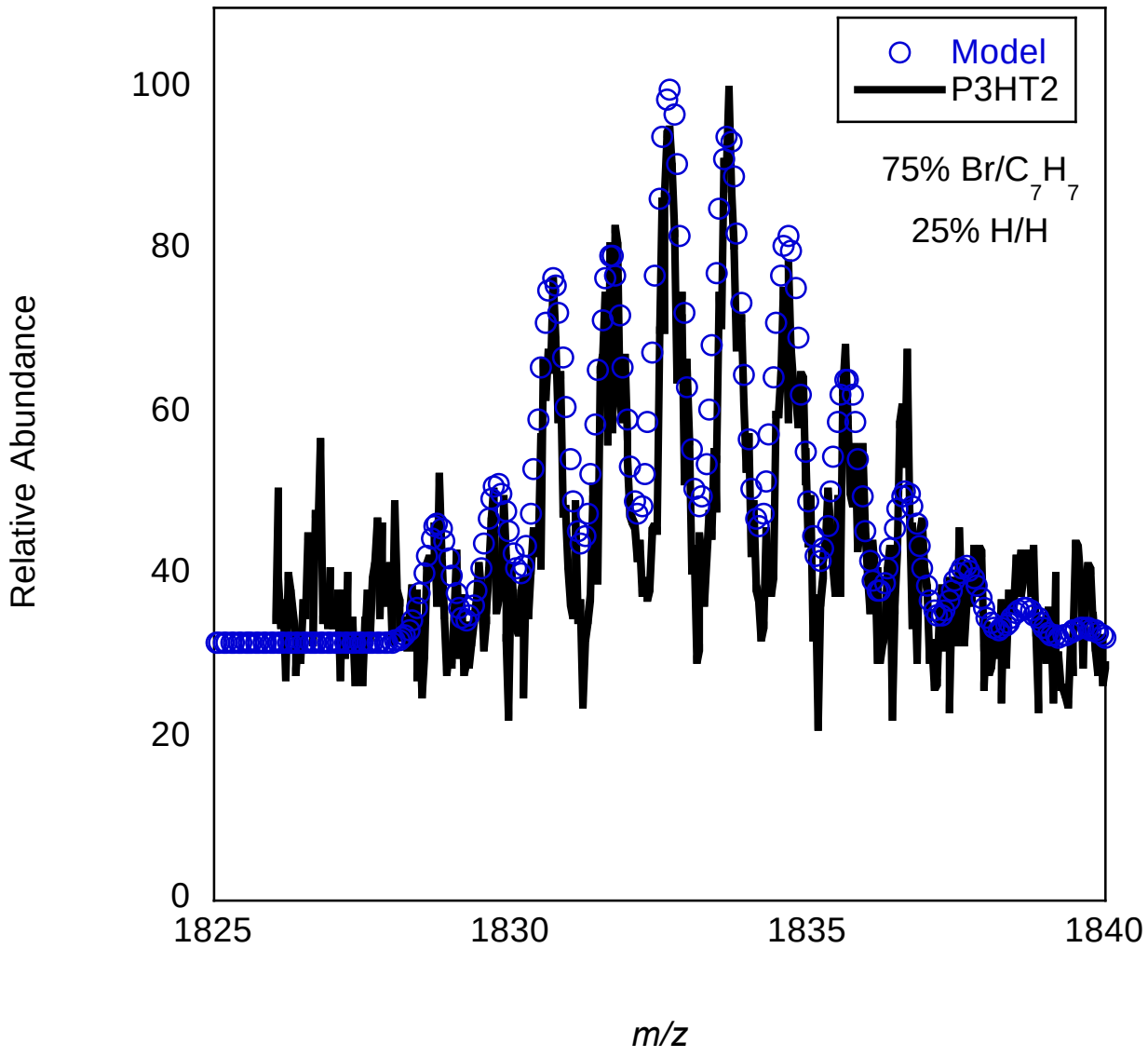

Figure B-4. Modeled spectrum for **P3HT2** showing the estimated abundance of Br/C_7H_7 and H/H terminated chains in the overlapping distribution.

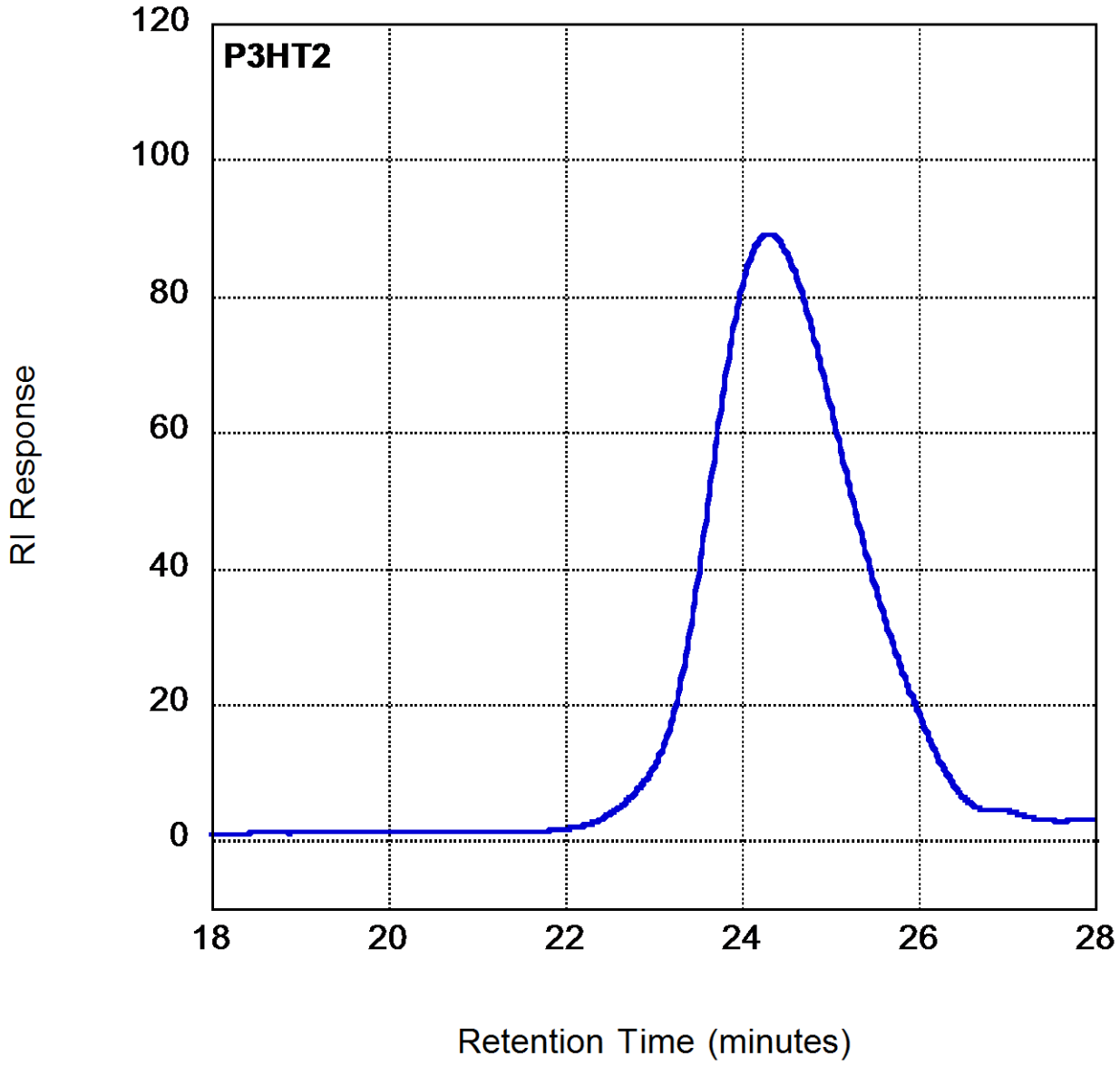

Figure B-5. SEC chromatogram for **P3HT2.**

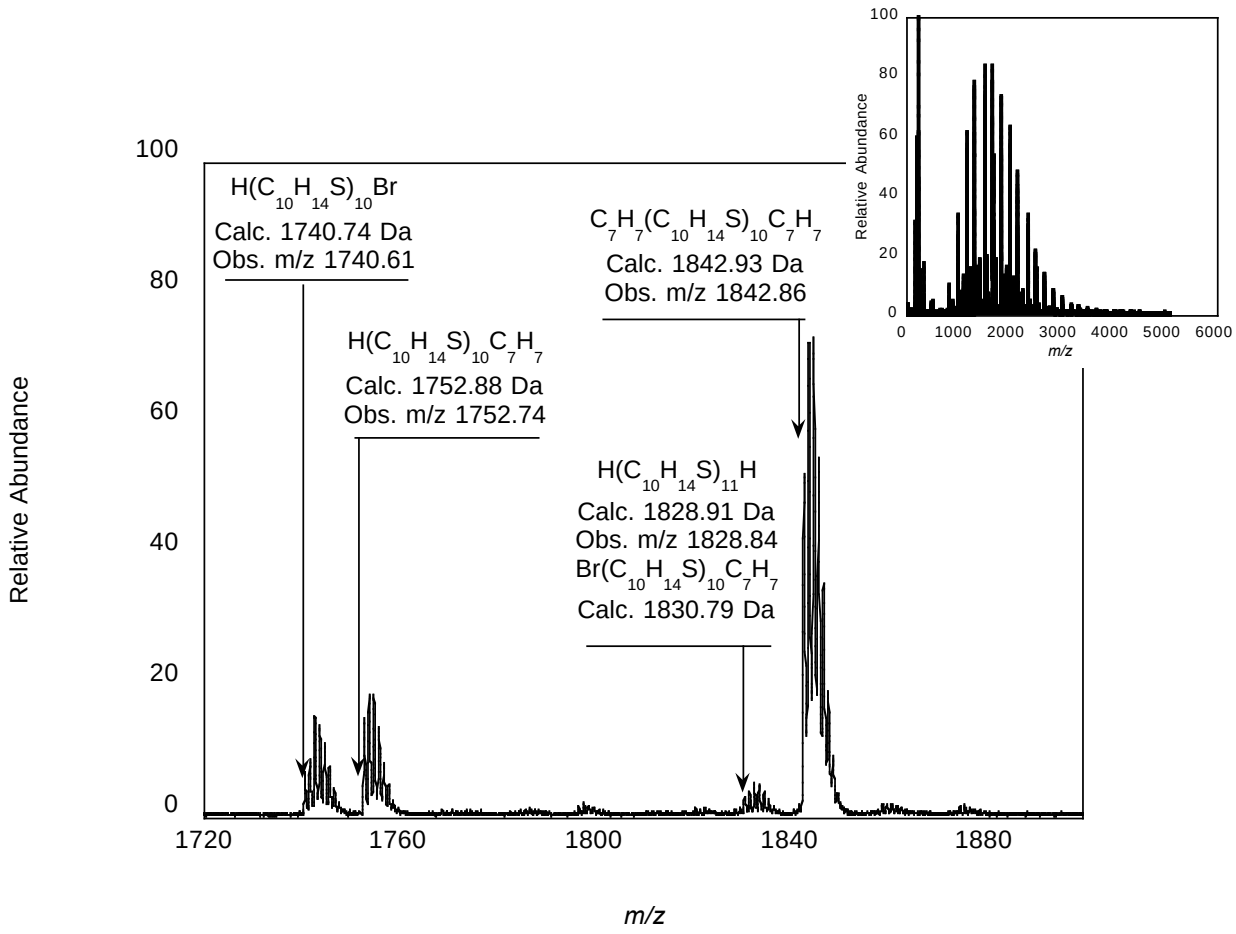

Figure B-6. Magnification of the 10-mer region of **P3HT3** with the full mass spectrum shown as an inset.

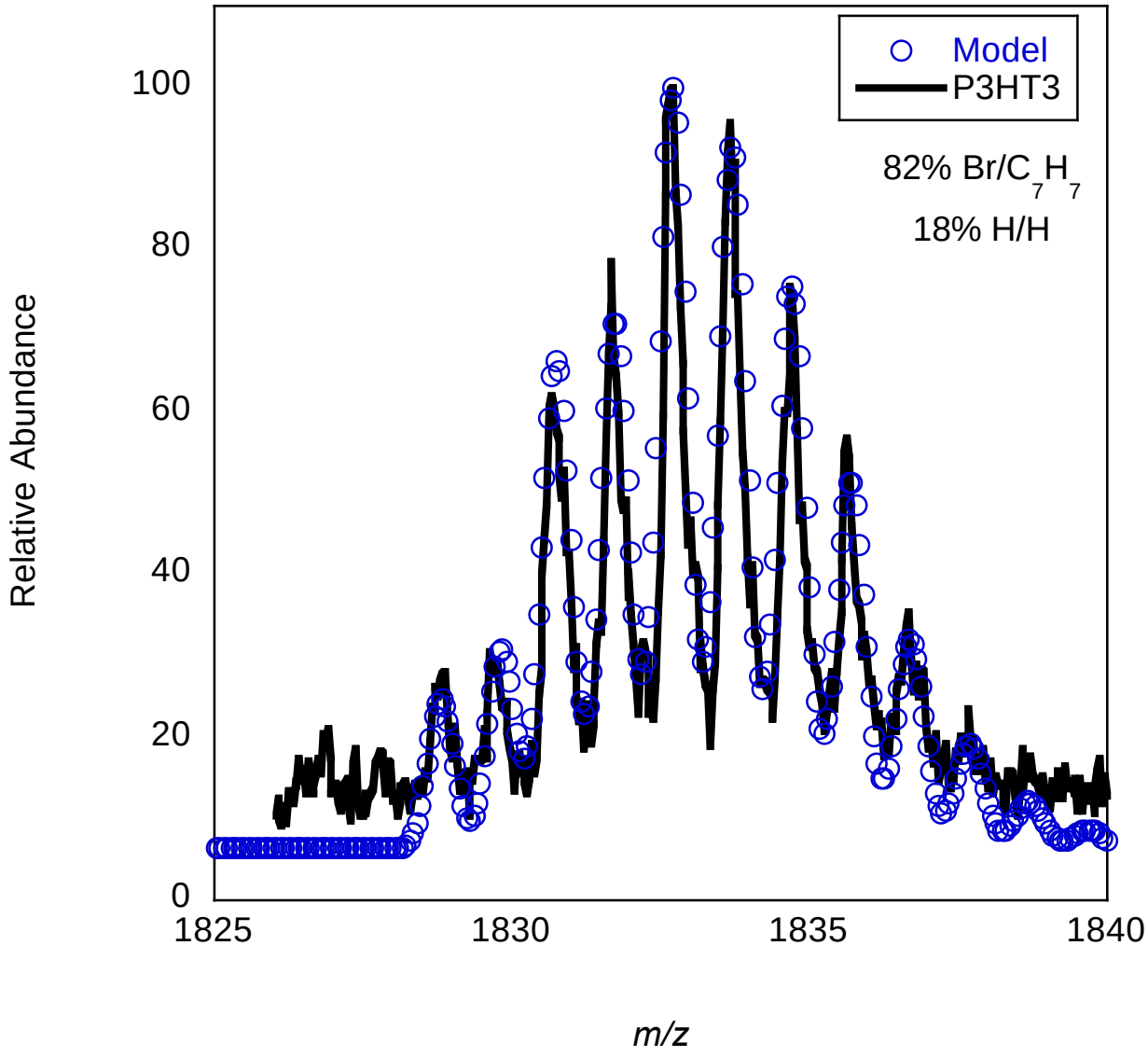

Figure B-7. Modeled spectrum for **P3HT3** showing the estimated abundance of Br/C_7H_7 and H/H terminated chains in the overlapping distribution.

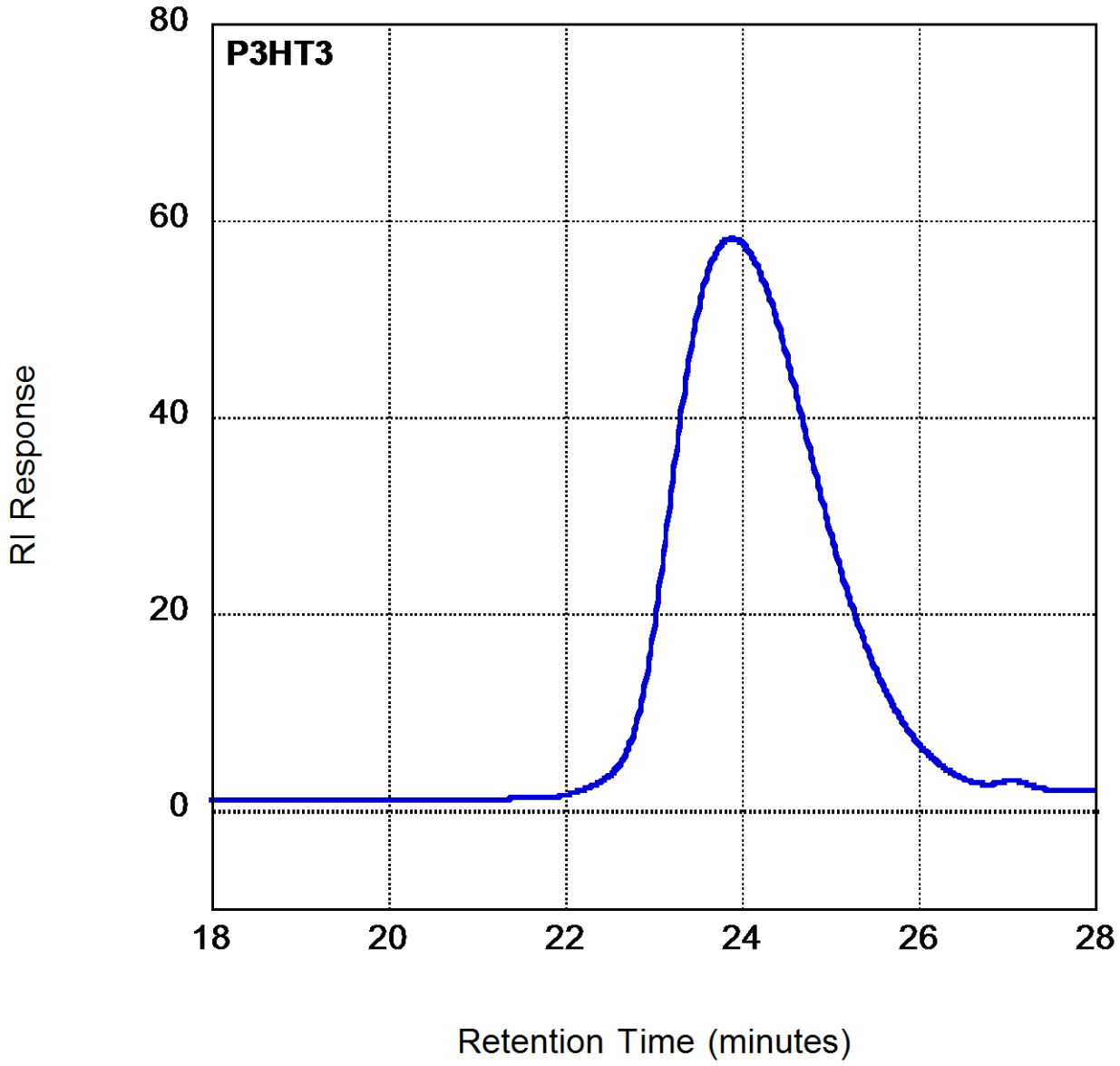

Figure B-8. SEC chromatogram for **P3HT3**.

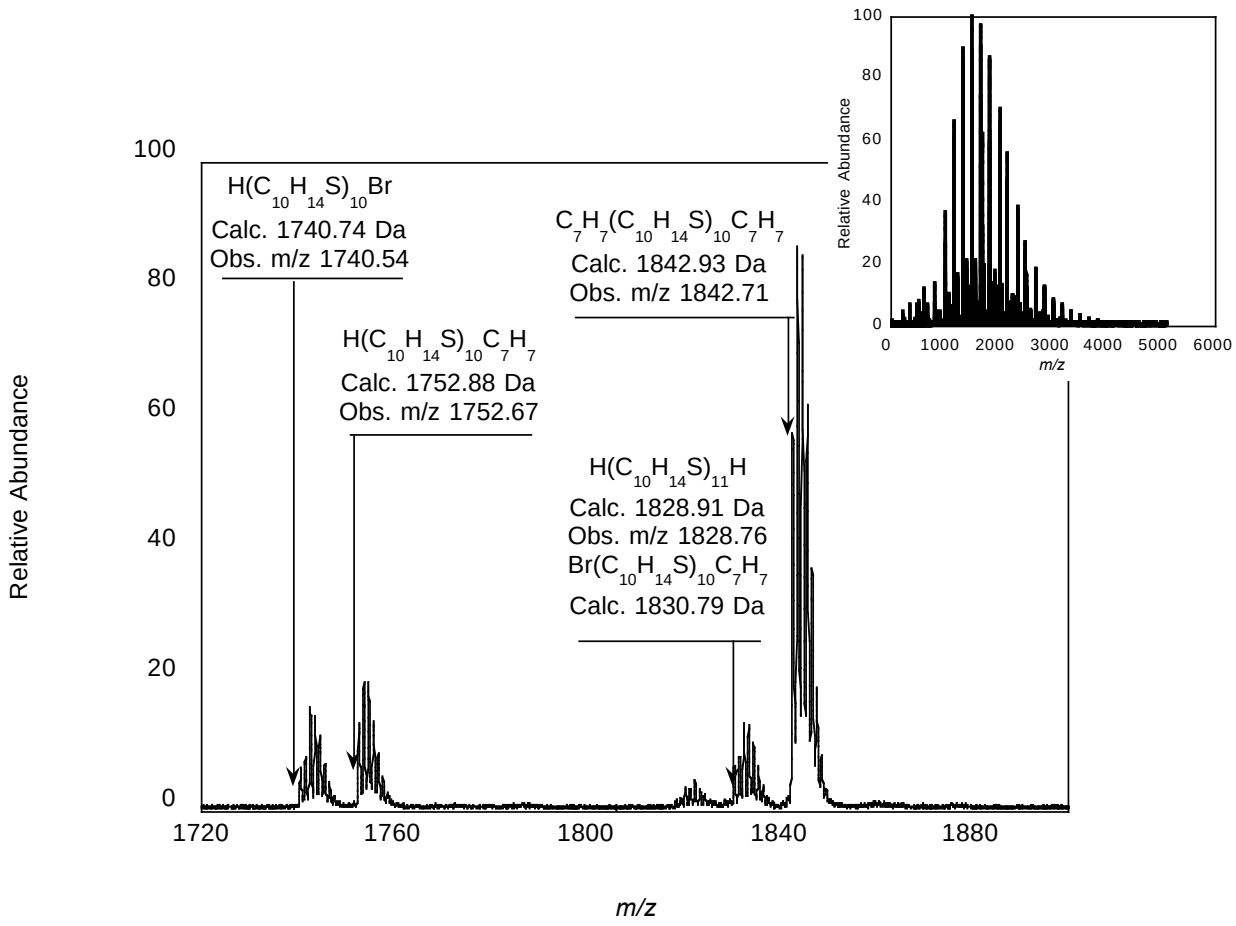

Figure B-9. Magnification of the 10-mer region of **P3HT4** with the full mass spectrum shown as an inset.

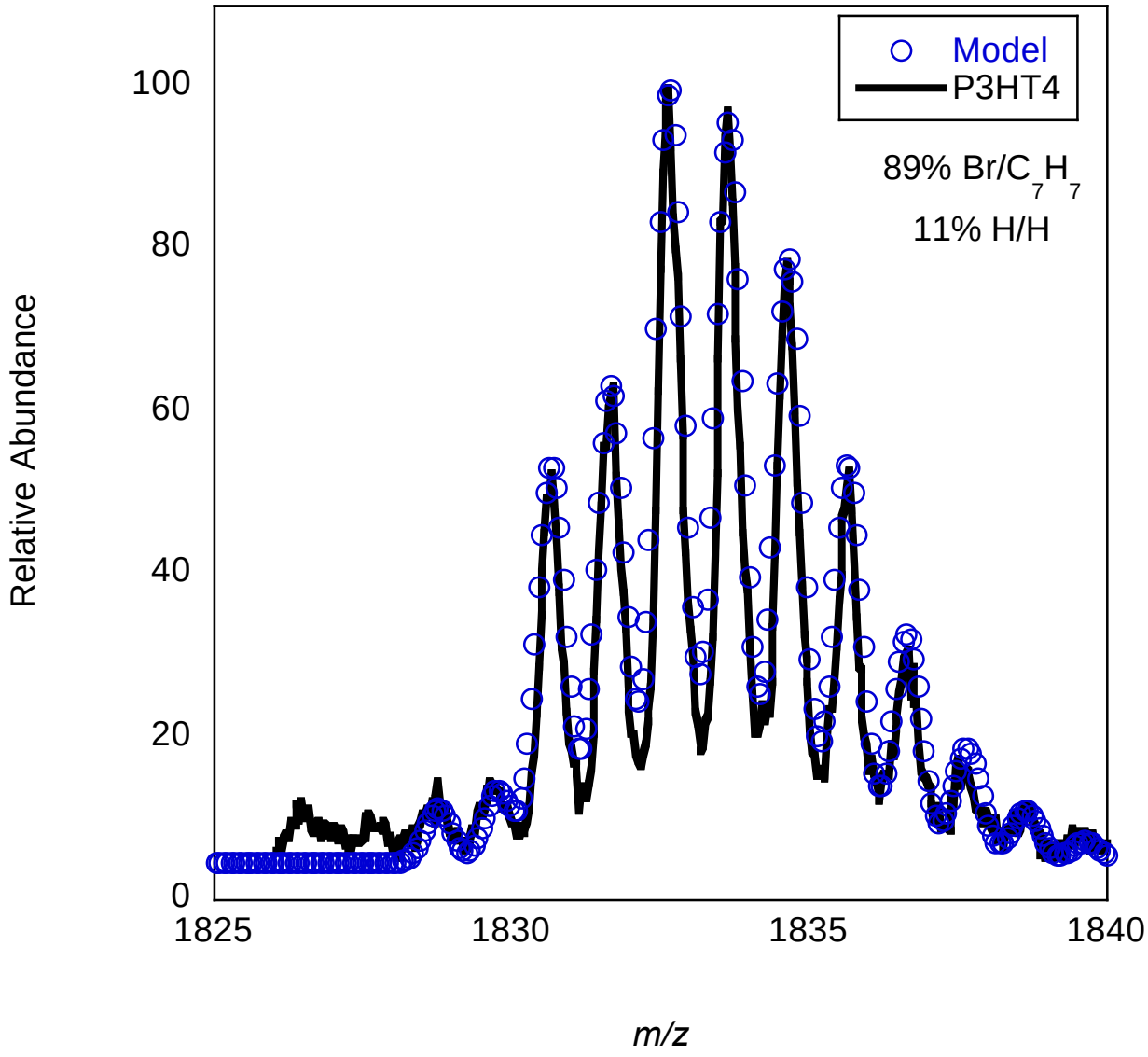

Figure B-10. Modeled spectrum for **P3HT4** showing the estimated abundance of Br/C_7H_7 and H/H terminated chains in the overlapping distribution.

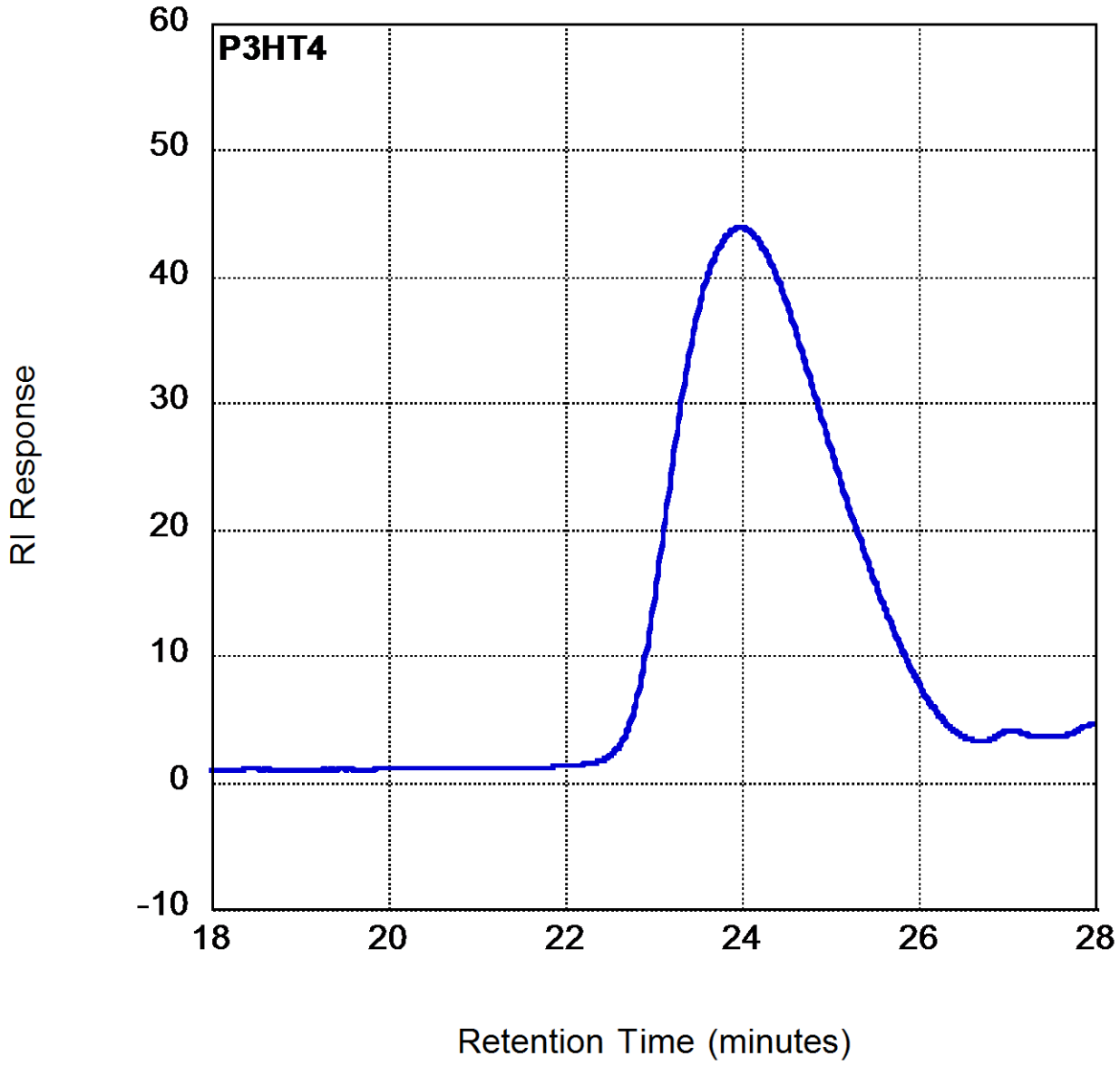

Figure B-11. SEC chromatogram for **P3HT4**.

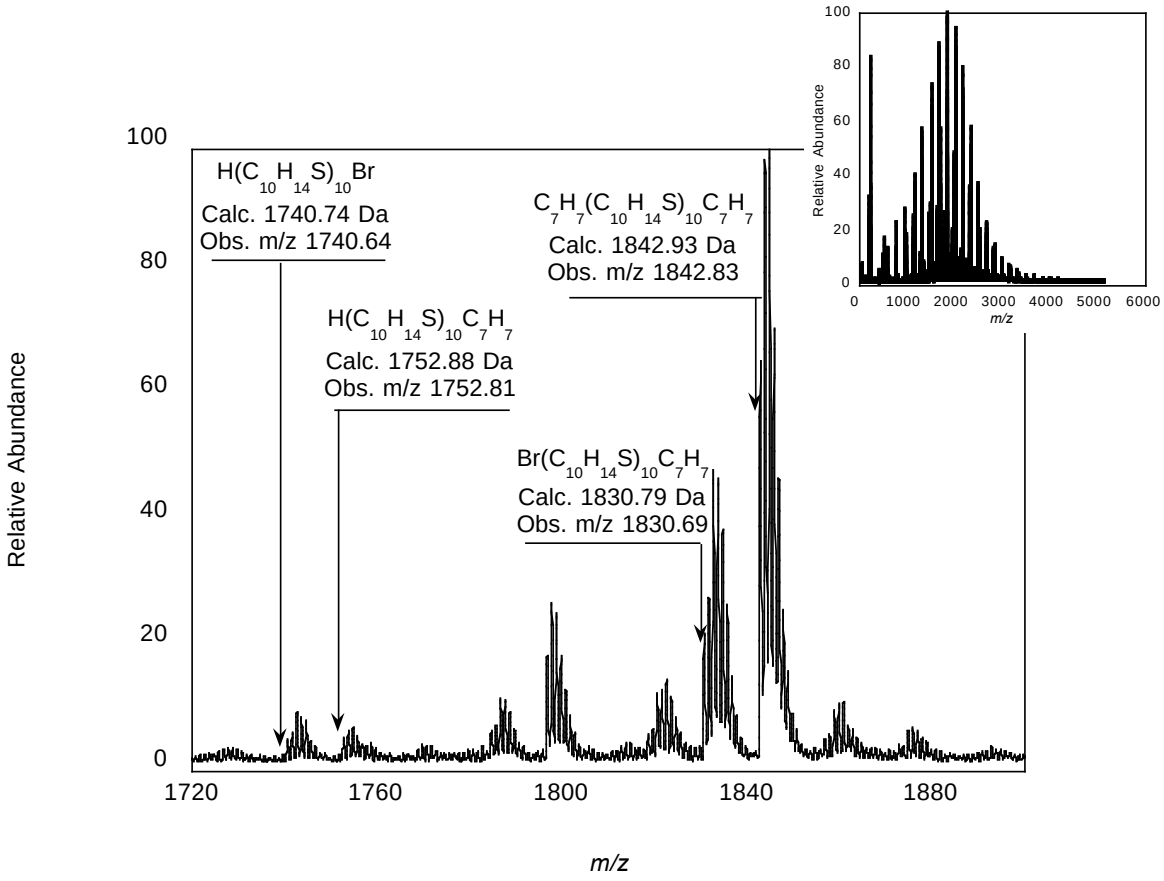

Figure B-12. Magnification of the 10-mer region of **P3HT5** with the full mass spectrum shown as an inset.

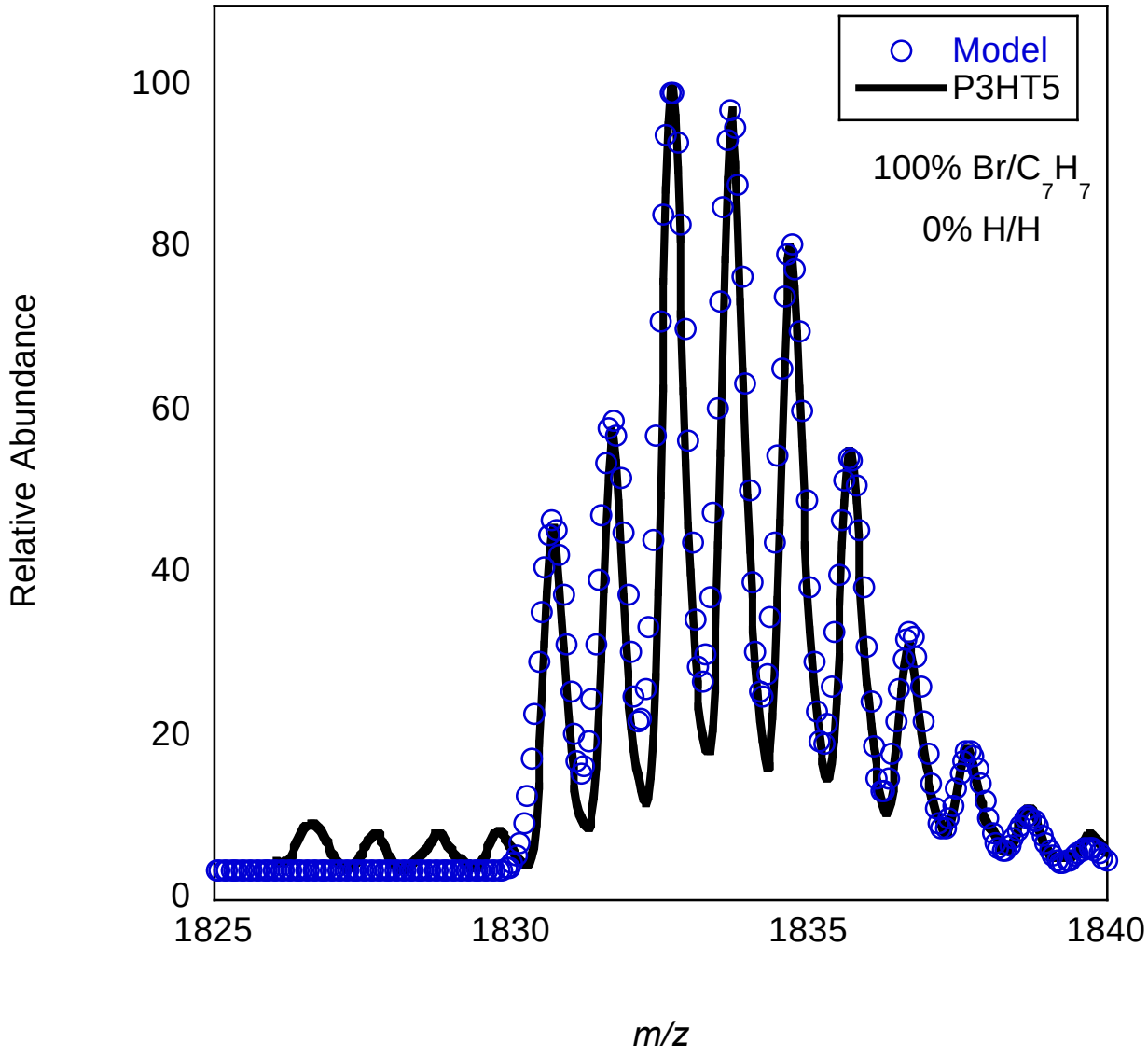

Figure B-13. Modeled spectrum for **P3HT5** showing the estimated abundance of Br/C_7H_7 and H/H terminated chains in the overlapping distribution.

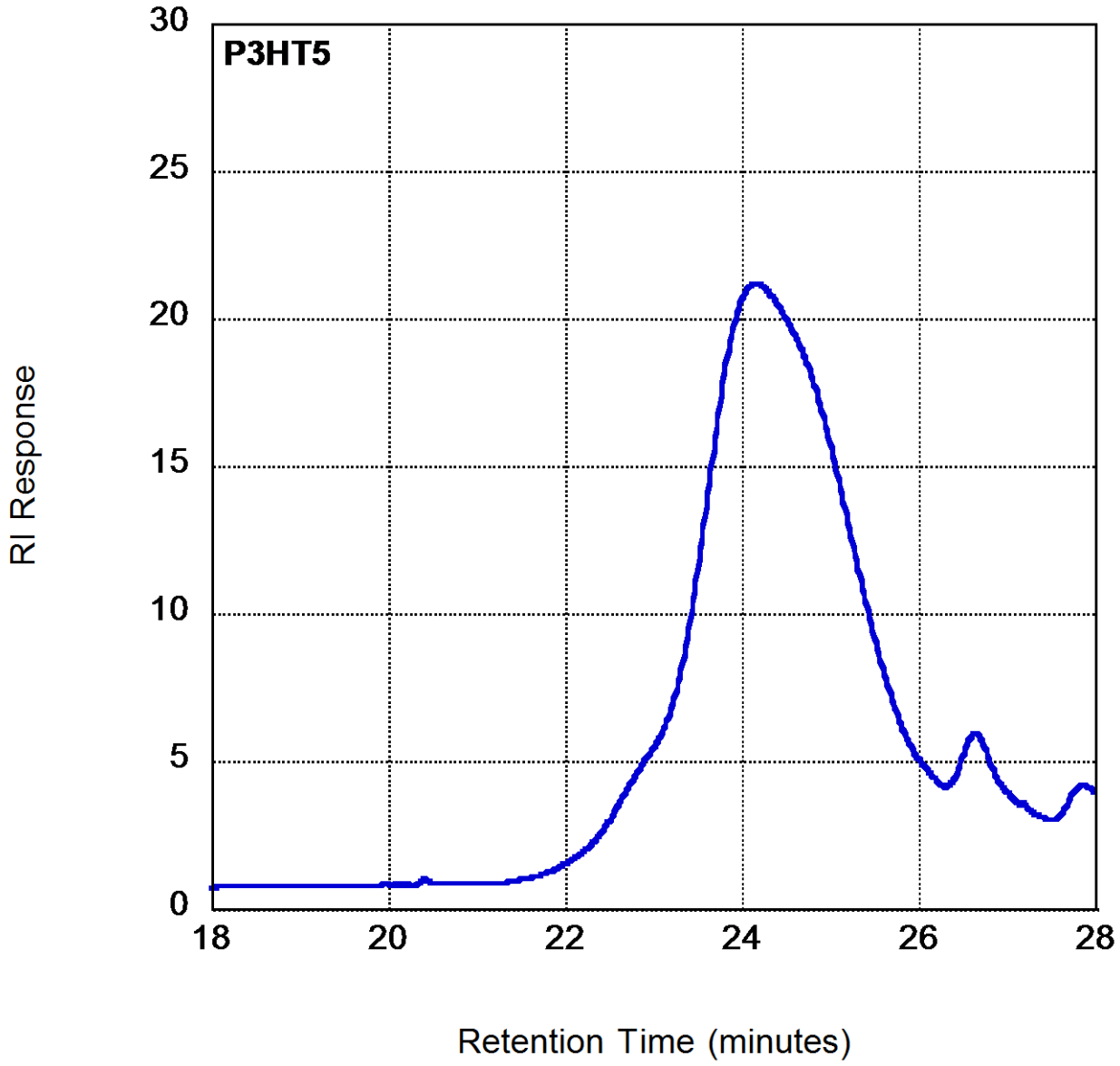

Figure B-14. SEC chromatogram for **P3HT5**.

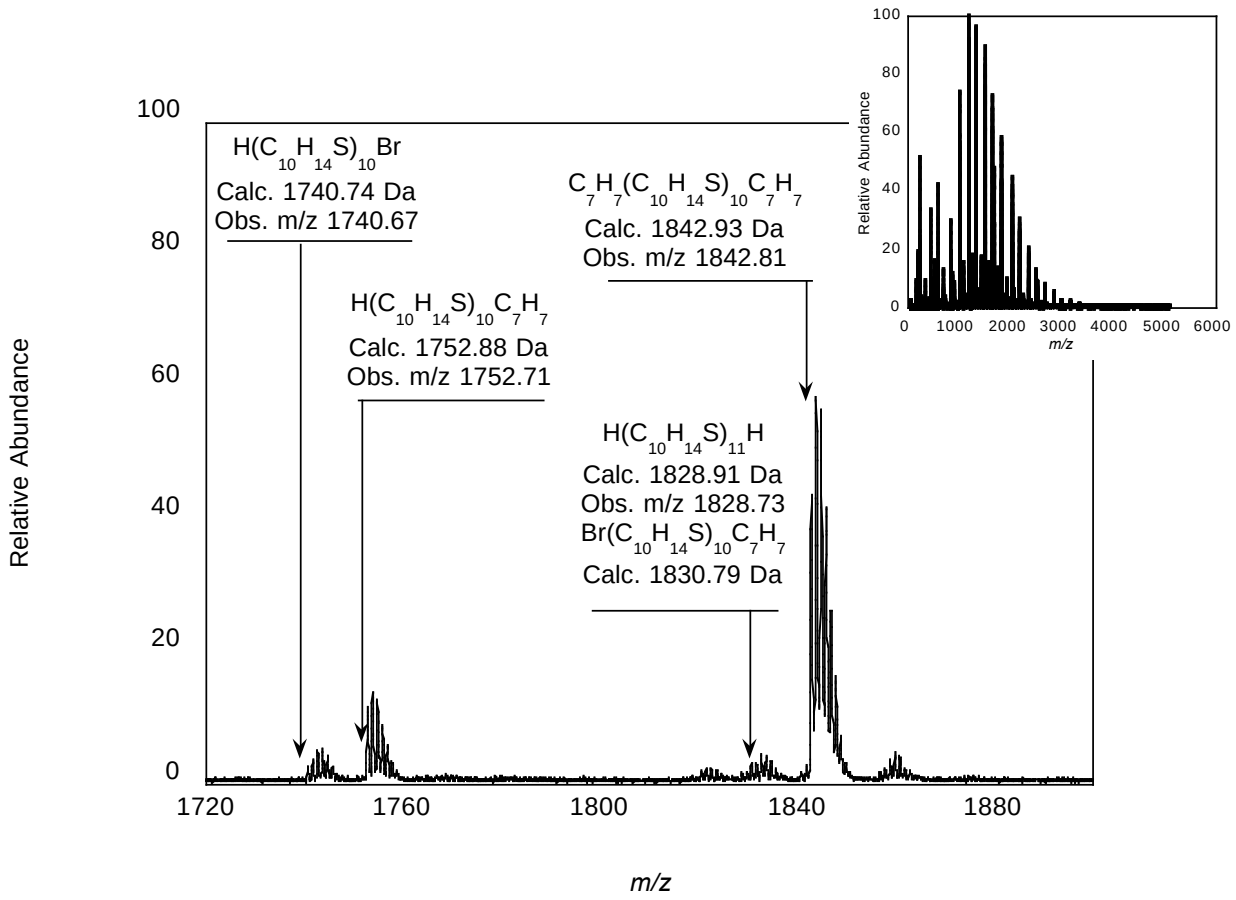

Figure B-15. Magnification of the 10-mer region of **P3HT6** with the full mass spectrum shown as an inset.

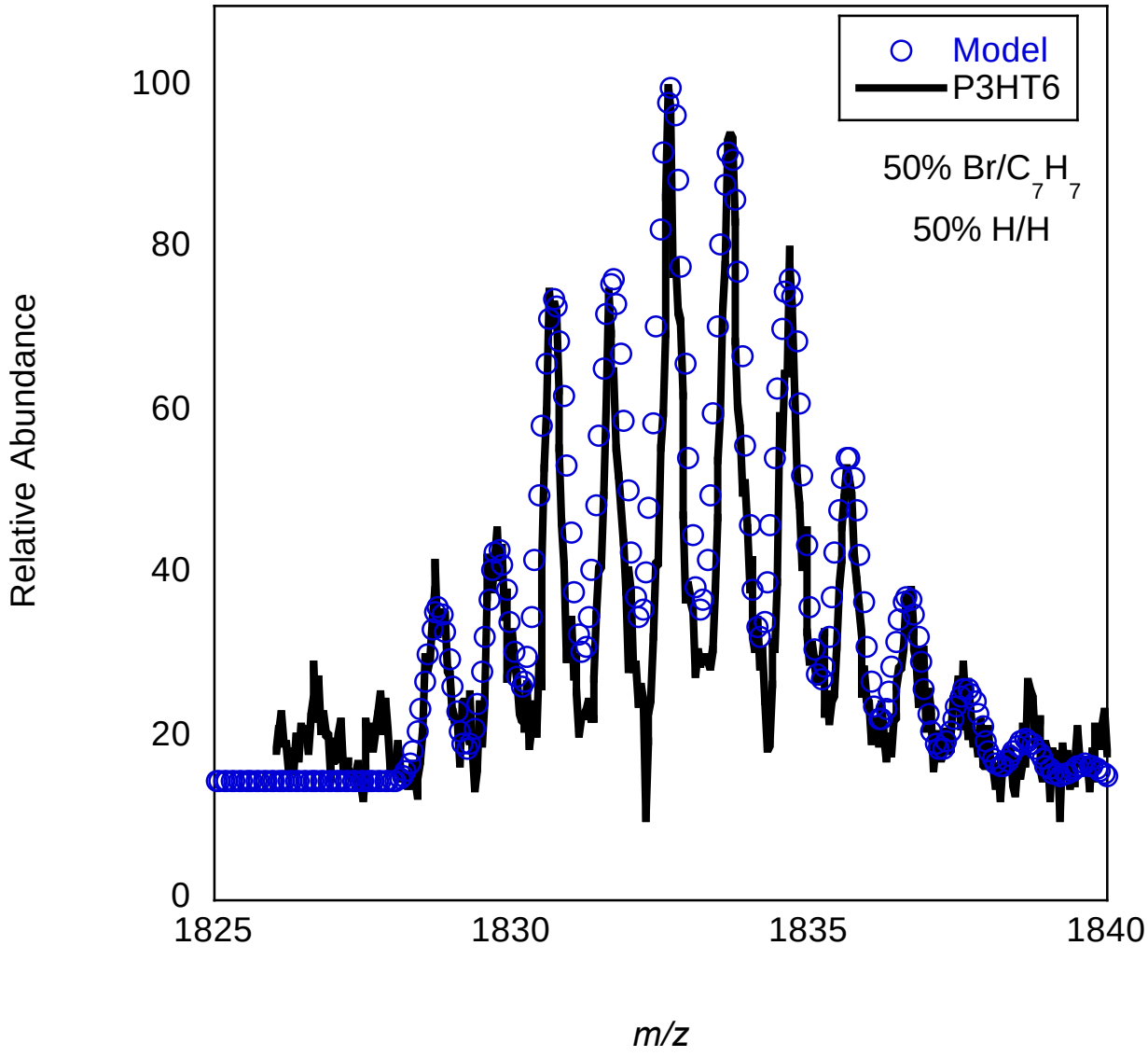

Figure B-16. Modeled spectrum for **P3HT6** showing the estimated abundance of Br/C_7H_7 and H/H terminated chains in the overlapping distribution.

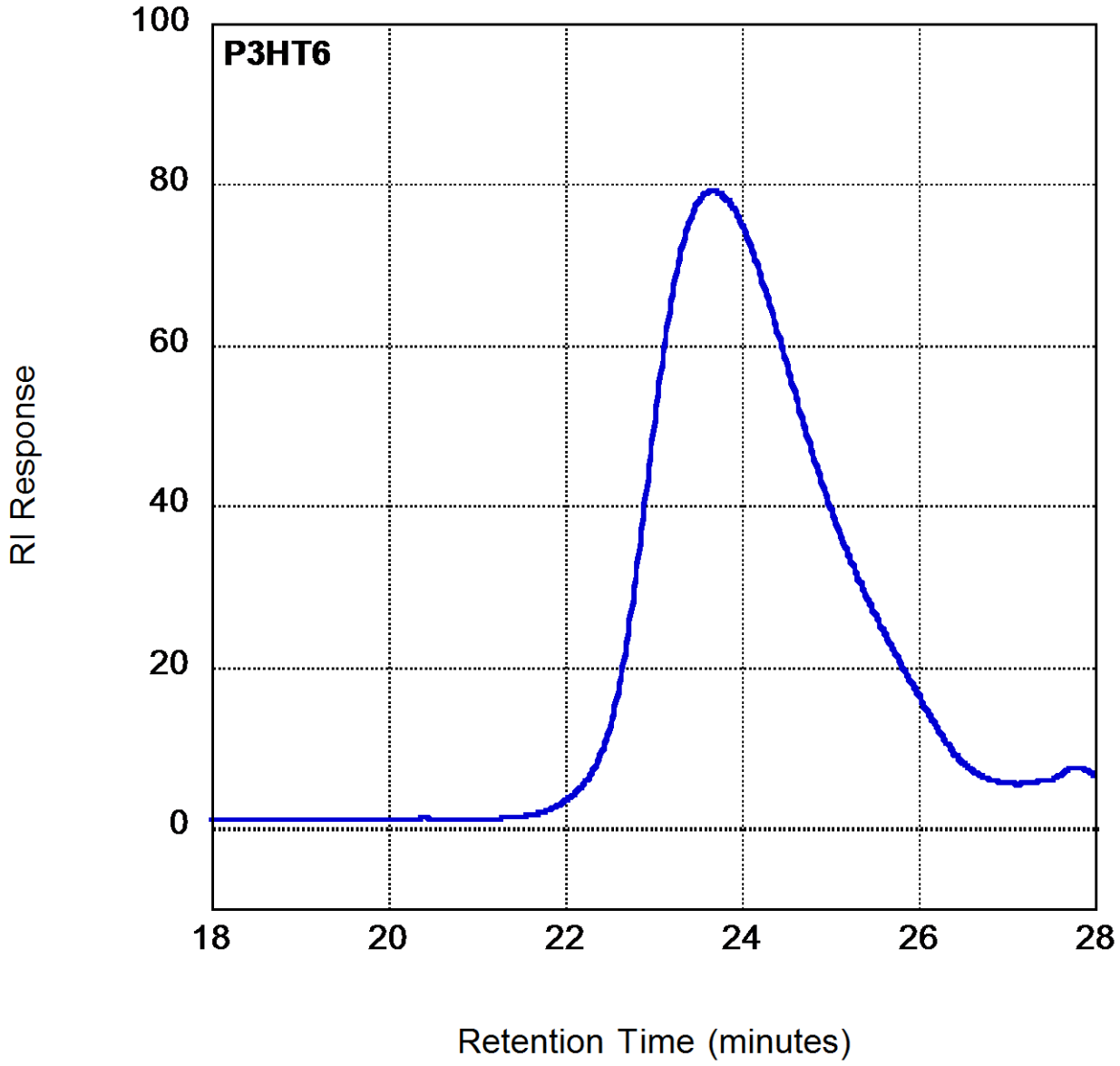

Figure B-17. SEC chromatogram for **P3HT6**.

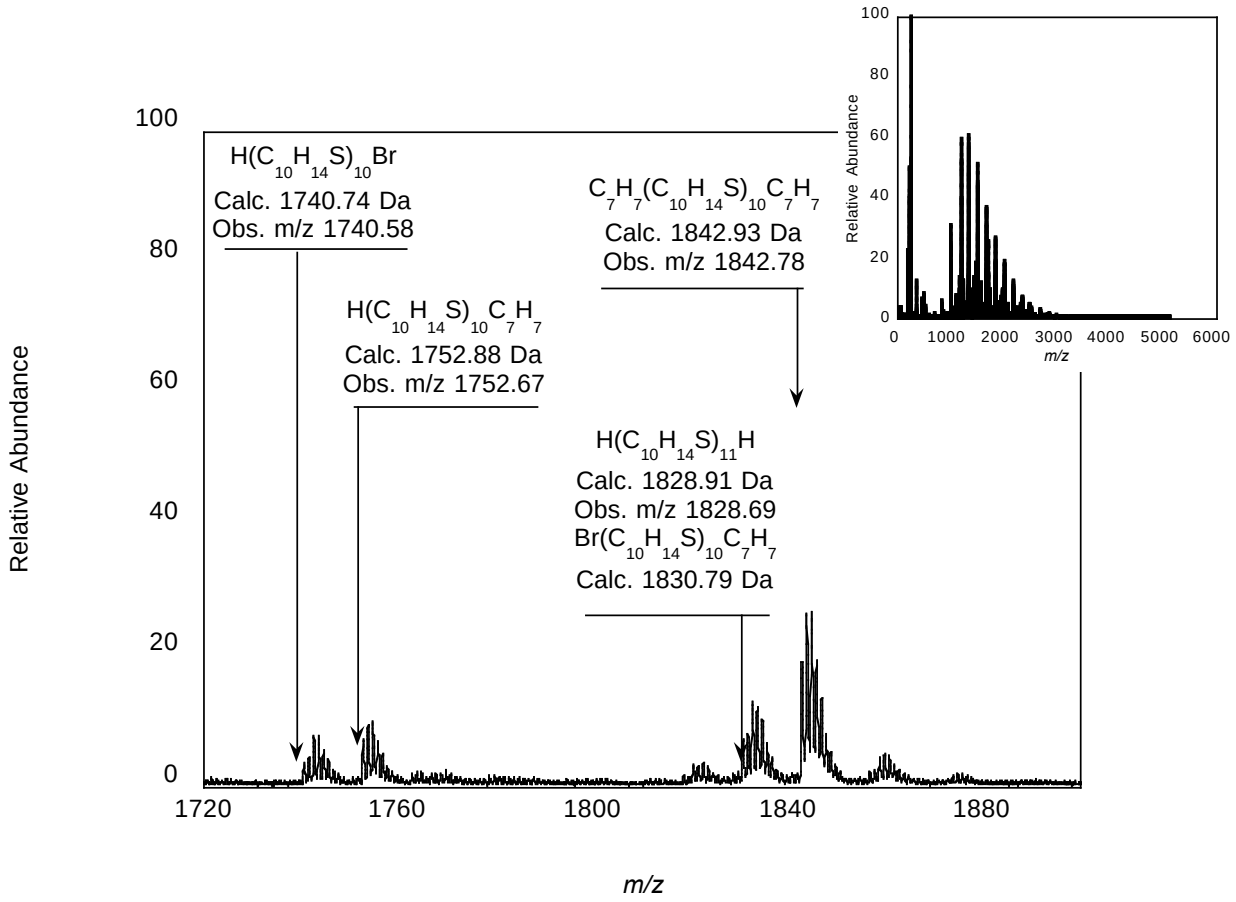

Figure B-18. Magnification of the 10-mer region of **P3HT7** with the full mass spectrum shown as an inset.

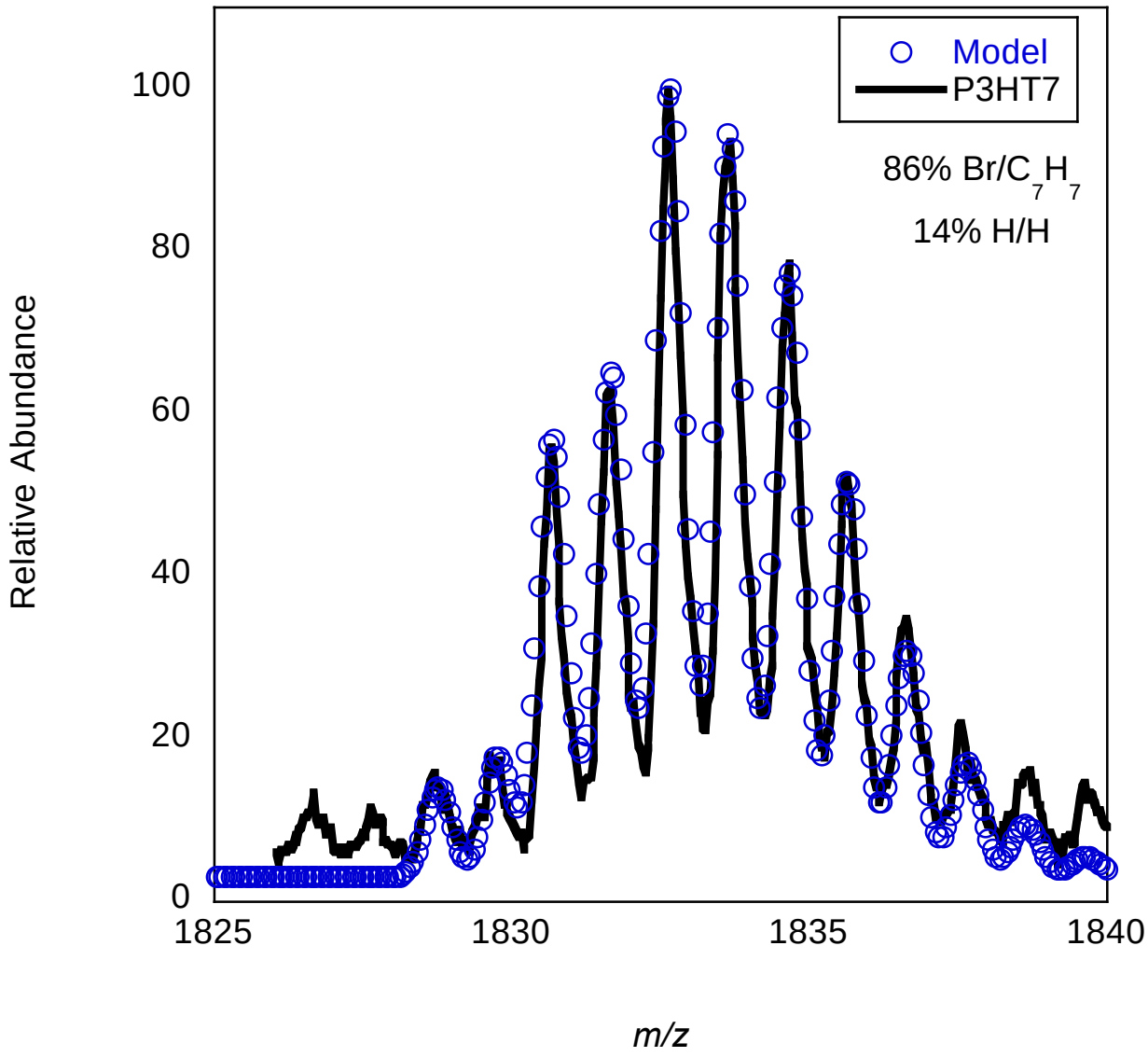

Figure B-19. Modeled spectrum for **P3HT7** showing the estimated abundance of Br/C_7H_7 and H/H terminated chains in the overlapping distribution.

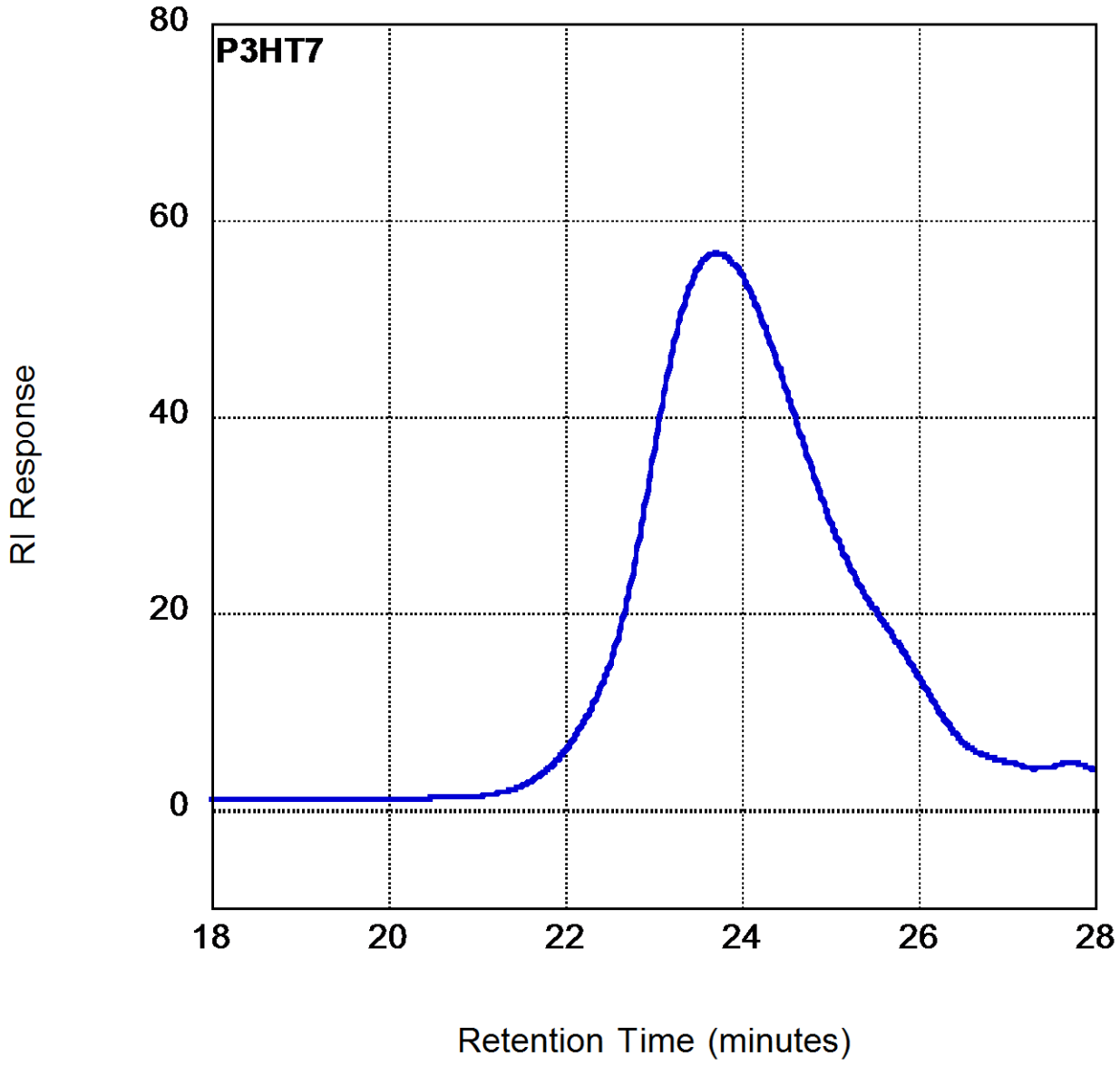

Figure B-20. SEC chromatogram for **P3HT7**.

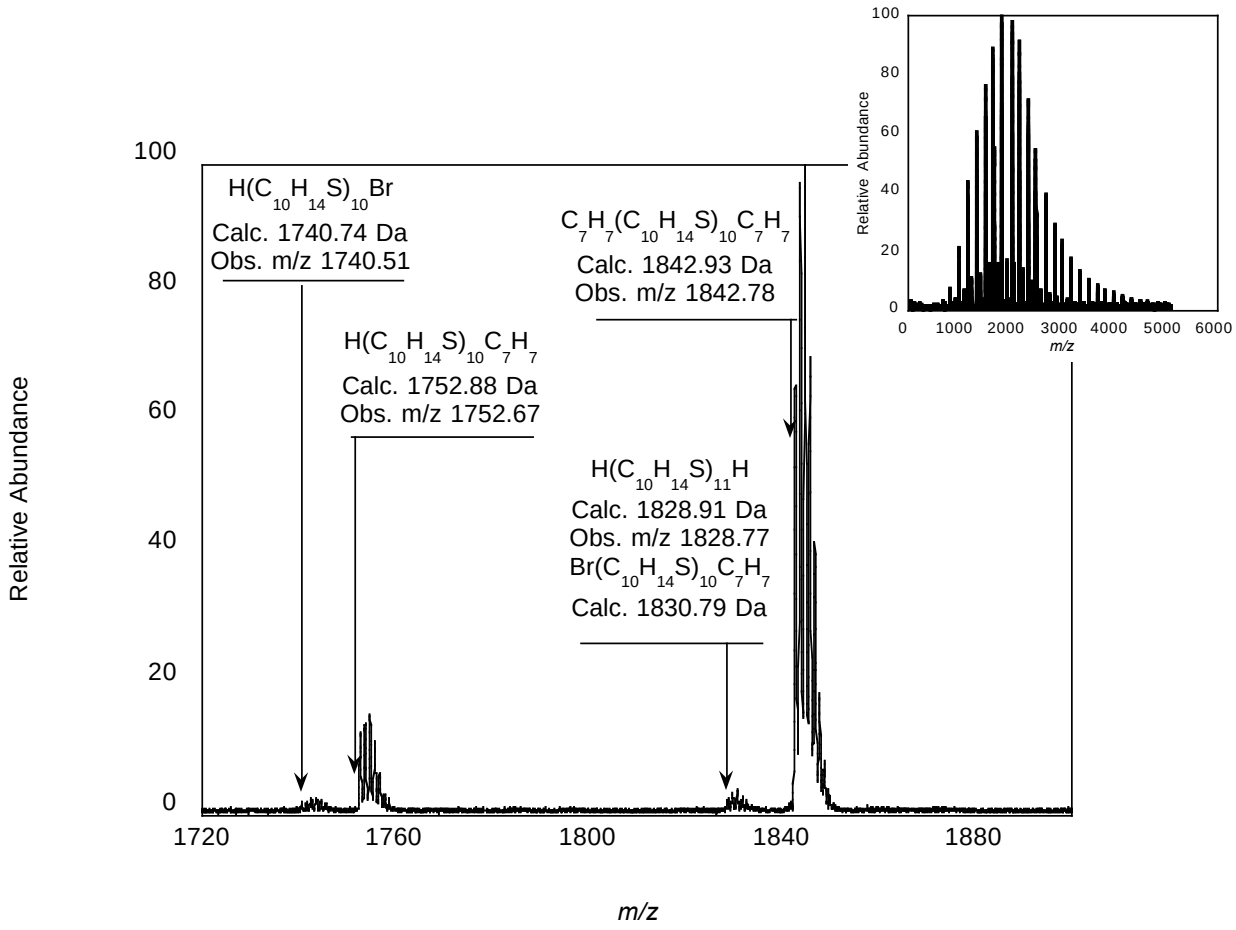

Figure B-21. Magnification of the 10-mer region of **P3HT8** with the full mass spectrum shown as an inset.

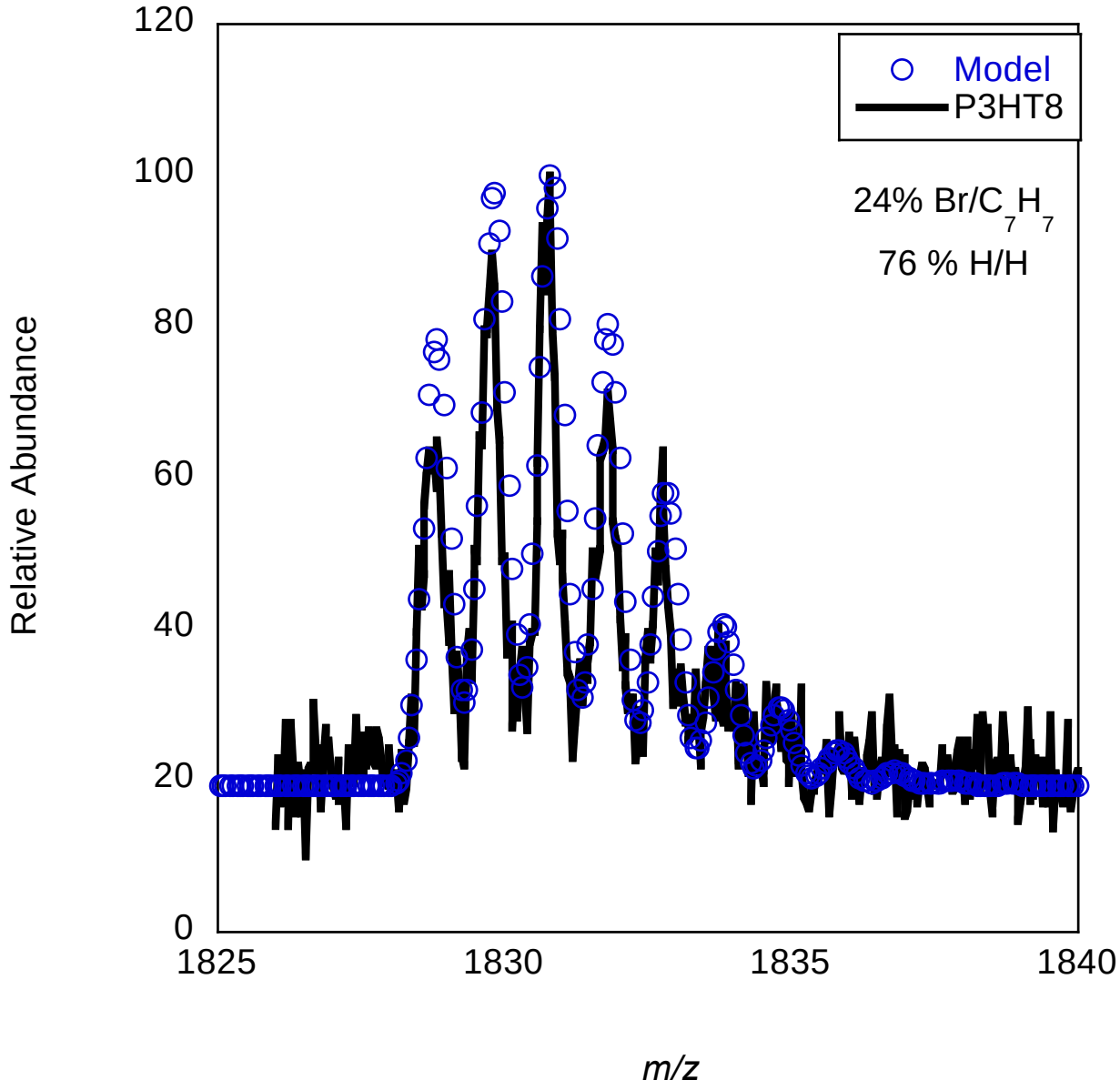

Figure B-22. Modeled spectrum for **P3HT8** showing the estimated abundance of Br/C_7H_7 and H/H terminated chains in the overlapping distribution.

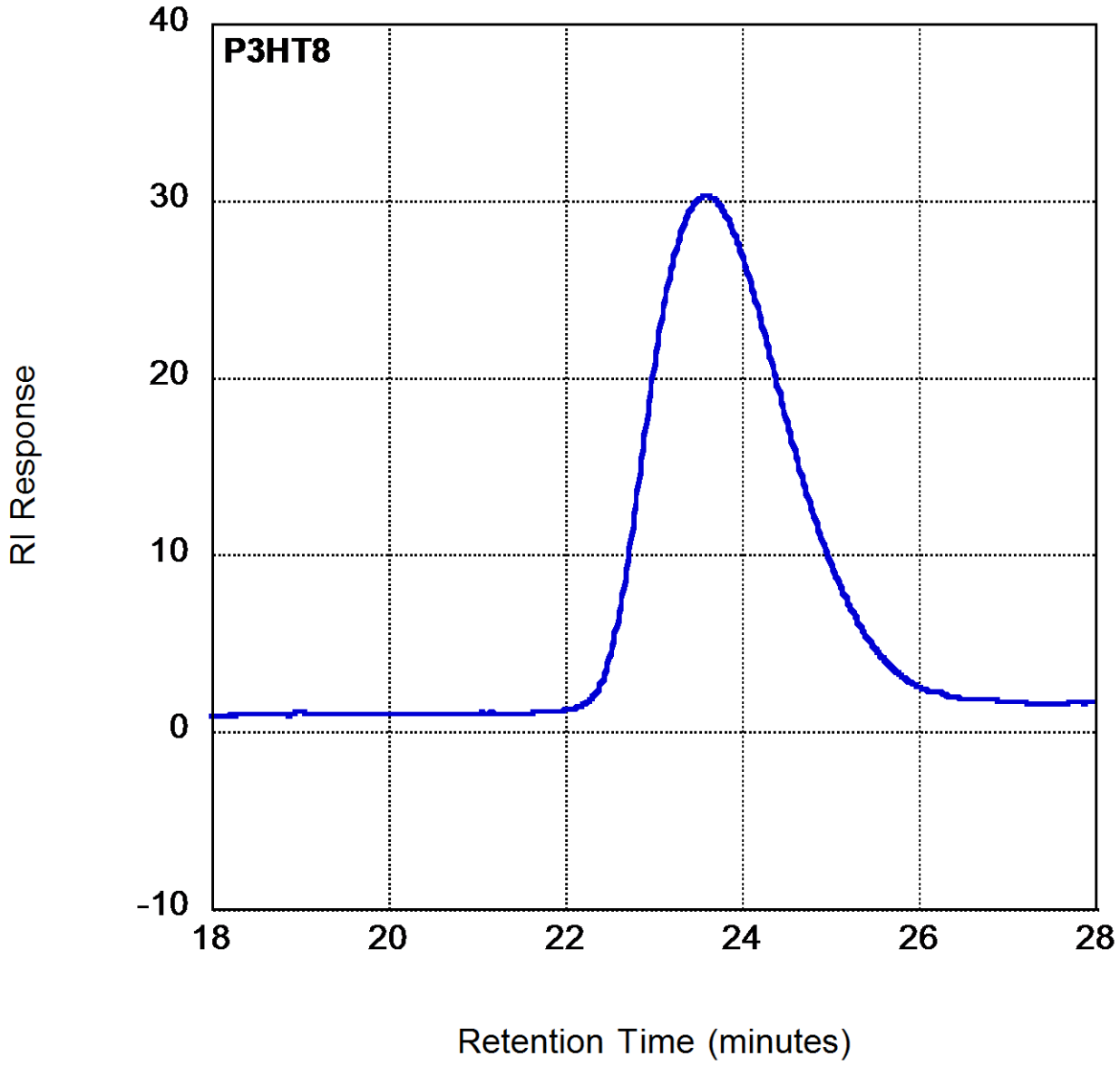

Figure B-23. SEC chromatogram for **P3HT8**.

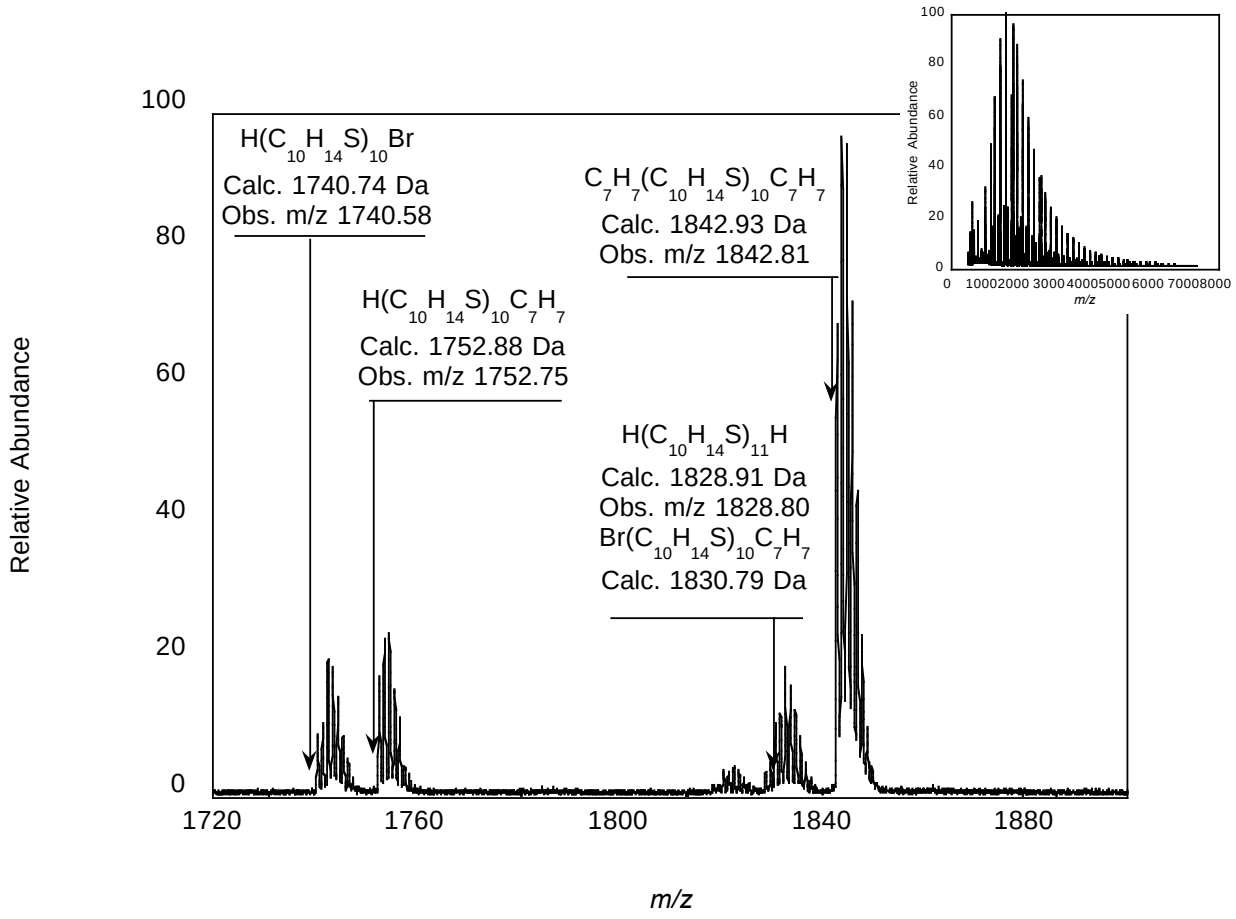

Figure B-24. Magnification of the 10-mer region of **P3HT9** with the full mass spectrum shown as an inset.

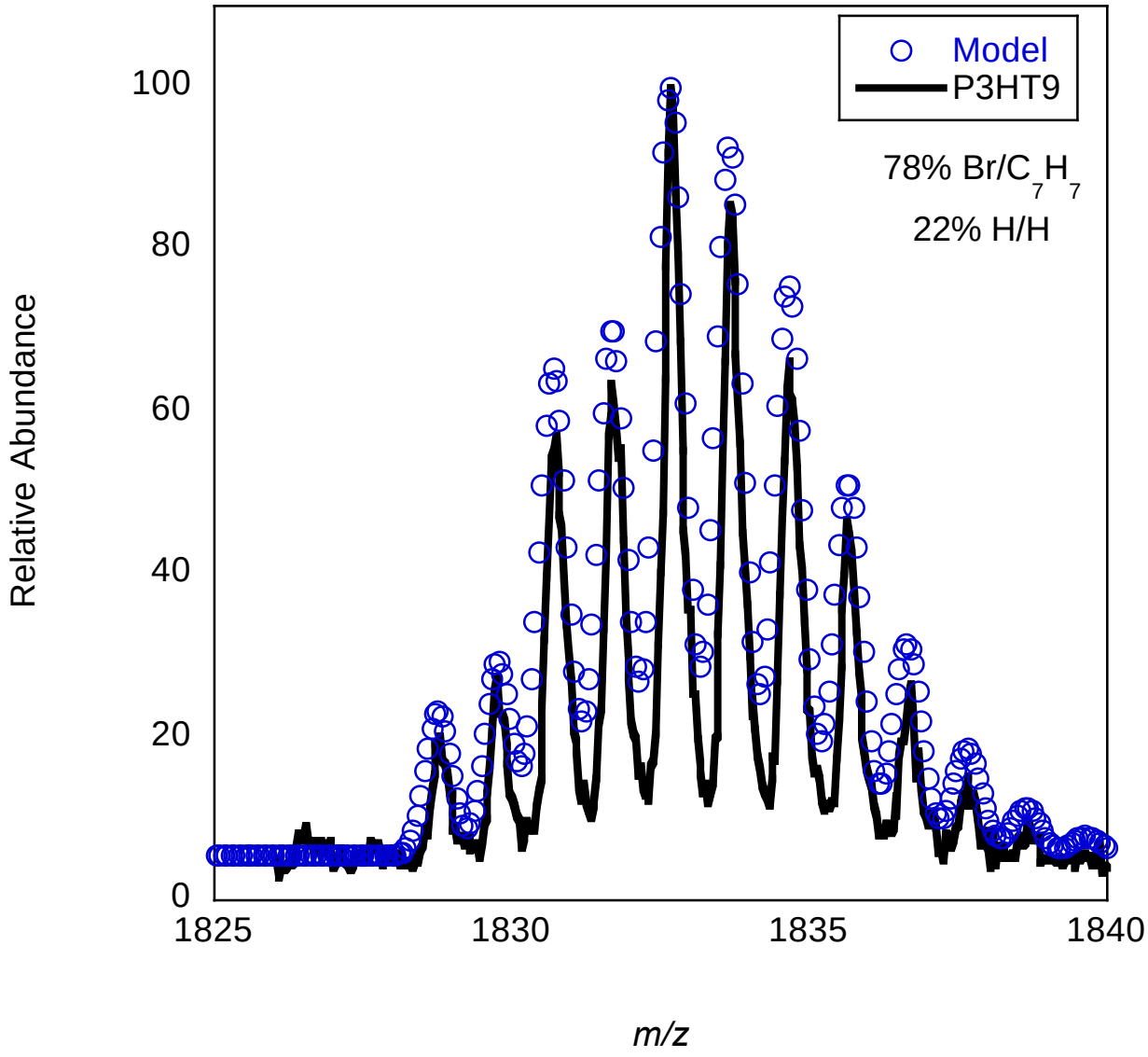

Figure B-25. Modeled spectrum for **P3HT9** showing the estimated abundance of Br/C_7H_7 and H/H terminated chains in the overlapping distribution.

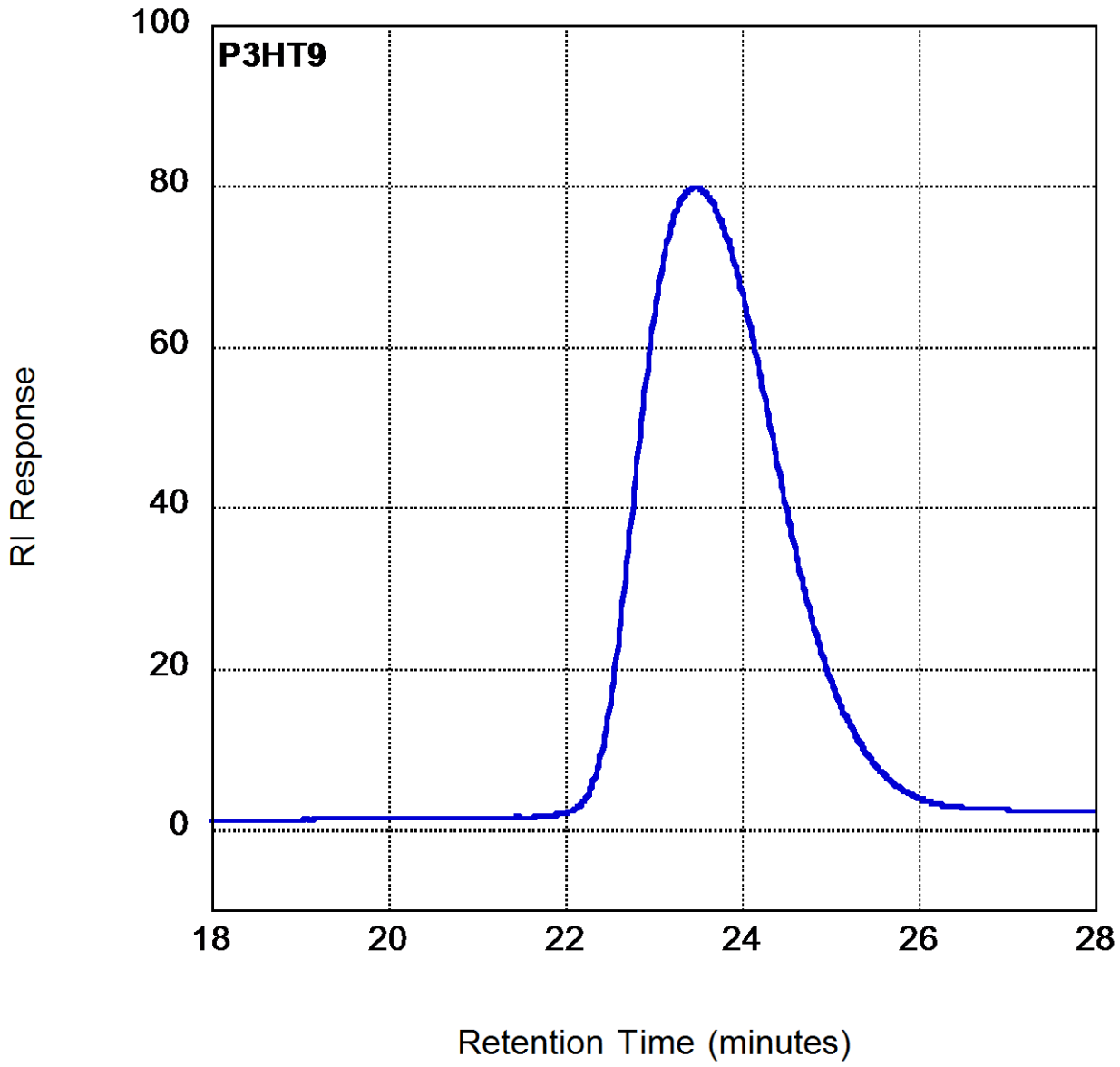

Figure B-26. SEC chromatogram for **P3HT9**.

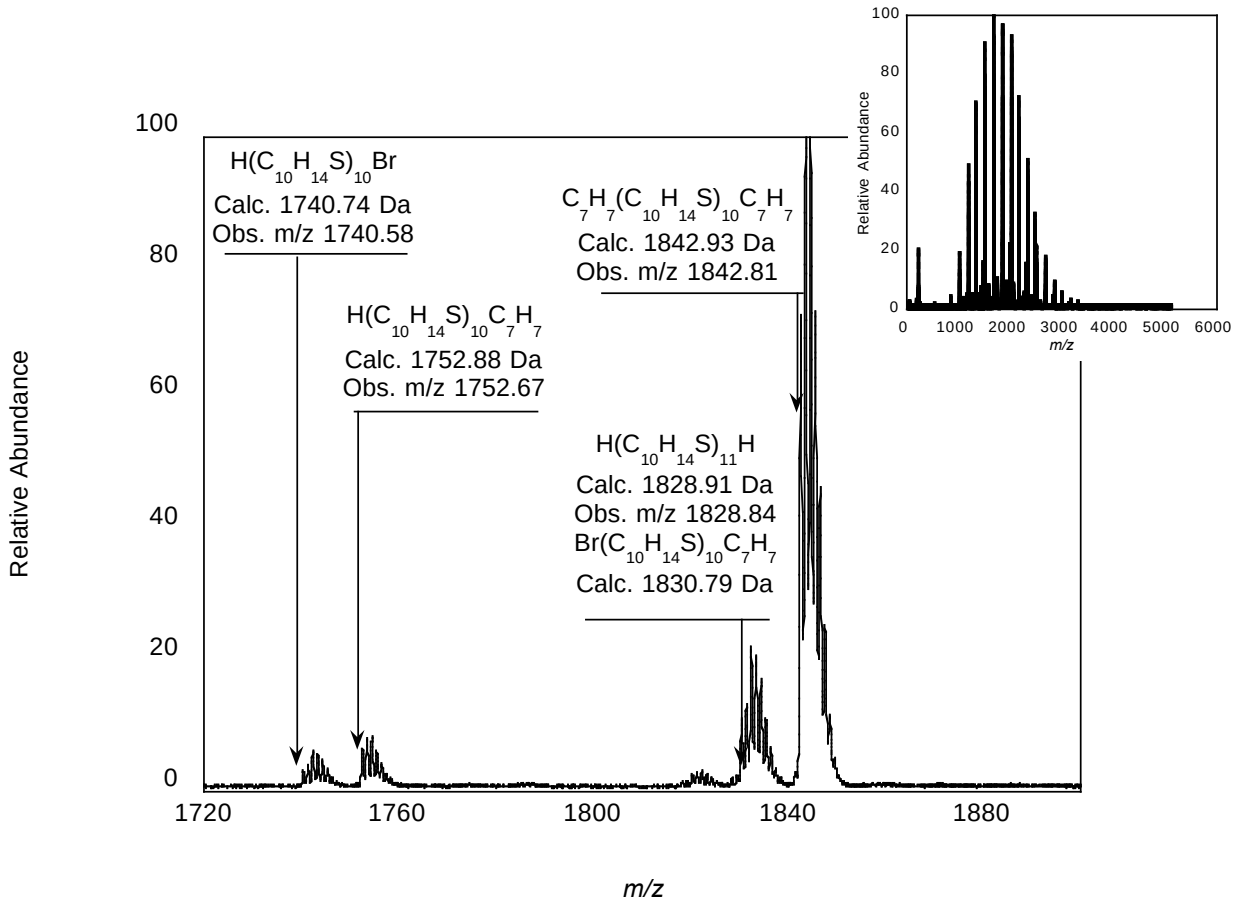

Figure B-27. Magnification of the 10-mer region of **P3HT10** with the full mass spectrum shown as an inset.

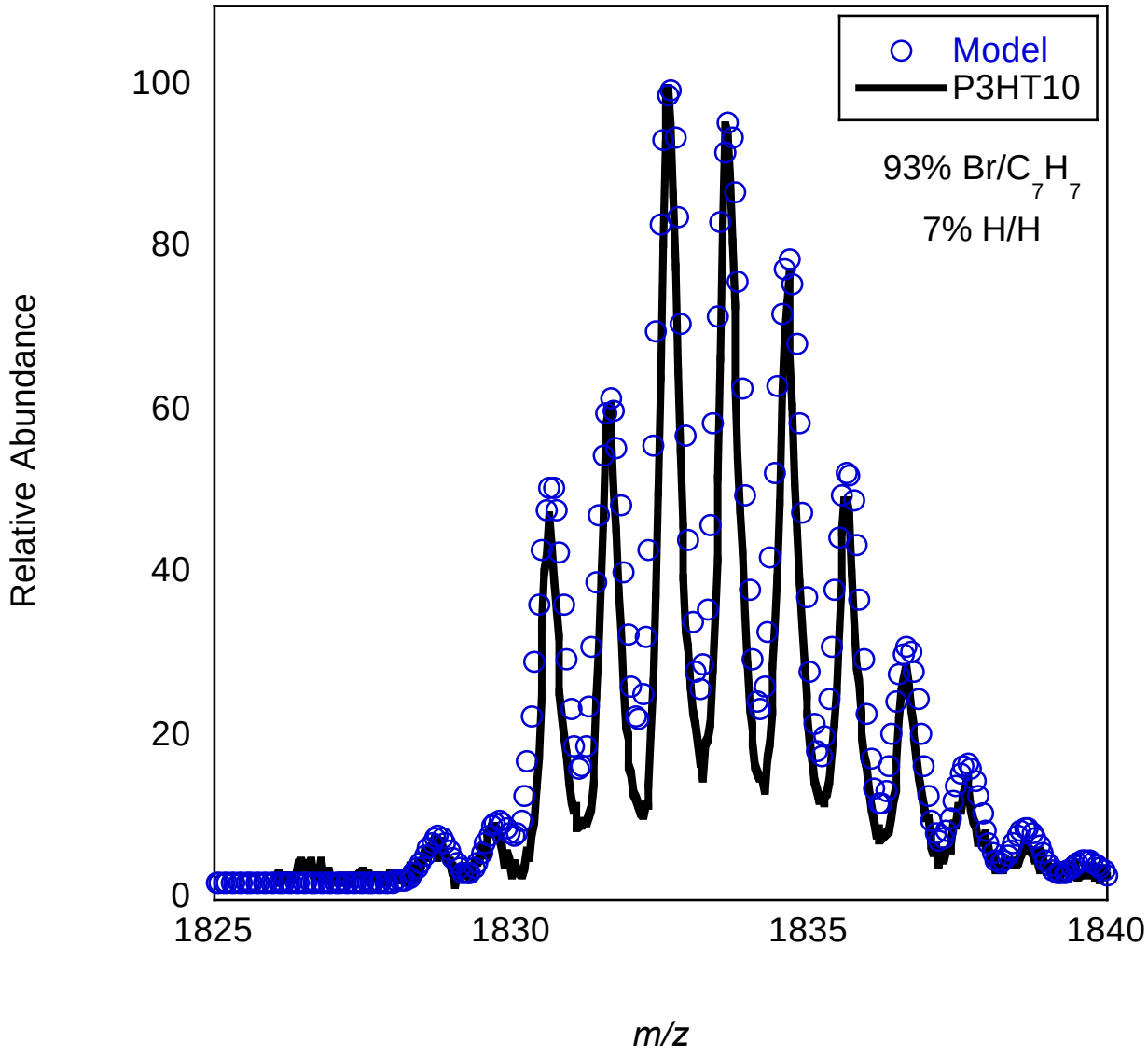

Figure B-28. Modeled spectrum for **P3HT10** showing the estimated abundance of Br/C_7H_7 and H/H terminated chains in the overlapping distribution.

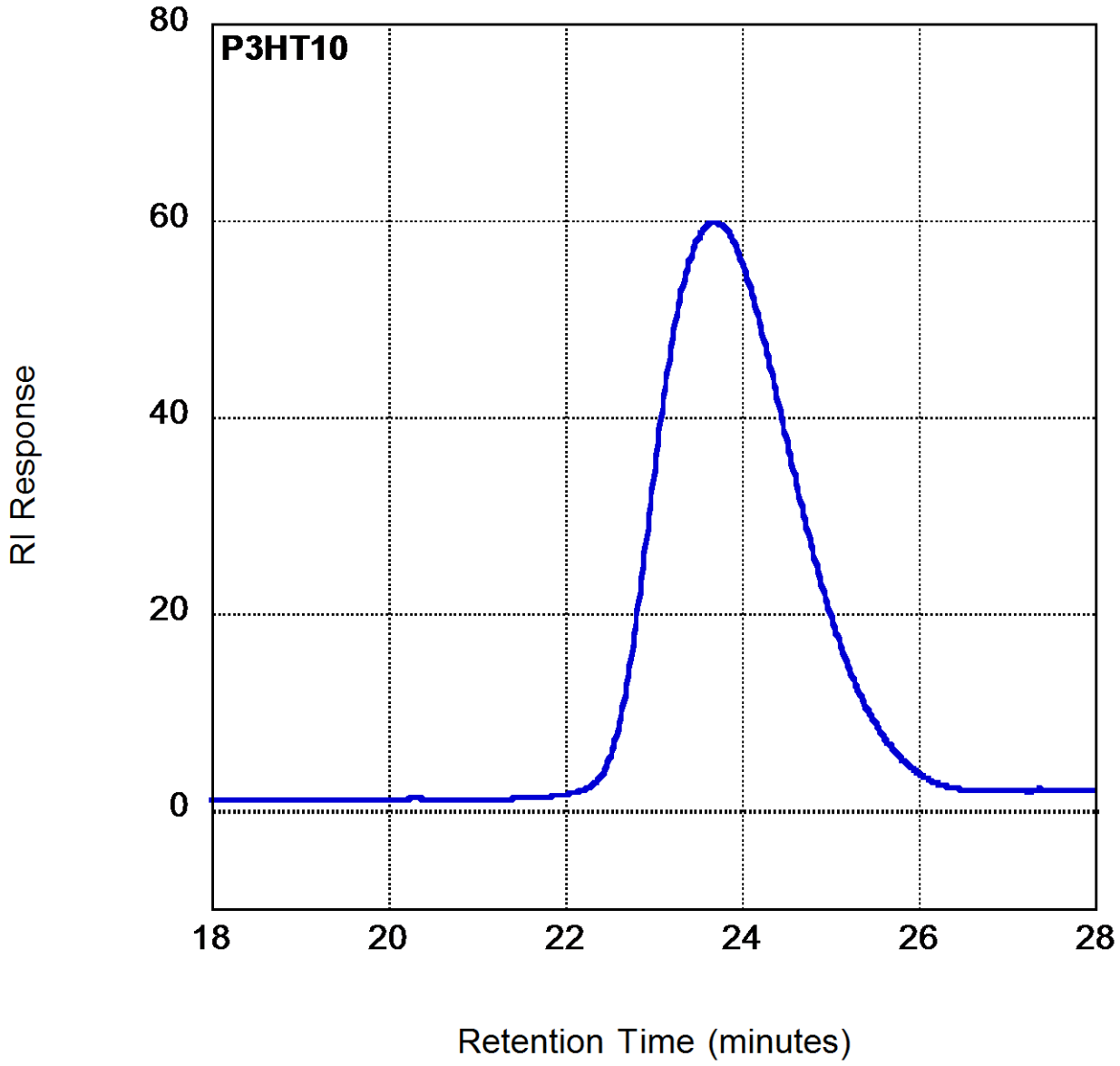

Figure B-29. SEC chromatogram for **P3HT10**.

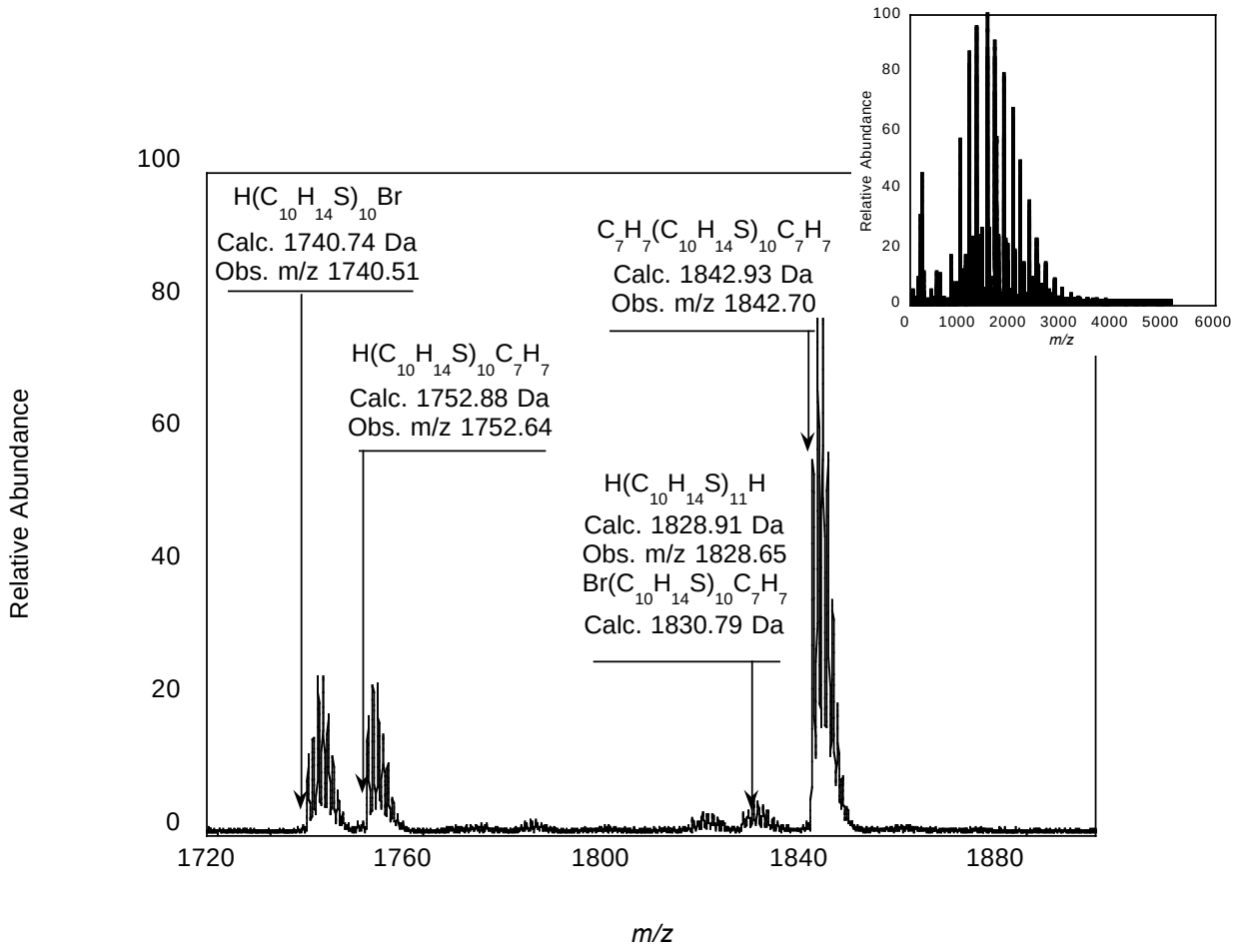

Figure B-30. Magnification of the 10-mer region of **P3HT11** with the full mass spectrum shown as an inset.

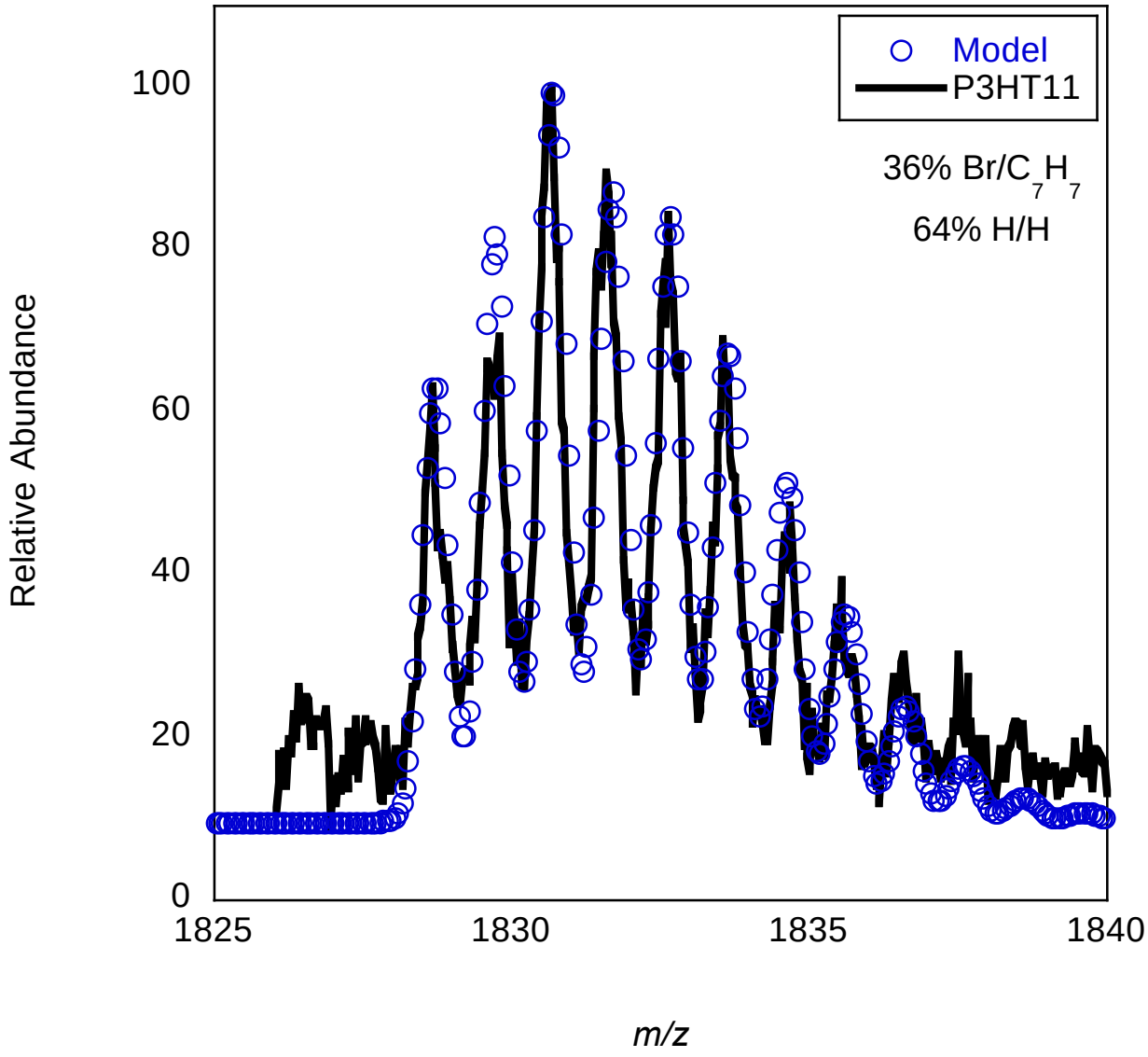

Figure B-31. Modeled spectrum for **P3HT11** showing the estimated abundance of Br/C_7H_7 and H/H terminated chains in the overlapping distribution.

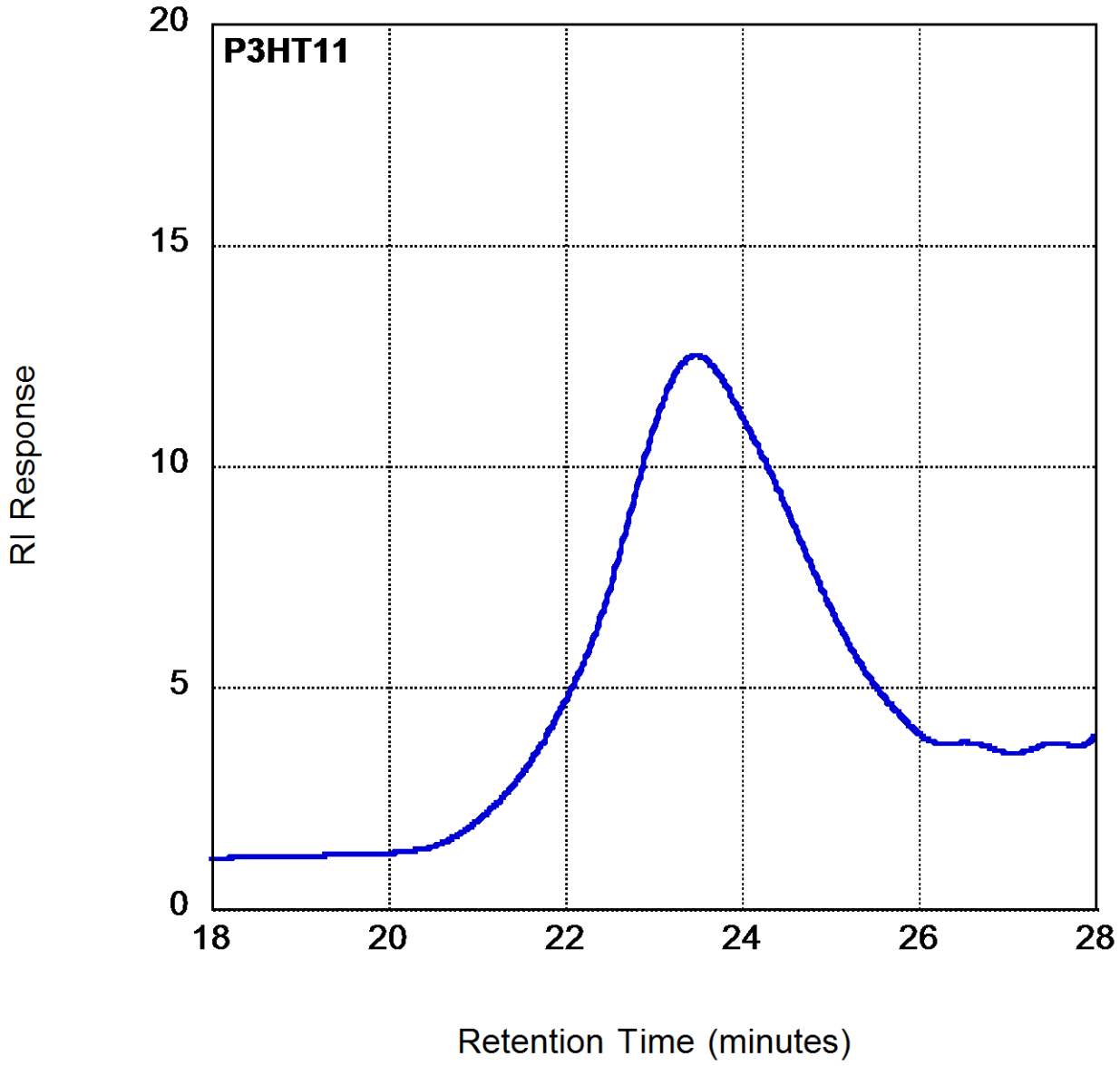

Figure B-32. SEC chromatogram for **P3HT11**.

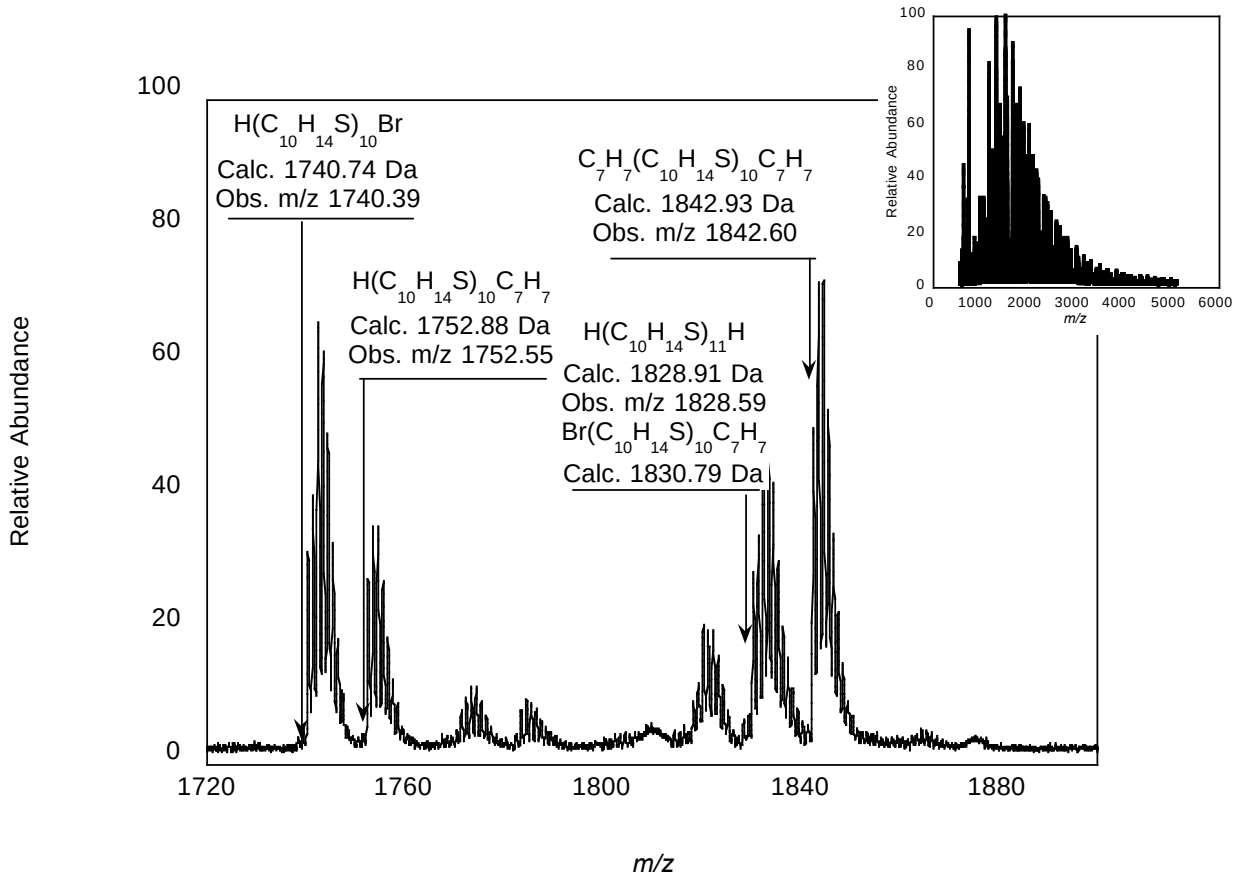

Figure B-33. Magnification of the 10-mer region of **P3HT12** with the full mass spectrum shown as an inset.

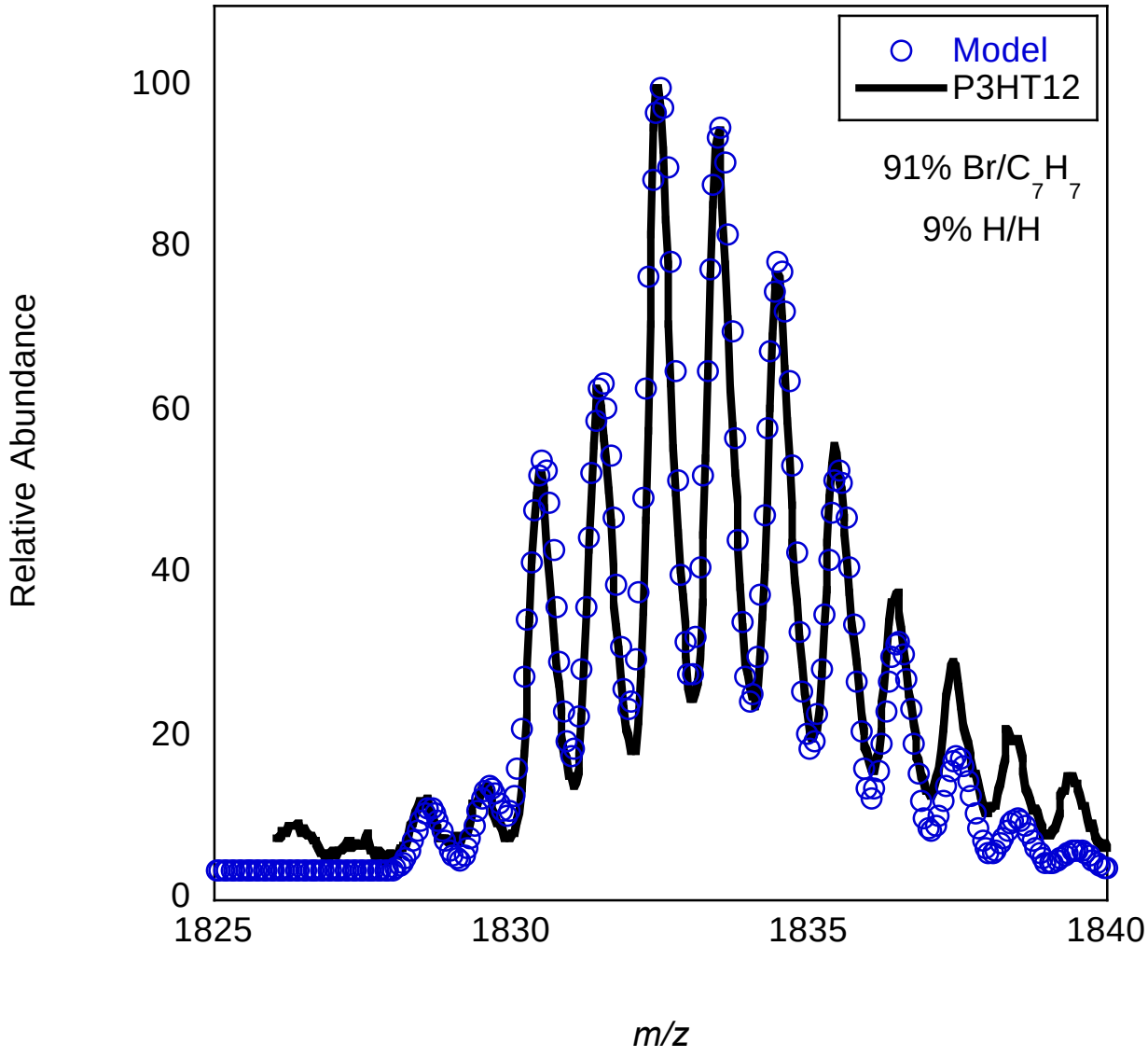

Figure B-34. Modeled spectrum for **P3HT12** showing the estimated abundance of Br/C_7H_7 and H/H terminated chains in the overlapping distribution.

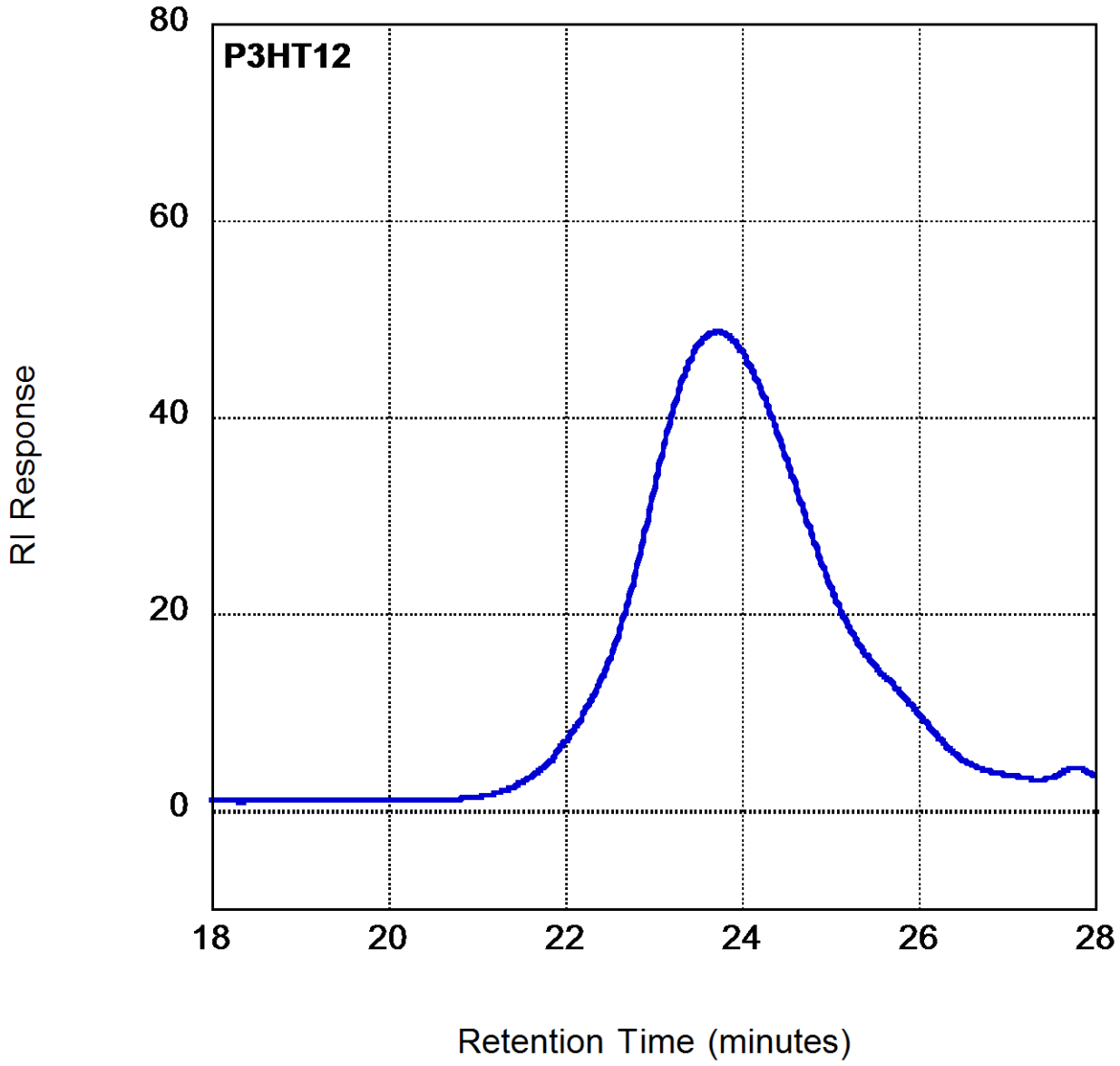

Figure B-35. SEC chromatogram for **P3HT12**.

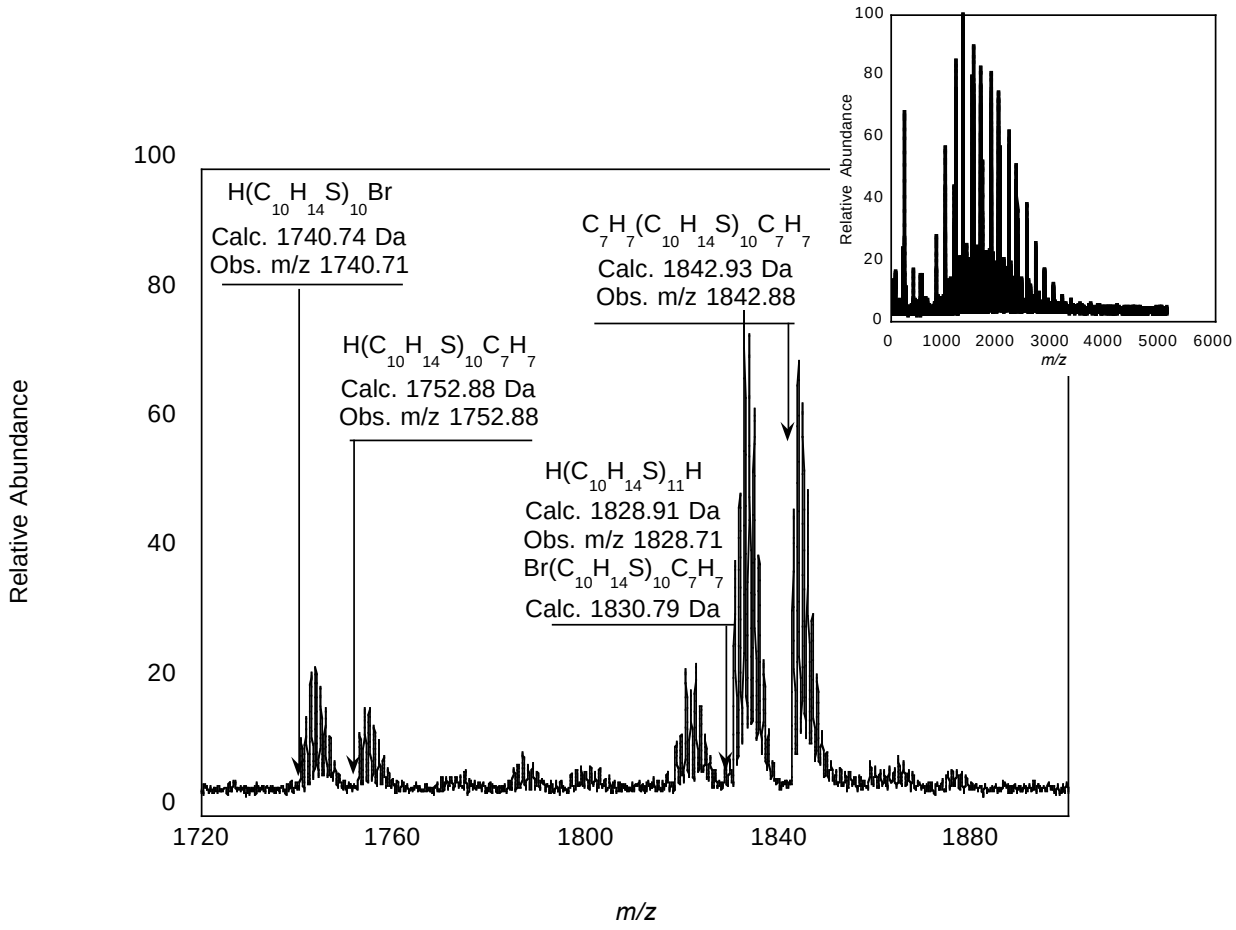

Figure B-36. Magnification of the 10-mer region of **P3HT13** with the full mass spectrum shown as an inset.

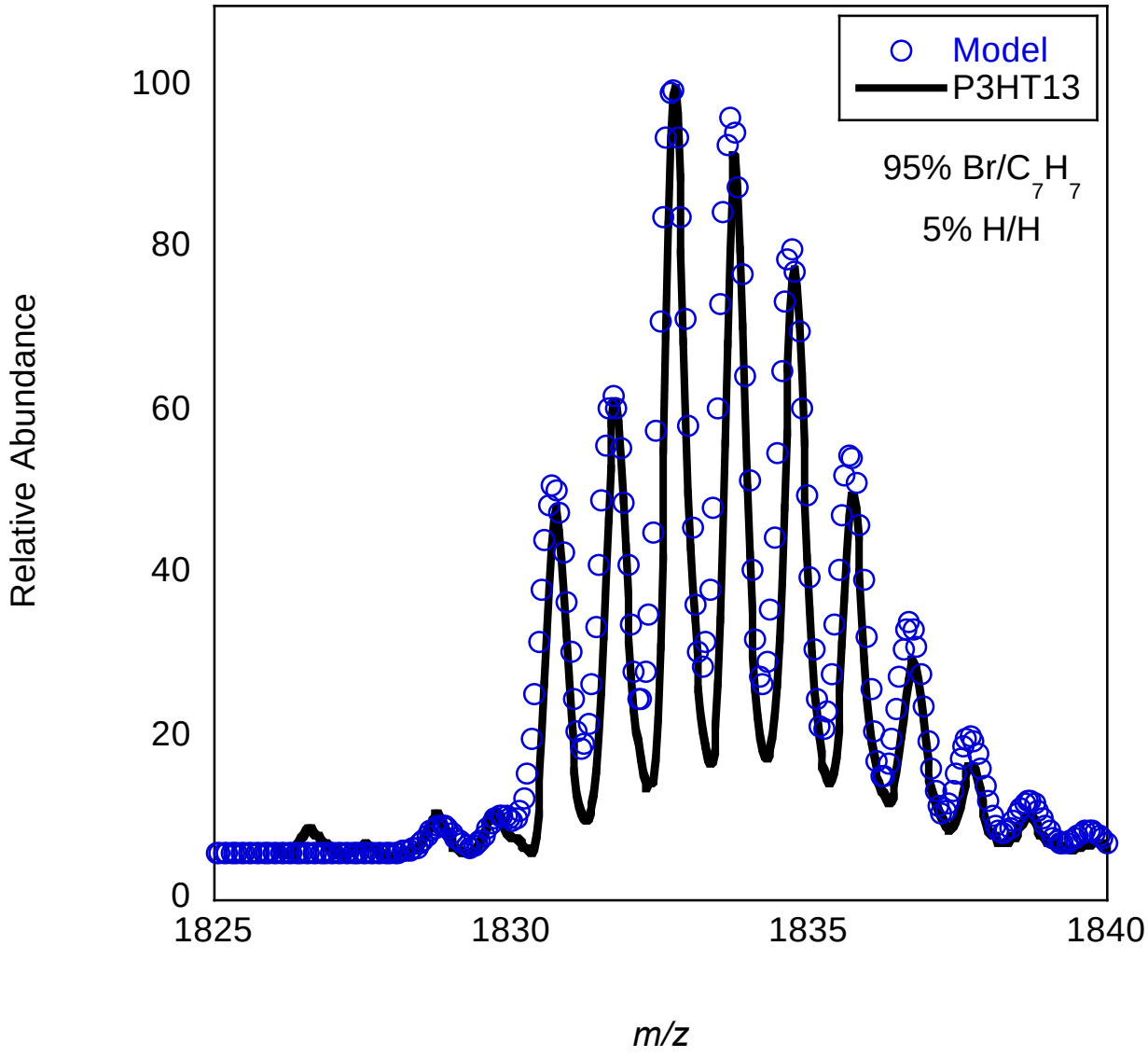

Figure B-37. Modeled spectrum for **P3HT13** showing the estimated abundance of Br/C_7H_7 and H/H terminated chains in the overlapping distribution.

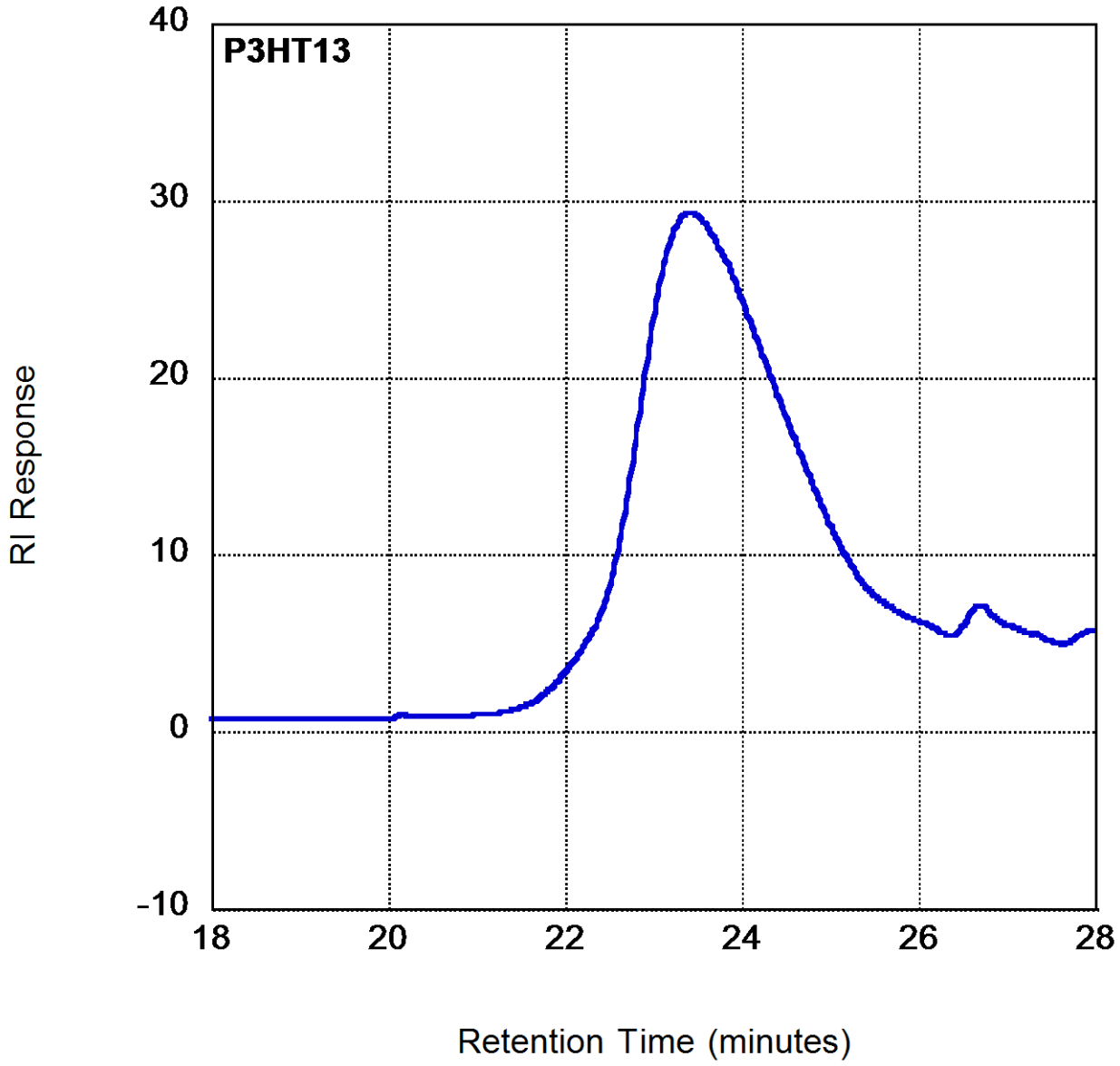

Figure B-38. SEC chromatogram for **P3HT13**.

^{1}H NMR spectra of the tolyl-functionalized P3HTs

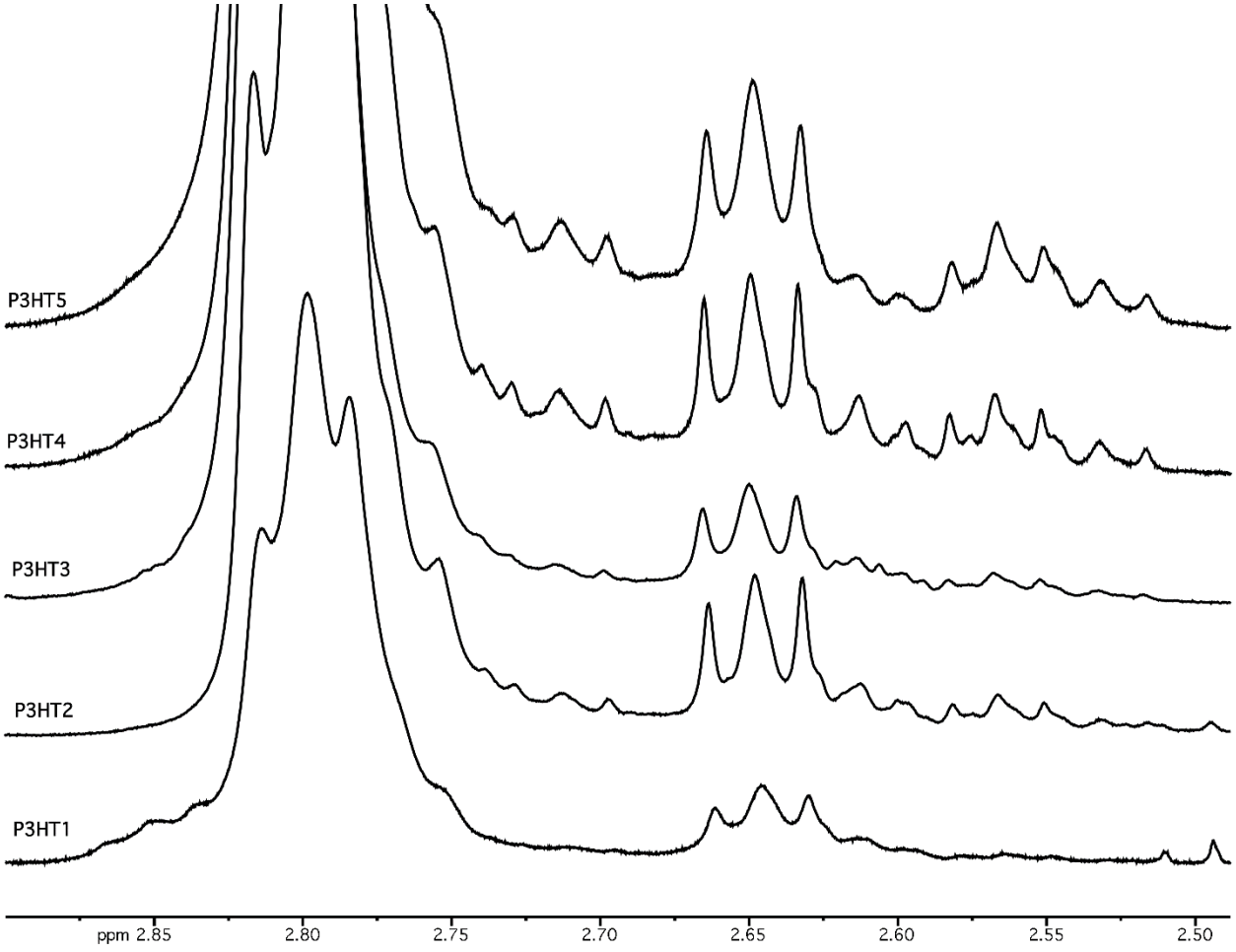

Figure B-39. ^{1}H NMR spectra showing the aliphatic region of **P3HT1**-**P3HT5**.

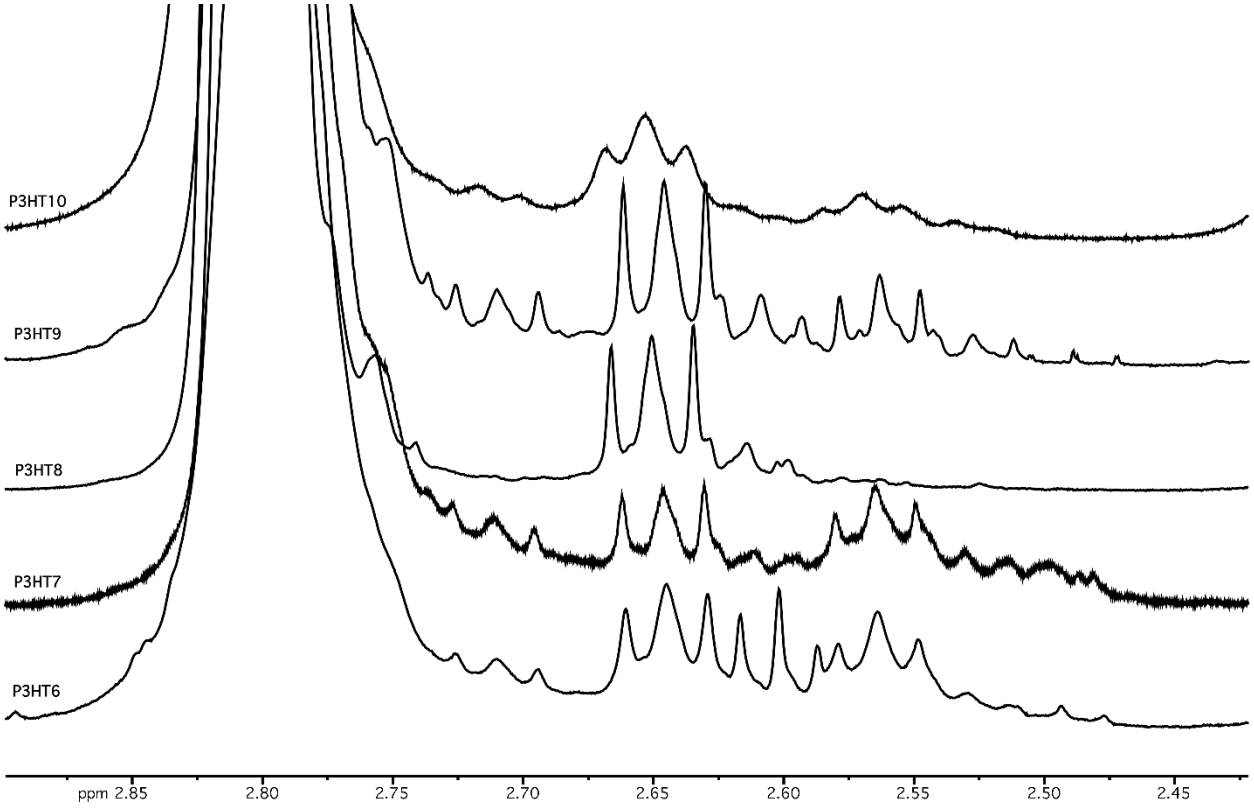

Figure B-40. ^{1}H NMR spectra showing the aliphatic region of **P3HT6**-**P3HT10**.

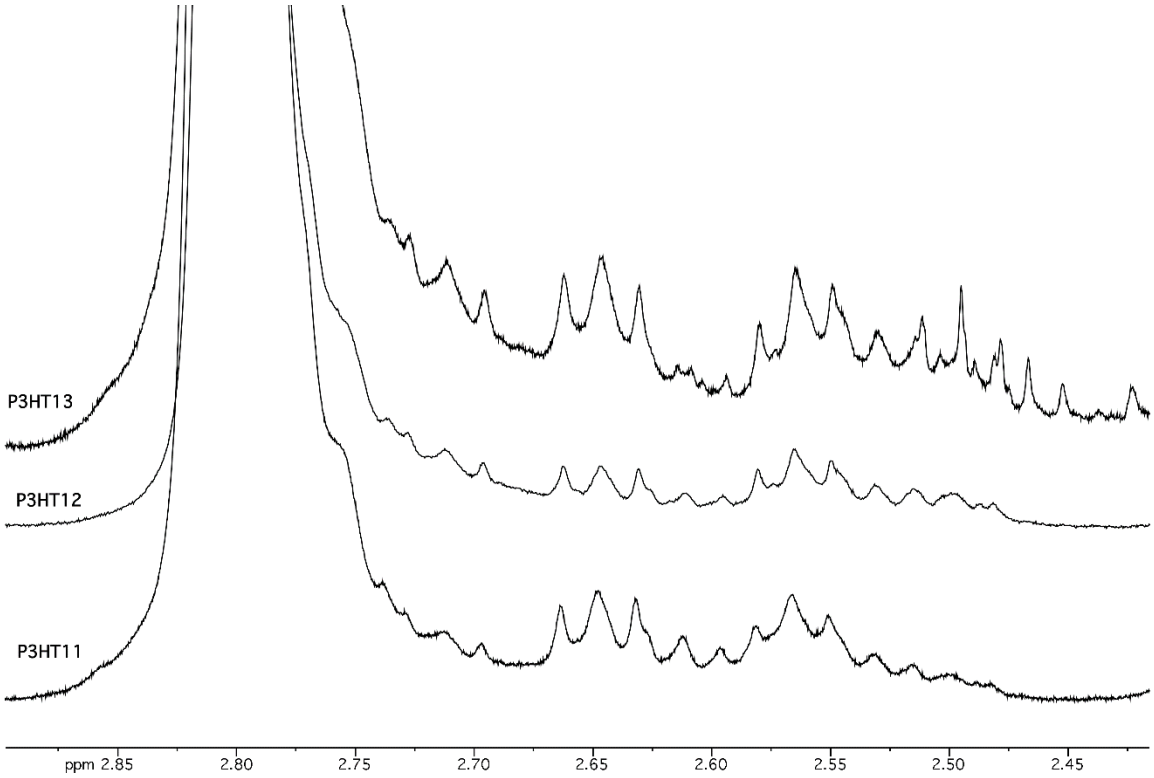

Figure B-41. ^{1}H NMR spectra showing the aliphatic region of **P3HT11**-**P3HT13**.

MALDI-TOF MS spectra of a vinyl-functionalized P3HT prepared by in situ quenching with vinyl magnesium bromide

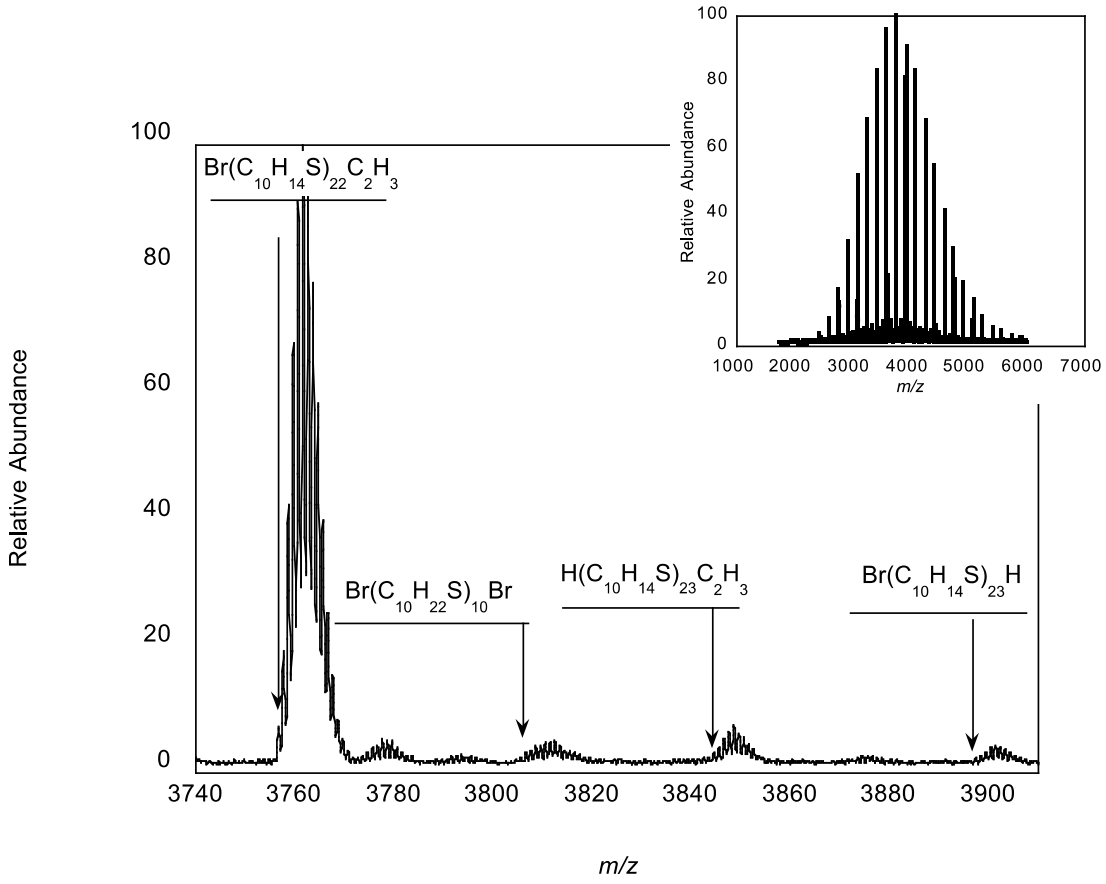

Figure B-42. Magnification of the 10-mer region of a vinyl functionalized P3HT with the full mass spectrum as an inset.

Appendix C- Chapter 3: In situ Formation of Pyridyl-Functionalized P3HTs via Quenching of the GRIM Polymerization

Optimized molecular and electronic structures

The optimized molecular and electronic structures that were calculated using density functional theory and discussed in Chapter 3 are given in Figures C-1 and C-2.

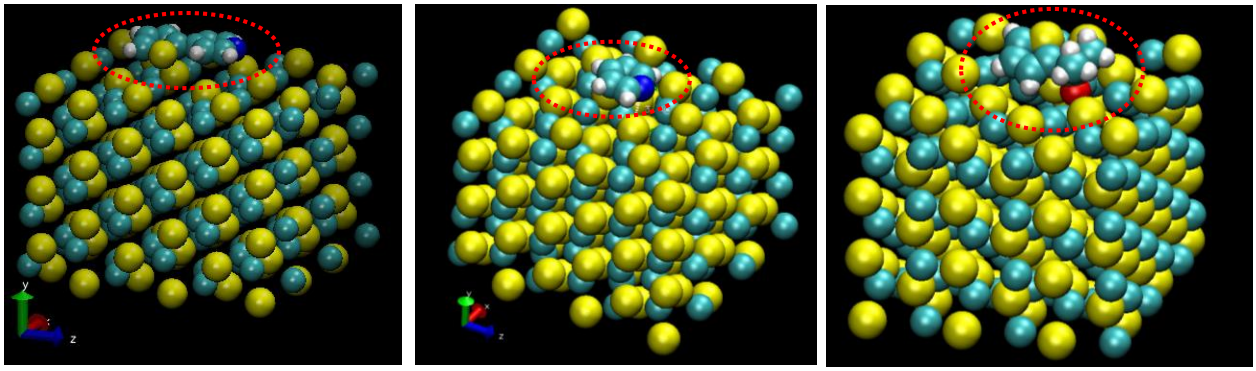

Figure C-1. Density functional theory (DFT) calculations using plane wave-pseudo potentials (see details in Chapter 3) to model (left) 3-pyridyl-2-thiophene (binding energy, B.E.= 14.73 kcal/mol), (middle) pyridine (B.E.= 7.45 kcal/mol), and (right) dimethyl(2-thienyl)phosphine oxide (B.E.=8.16 kcal/mol) binding to a CdSe surface.

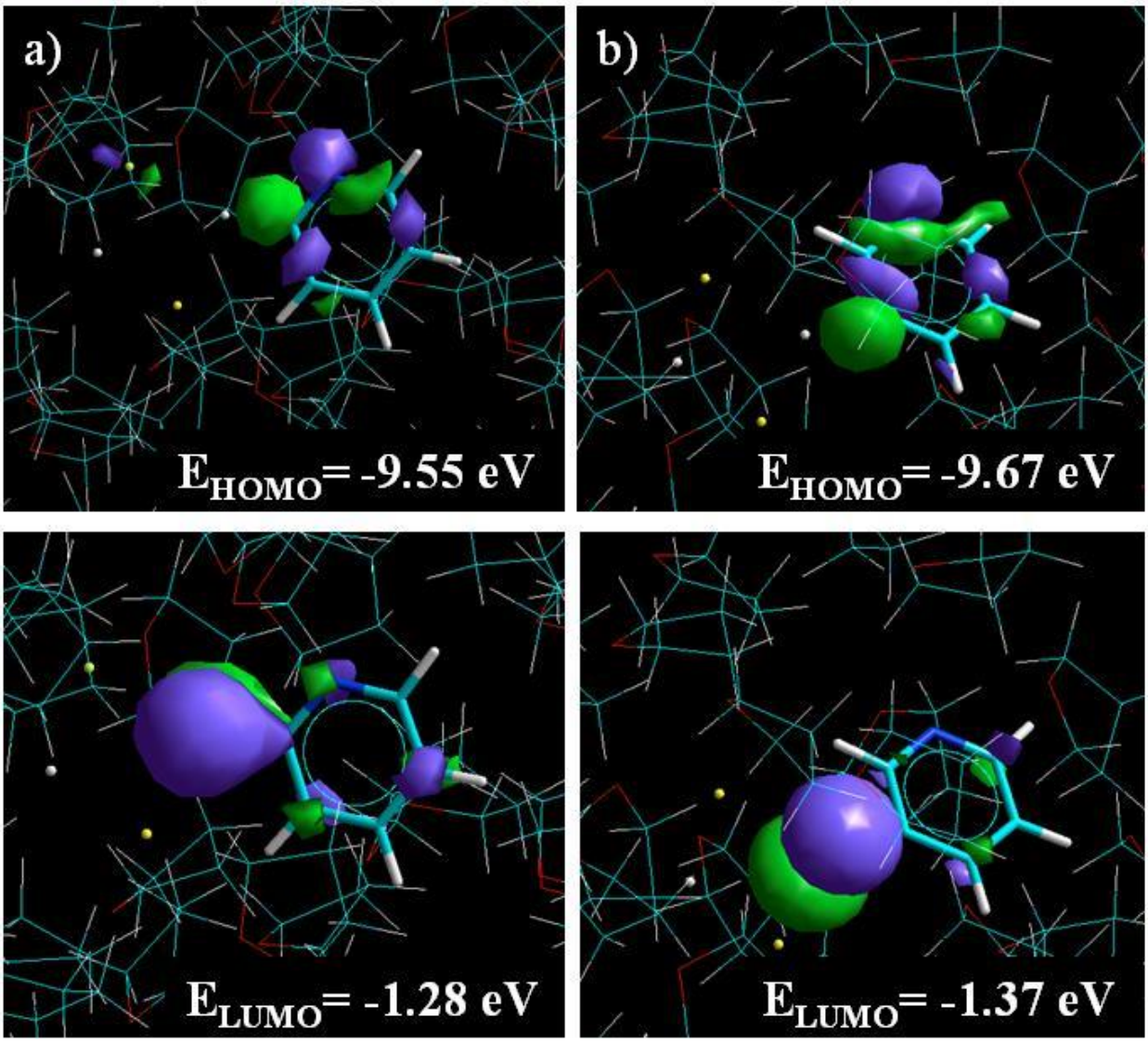

Figure C-2. Molecular orbitals for a) 2-pyridyl-MgCl·LiCl (heat of formation, ΔH_f = -110 kcal/mol) and b) 3-pyridyl-MgCl·LiCl (ΔH_f = -105 kcal/mol) in THF showing the HOMO (top) and the LUMO (bottom) and their respective energies.

Molecular weight data for pyridyl-functionalized P3HTs

The molecular weight data for all of the pyridyl-functionalized P3HTs from Chapter 3 are shown in Table C-1.

Table C-1. Molecular weight data for pyridyl-functionalized P3HTs obtained by SEC and MALDI-TOF MS.

	SEC-RI			**MALDI-TOF MS**		
	M_n	M_w	PDI	M_n	M_w	PDI
P3HT1	6200	7960	1.28	2460	2770	1.13
P3HT2	5040	6170	1.22	2090	2190	1.05
P3HT3	5100	6040	1.18	2420	2680	1.11
P3HT4	5070	6250	1.23	2400	2550	1.06
P3HT5	4270	5220	1.22	2060	2200	1.07
P3HT6	4300	5300	1.23	2310	2390	1.03
P3HT7	5300	6200	1.17	2550	2640	1.04
P3HT8	5000	5800	1.16	2490	2590	1.04

MALDI-TOF MS spectrum of Br/H P3HT

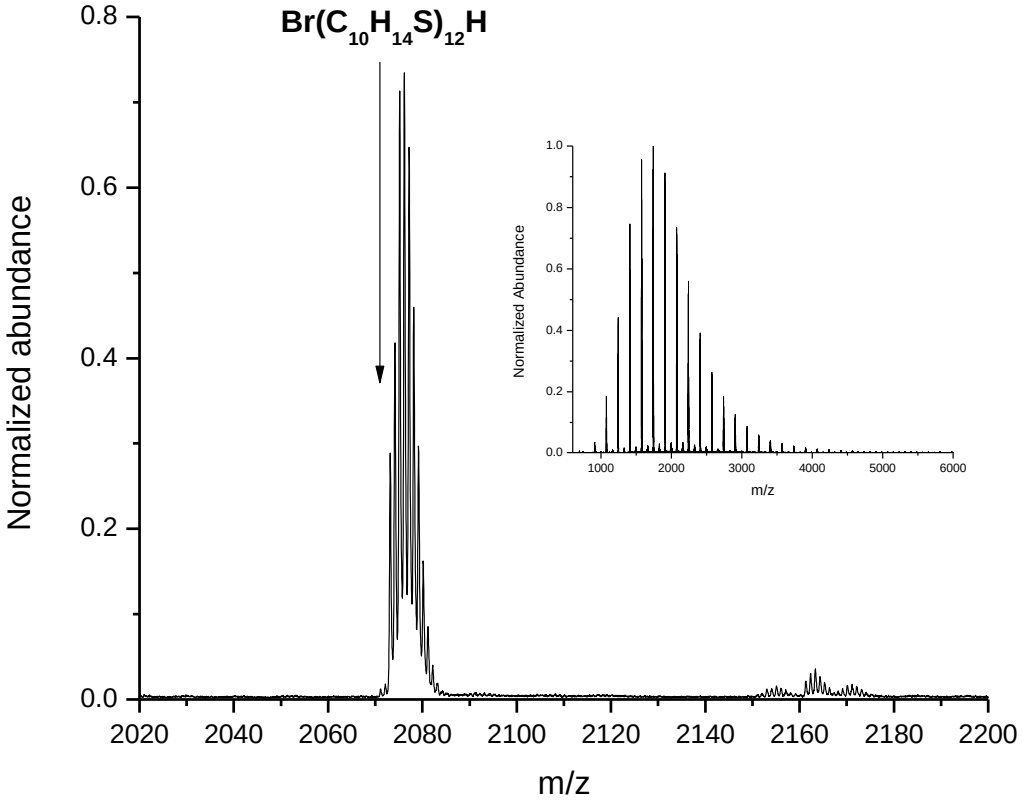

Figure C-3. MALDI-TOF MS of P3HT obtained when the GRIM polymerization is quenched with 5M HCl showing magnification of the 12-mer region and the full spectrum (inset). Nearly 100% of chains contain **Br/H** end groups.

Fitting of overlapping isotope distributions

As described in the Chapter 3, the shape of the isotope distributions observed for the 13-mer at *m/z* 2238.10 and 2315.13 in the mass spectrum of pyridyl-functionalized P3HT are different than the calculated isotope distributions of the expected products $H(C_{10}H_{14}S)_{13}C_5H_4N$ and $C_5H_4N(C_{10}H_{14}S)_{13}C_5H_4N$, due to overlap with other products of similar mass. A MATLAB program was developed that calculates a model spectrum using the ratio of the constituent spectra as a fitting parameter, which I described in detail in Appendix B. This program allows the relative amounts of the constituent species within the observed distribution to be determined, which can then be used to calculate the overall end-group composition of the sample. For example, **Figure S4** shows the calculated isotope distributions of the constituent spectra on the left and the modeled spectrum of **P3HT1** at *m/z* 2238.10 on the right in **Figure S4**. Based on the model, the observed isotope distribution corresponds to a mixture of 80% $H(C_{10}H_{14}S)_{13}C_5H_4N$ and 20% $Br(C_{10}H_{14}S)_{13}H$. The modeled spectra for all of the P3HTs presented in Chapter 3 are provided on the following pages, along with the calculated composition for each distribution.

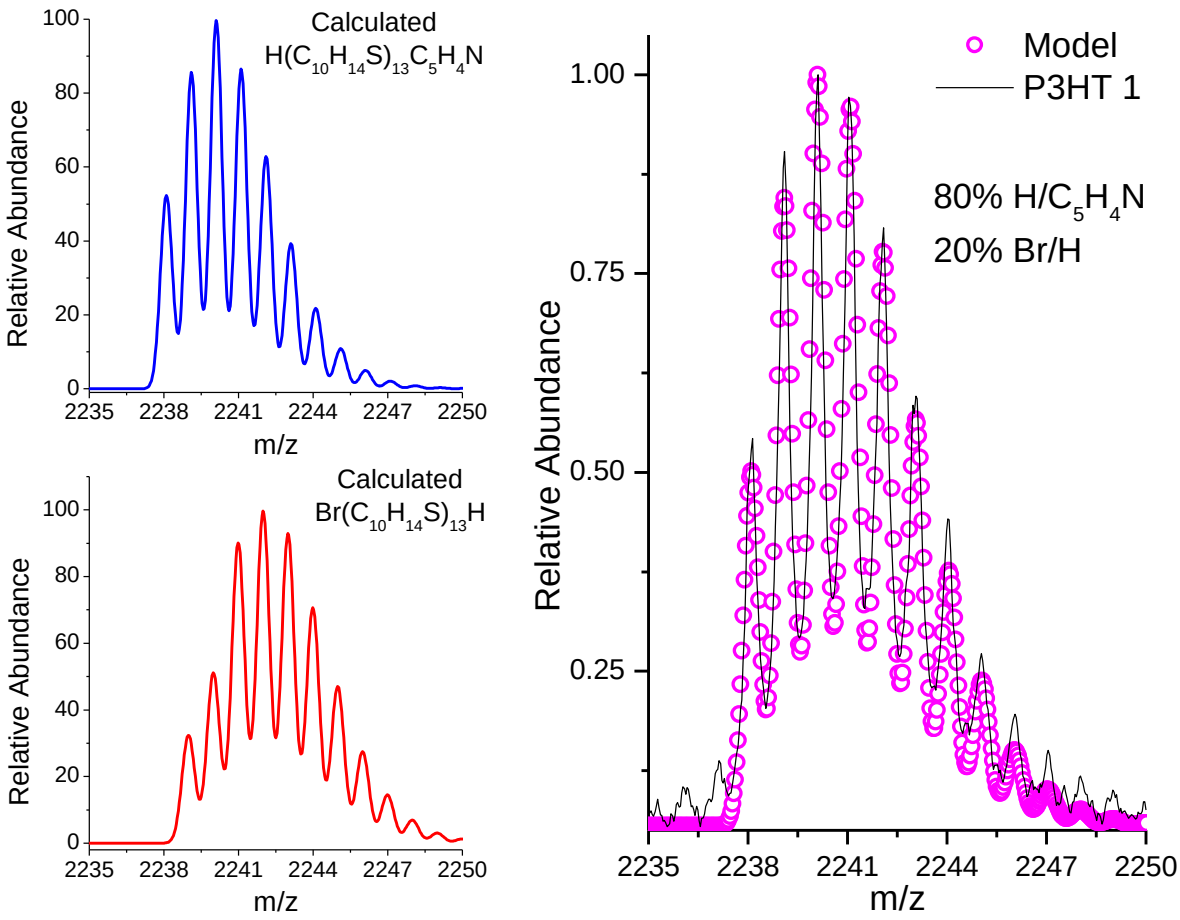

Figure C-4. The calculated isotope distributions for $H(C_{10}H_{14}S)_{13}C_5H_4N$ (blue line) and $Br(C_{10}H_{14}S)_{13}H$ (red line) and the calculated spectrum of **P3HT1** (pink circles) obtained using the ratio of the two constituent spectra.

SEC chromatograms, MALDI-TOF MS spectra, and modeled spectra of pyridyl-functionalized P3HTs

In this section of Appendix C, the SEC chromatograms, MALDI-TOF mass specta, and modelled spectra for each pyridyl-functionalized P3HT are given. It should be noted that there are two sets of overlapping distributions for each sample, therefore, two modeled spectra are provided for each P3HT sample.

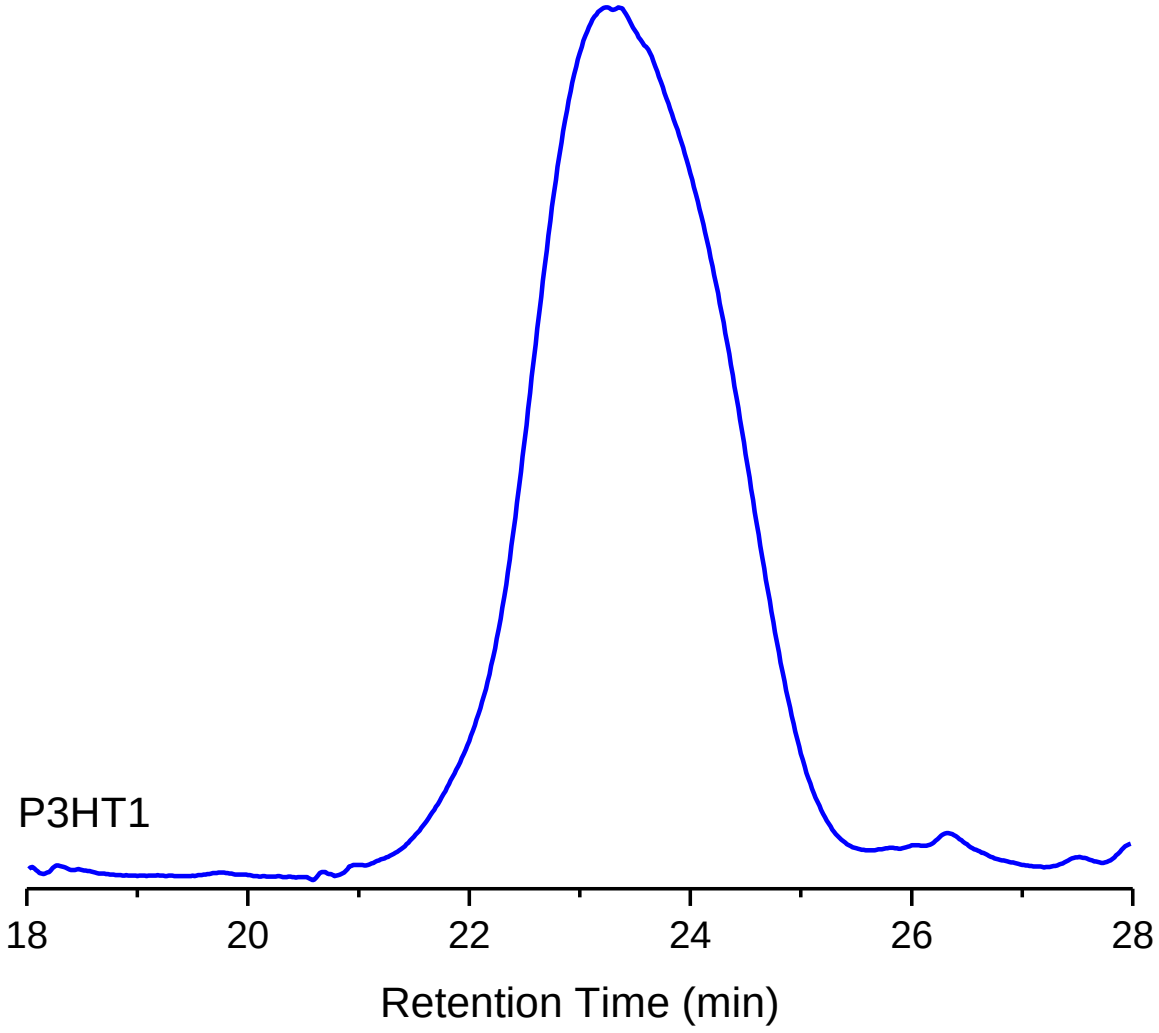

Figure C-5. SEC chromatogram for **P3HT1**.

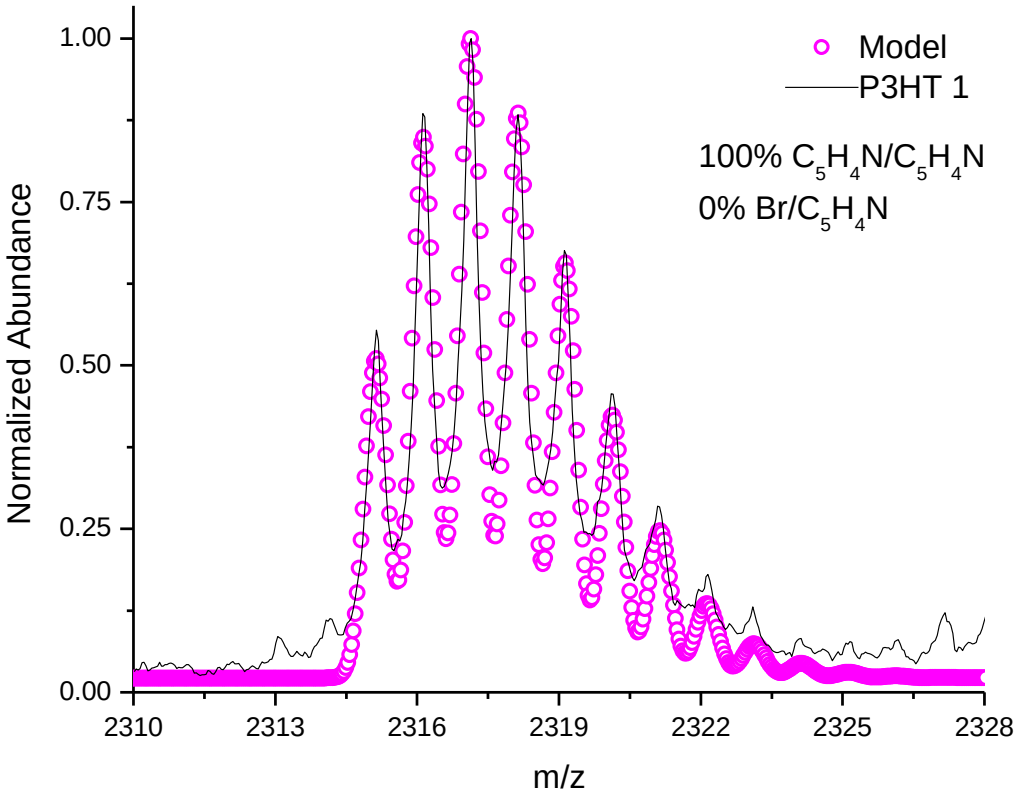

Figure C-6. Modeled spectrum for **P3HT1** showing the estimated abundance of C_5H_4N/C_5H_4N and Br/C_5H_4N terminated chains in the overlapping distribution.

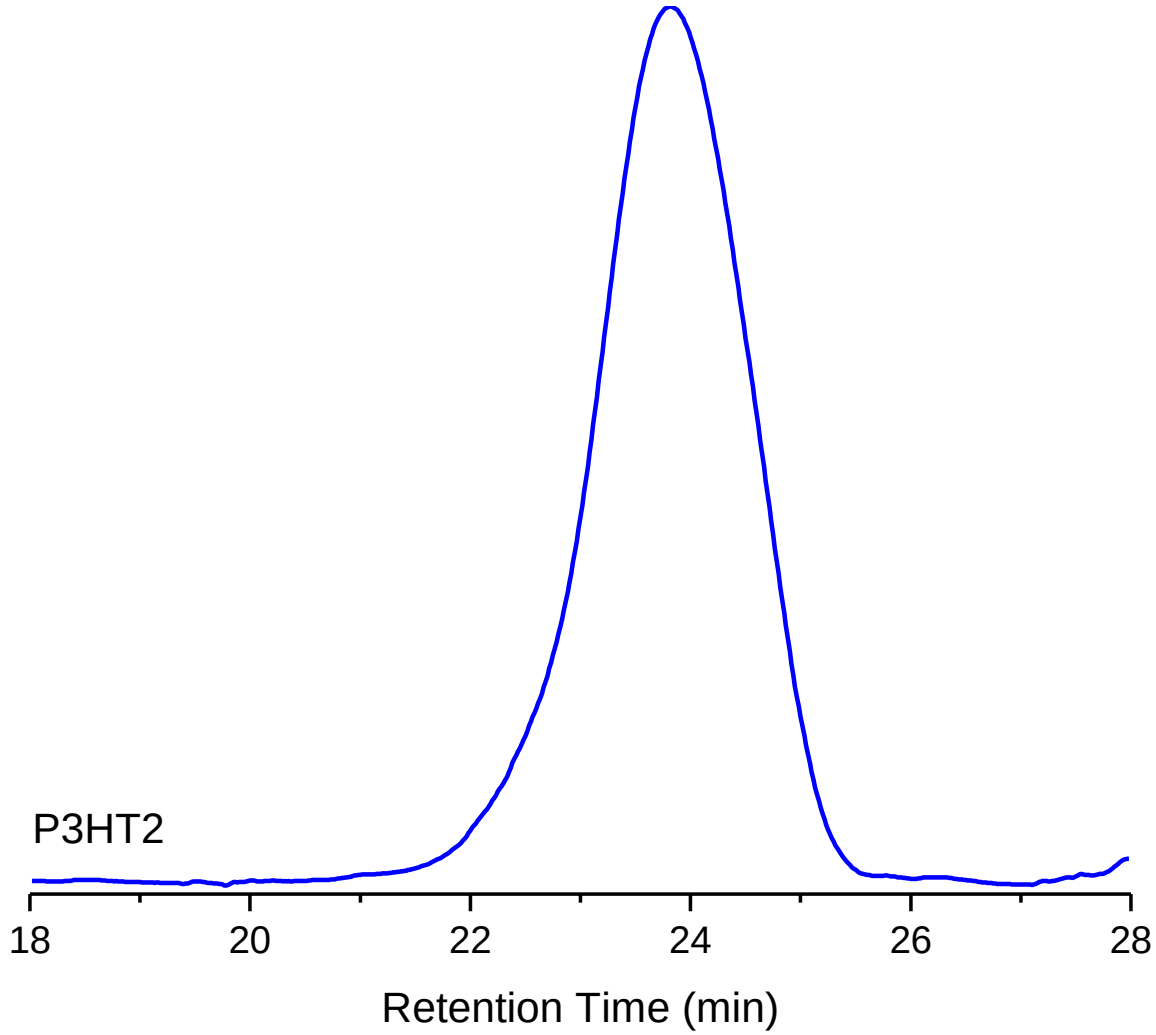

Figure C-7. SEC chromatogram for **P3HT2**.

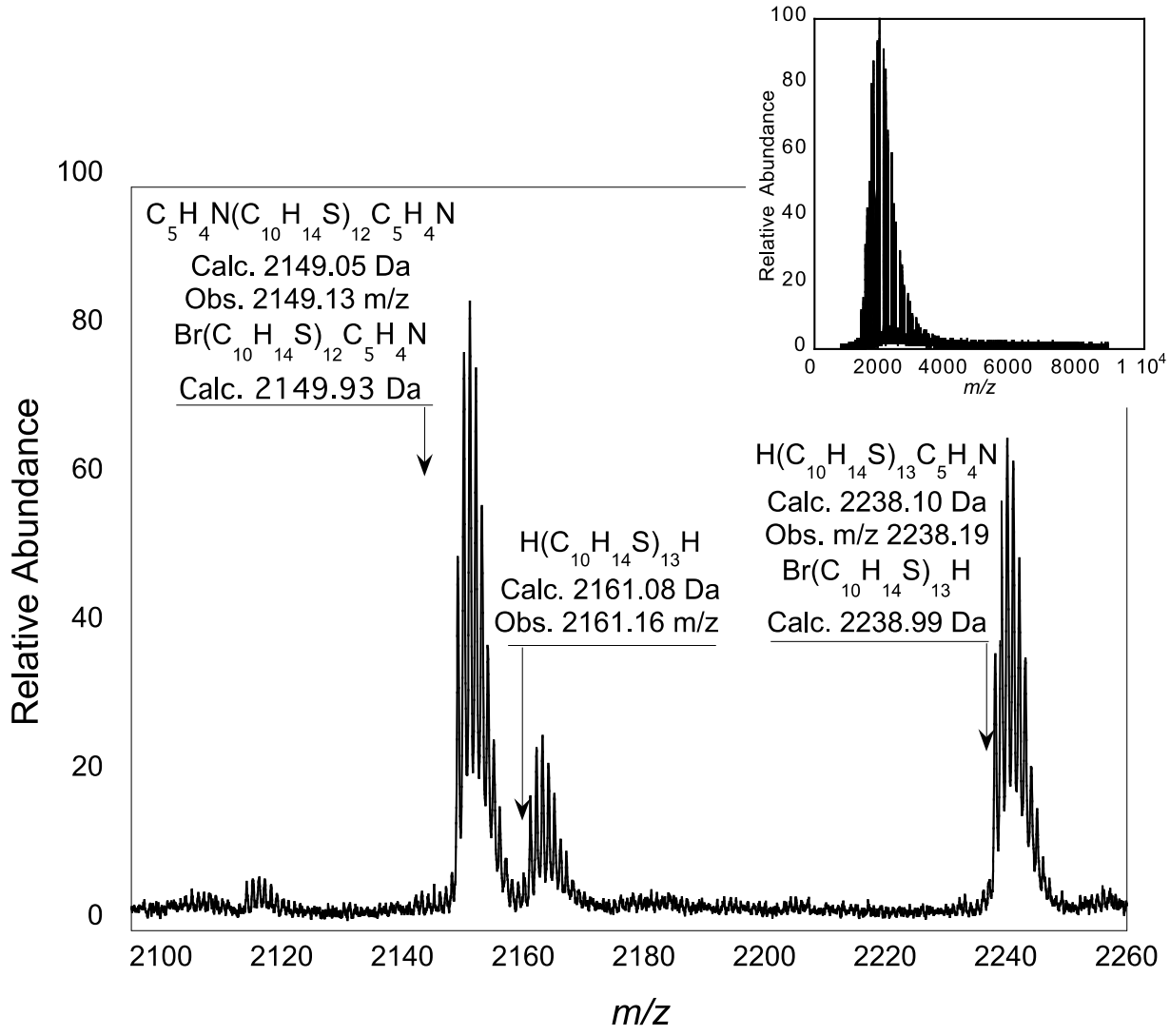

Figure C-8. Mass spectrum of **P3HT2** showing magnification of the 13-mer region and the full spectrum (inset).

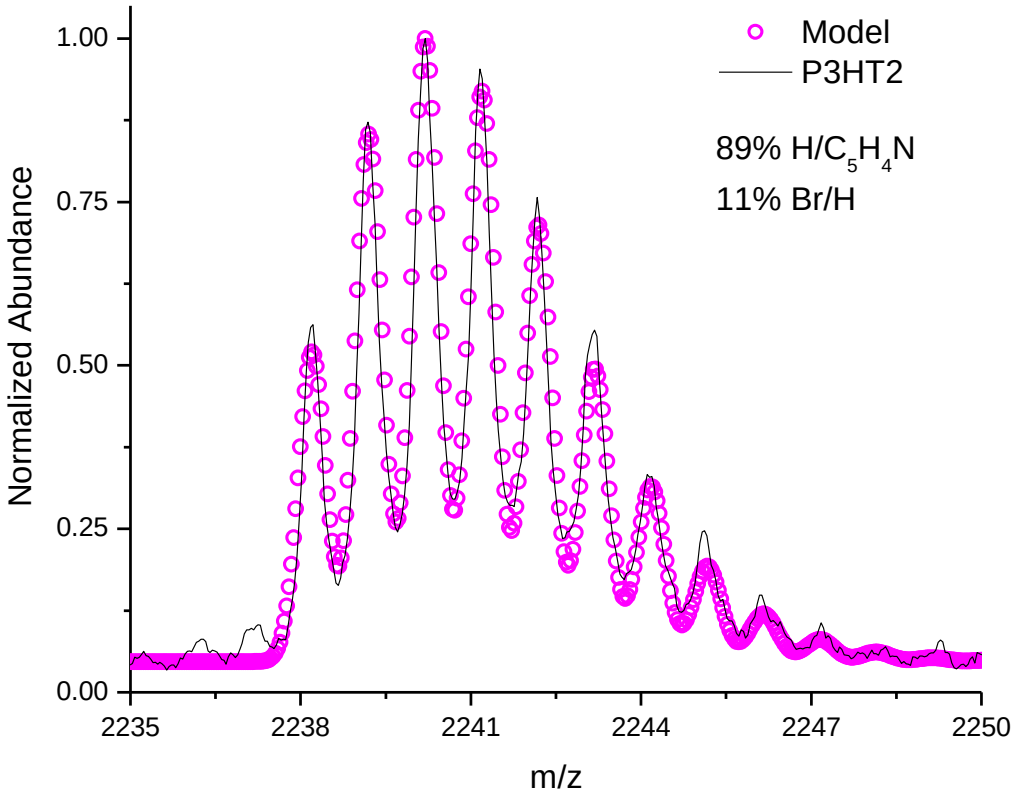

Figure C-9. Modeled spectrum for **P3HT2** showing the estimated abundance of H/C_5H_4N and Br/H terminated chains in the overlapping distribution.

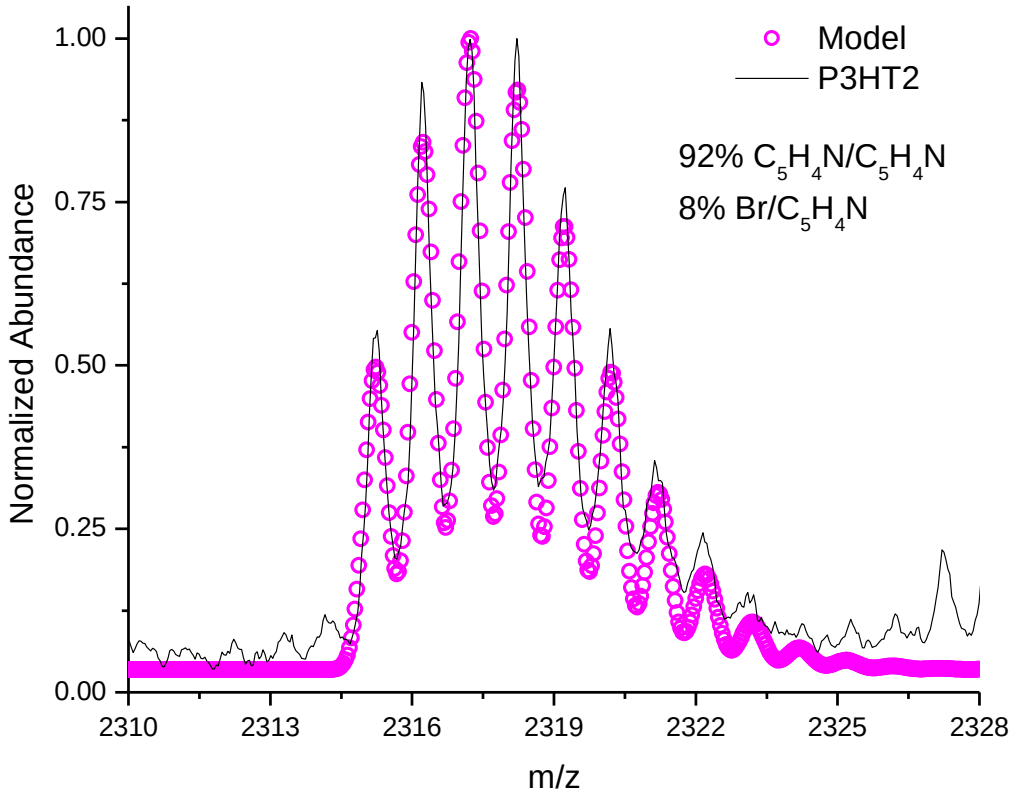

Figure C-10. Modeled spectrum for **P3HT2** showing the estimated abundance of C_5H_4N/C_5H_4N and Br/C_5H_4N terminated chains in the overlapping distribution.

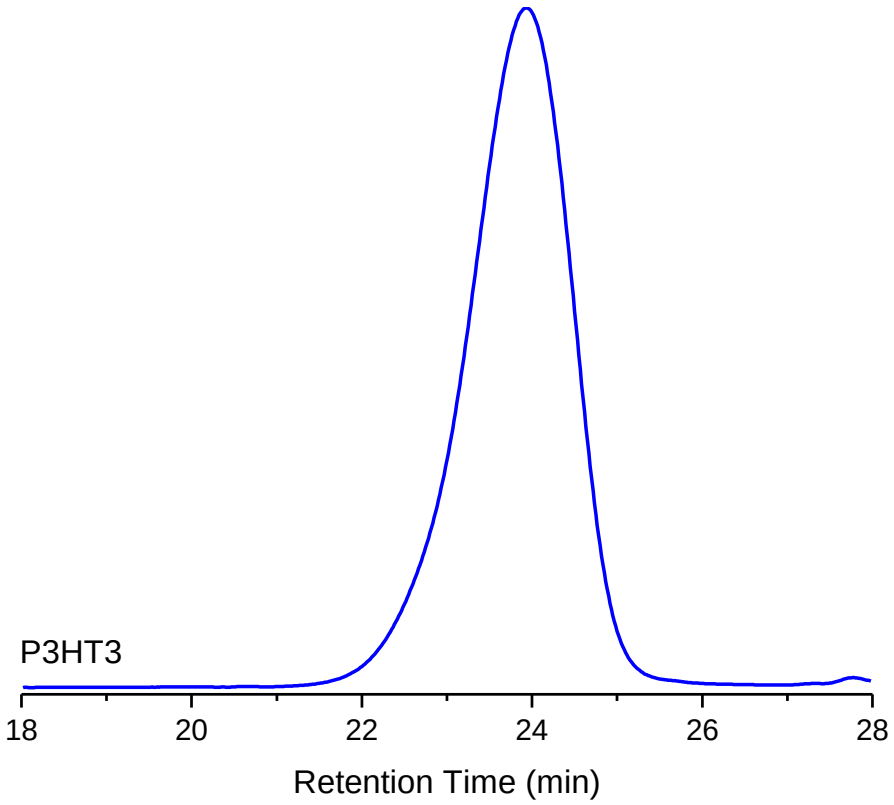

Figure C-11. SEC chromatogram for **P3HT3**.

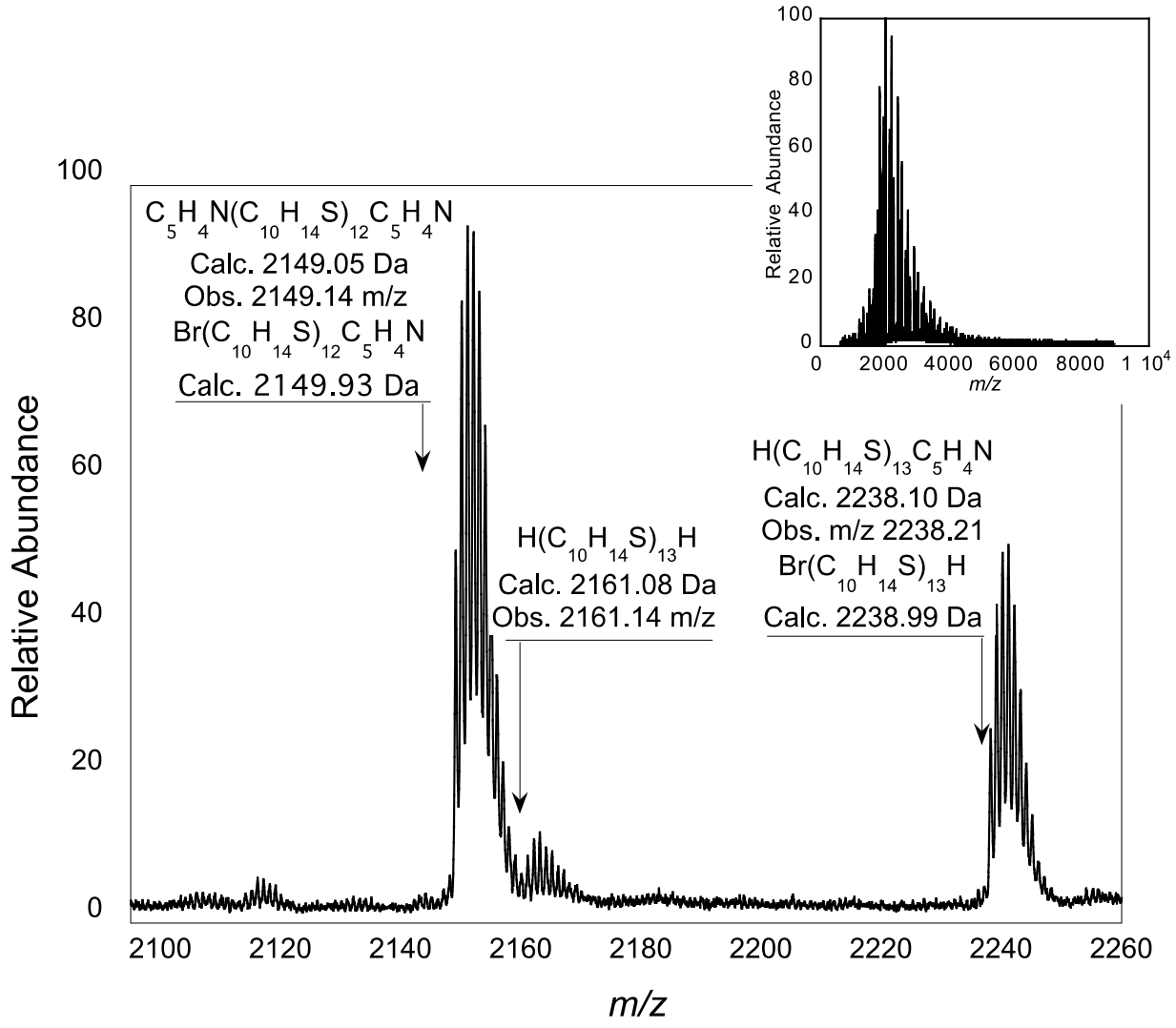

Figure C-12. Mass spectrum of **P3HT3** showing magnification of the 13-mer region and the full spectrum (inset).

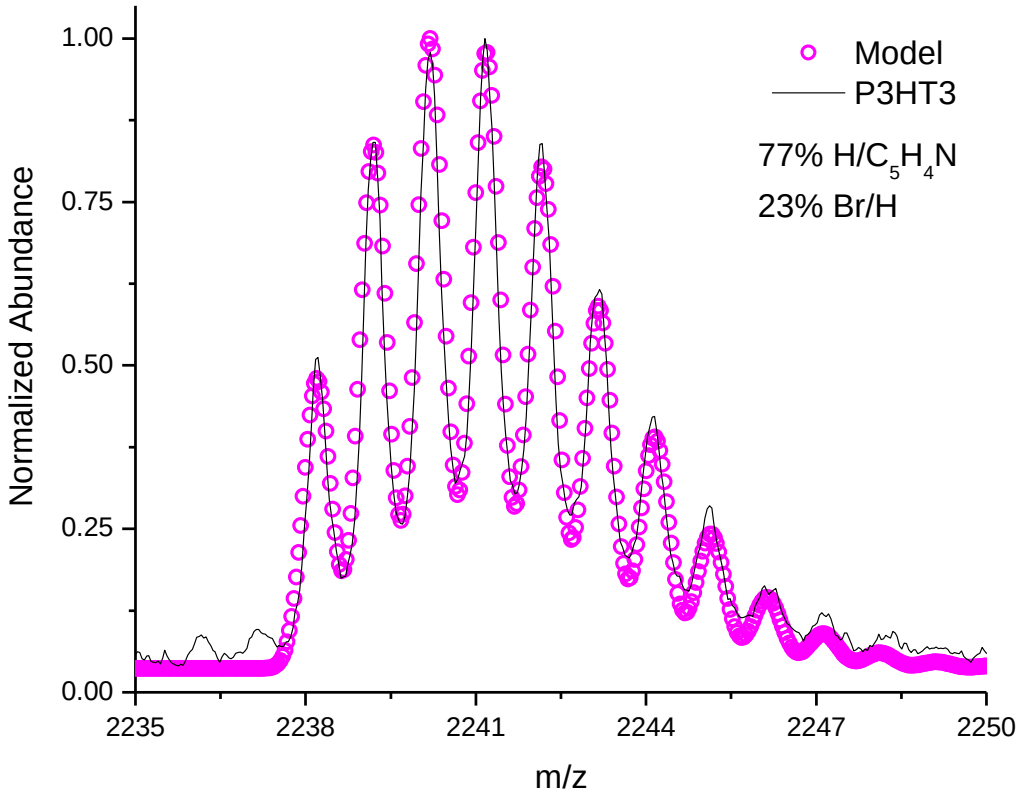

Figure C-13. Modeled spectrum for **P3HT3** showing the estimated abundance of H/C_5H_4N and Br/H terminated chains in the overlapping distribution.

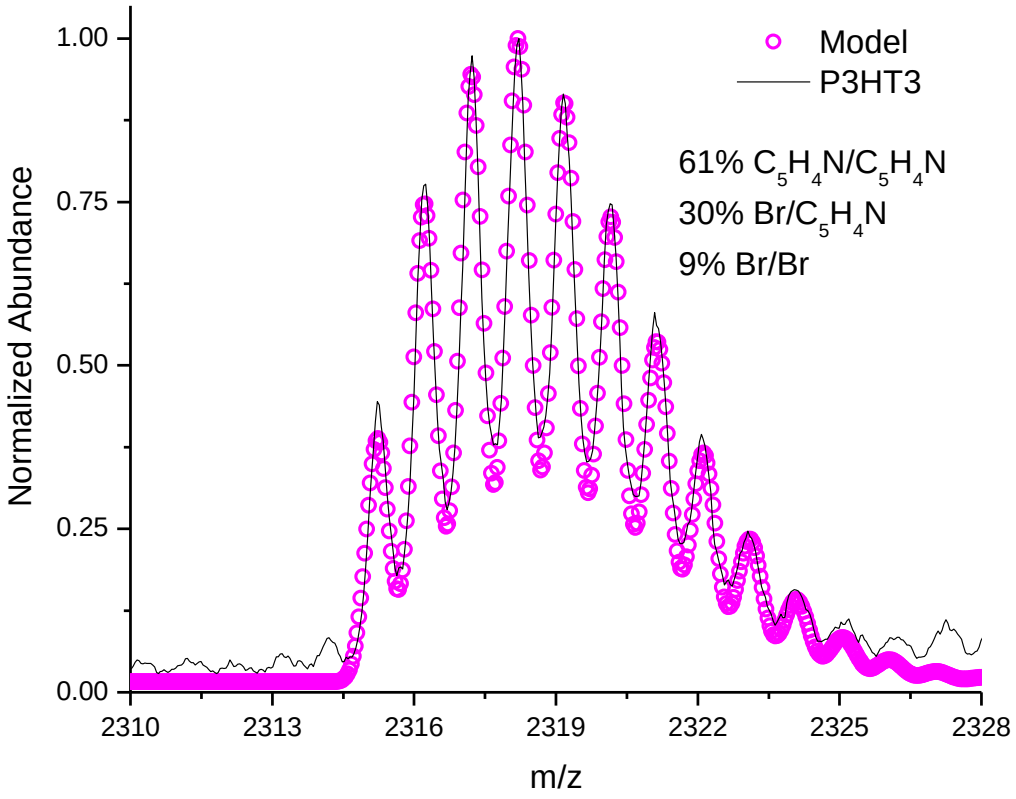

Figure C-14. Modeled spectrum for **P3HT3** showing the estimated abundance of C_5H_4N/C_5H_4N, Br/C_5H_4N, and Br/Br terminated chains in the overlapping distribution.

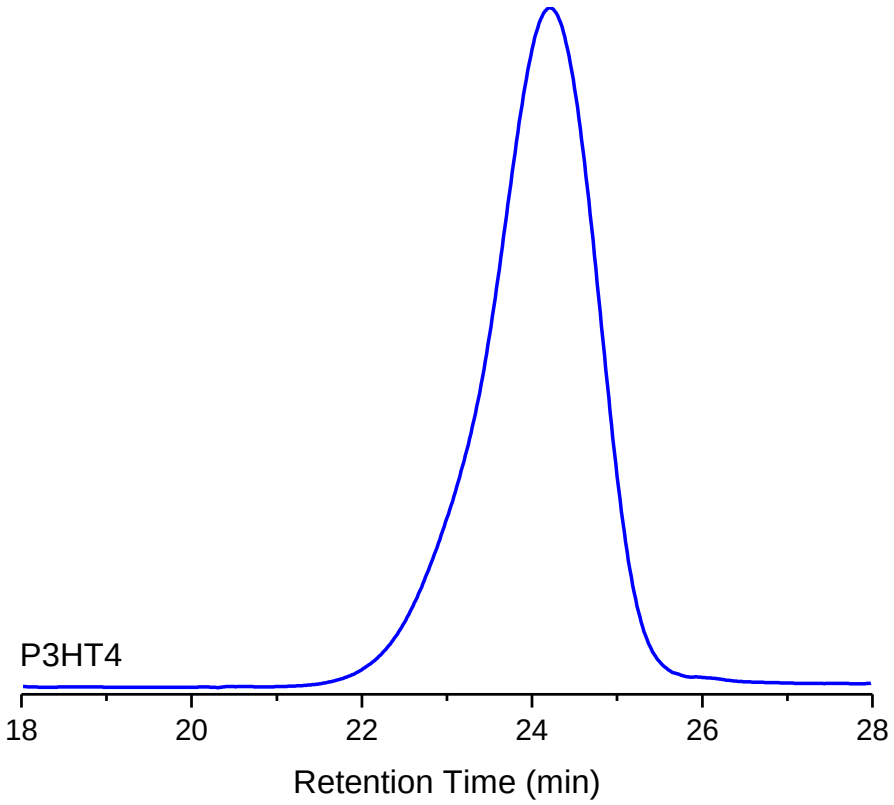

Figure C-15. SEC chromatogram for **P3HT4**.

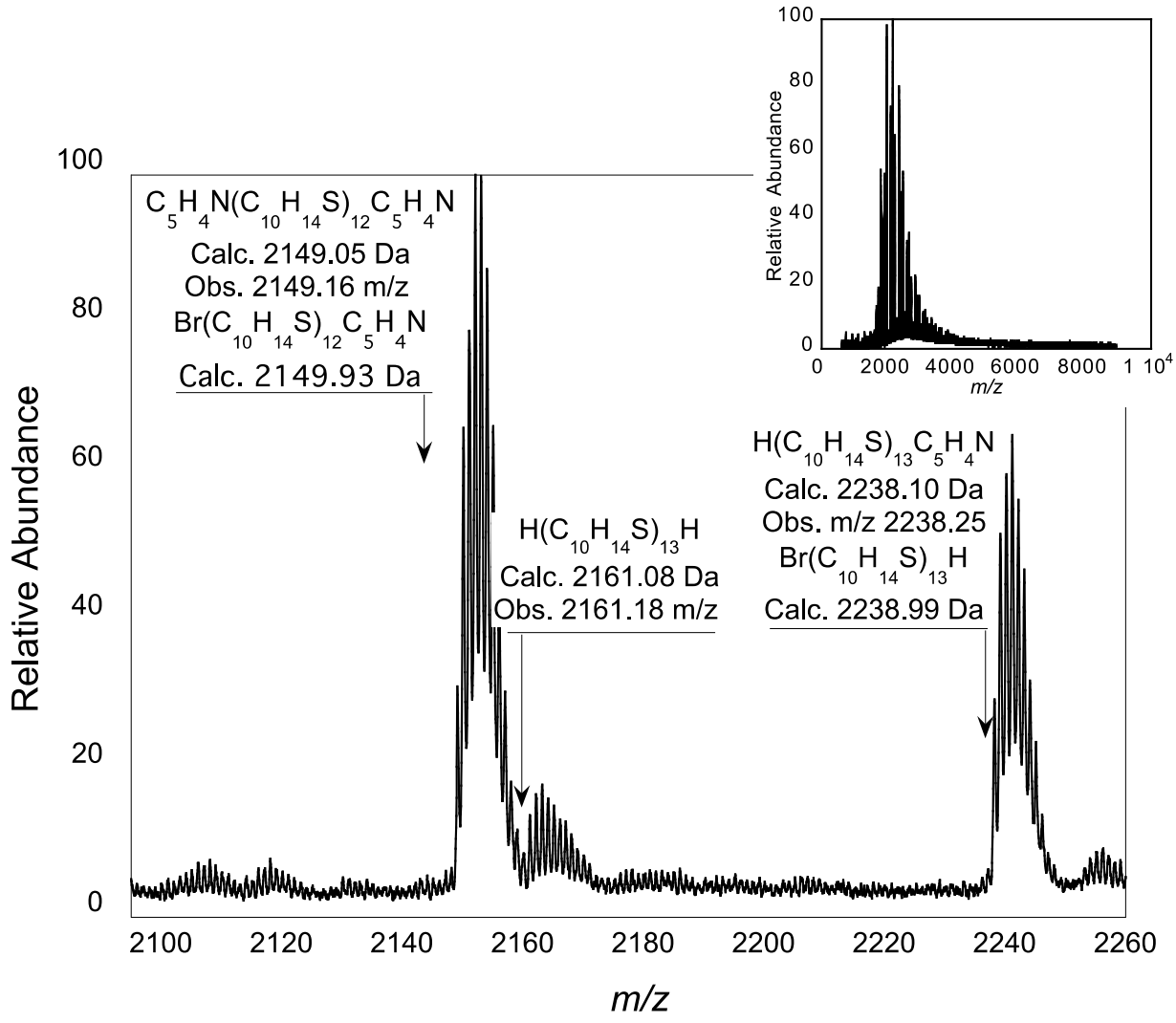

Figure C-16. Mass spectrum of **P3HT4** showing magnification of the 13-mer region and the full spectrum (inset).

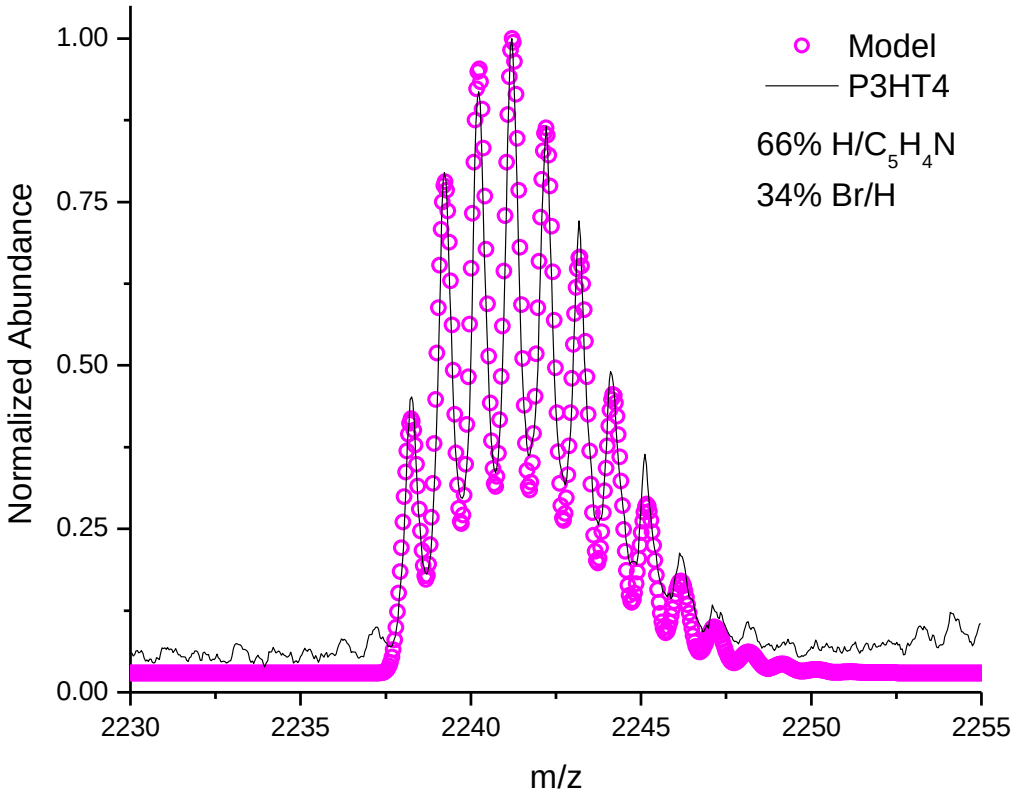

Figure C-17. Modeled spectrum for **P3HT4** showing the estimated abundance of H/C_5H_4N and Br/H terminated chains in the overlapping distribution.

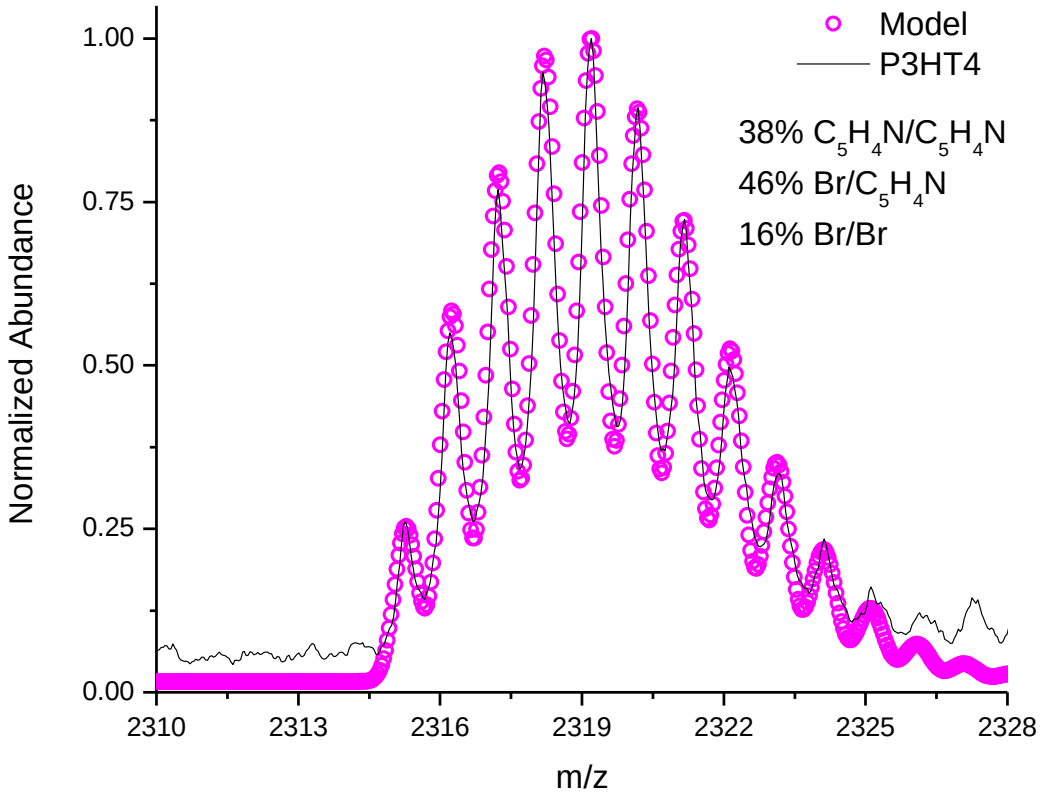

Figure C-18. Modeled spectrum for **P3HT4** showing the estimated abundance of C_5H_4N/C_5H_4N, Br/C_5H_4N, and Br/Br terminated chains in the overlapping distribution.

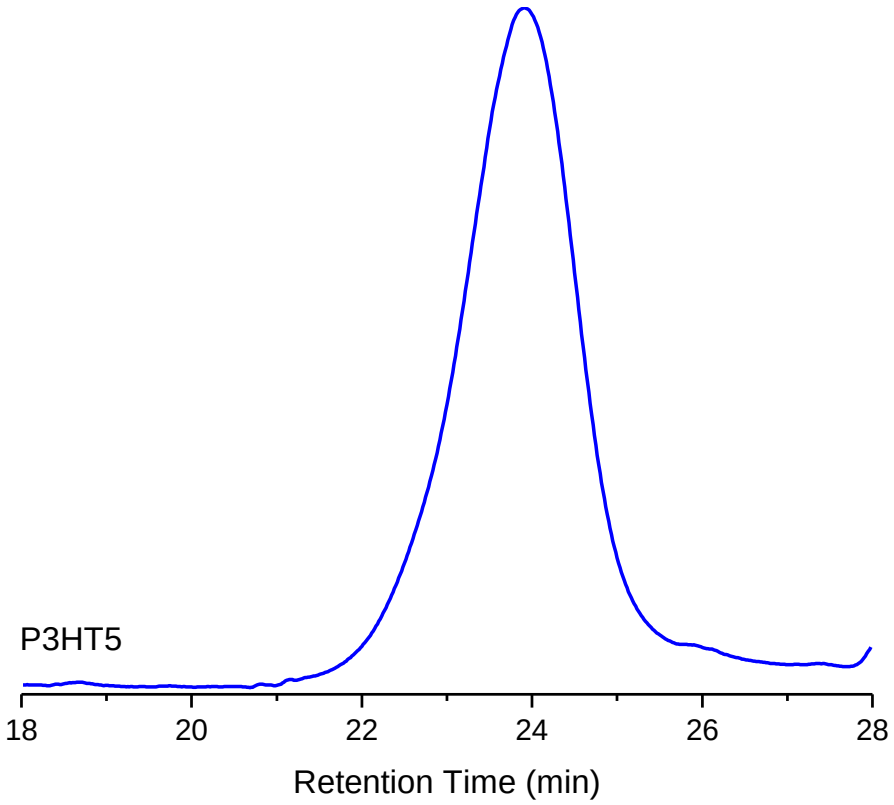

Figure C-19. SEC chromatogram for **P3HT5**.

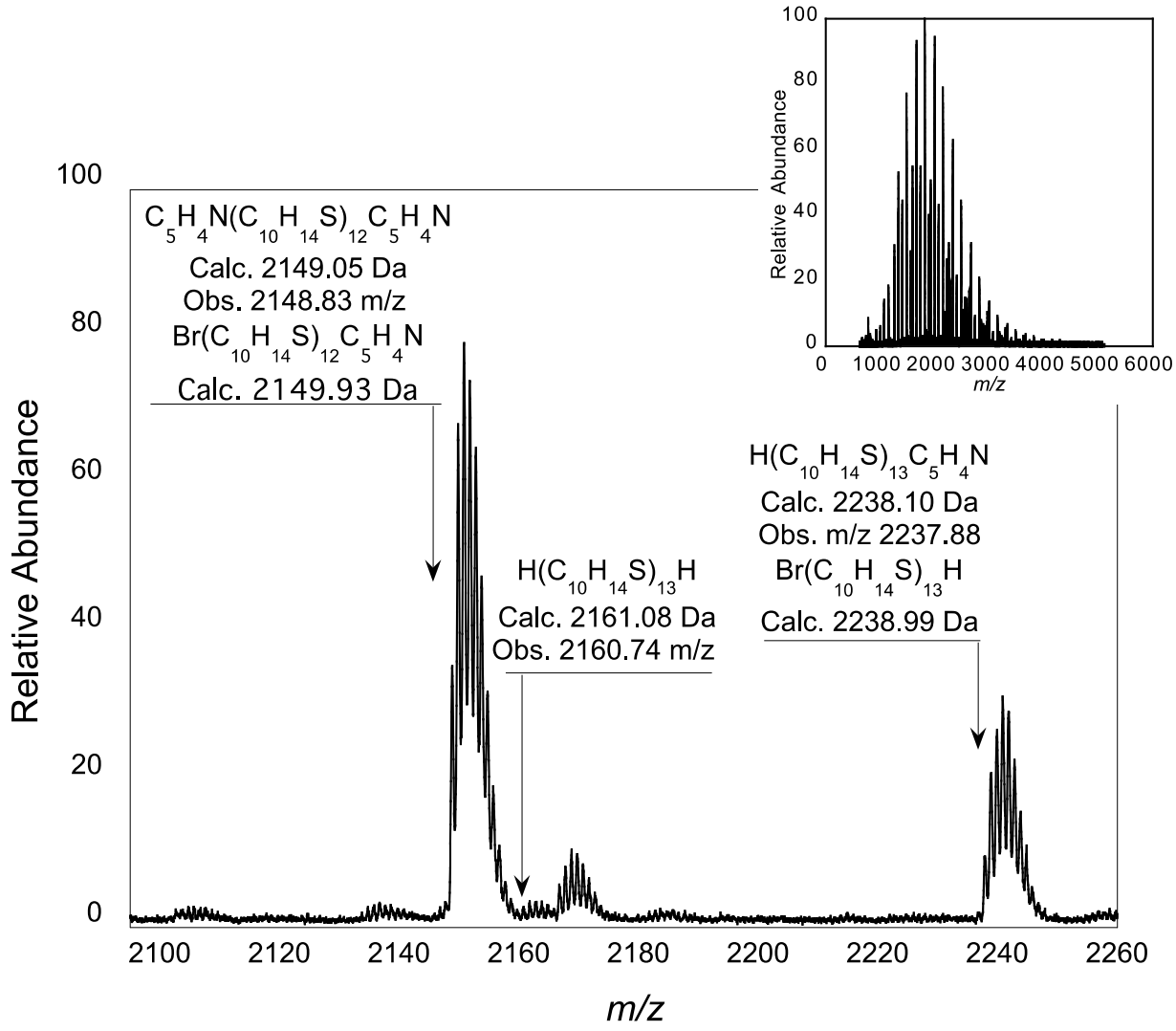

Figure C-20. Mass spectrum of **P3HT5** showing magnification of the 13-mer region and the full spectrum (inset).

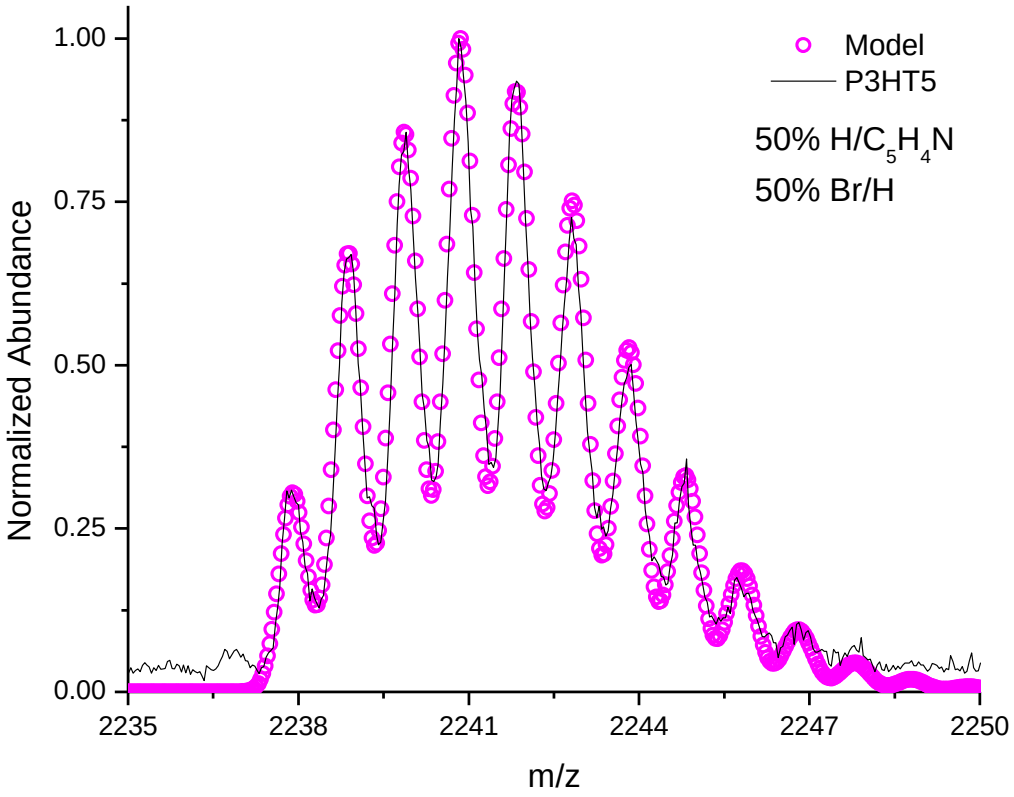

Figure C-21. Modeled spectrum for **P3HT5** showing the estimated abundance of H/C_5H_4N and Br/H terminated chains in the overlapping distribution.

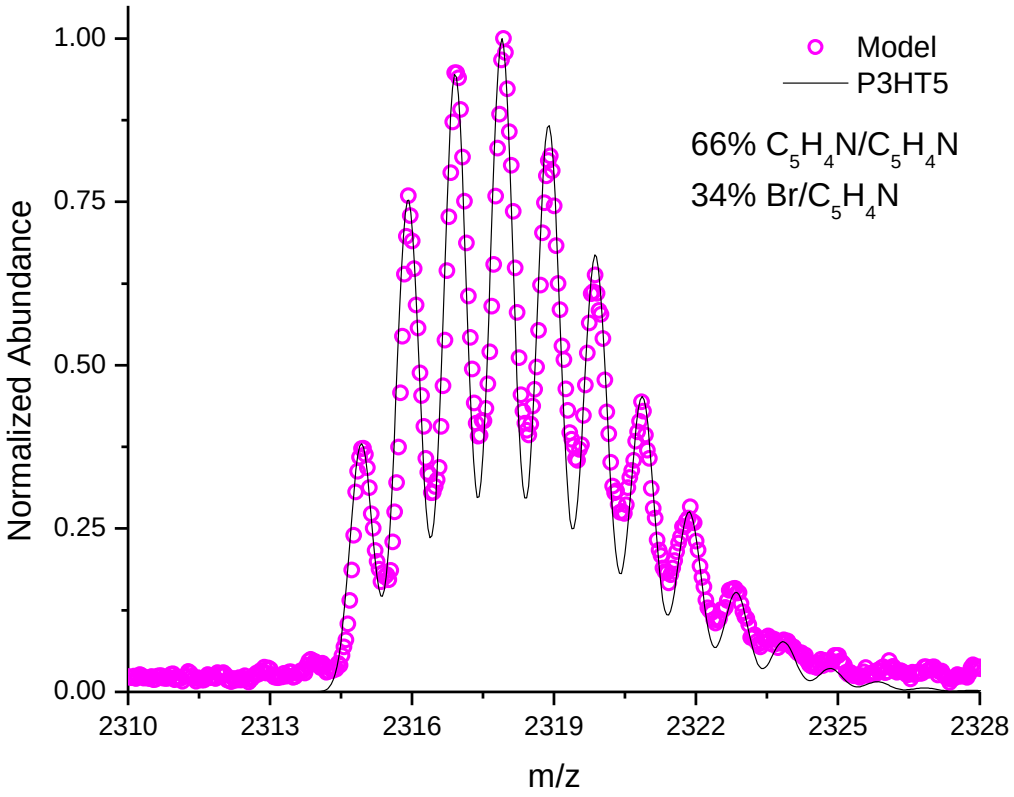

Figure C-22. Modeled spectrum for **P3HT5** showing the estimated abundance of C_5H_4N/C_5H_4N and Br/C_5H_4N terminated chains in the overlapping distribution.

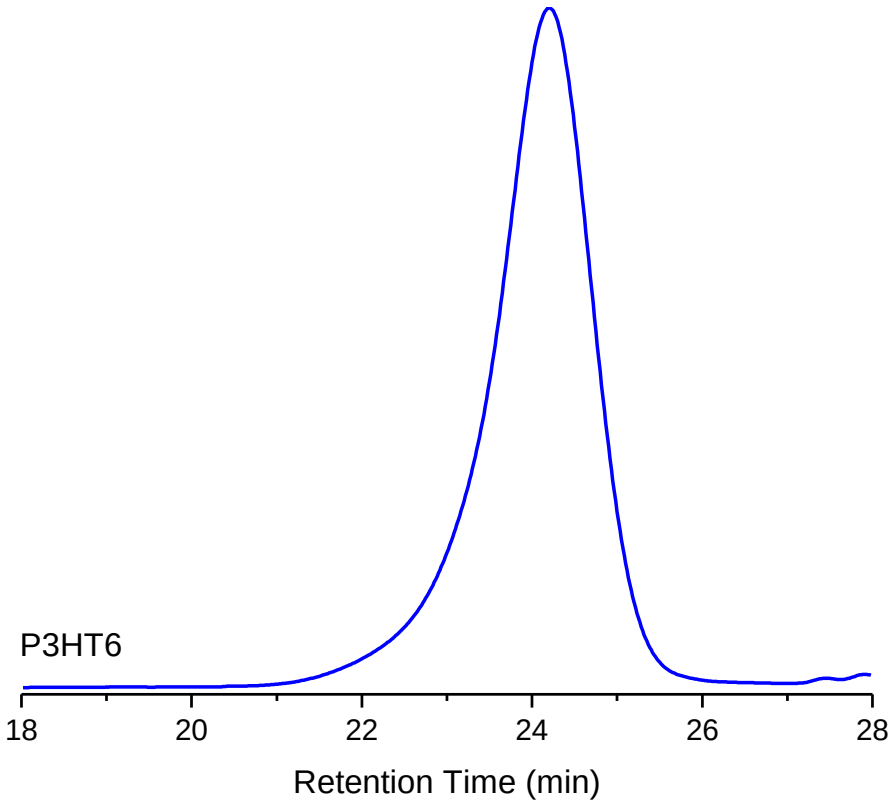

Figure C-23. SEC chromatogram for **P3HT6**.

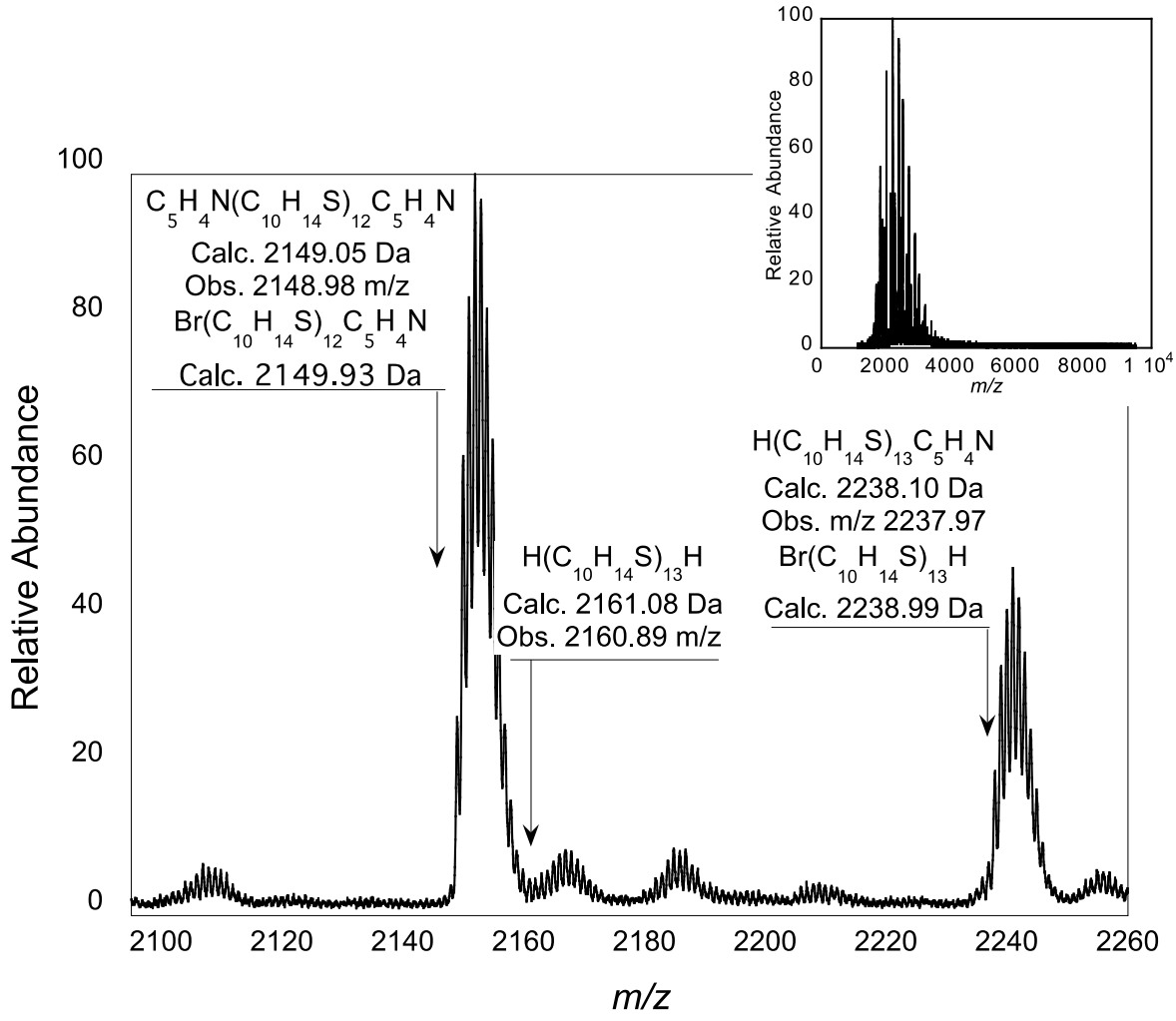

Figure C-24. Mass spectrum of **P3HT6** showing magnification of the 13-mer region and the full spectrum (inset).

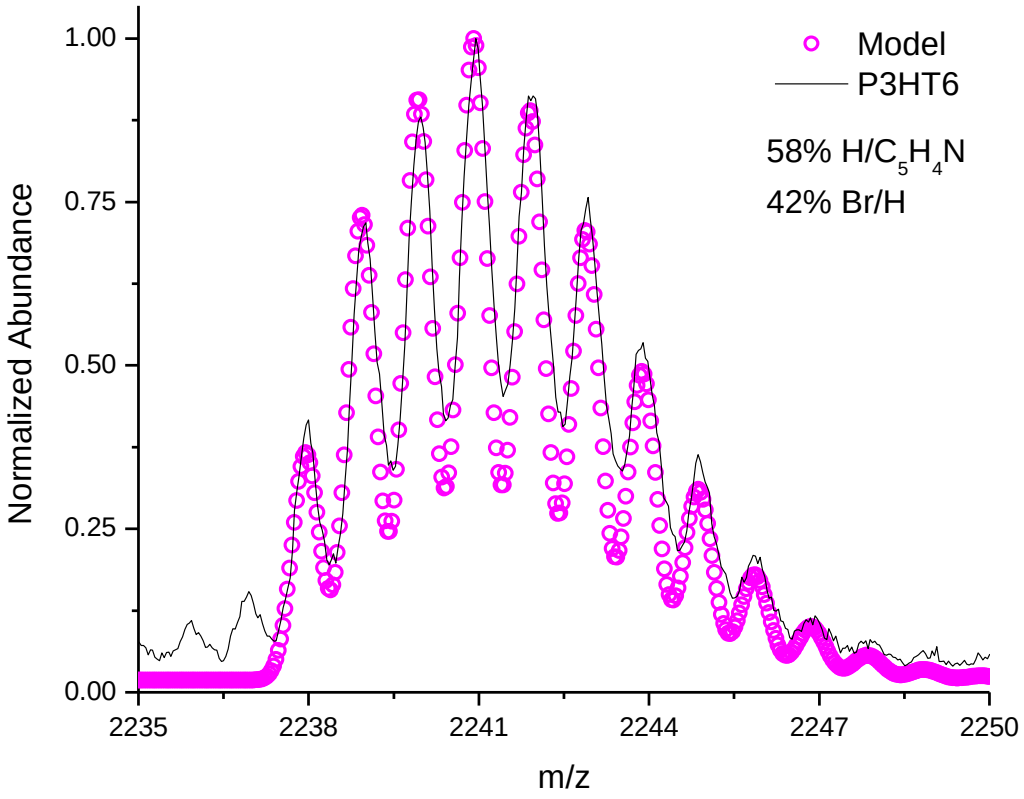

Figure C-25. Modeled spectrum for **P3HT6** showing the estimated abundance of H/C_5H_4N and Br/H terminated chains in the overlapping distribution.

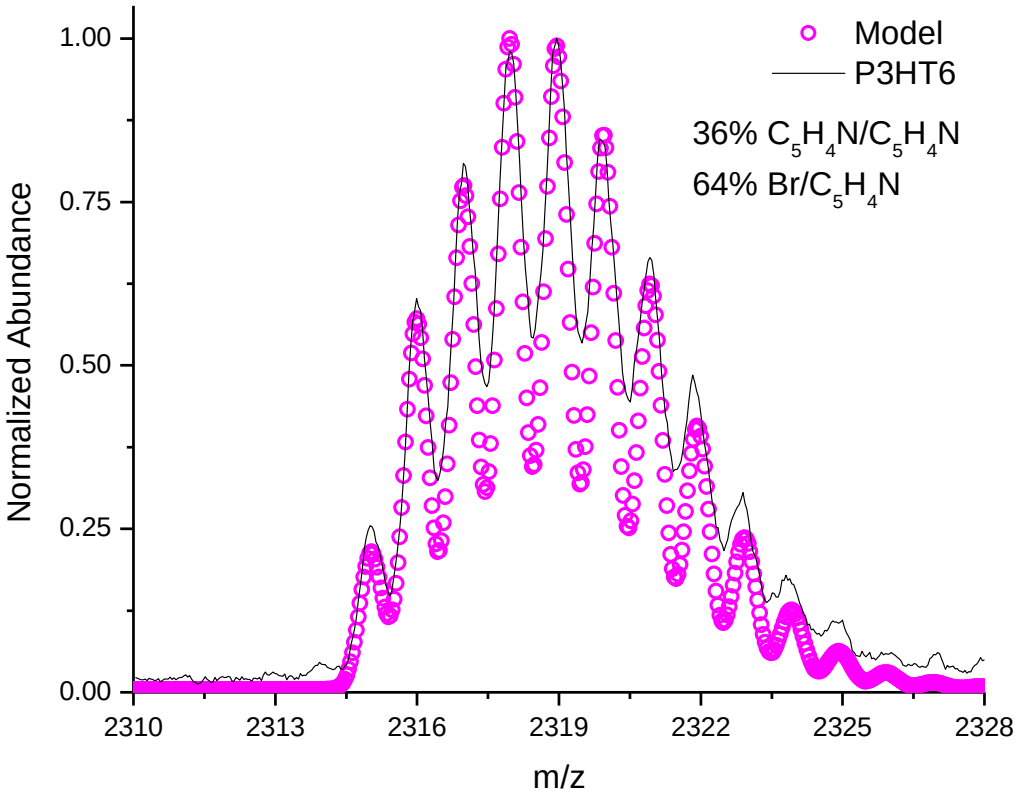

Figure C-26. Modeled spectrum for **P3HT6** showing the estimated abundance of C_5H_4N/C_5H_4N and Br/C_5H_4N terminated chains in the overlapping distribution.

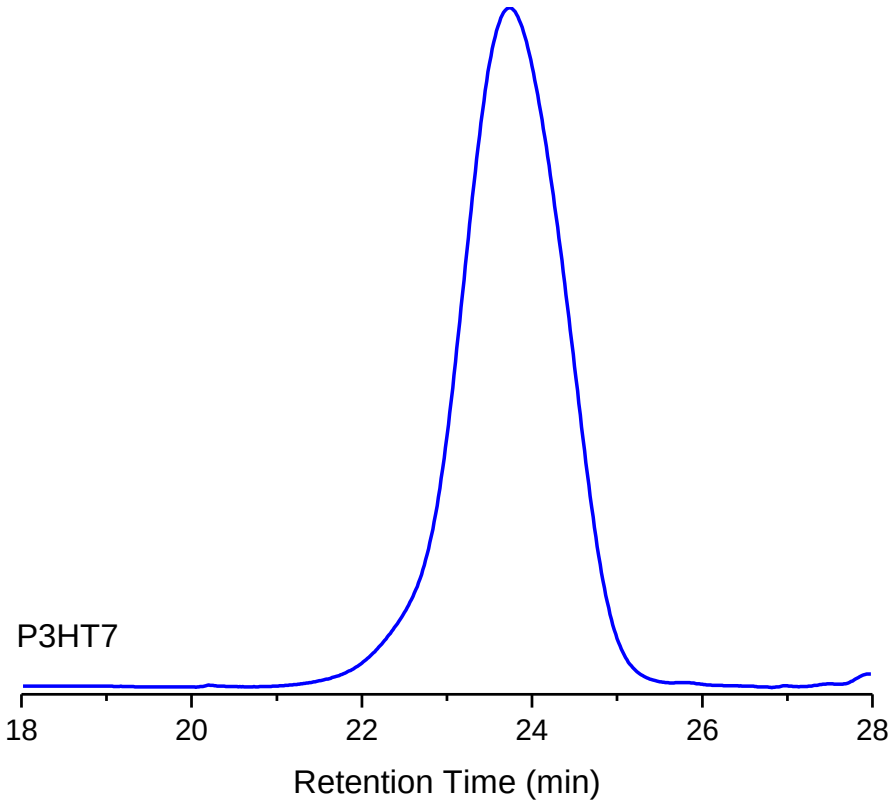

Figure C-27. SEC chromatogram for **P3HT7**.

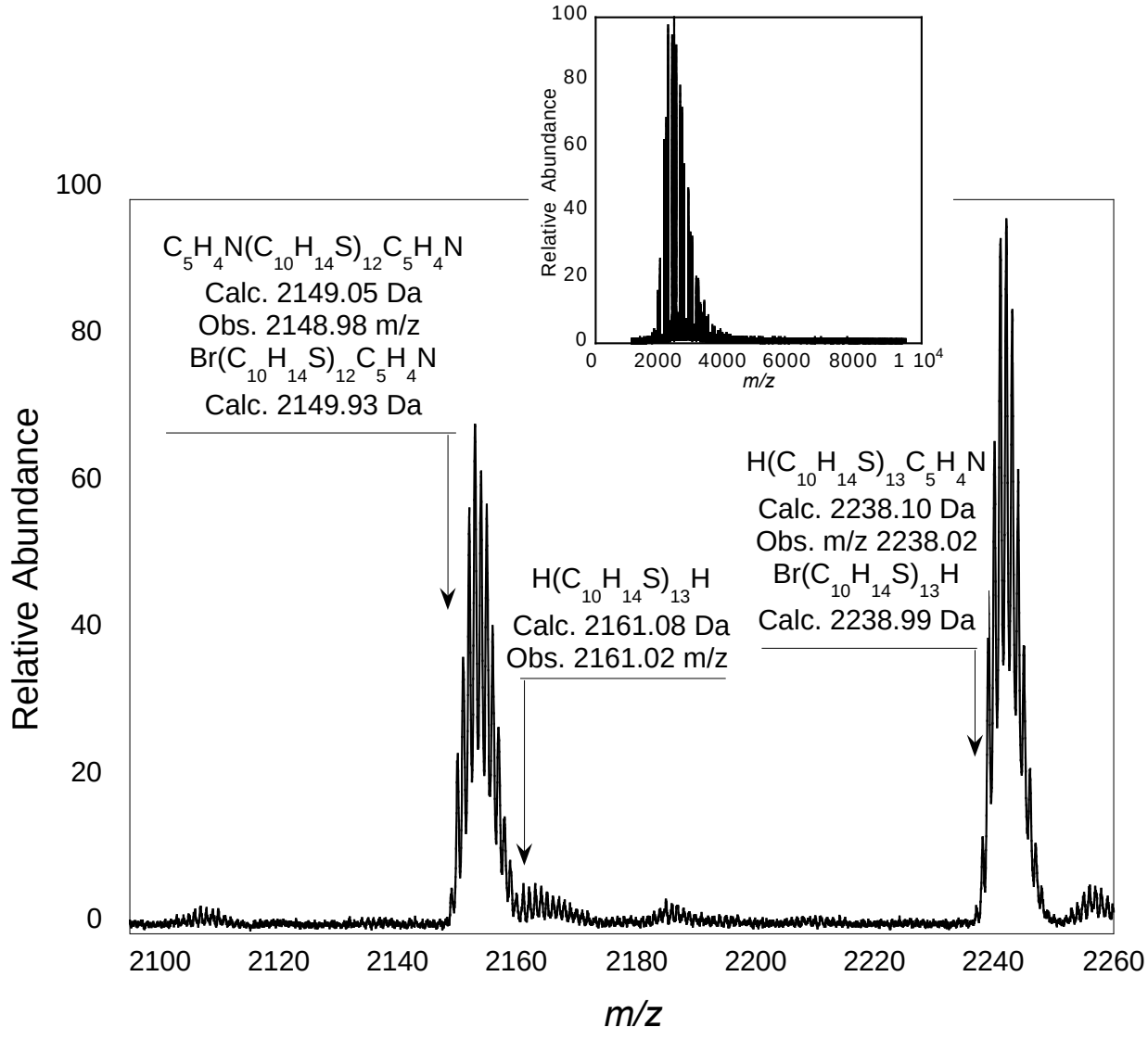

Figure C-28. Mass spectrum of **P3HT7** showing magnification of the 13-mer region and the full spectrum (inset).

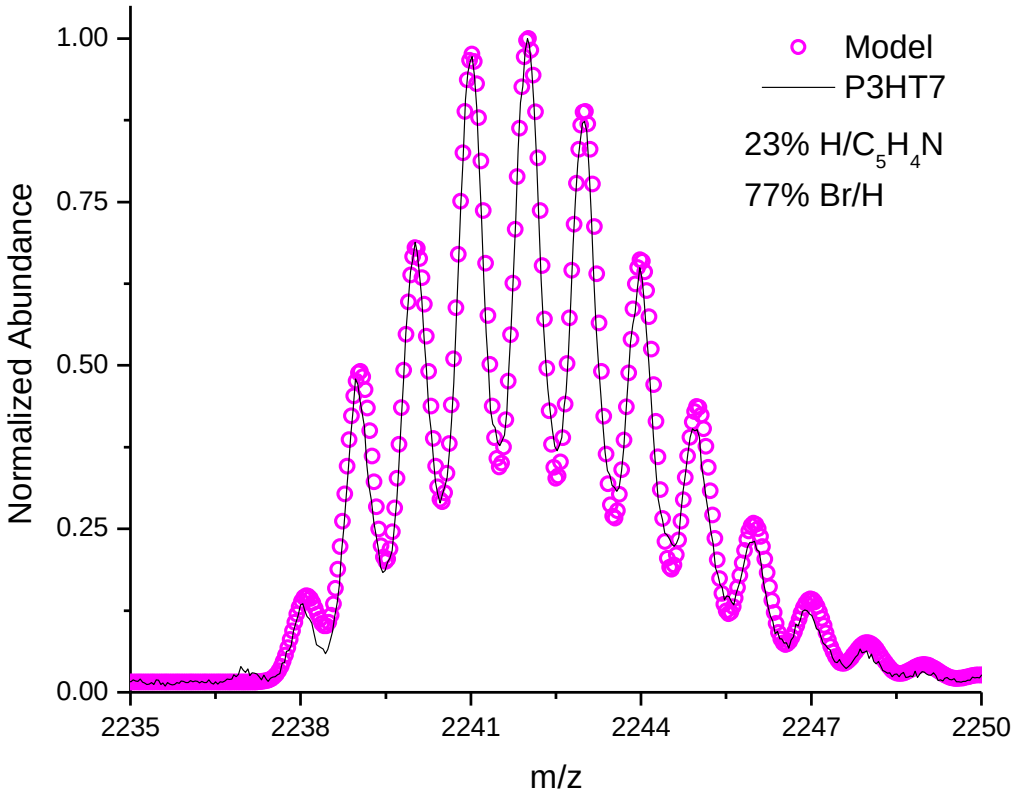

Figure C-29. Modeled spectrum for **P3HT7** showing the estimated abundance of H/C_5H_4N and Br/H terminated chains in the overlapping distribution.

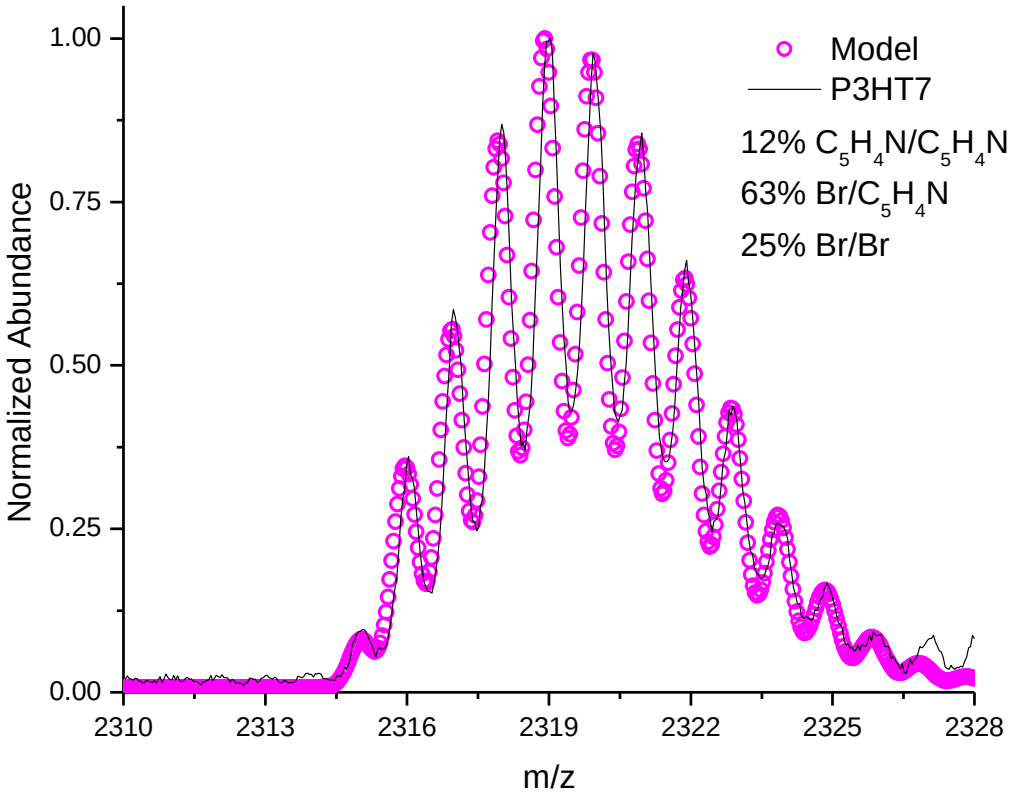

Figure C-30. Modeled spectrum for **P3HT7** showing the estimated abundance of C_5H_4N/C_5H_4N, Br/C_5H_4N, and Br/Br terminated chains in the overlapping distribution.

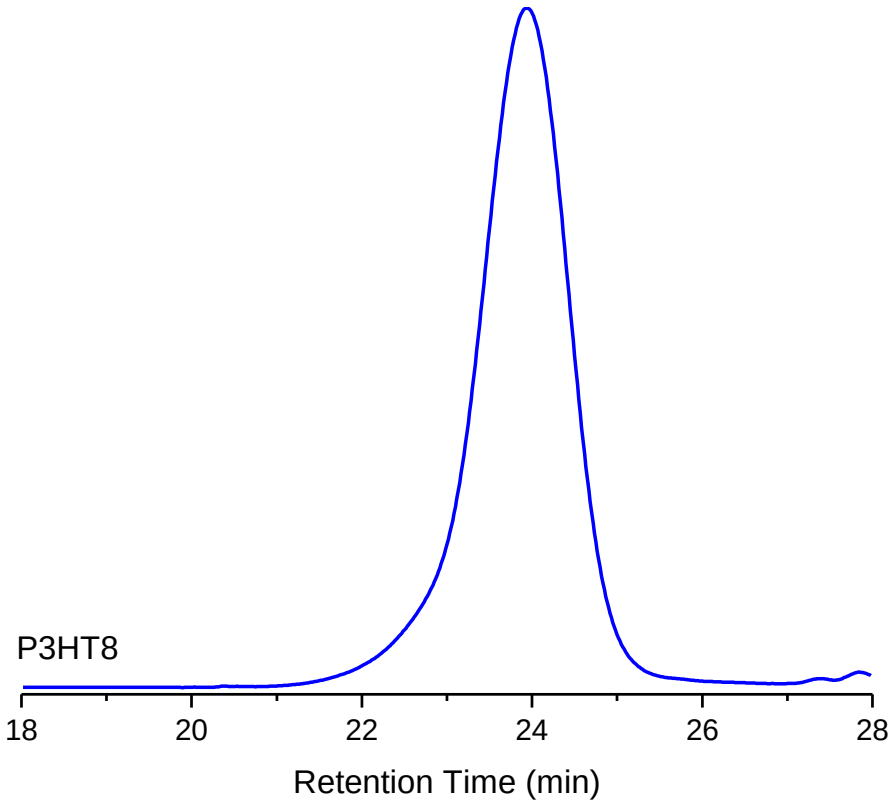

Figure C-31. SEC chromatogram for **P3HT8**.

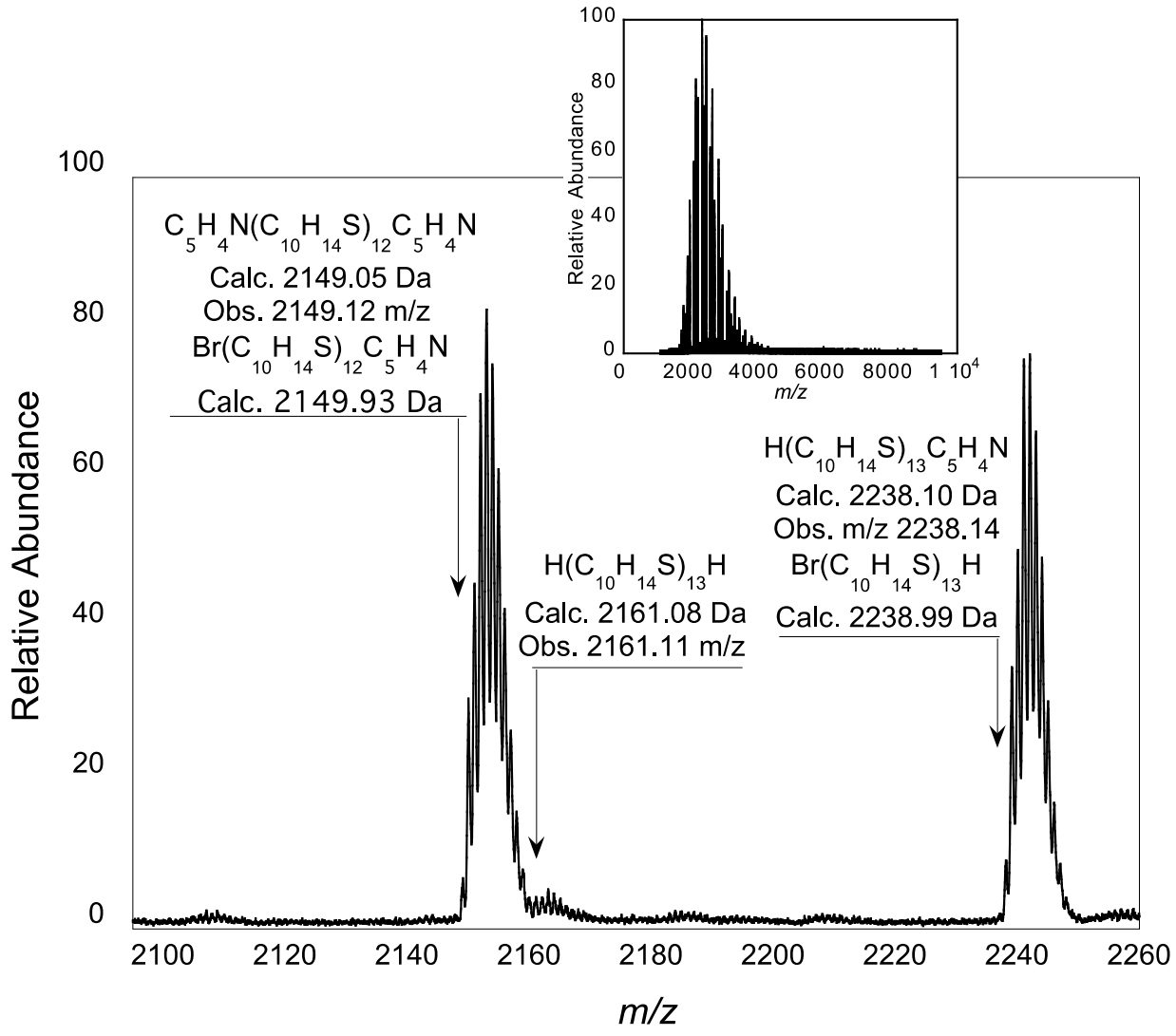

Figure C-32. Mass spectrum of **P3HT8** showing magnification of the 13-mer region and the full spectrum (inset).

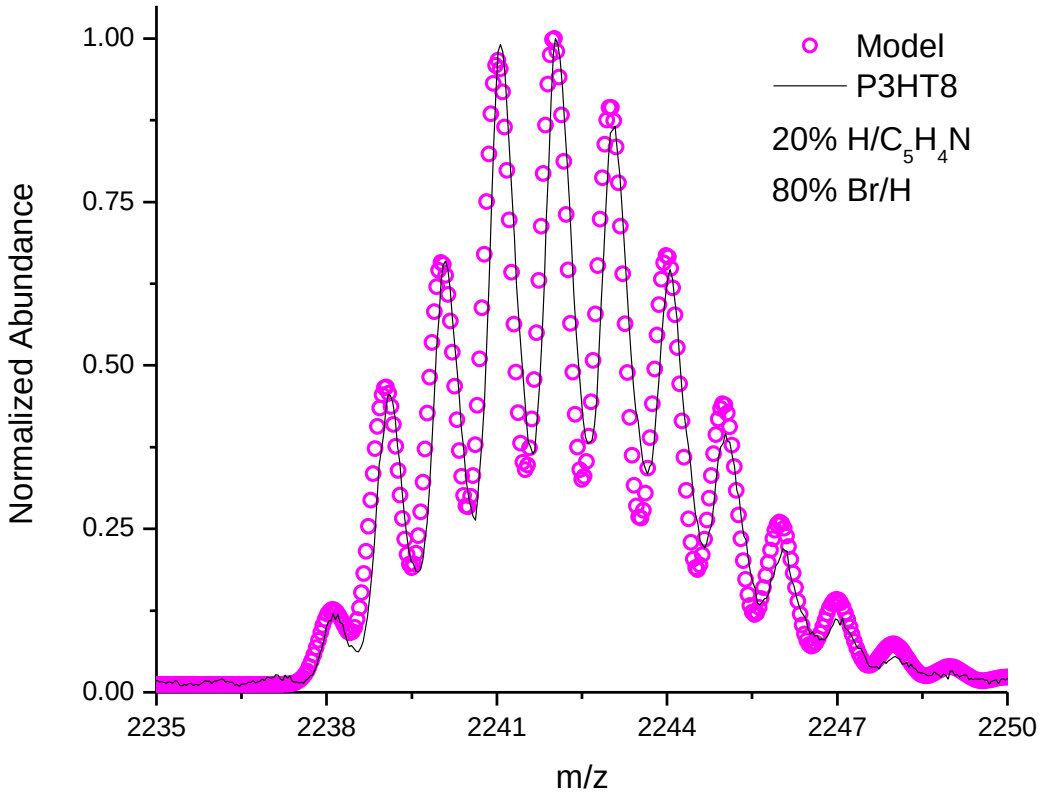

Figure C-33. Modeled spectrum for **P3HT8** showing the estimated abundance of H/C_5H_4N and Br/H terminated chains in the overlapping distribution.

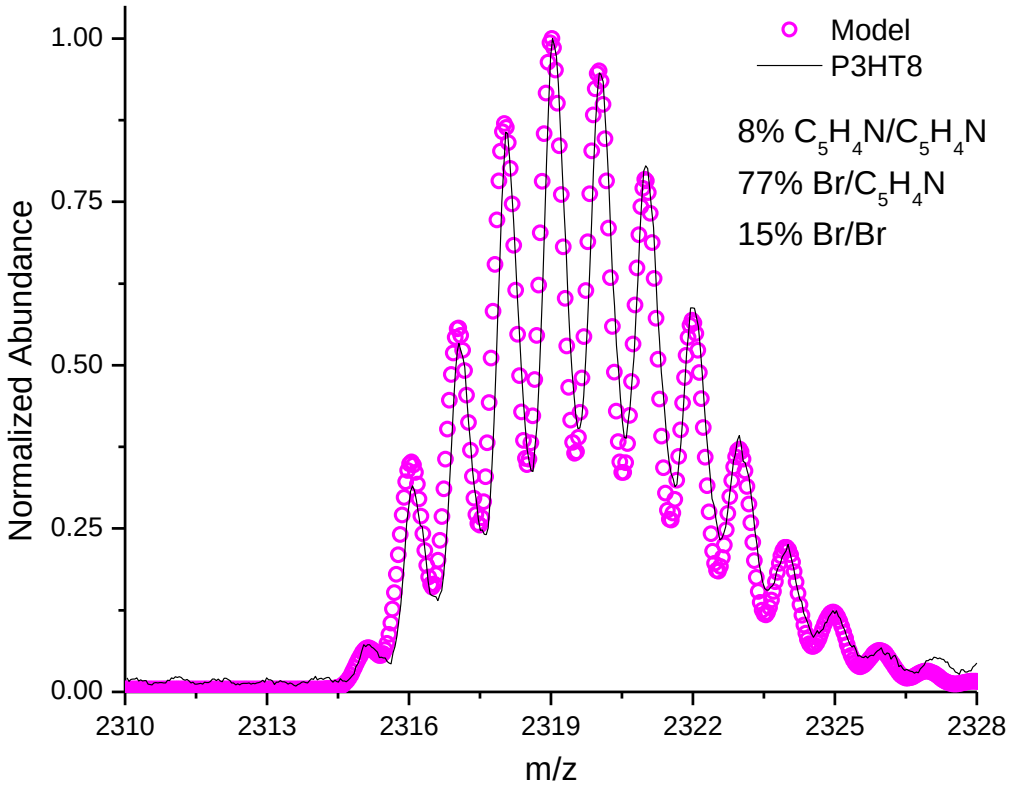

Figure C-34. Modeled spectrum for **P3HT8** showing the estimated abundance of C_5H_4N/C_5H_4N, Br/C_5H_4N, and Br/Br terminated chains in the overlapping distribution.

^{1}H NMR of P3HT5-P3HT8

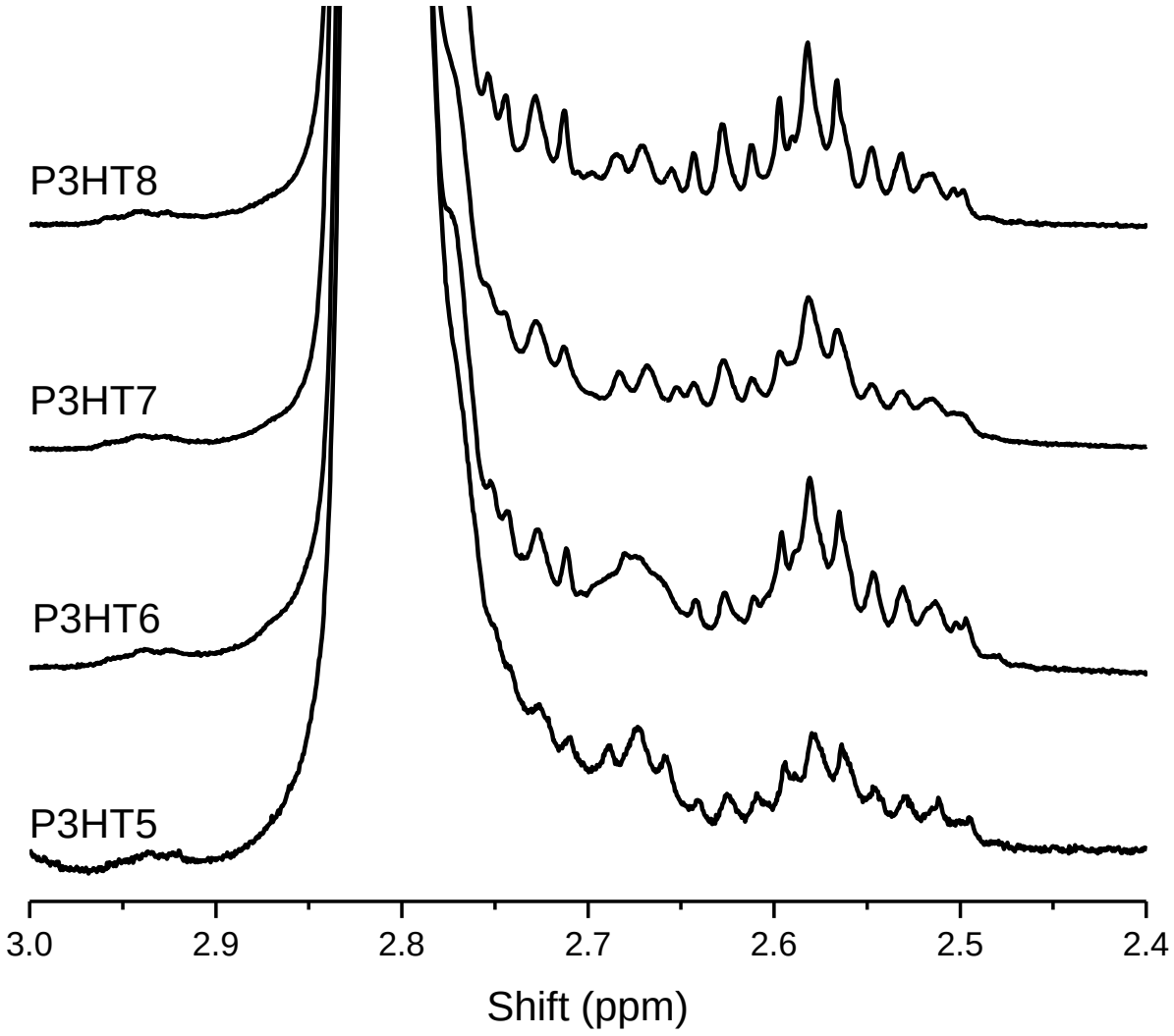

Figure C-35. ^{1}H NMR spectra showing the aliphatic region that corresponds to the α-methylene protons adjacent to the chain ends for **P3HT5-P3HT8**. The triplet at 2.65 ppm is attributed to the α-methylene protons adjacent to the pyridine ring with nitrogen in the 3-position.

TEM micrographs at 100 nm scale

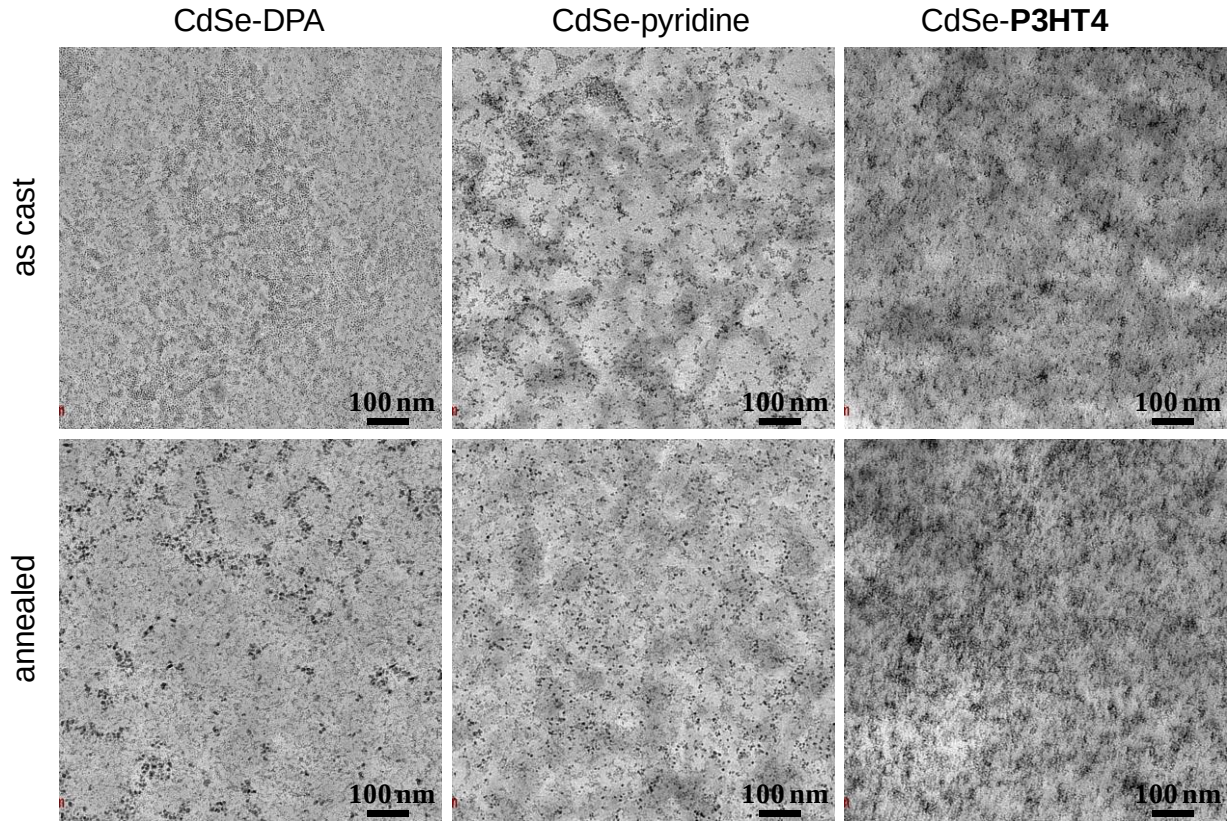

Figure C-36. TEM micrographs of films consisting of 20 wt % surface-modified CdSe in a P3HT matrix (M_n = 25 kDa) made by drop casting from a 0.2 wt% solution in $CHCl_3$. The ligands decorating the CdSe surface from left to right are DPA, pyridine and **P3HT4**. The scale bar shown is 100 nm.

Appendix D- Chapter 4: Tailoring Nanoscale Organization of CdSe/poly (3-hexylthiophene) (P3HT) Blends by Ligand Modification

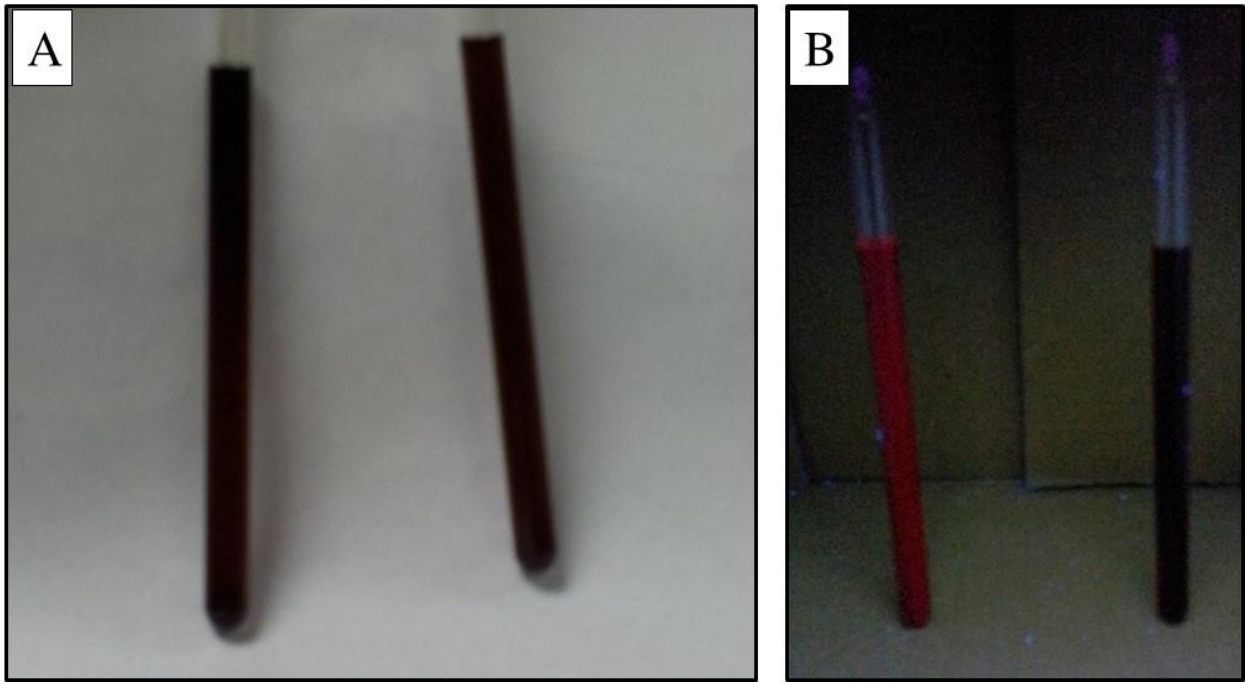

Figure D-1. Pictures of OA-CdSe (left vessel) and pyr-CdSe (right vessel) dispersed in pyridine under ambient light (A) and under UV radiation (B).

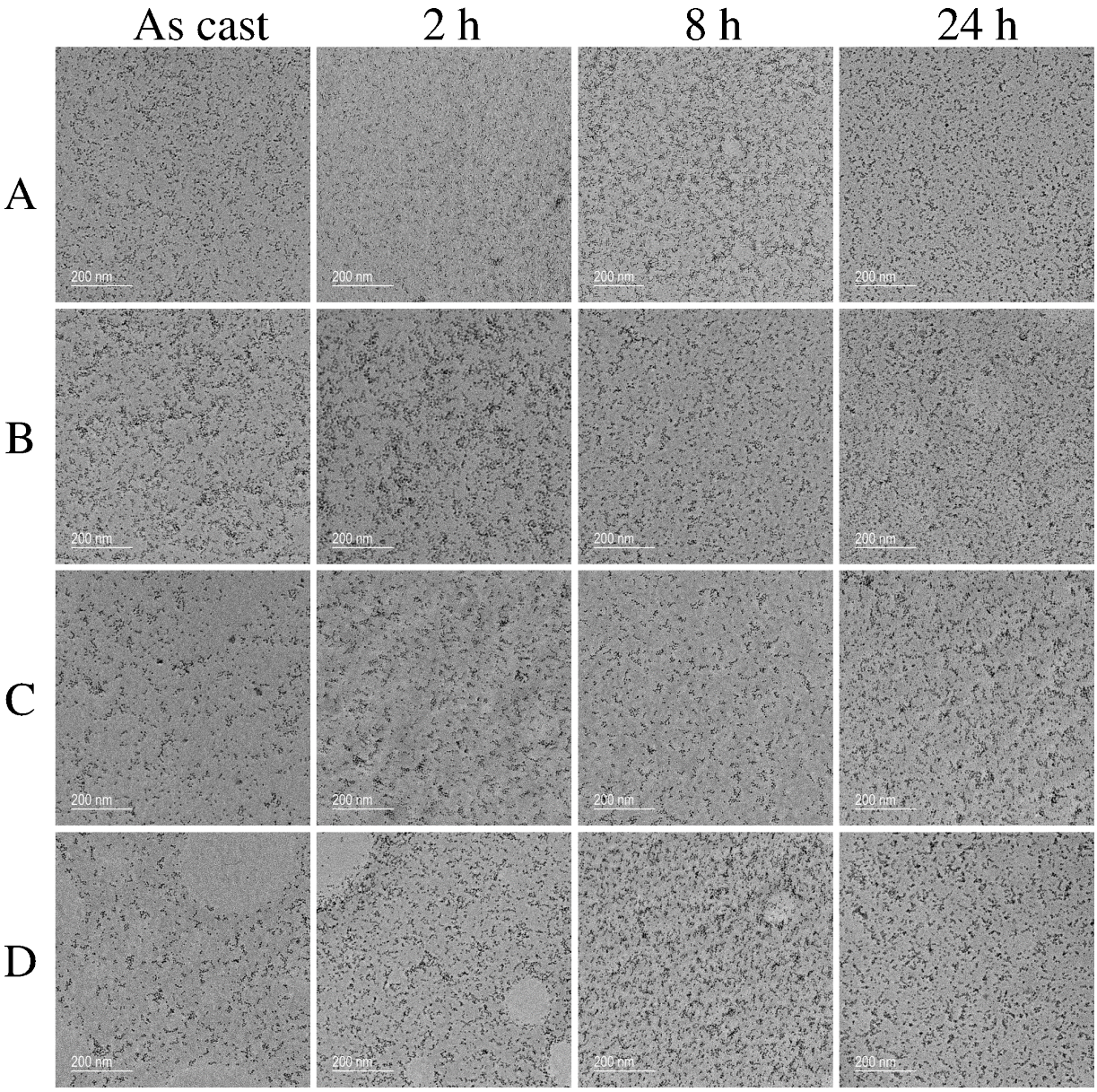

Figure D-2. TEM images for 5L6.5M (A), 5L-26.2M (B), 14L-6.5M (C),and 14L-26.2M (D) as cast and after 2 h, 8 h, and 24 h of thermal annealing treatment at 150^{o}C.

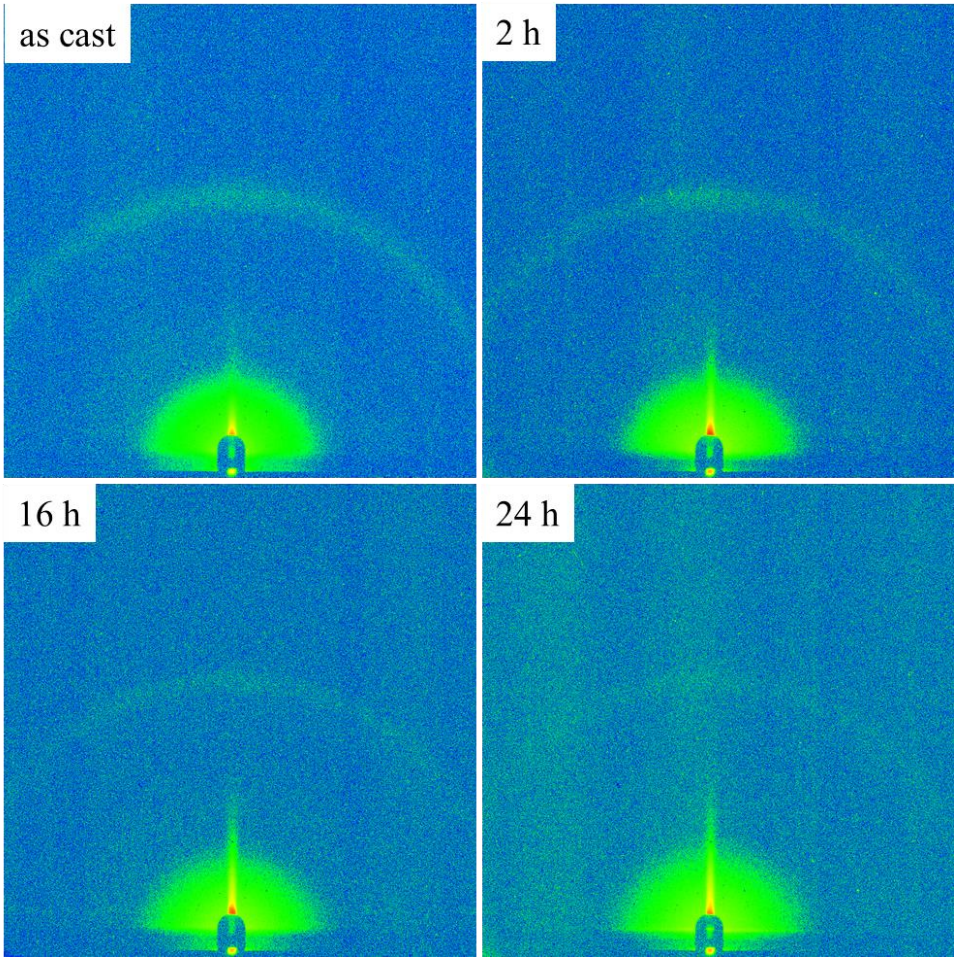

Figure D-3. Two-dimensional GISAXS patterns for 5L-6.5M films.

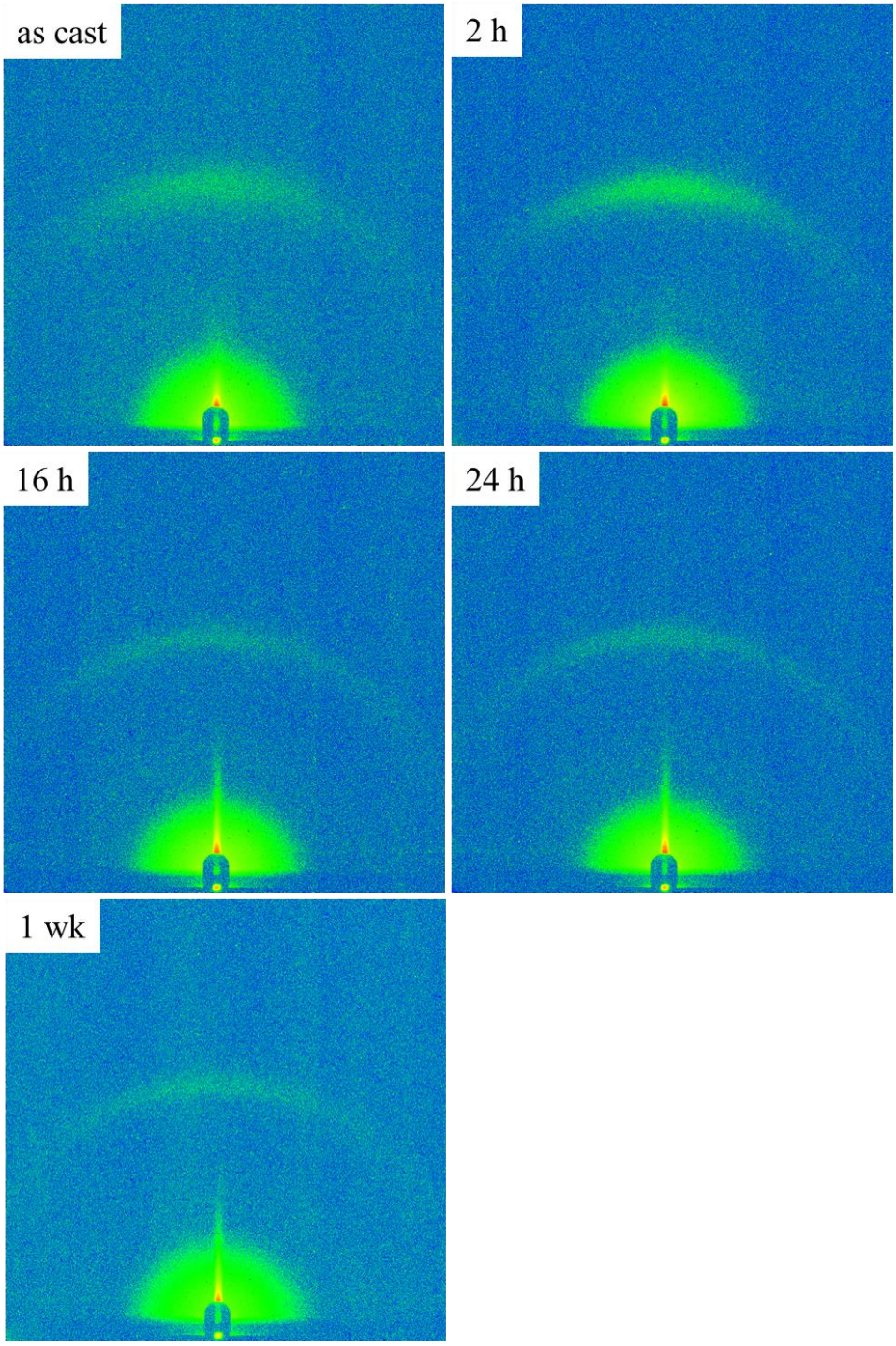

Figure D-4. Two-dimensional GISAXS patterns for 5L-26.2M films.

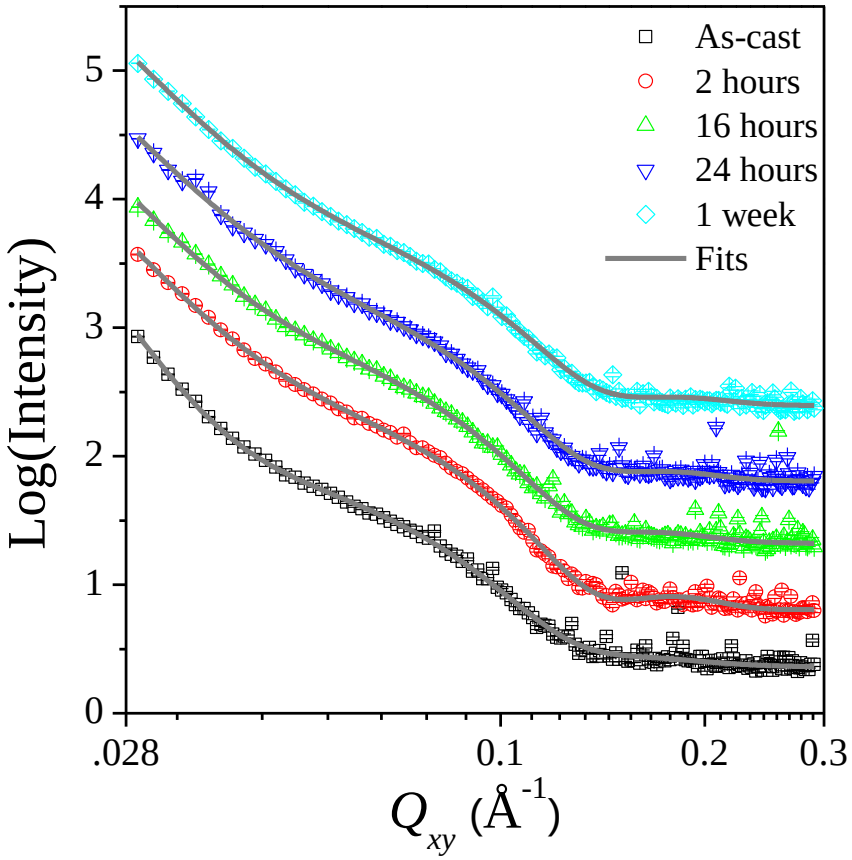

Figure D-5. In-plane GISAXS curves and model fits for 5L-26.2M films.

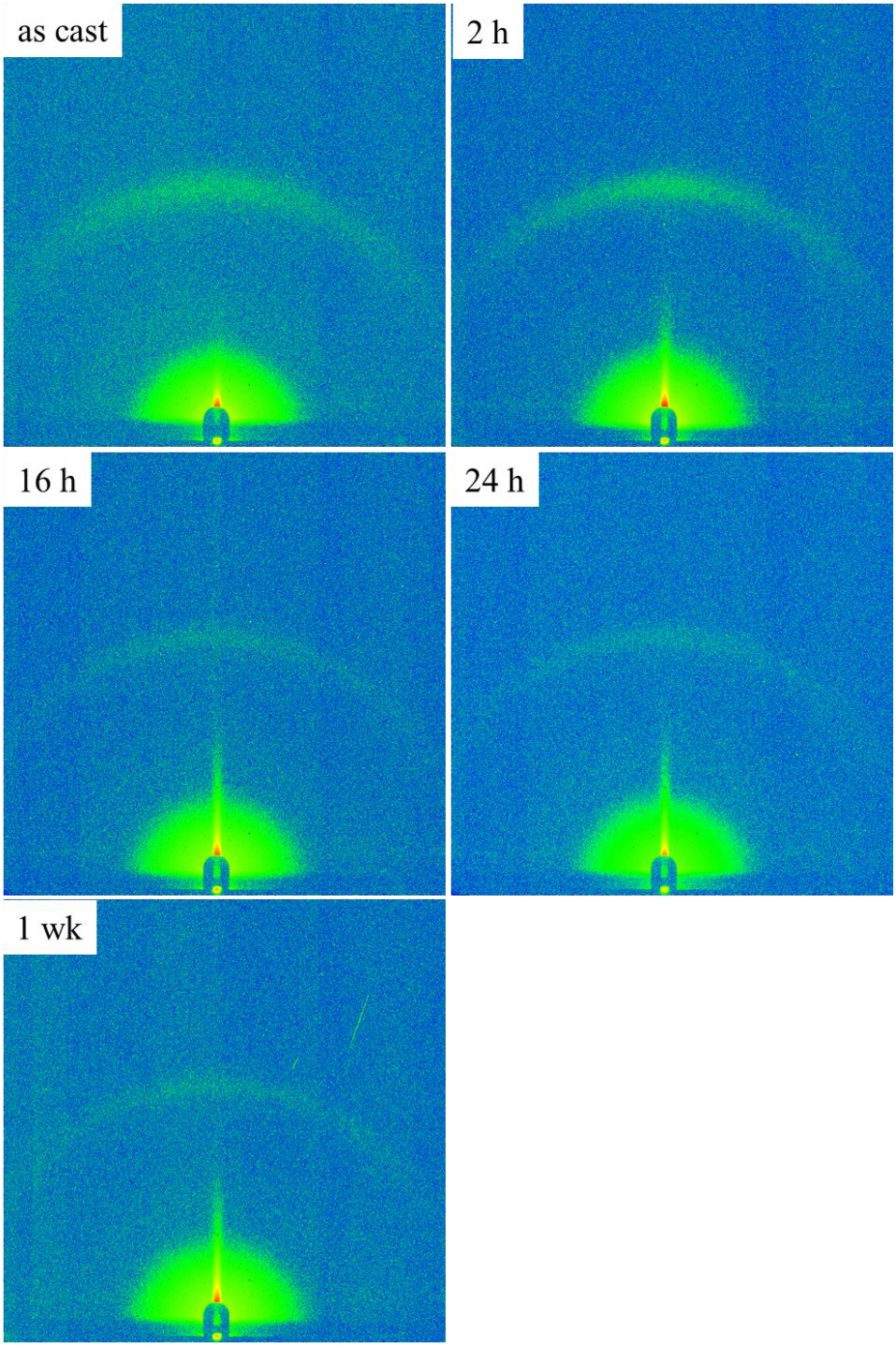

Figure D-6. Two-dimensional GISAXS patterns for 14L-6.5M films.

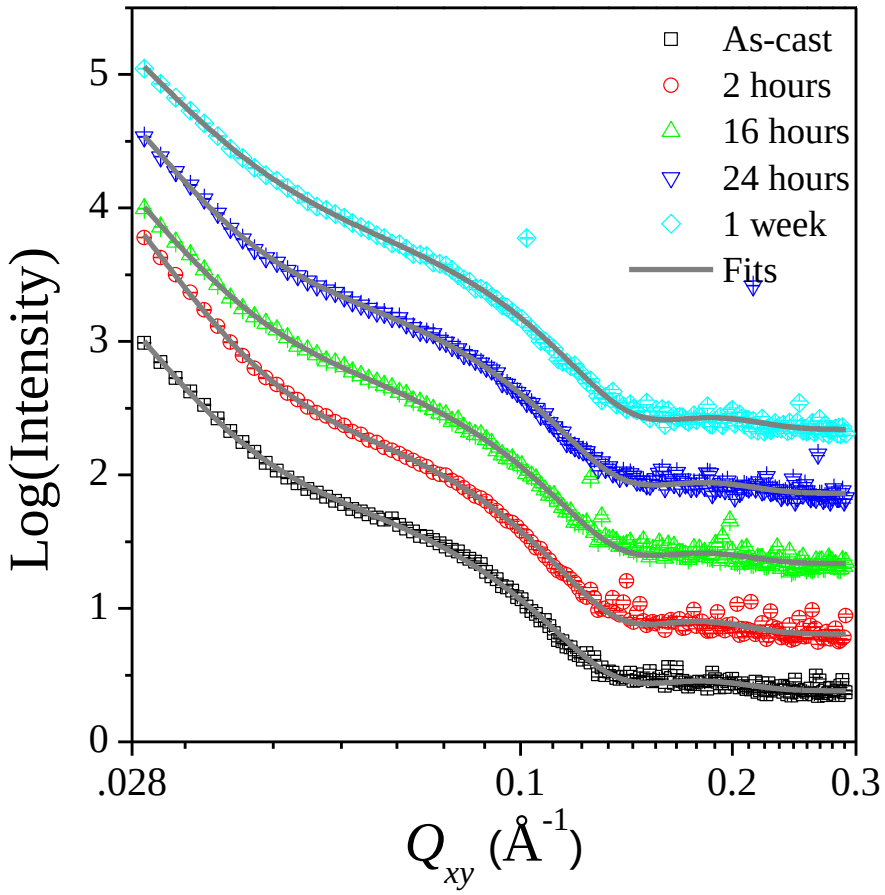

Figure D-7. In-plane GISAXS curves and model fits for 14L-6.5M films.

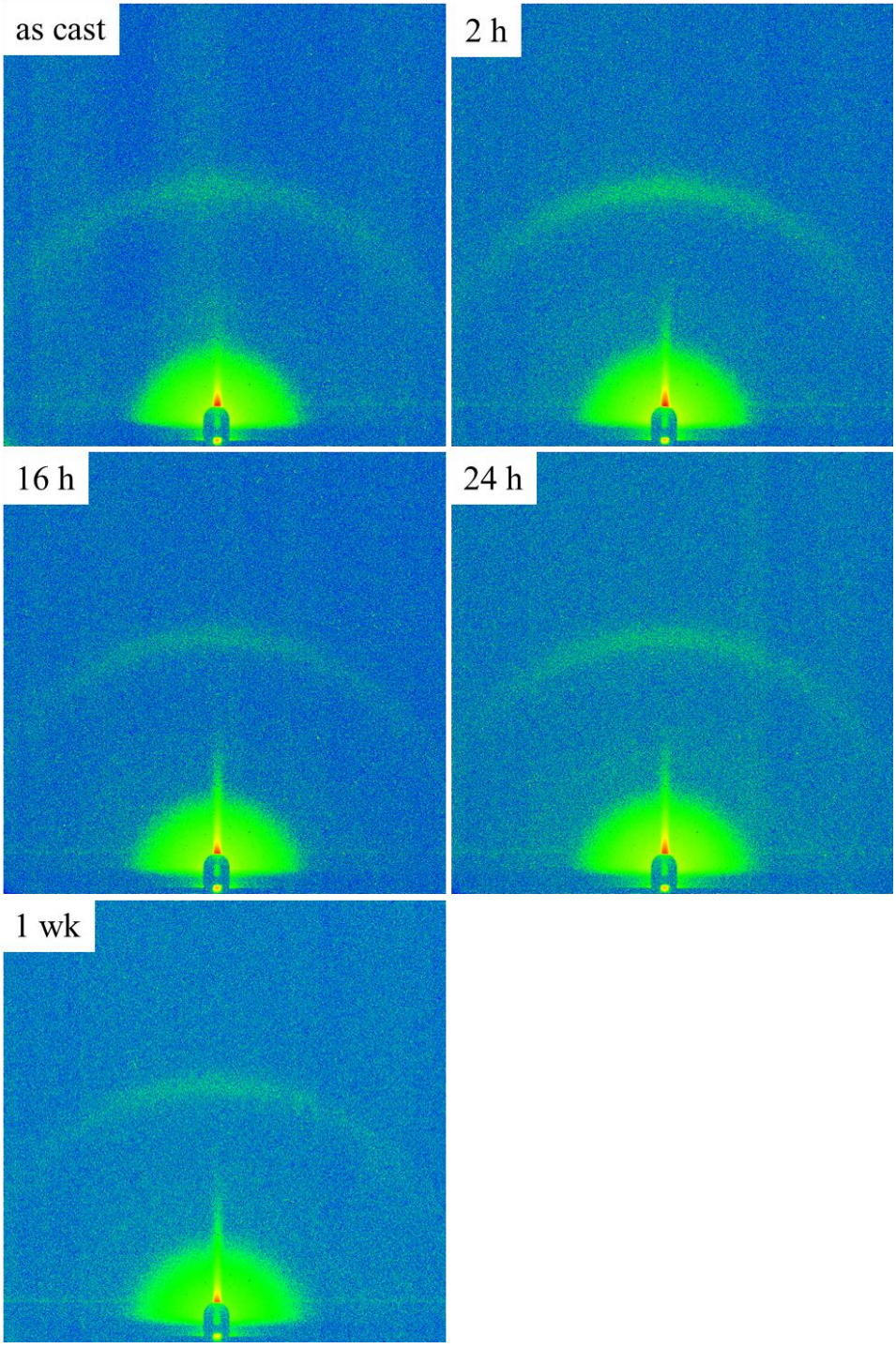

Figure D-8. Two-dimensional GISAXS patterns for 14L-26.2M films.

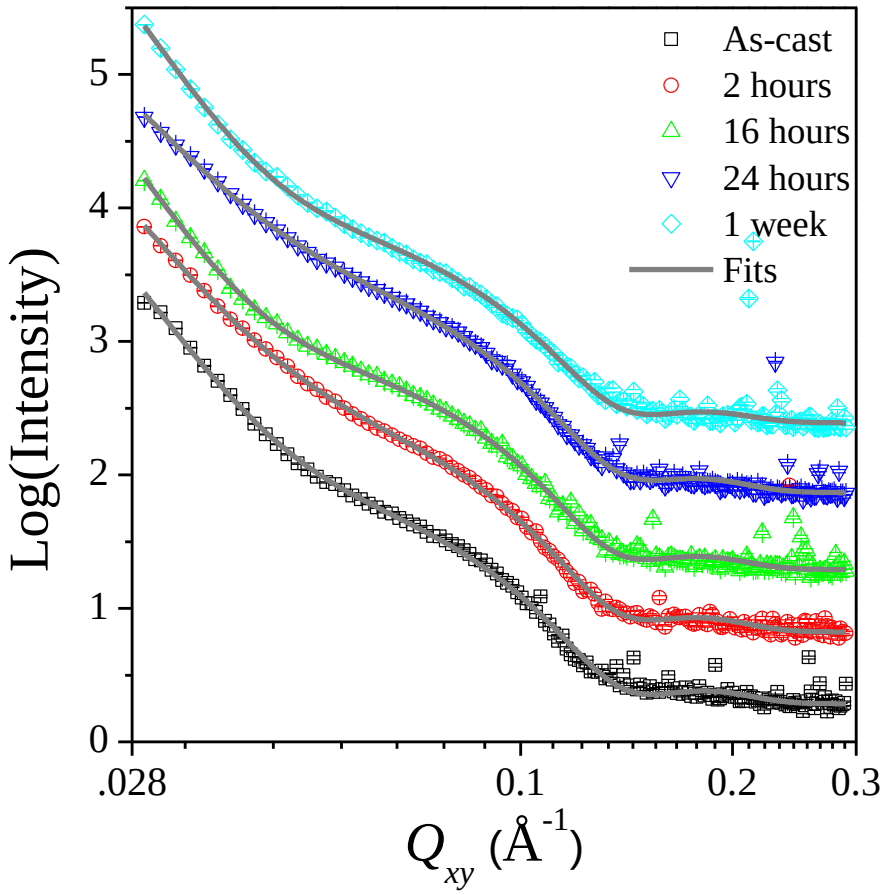

Figure D- 9. In-plane GISAXS curves and model fits for 14L-26.2M films.

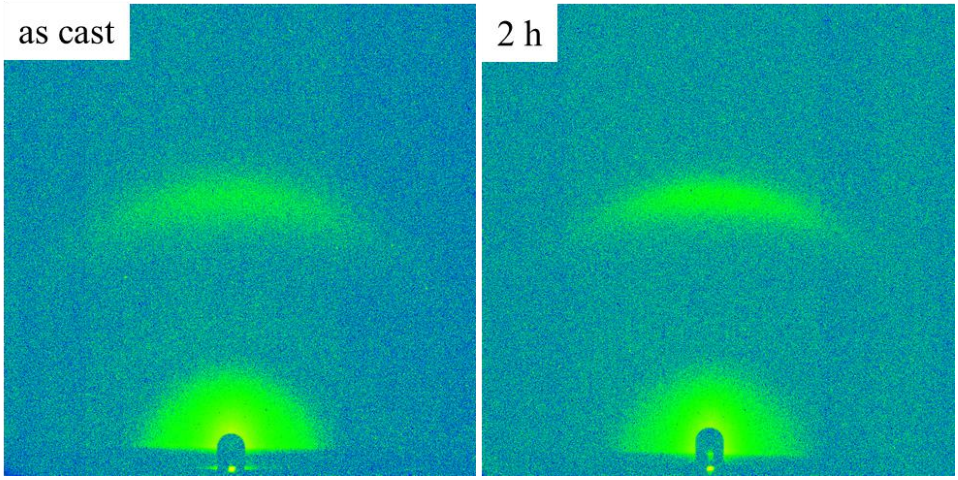

Figure D-10. Two-dimensional GISAXS patterns for pyrL-26.2M films.

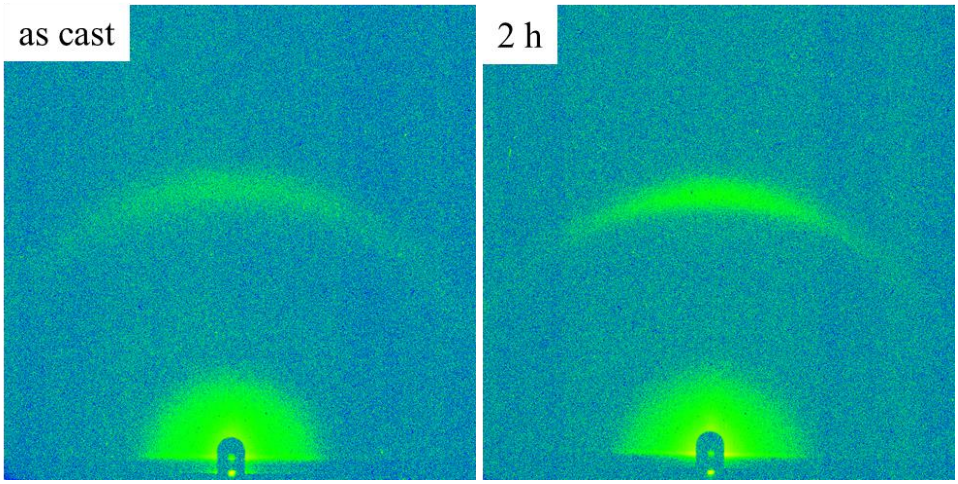

Figure D-11. Two-dimensional GISAXS patterns for pyrL-6.5M films.

Vita

William Michael Kochemba was born in Greenville, Pennsylvania and raised in Trumbull county Ohio through elementary school. His family then moved to Grove City, PA where he attended middle school and high school, graduating in 2005. Directly following high school, Michael began his undergraduate studies at Westminster College in New Wilmington, Pennsylvania, where he earned a B.S. in Chemistry. He came to the University of Tennessee in 2009 and joined the research group of Prof. S. Michael Kilbey II where his research has focused on developing a method to tailor the morphology of inorganic nanoparticles in a polymer matrix for organic photovoltaic applications.